Copyright Warning & Restrictions

The copyright law of the United States (Title 17, United States Code) governs the making of photocopies or other reproductions of copyrighted material.

Under certain conditions specified in the law, libraries and archives are authorized to furnish a photocopy or other reproduction. One of these specified conditions is that the photocopy or reproduction is not to be "used for any purpose other than private study, scholarship, or research." If a, user makes a request for, or later uses, a photocopy or reproduction for purposes in excess of "fair use" that user may be liable for copyright infringement,

This institution reserves the right to refuse to accept a copying order if, in its judgment, fulfillment of the order would involve violation of copyright law.

Please Note: The author retains the copyright while the New Jersey Institute of Technology reserves the right to distribute this thesis or dissertation

Printing note: If you do not wish to print this page, then select "Pages from: first page # to: last page #" on the print dialog screen

INVESTIGATION AND OPTIMUM DESIGN OF THE GENERALIZED SECOND-ORDER PHASE-LOCKED LOOP

BY

WILLIAM A. NOVICK

A DISSERTATION

PRESENTED IN PARTIAL FULFILLMENT OF

THE REQUIREMENTS FOR THE DEGREE

OF

DOCTOR OF ENGINEERING SCIENCE IN ELECTRICAL ENGINEERING

AT

NEW JERSEY INSTITUTE OF TECHNOLOGY

Newark, New Jersey

1976

ABSTRACT

In this dissertation, a second-order phase-locked loop (PLL) in which the loop filter contains complex zeros is investigated in both its linear and nonlinear modes of operation; prior designs used a filter containing a simple zero on the negative real axis. This "generalized" second-order PLL had been heretofore essentially unexplored.

The basic characteristics of the generalized second-order PLL operating in the linear mode including the open and closed-loop responses and the corresponding root locus were generated and compared against those of the conventional second-order PLL. As in the conventional case, the generalized second-order PLL is found to be unconditionally stable. The closed-loop response of the generalized second-order PLL indicates a noise bandwidth which is theoretically infinite, thus making the predetection filter critical to the performance of this PLL. Such is not the case in the conventional PLL.

A method is presented for achieving an optimum design for the generalized second-order PLL for a number of useful modulation types including a single-channel FM speech signal, FDM-FM and FDM-PM. This optimum design is in terms of threshold performance and theoretically predicts that superior performance is possible over the conventional second-order PLL.

Using the Continuous System Modeling Program (CSMP), a nonlinear model of the generalized second-order PLL was simulated for the test-

tone modulation case, both in the absence of noise and with the signal corrupted by bandpass additive Gaussian noise. In addition, preliminary simulation results were obtained for the case of a single-channel FM speech signal. Using simulation techniques, a measure of the mean-square phase error at threshold for the generalized second-order PLL was obtained. This parameter is useful in the optimum design procedure.

Additional insight into the operation of the generalized second-order PLL was obtained through investigation of its acquisition and tracking behavior. This was accomplished using phase plane techniques to study the nonlinear differential equation which governs the loop operation. The results indicate that two distinct types of behavior are theoretically possible depending upon the loop parameters. In one case the behavior is not unlike that of the conventional second-order PLL. In the second case, however, additional singularities are introduced into the phase plane and the behavior is seen to change markedly.

APPROVAL OF DISSERTATION

INVESTIGATION AND OPTIMUM DESIGN OF THE GENERALIZED SECOND-ORDER PHASE-LOCKED LOOP

BY

WILLIAM A. NOVICK

FOR

DEPARTMENT OF ELECTRICAL ENGINEERING

NEW JERSEY INSTITUTE OF TECHNOLOGY

BY

FACULTY COMMITTEE

APPROVED: _____ CHAIRMAN

_____

_____

_____

_____

NEWARK, NEW JERSEY

MAY 1976

DEDICATION

To my wife, Georgine, for her patience, her understanding, and her encouragement and to our children Brett and Jill for their refreshing joy.

ACKNOWLEDGEMENTS

The author gratefully acknowledges the guidance and assistance of Dr. Jacob Klapper, Professor of Electrical Engineering. He also expresses his gratitude to the faculty and staff of New Jersey Institute of Technology for the aid that they have rendered; in particular to Dr. Joseph Frank, Dr. Stanley Habib, and Dr. Solomon Rosenstark.

The author also acknowledges the financial support of New Jersey Institute of Technology and the US Army Electronics Command.

TABLE OF CONTENTS

APPENDICES

LIST OF FIGURES

LIST OF TABLES

CHAPTER I

INTRODUCTION AND REVIEW OF PHASE-LOCKED LOOP THEORY

1.1 Introduction.

The Phase-Locked Loop is now in widespread use. Its superior performance is recognized in many applications, encompassing the fields of communications, control, instrumentation and telemetry. For communications systems the PLL is particularly useful in a low signal-to-noise ratio (SNR) environment because of improved performance in the threshold region. The second-order PLL is most commonly used in practice because of its superior performance over the first-order PLL in most applications and because of the complexity and instability problems often associated with third and higher order loops. The standard second-order PLL design utilizes a filter having a simple zero on the negative real axis. This dissertation involves the investigation and optimum design of a second-order PLL in which the loop filter contains complex zeros. This "generalized" second-order PLL had been heretofore essentially unexplored. This chapter briefly reviews the basic theory of the PLL and introduces the terminology used as a prelude to the subsequent analysis of the generalized second-order PLL.

1.2 Review of Phase-Locked Loop Theory.

1.2.1 General. A block diagram of the basic PLL is given in Fig. 1-1. The elements comprising the PLL are the phase detector, loop filter and amplifier, and the voltage controlled oscillator (VCO). The PLL acts in a manner to keep the VCO output in synchronism with the loop input, i.e., for each cycle of the input signal, there is a corresponding cycle of the VCO output signal. This is accomplished as follows: the phase detector forms a voltage which is proportional to the phase difference between the loop input signal and the VCO output signal. The phase detector output, termed the phase error, is of such a magnitude and polarity, that when it is amplified, filtered (to remove noise and other extraneous signals), and applied to the VCO, it causes the VCO frequency to be exactly that of the loop input signal. A change in input frequency causes readjustment of the phase error to maintain synchronism. The input to the PLL is generally a carrier wave with the intelligence incorporated into its angle, plus additional noise components. Depending upon the application, the output from the PLL is taken at one of the two places. If the PLL operates as an FM demodulator, the output signal is taken from the VCO input. On the other hand, if the PLL operates as a phase extractor, the output signal is taken from the VCO output.

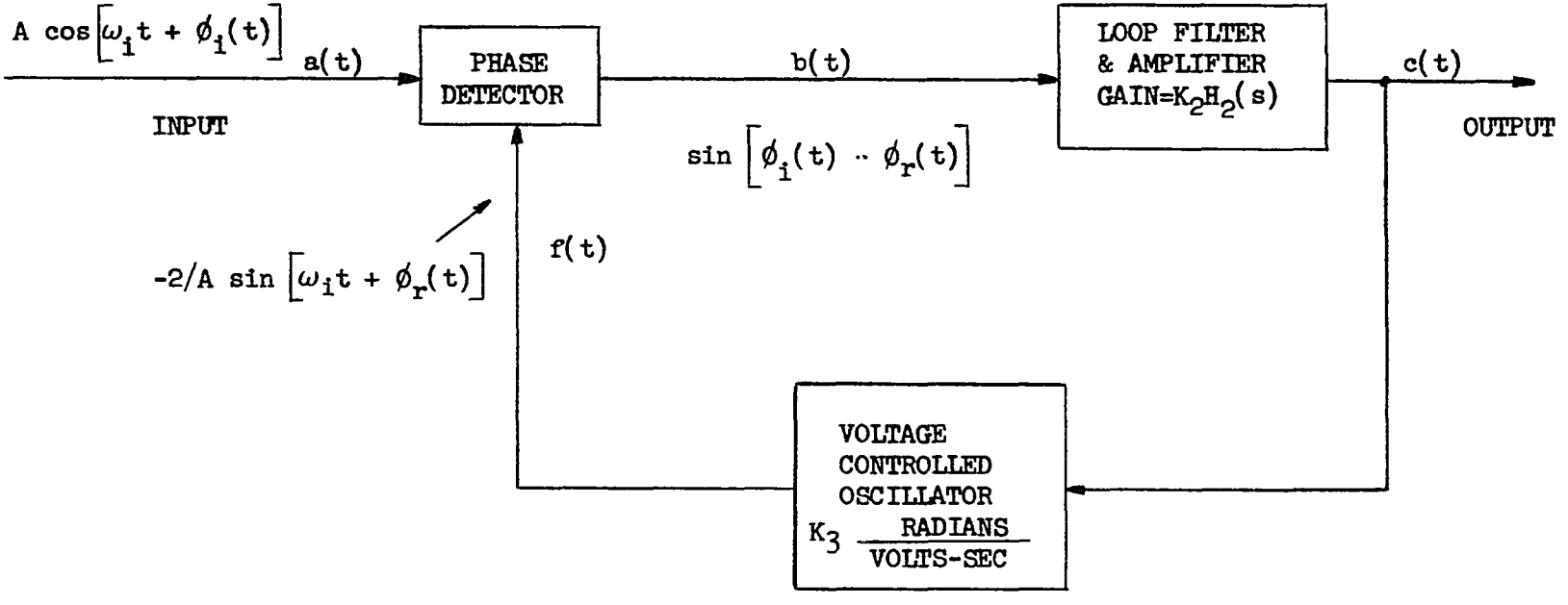

Fig. 1-1. Block diagram of the basic PLL in synchronized mode.

1.2.2 Formulation of the Differential Equation of the PLL. Referring back to the basic PLL of Fig. 1-1, the input signal in the absence of noise may be expressed as

$$a(t) = A \cos \left[\omega_i t + \phi_i(t) \right] \tag{1-1}$$

where A is the peak signal amplitude, ω_i is the center frequency of the input signal and $\phi_i(t)$ is the input signal phase modulation. The VCO output signal is assumed to be of the form

$$f(t) = - (2/A) \sin \left[\omega_i t + \phi_r(t) \right] \tag{1-2}$$

where $\phi_r(t)$ is the phase modulation of the VCO. Note that the VCO signal is chosen to be in quadrature with the input signal. The 2/A amplitude is chosen for convenience as will become evident shortly. Finally, the static frequency error between the input signal and the VCO output signal is assumed to be zero, indicative of the PLL being in the synchronized or locked mode [Ref. 1, p. 78]. Assuming a multiplier type phase detector is used, produces a phase detector output given by

$$b(t) = a(t)f(t) = -\sin \left[2\omega_i t + \phi_i(t) + \phi_r(t) \right] + \sin \left[\phi_i(t) - \phi_r(t) \right] \tag{1-3}$$

Assuming that the double frequency component is rejected by the loop yields an output at the loop filter given by

$$c(t) = K_2\, h_2(t) * \sin\ \phi_e(t) \tag{1-4}$$

where K_2 is the gain of the loop amplifier, $h_2\ (t)$ is the impulse response of the loop filter, * denotes convolution and $\phi_e(t)$ is the phase error which is expressed as

$$\phi_e(t) = \phi_i(t) - \phi_r(t) \tag{1-5}$$

The voltage c(t) is applied to the VCO which produces an FM signal with a frequency deviation which is directly proportional to this voltage, yielding the condition

$$\frac{d\phi_r}{dt} = K_2 K_3 h_2\ (t) * \sin\ \phi_e(t) \tag{1-6}$$

where K_3 is the VCO sensitivity. Eq. 1-6 may be reexpressed in terms of operational notation p = d/dt as follows

$$\dot{\phi}_e(t) = \dot{\phi}_i(t) - KH_2(P) \sin\ \phi_e(t) \tag{1-7}$$

where

$$K = K_2\ K_3 \tag{1-8}$$

Eq. 1-7 is a nonlinear differential which governs the operation of the PLL and for which a general analytic solution is not available. However, as will be subsequently shown, using "phase plane" techniques, a number of important properties of the system response can be obtained.

1.2.3 The Linear Equivalent Model. In addition to the nonlinearity associated with the periodicity of the phase detector characteristic, the particular PLL discussed here contains a basic nonlinearity due to the choice of a phase detector having a sinusoidal characteristic. This obviously presents a limitation on the performance of the PLL and brings up the question as to why a more linear type of phase detector is not used. The answer lies in several factors, most important of which are the simplicity of its implementation and the linear translational characteristic in frequency exhibited by the multiplier-type phase detector to additive input noise. More sophisticated phase detectors having more linear characteristics are discussed in the next chapter.

Returning once more to the sinusoidal-type phase detector, it is noted that for proper operation of the PLL, the input signal and noise components must be such that the phase error be less than $\pi/2$. Beyond this value, the slope of the phase detector characteristic changes sign and a regenerative mode occurs. Furthermore, the dynamic phase error must be small (generally less than

one radian) so that the portion of the characteristics over which operation takes place is essentially linear. With these restrictions, a linear equivalent model can be derived for the PLL. This model, shown in Fig. 1-2 has obvious analytical significance.

1.2.4 Effects Due to Input Noise. Under normal circumstances, the PLL is subjected to a signal with additive input noise. In this section, the representative case of signal corruption by band-limited Gaussian noise will be considered. The input to the PLL may be expressed as

$$a(t) = A \cos\left[\omega_i t + \phi_i(t)\right] + N(t) \qquad (1\text{-}9)$$

The VCO output signal now contains a signal component and a noise component which are designated $\phi_{rs}(t)$ and $\phi_{rn}(t)$, respectively, and therefore

$$f(t) = -(2/A) \sin\left[\omega_i t + \phi_r(t)\right] \qquad (1\text{-}10)$$

where

$$\phi_r(t) = \phi_{rs}(t) + \phi_{rn}(t) \qquad (1\text{-}11)$$

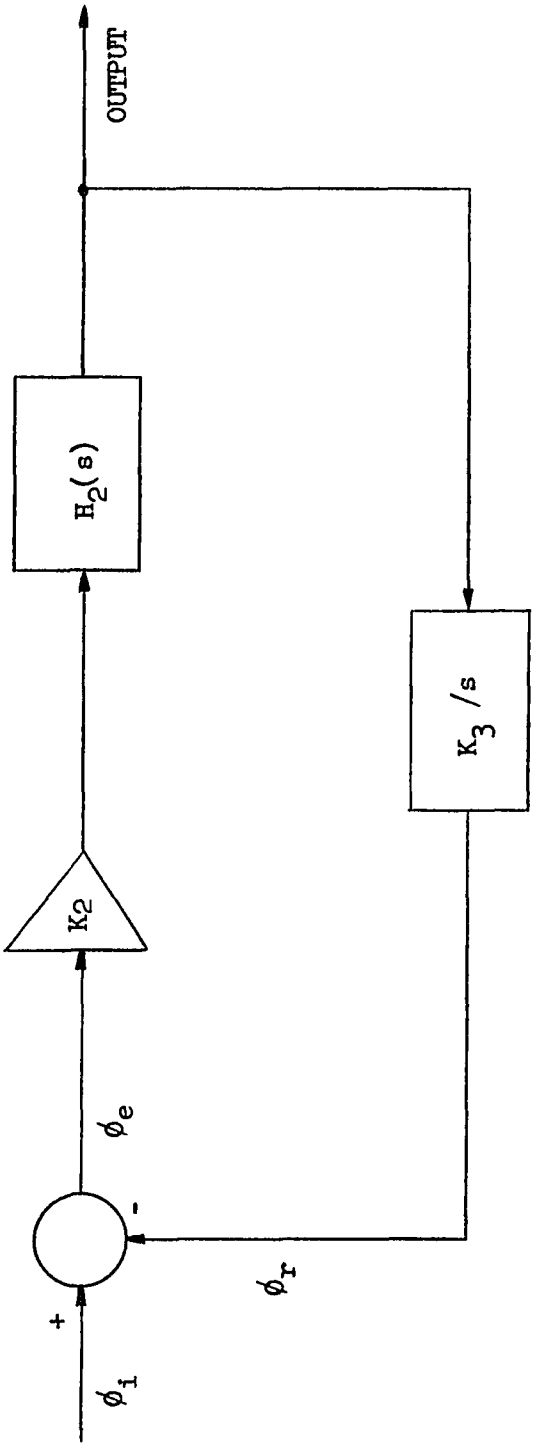

Fig. 1-2. Linear model of the basic PLL.

The phase detector output may be expressed as

$$b(t) = \text{Sin}\left[\phi_{es}(t) - \phi_{rn}(t)\right] + n(t) \tag{1-12}$$

where

$$n(t) = -\left(2N(t)/A\right) \text{Sin}\left[\omega_i t + \phi_r(t)\right] \tag{1-13}$$

and

$$\phi_{es}(t) = \phi_i(t) - \phi_{rs}(t) \tag{1-14}$$

Note that the double frequency term is again assumed to be rejected by the loop and is omitted from Eq. 1-12. The bandpass input noise may be expressed as follows

$$N(t) = x(t) \cos \omega_i t - y(t) \sin \omega_i t \tag{1-15}$$

substituting Eq. 1-15 into Eq. 1-13 yields

$$n(t) = -(2/A) \left[x(t) \cos \omega_i t - y(t) \sin \omega_i t \right] \sin\left[\omega_i t + \phi_r (t)\right] \tag{1-16}$$

Multiplying through and again eliminating the double frequency terms yields

$$n(t) = -\left[x(t)/A\right] \operatorname{Sin} \phi_r(t) + \left[y(t)/A\right] \operatorname{Cos} \phi_r(t) \qquad (1\text{-}17)$$

n(t) is called the "equivalent noise input" and may be incorporated into the PLL model to fully account for the input noise [Ref. 1, pp. 82-83 and Ref. 3, pp. 1737-1738] as shown in Fig. 3-1. Note

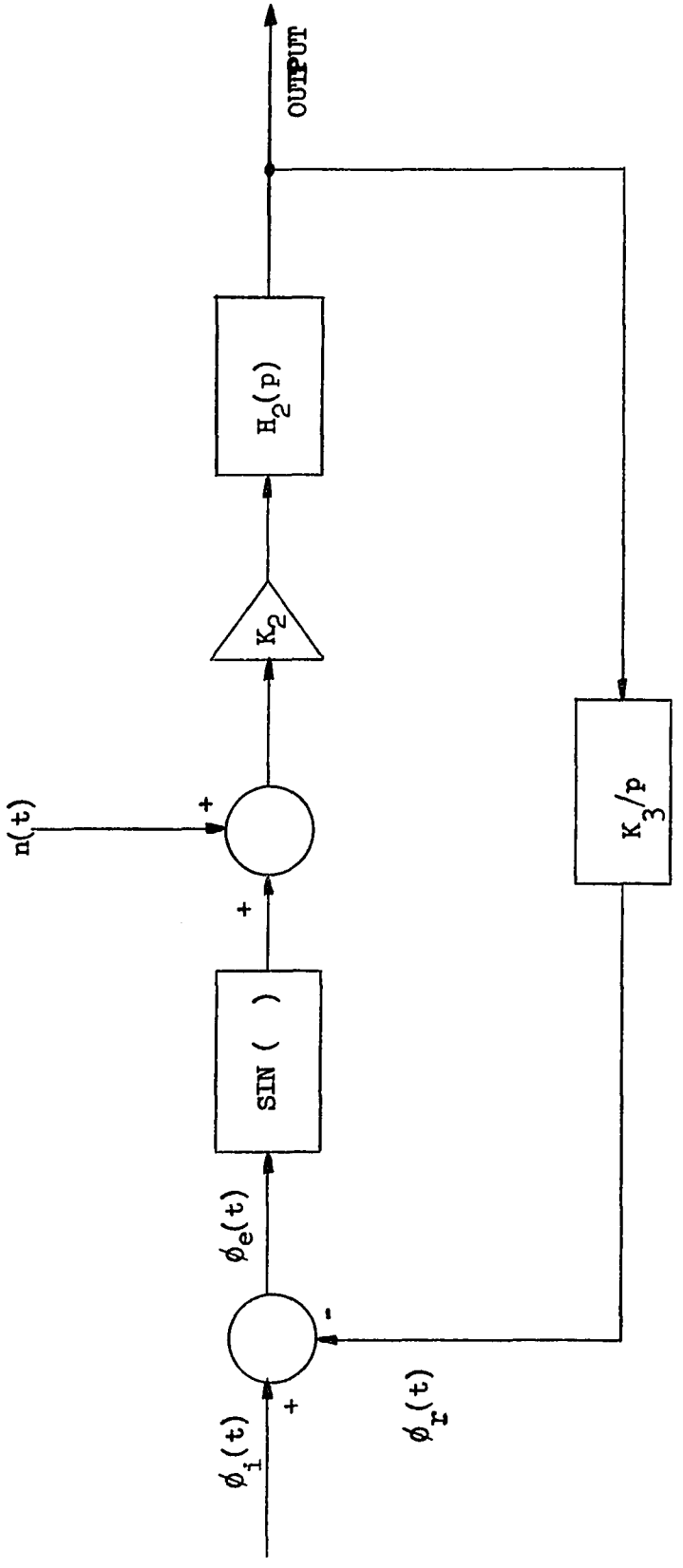

Fig. 1-3. PLL model incorporating the equivalent noise input.

that by applying the criteria discussed in Sec. 1.2.3 the model of Fig. 3-1 can be reduced to the linear case.

The determination of the power spectral density (PSD) of n(t) is in general a complex problem, however, for the case where N(t) has a symmetrical bandpass, PSD which is much wider than the bandwidth of $\phi_r(t)$, it has been shown [Ref. 1, pp. 28-34] that n(t) is essentially the lowpass equivalent of N(t) with the appropriate scaling. For example, if the input noise is white with a PSD of height η, the PSD of n(t) is white with height $2\eta/A^2$ [Ref. 1, p. 84].

1.2.5 Open and Closed-Loop Transfer Functions. It is of interest to determine the open and closed-loop transfer functions for the linear model of the PLL since they will be of use in later analysis. The open-loop transfer function for the PLL (see Fig. 1-2) is given by

$$\left.\frac{\Phi_r(s)}{\Phi_i(s)}\right|_{\substack{\text{Open}\\\text{Loop}}} = G(s) = \frac{K\,H_2(s)}{s} \qquad (1\text{-}18)$$

where

$$K = K_2\,K_3 \qquad (1\text{-}19)$$

and serves as the means by which PLL's are normally classified. The "loop type" is the number of poles in (s) located at the origin, while the "loop order" is the total number of poles in G(s). Thus, a PLL containing no loop filter is of first order. On the other hand, if $H_2(s)$ introduces a pole, then the loop becomes second-order. The closed-loop transfer function is given by

$$\left.\frac{\Phi_r(s)}{\Phi_i(s)}\right|_{\substack{\text{Closed}\\\text{Loop}}} = H(s) = \frac{G(s)}{1 + G(s)} = \frac{KH_2(s)}{s + KH_2(s)} \qquad (1\text{-}20)$$

from which the stability of the PLL may be determined. As discussed earlier, the second-order PLL is most widely used in practice. In particular, the second-order, type one, PLL is the practical configuration associated with this case. Since the second-order, type one, PLL shall be referred to frequently during the course of this dissertation, it is of interest to determine some of its important characteristics. The loop filter for the second-order, type one PLL is of the form

$$H_2(s) = \frac{s/a + 1}{s/b + 1} \qquad (1\text{-}21)$$

Substituting Eq. 1-21 into Eq. 1-20 yields the closed-loop transfer function for the second-order, type one PLL as

$$H(s) = \frac{\frac{s}{a} + 1}{\frac{s^2}{Kb} + \left(\frac{1}{K} \quad \frac{1}{a}\right)s + 1} \tag{1-22}$$

Fig. 1-4 shows the root locus plot of H(s) for the second-order, type one PLL. It is noted that this PLL is unconditionally stable.

Finally, it is of interest to determine the equivalent noise bandwidth which is defined as

$$B_n = \frac{1}{H_o^2}\int_0^\infty H\left|j\omega\right|^2 df \tag{1-23}$$

For the case at hand, H_o^2 is the power response at f = 0 which from Eq. 1-22 is unity. The definite integral in Eq. 1-23 can be evaluated directly from tabulated integrals [Ref. 1, p. 21 and p. 93] yielding

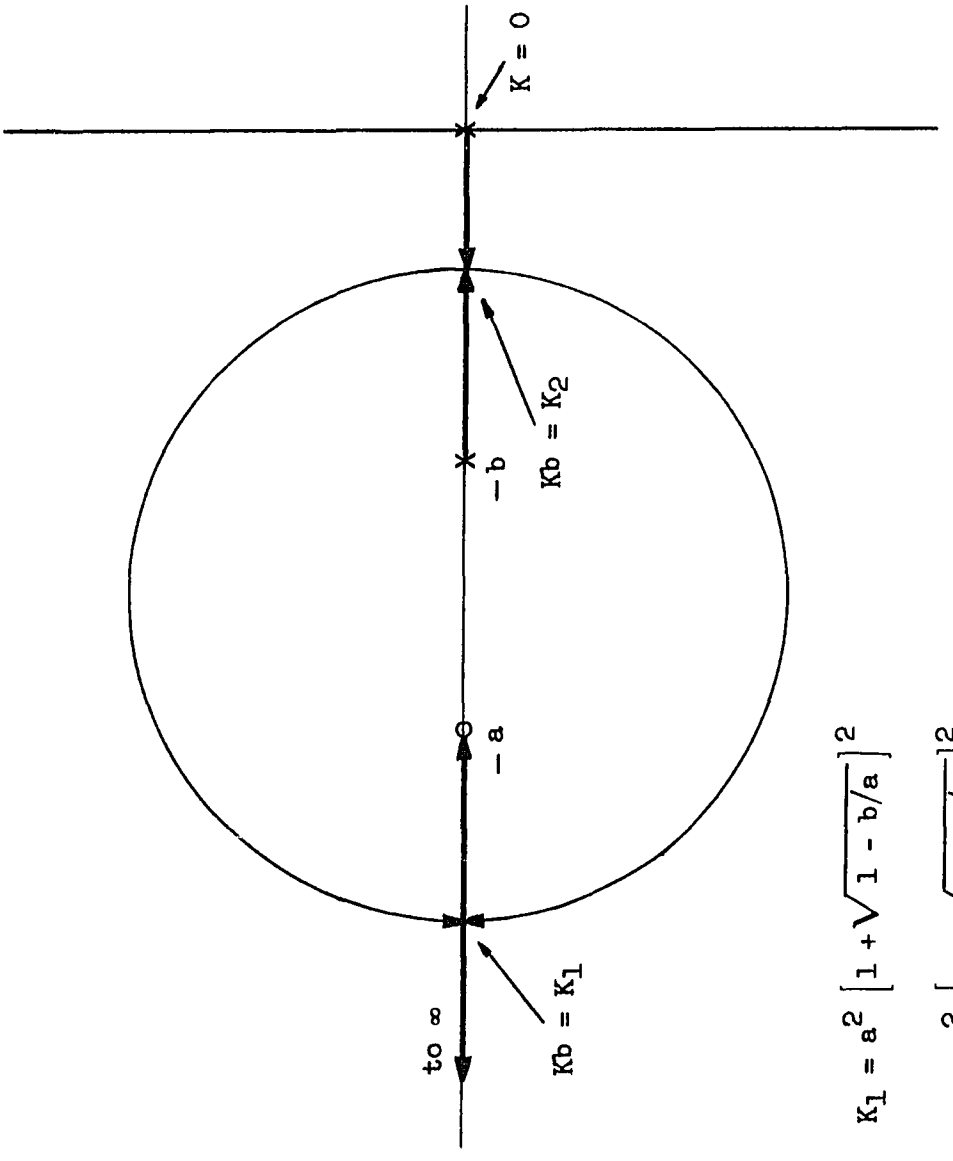

$$K_1 = a^2\left[1 + \sqrt{1 - b/a}\right]^2$$

$$K_2 = a^2\left[1 - \sqrt{1 - b/a}\right]^2$$

Fig. 1-4. Root locus plot for the second-order, type one PLL.

$$B_n = \frac{Kb\left(\frac{Kb}{a}+a\right)}{4a\left(\frac{Kb}{a}+b\right)} \qquad (1\text{-}24)$$

1.2.6 Cycle Slipping. In most applications of the PLL, the critical parameter is the "rate of cycle slippings". This refers to the occasional deletion (or insertion) of a cycle in the VCO output signal as compared to the pure signal at the loop input.

There are two different sources of cycle slippings in a PLL [Ref. 5] . The first type is referred to as ThI (threshold impulses). These come about when the resultant phasor of carrier and noise at the loop input encircles the origin. Only a relatively small percentage of the ThI are normally tracked by the loop due to its compressive and filtering actions. If a ThI is tracked, it results in a spike in the output of the PLL. The rate of these ThI is seen to increase with increasing PLL bandwidth.

The second source of cycle slippings, called LLI (loss of lock impulses), comes about when the PLL encounters noise and/or signal transients which it is not able to follow due to the multi-valued characteristic of the phase detector. For the case of a phase detector with a sinusoidal characteristic, if the phase

error is forced beyond $\pi/2$, the PLL enters a regenerative mode because of the change in the sign of the slope, usually resulting in a shifting of the stable operating point by 2π or a multiple of 2π thereby causing LLI. The rate of these LLI decreases with increasing bandwidth. The optimum design of a PLL is achieved by minimization of the combined total rate of ThI and LLI. The ability of a PLL to achieve lower thresholds than a conventional FM demodulator is based on the fact that the combined rate of ThI and LLI in a PLL may be made less than that of the ThI alone in a conventional FM demodulator [Ref. 1, p. 109].

These cycle slippings are the cause of threshold in FM demodulation and thus limits the tradeoff capability in an FM system between required transmitter power and transmission bandwidth. Their effect is felt particularly in satellite communications systems. The cycle slippings are further known to be the major cause of errors in digital FM transmissions [Ref. 5]. They are also of critical significance in tracking and whenever absolute phase estimation is required.

In the next chapter, devices which possess a phase detector characteristic having greater than $\pm \pi/2$ monotonic range are discussed and it is shown how one such device leads to the generalized second-order PLL configuration.

References - Chapter 1

1. J. Klapper and J. Frankle, Phase-Locked and Frequency-Feedback Systems: Principles and Techniques, Academic Press, New York, 1972.

2. A. Acampora and A. Newton, "Use of Phase Subtraction to Extend the Range of a Phase-Locked Demodulator," RCA Review, Vol. 27, No. 3, pp. 577-599, December 1966.

3. A. J. Viterbi, "Phase-Locked Loop Dynamics in the Presence of Noise by Fokker-Planck Techniques," Proc. IEEE, Vol. 51, pp. 1737-1753, December 1963.

4. A. J. Viterbi, Principles of Coherent Communication, McGraw-Hill Book Co., New York, 1966.

5. J. Klapper, "Demodulator Threshold Performance and Error Rates in Angle-Modulated Digital Signals," RCA Review, Vol. 27, No. 2, pp. 226-244, June 1966.

CHAPTER II

THE EXTENDED-RANGE PHASE-LOCKED DEMODULATOR (ERPLD) AND THE GENERALIZED SECOND-ORDER PLL

2.1 Introduction

As discussed in the preceding chapter, the conventional PLL incorporates a phase detector having a sinusoidal characteristic, and thus has a monotonic range of $\pm \pi/2$. Whenever the signal and/or noise cause the phase error to exceed $\pm \pi/2$, the PLL enters a regenerative mode due to the change in sign of the slope of the phase detector characteristic. When this occurs it is highly probable that loss of lock will occur and an LLI will be produced. This suggests the use of a phase detector with a monotonic range greater than $\pm \pi/2$ to reduce the rate of LLI. Under such conditions, it would be possible to reduce the bandwidth of the PLL thus reducing the rate of ThI. The net outcome of such a scheme would be a device whose spike rate would be less than that for a conventional PLL under the same input conditions, thus permitting lower thresholds. It is this concept that provides the basis for all ERPLDs.

It is subsequently shown that one such ERPLD configuration i.e. the ERPLD using phase feedback can be reduced to a conventional PLL with a more complicated loop filter. This "equi-

valent filter realization" is shown to lead directly to the "generalized second-order PLL."

2.2 Implementations of the ERPLD

2.2.1 General. The threshold performance of a PLL with a phase detector having a greater than $\pm \pi/2$ monotonic range has been analyzed by Frankle [Ref. 1]. In this analysis, both a sawtooth and a truncated sine phase-detector characteristic were considered as shown in Fig. 2-1. Threshold reductions of 4dB for the sawtooth and 7dB for the truncated sinusoid were predicted in comparison to the conventional second-order PLL. In light of these results, it is apparent that besides monotonic range, the shape of the phase-detector characteristic is also very important and linearity of the characteristic is not necessarily desirable.

The actual realization of the extended-range type phase detector has thus far been found to fall into three categories: waveshaping of the carrier signal, postdetection linear synthesis and postdetection non-linear synthesis [Ref. 2, p. 250]. The first method involves choosing shapes for the input and reference carrier signals, which when passed through a multiplier-type phase detector produce, in the low frequency output component, the desired characteristic. Because of the problems involved in

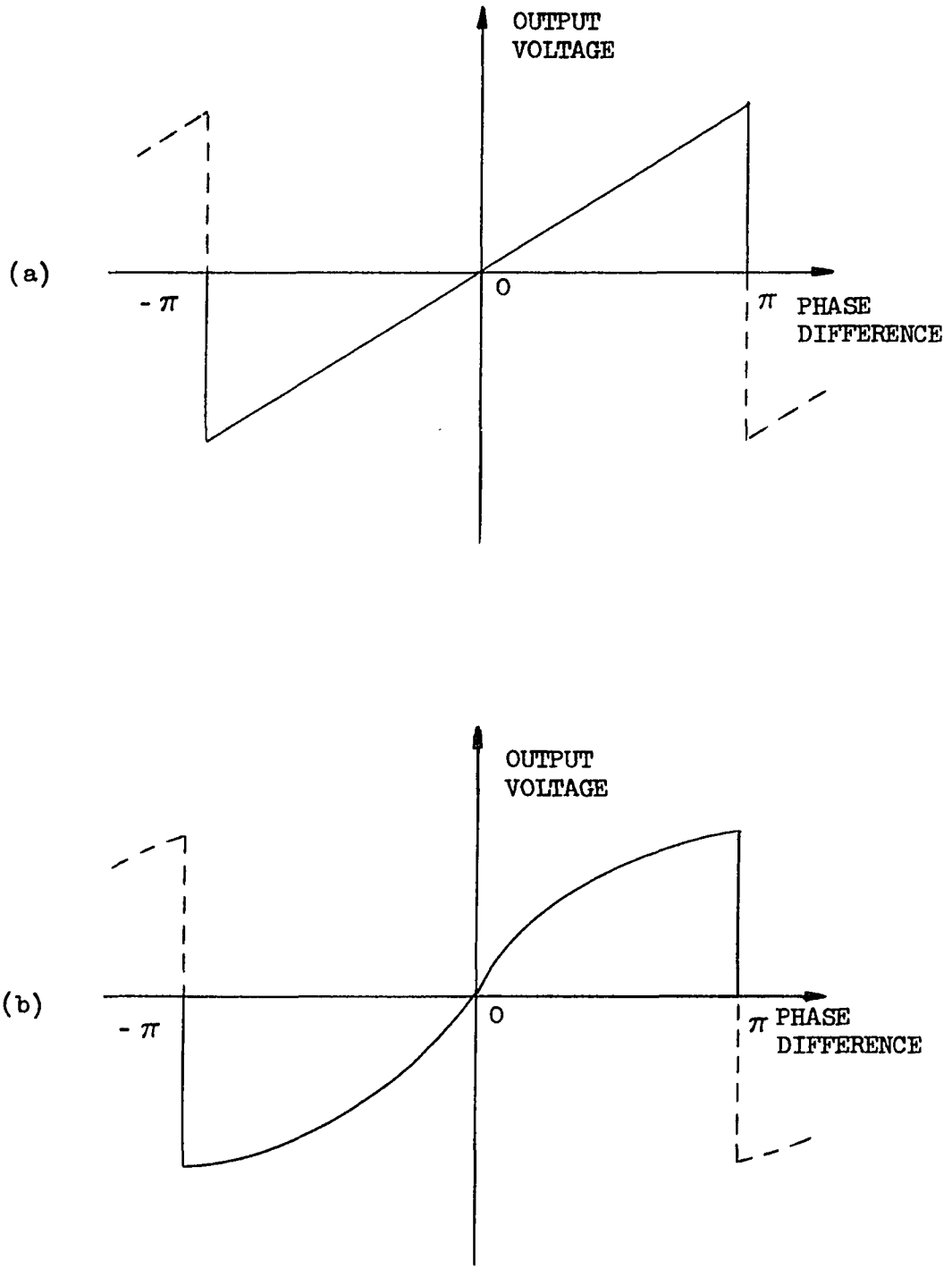

Fig. 2-1. Extended-range phase detector characteristics.
(a) Sawtooth; (b) Truncated sinusoid.

transmitter waveshaping, this method is, in general, not practical. It does, however, provide the basis for more practical procedures to be discussed presently.

2.2.2 ERPLD Realization by Postdetection Linear Synthesis. Referring to the conventional PLL of Fig. 1-1, it is noted that the shaped input and reference signals in the absence of noise and without modulation may be represented by their Fourier series expansions as follows

$$a(t) = \sum_{m=1}^{\infty} a_m \cos(m \omega_i t) \qquad (2\text{-}1)$$

and

$$f(t) = \sum_{n=1}^{\infty} b_n \sin(n\omega_i t - n \phi_e) \qquad (2\text{-}2)$$

where ϕ_e is the relative phase shift between the input and reference signals. For a multiplying type of phase detector, the low-frequency output components are

$$e = a(t)\, f(t) = \sum_{n=1}^{\infty} \frac{a_n b_n}{2} \sin(n \phi_e) \qquad (2\text{-}3)$$

The result is that the phase detector characteristic (e vs. ϕ_e) is dependent on the superposition of the Fourier terms

$a_n b_n \sin(n \phi_e)$. Various phase-detector responses can be synthesized by proper choice of the $a_n b_n$ coefficient, which are controlled by the shape of the carrier signals [Ref 2, p. 253].

Eq. 2-3 can also be generated without carrier signal waveshaping by postdetection synthesis, an example of which is shown in Fig. 2-2 [Ref. 2, p. 253]. In this system, called the "phase-error feedback method," a voltage which is linearly proportional to the phase error is fed back through a system of phase modulators and phase detectors to produce a series of outputs with voltages proportional to $\sin \phi_e$ and its harmonics. These outputs are then properly weighted and summed to form the required linear function of ϕ_e. The system has the practical limitation of requiring a large number of phase detectors and phase modulators which still limit the system to only a finite summation of harmonic components. The effectiveness of this system is not fully known because the formidable task of its analysis in the presence of noise remains yet to be accomplished.

2.2.3 ERPLD Realization by Postdetection Non-linear Synthesis.

The technique of postdetection non-linear synthesis is exemplified by the system shown in Fig. 2-3 known as the Tanlock PLL [Ref. 3]. This system produces a phase comparator characteristic given by

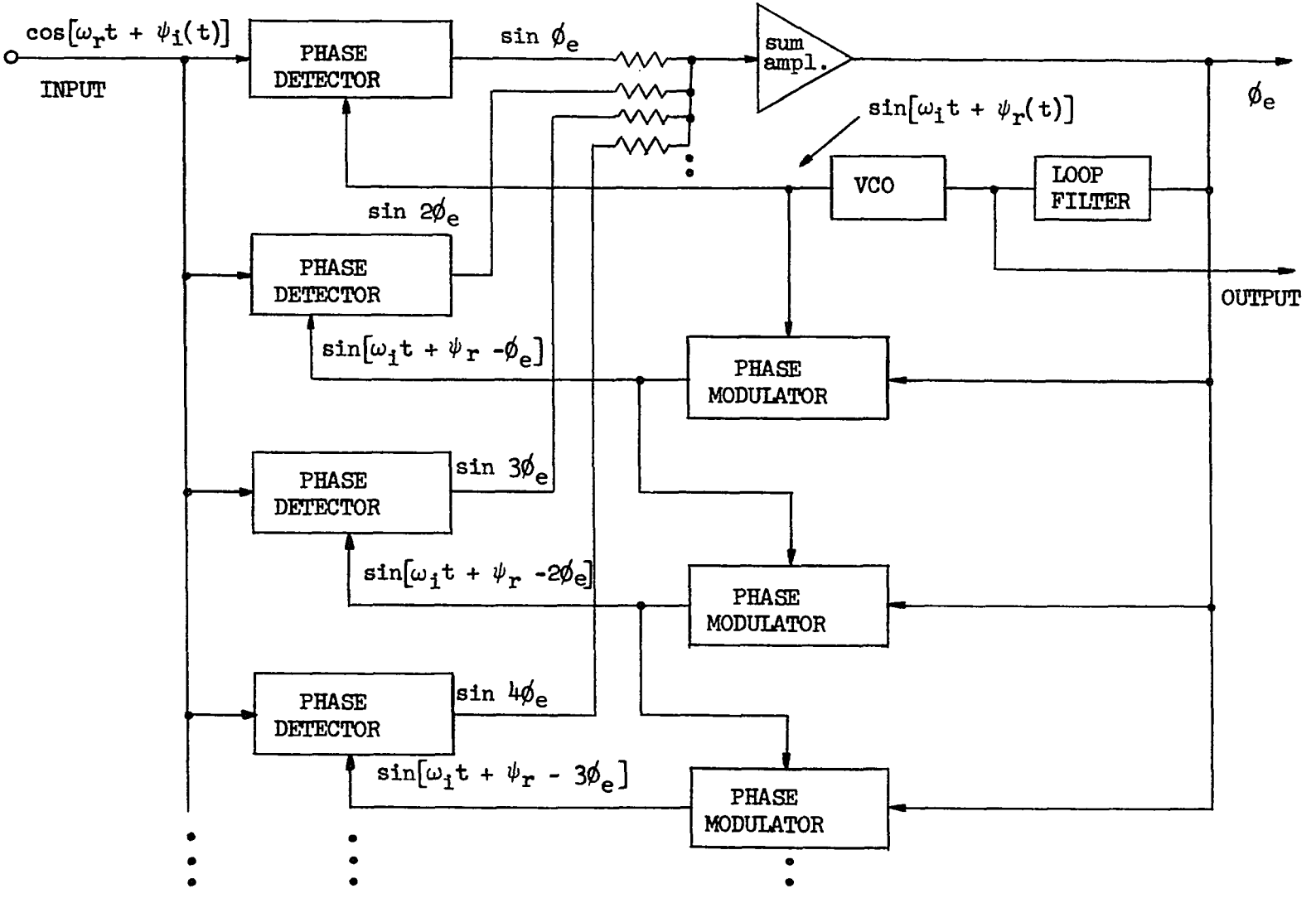

Fig. 2-2. ERPLD using multiterm synthesis: Phase-error feedback method (from Klapper and Frankle [Ref. 2, p.253]).

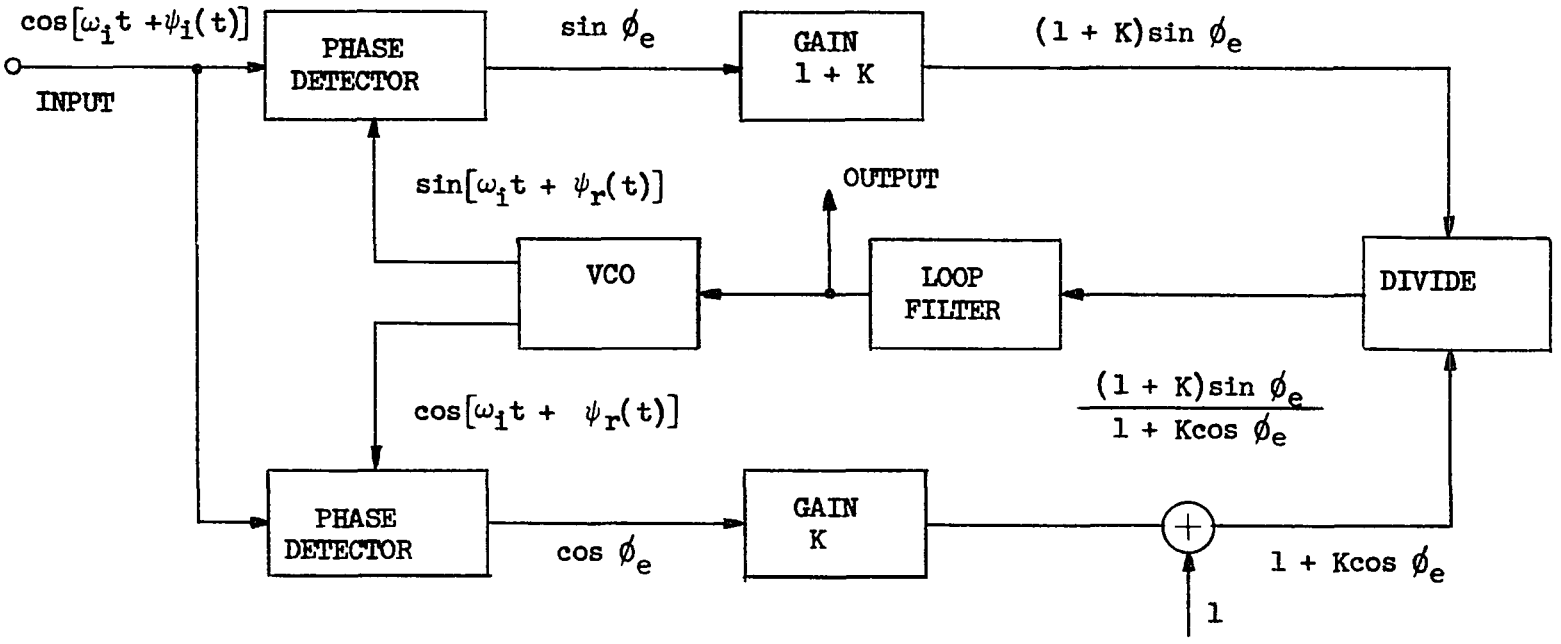

Fig. 2-3. The Tanlock PLL (from Klapper and Frankle [Ref. 2, p.256]).

$$q(\phi_e) = \frac{(1 + K)\sin\phi_e}{1 + K\cos\phi_e}, \quad 0 \leq K < 1 \qquad (2\text{-}4)$$

This function is plotted in Fig. 2-4 for a number of values of K. This system is capable of a monotonic range approaching $\pm \pi$ as K approaches unity, but with increasing non-linearity. Currently, there is some doubt as to whether the Tanlock system under modulation conditions does actually provide threshold reduction in comparison to the conventional PLL [Ref. 3 and Ref. 4] .

Of particular interest to the research undertaken in this dissertation is the ERPLD which uses phase feedback [Ref. 5] which shall be discussed in detail in the next section.

2.2.4 The ERPLD Using Phase Feedback. The ERPLD which uses phase feedback described by Acampora and Newton [Ref. 5] is shown in Fig. 2-5. This device was implemented for a single-channel FM receiver with the following parameters:

Base-band voice channel: 300-3300 Hz

Center frequency: 11.5 MHz

Deviation: $\pm$ 10 KHz peak

IF bandwidth: 35 KHz

Base-band bandwidth: 3.5 KHz

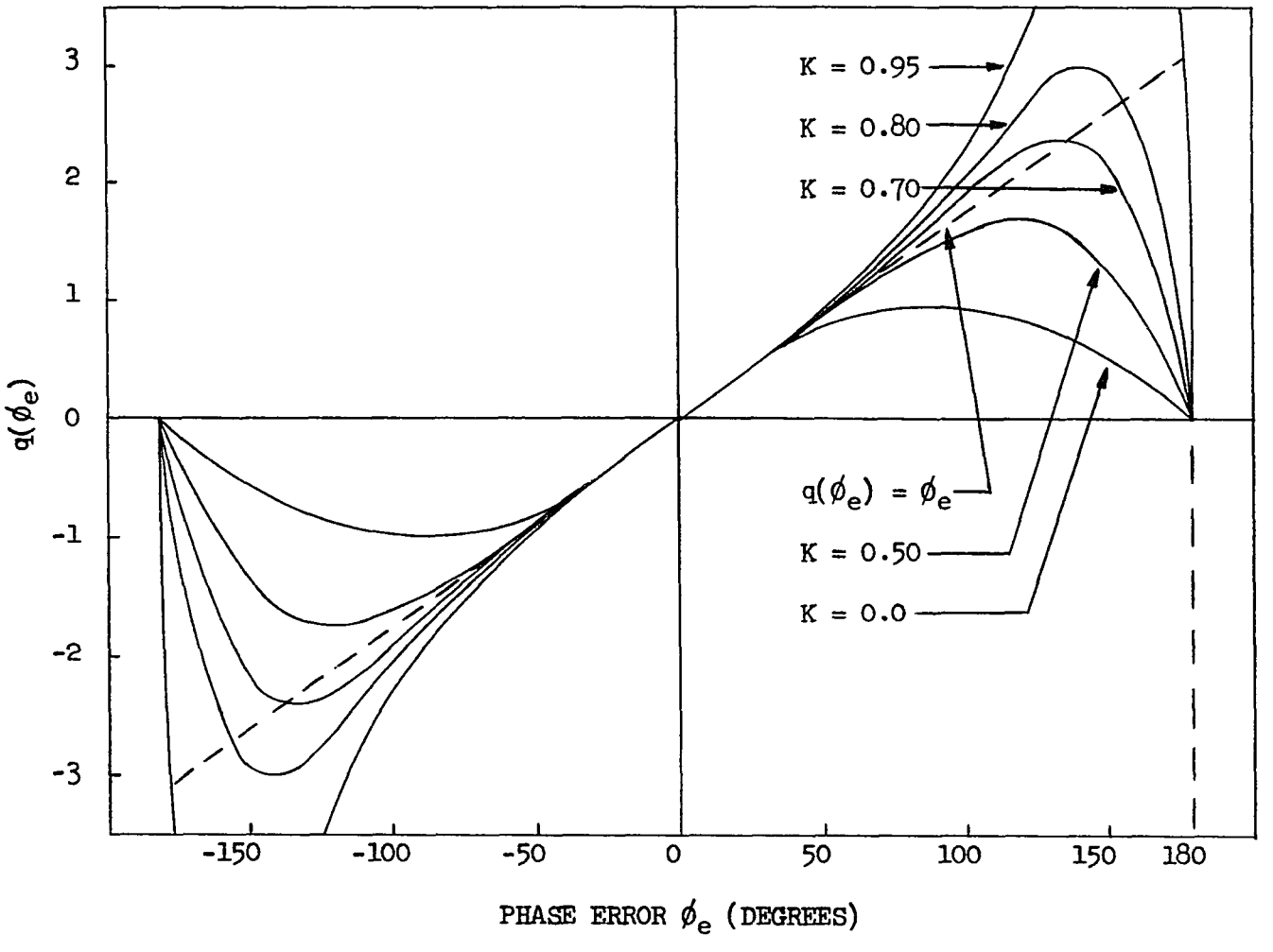

Fig. 2-4. Tanlock phase comparator characteristics (from Robinson[Ref. 3]).

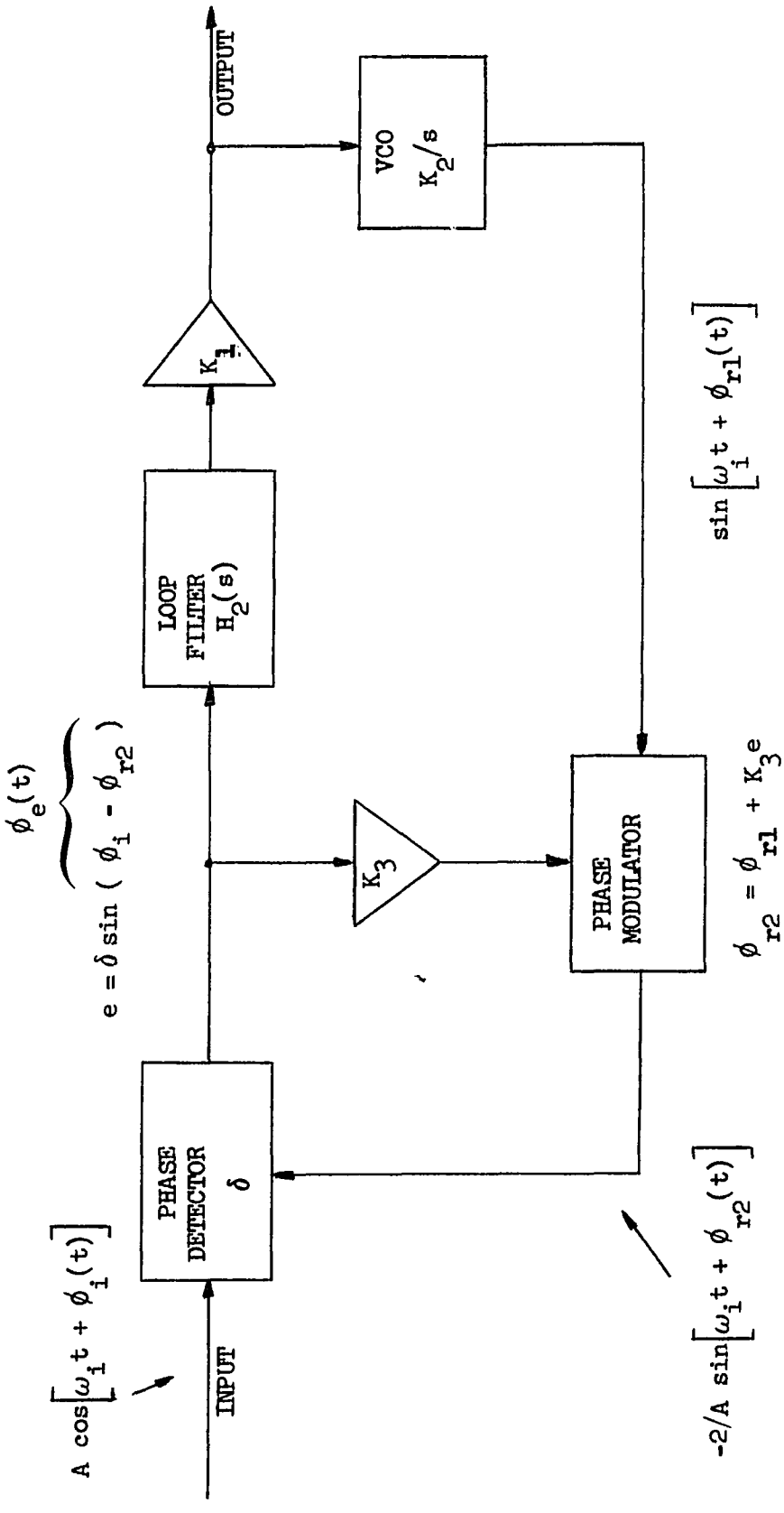

Fig. 2-5. The ERPLD using phase feedback.

The design parameters of the device included a standard second-order, type one loop filter of the form

$$H_2(s) = \frac{s/a + 1}{s/b + 1} \qquad (2\text{-}5)$$

with "a" and "b" chosen at $2.94\text{x}10^4$ and $1.88\text{x}10^3$ rad/sec respectively. The combined main loop gain was set at $4.7\text{x}10^5 \text{sec}^{-1}$, and the product of the phase-detector and phase-modulator sensitivities δK_3 was adjusted to unity. The threshold performance of the device was determined for a 1KHz test-tone in the voice channel. The results indicated a 3dB threshold reduction over the conventional PLL [Ref. 5, p. 591] .

It is of interest to determine the response characteristic for the extended-range phase detector shown in Fig. 2-6. From this figure, the characteristic equation of the phase feedback phase detector in the absence of noise is given by

$$e = \delta \sin(\psi - K_3 e) \qquad (2\text{-}6)$$

where

$$\psi = \phi_i(t) - \phi_{r_1}(t) \qquad (2\text{-}7)$$

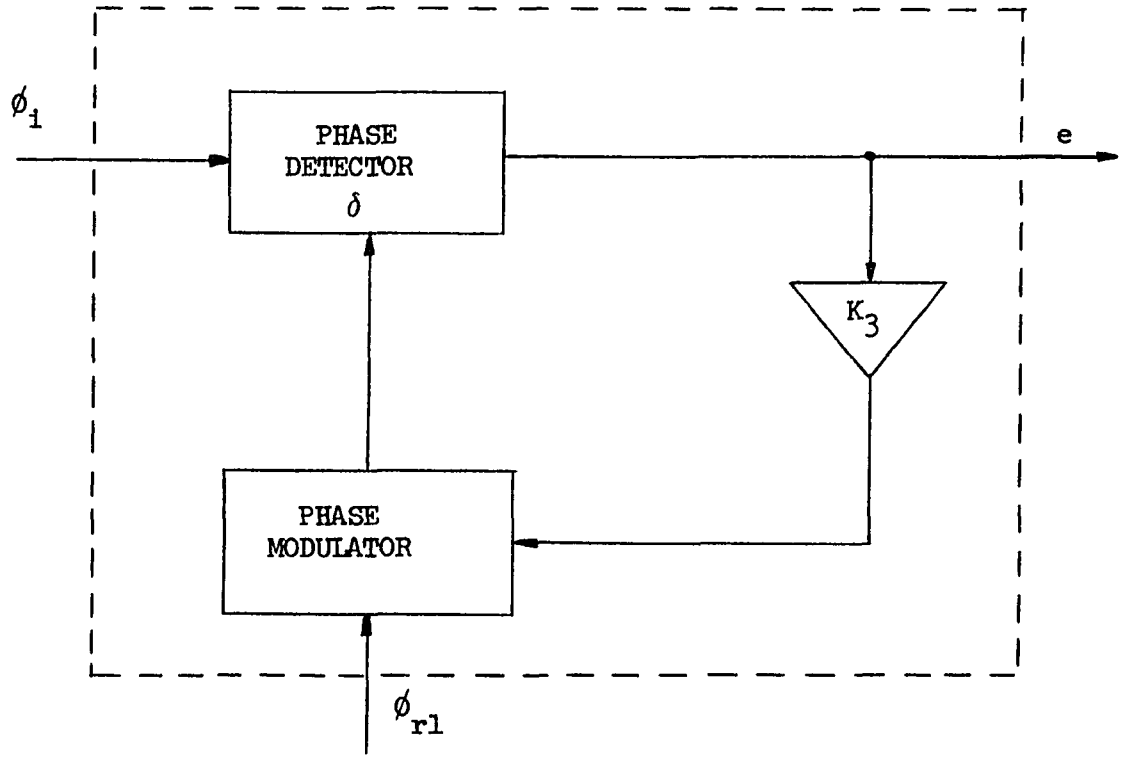

Fig. 2-6. Block diagram of the extended-range phase detector.

It is convenient to normalize Eq. 2-6 by letting $e_n = e/\delta$ resulting in

$$e_n = \sin(\psi - \alpha e_n) \tag{2-8}$$

where

$$\alpha = K_3 \delta \tag{2-9}$$

Fig. 2-7 shows a plot of Eq. 2-8 for a number of values of α. For $\alpha = 0$, the phase detector reverts back to a purely sinusoidal characteristic as expected. As α is increased, the extension of the monotonic range is readily apparent. It is significant to note that maximum monotonic range extension for which the characteristic is single-valued is $\alpha = 1.0$ which results in a monotonic range of

$$-(\pi/2 + 1) \leq \psi \leq (\pi/2 + 1) \tag{2-10}$$

The transition of the characteristic from a single-valued to a multi-valued function as α exceeds unity will take on added significance when the acquisition and tracking behavior of ERPLD with phase feedback and the generalized second-order PLL are discussed in Chapter 5. The improved performance of this system has been explained by the increased monotonic range of the phase

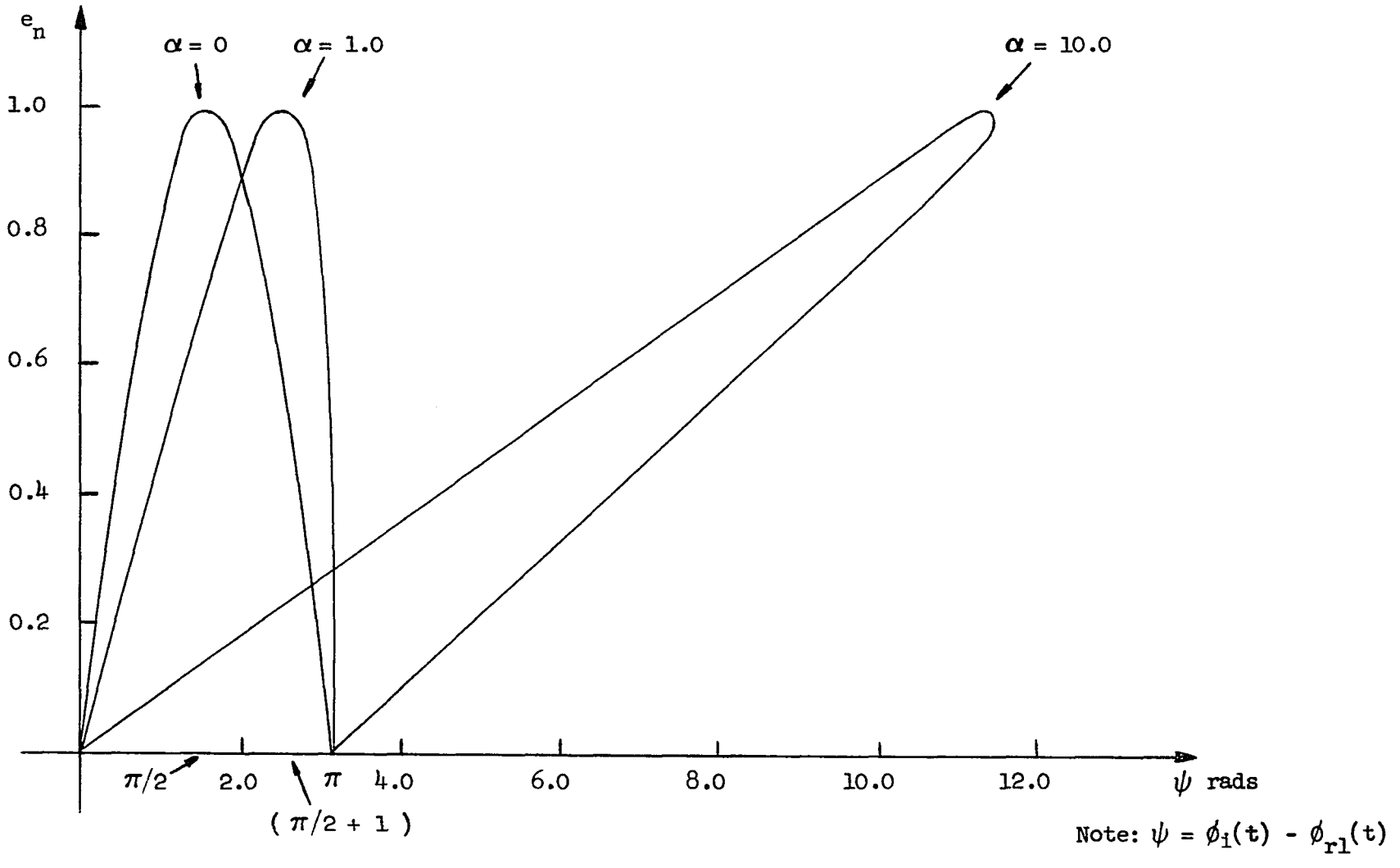

Fig. 2-7. Normalized response characteristic of the extended-range phase detector using phase feedback.

detector beyond $\pm \pi/2$. This explanation is correct for the case of no noise operation. However, under operation with noise a more extensive analysis is necessary. An analysis by Klapper and Veiga [Ref. 6] of the ERPLD with phase feedback which includes the effects of noise has shown the device to indeed be capable of a threshold significantly below that of the conventional PLL. In addition, the analysis showed the performance of this ERPLD to be critically dependent on the predetection bandwidth Bp. Specifically, the threshold reduction of the Acampora and Newton ERPLD with respect to the conventional PLL is predicted only for $B_p/a < 2.75$ [Ref. 6]. The reason for this dependence on predetection bandwidth will become apparent shortly.

An alternate way of viewing the ERPLD with phase feedback is the "equivalent filter approach" [Ref. 2, p. 260]. This analysis begins with the formulation of the loop differential equation of Fig. 2-5 which results in

$$\dot{\phi}_e(t) = \dot{\phi}_i(t) - K_1 K_2 \delta F(P) \sin\phi_e \qquad (2\text{-}11)$$

where

$$\phi_e(t) = \phi_i(t) - \phi_{r2}(t) \qquad (2\text{-}12)$$

and

$$F(p) = \left[H_2(p) + \frac{K_3}{K_1 K_2} \cdot P \right] \qquad (2\text{-}13)$$

Eq. 2-11 is identical in form to the loop differential equation of the conventional PLL, except for the difference in the filter function F(p). Substitution of $H_2(s)$ from Eq. 2-5 into Eq. 2-13 yields

$$F(s) = \frac{s^2\left(\frac{K_3}{K_1 K_2 b}\right) + s\left(\frac{1}{a} + \frac{K_3}{K_1 K_2}\right) + 1}{\frac{s}{b} + 1} \qquad (2\text{-}14)$$

The equivalent filter realization of the ERPLD with phase feedback is thus seen to be a second-order PLL in which the loop filter F(s) contains a pair of complex zeros. This is in contrast to the conventional design of the PLL which utilizes a filter having a simple zero on the negative real axis. Eq. 2-14 can be put into more convenient form by first noting that the main loop gain in Fig 2-5 can be expressed as

$$K = K_1 K_2 \delta \qquad (2\text{-}15)$$

Substitution of Eq. 2-15 and the auxiliary loop gain expression of Eq. 2-9 into Eq. 2-14 yields

$$F(s) = \frac{s^2\left(\frac{\alpha}{Kb}\right) + s\left(\frac{1}{a} + \frac{\alpha}{K}\right) + 1}{\frac{s}{b} + 1} \qquad (2\text{-}16)$$

It is of interest to investigate some additional properties of this "equivalent filter" ERPLD. Figs. 2-8 and 2-9 show the closed-loop magnitude response of the equivalent filter ERPLD for α over a range of 0.0 to 10.0 with the remaining parameters those of Acampora and Newton [Ref. 5] . Note that for $\alpha = 0$ the system reverts to a conventional second-order, type one PLL. For $\alpha > 0$ it is significant to note that the closed-loop magnitude response does not fall off to zero as the frequency becomes unbounded as is the case for the conventional PLL. This theoretically implies an "infinite" noise bandwidth and in essence explains the critical dependence of the response on the predetection bandwidth as discussed earlier, since the predetection noise bandwidth limits the performance of the device. On the other hand, it shows a reduction in the peak of the response with α. Fig 2-10 shows the closed-loop phase response of the equivalent filter ERPLD for α over a range of 0.0 to 10.0. For $\alpha = 0$, the system again reverts to a conventional second-order, type one PLL with the phase angle starting at 0°

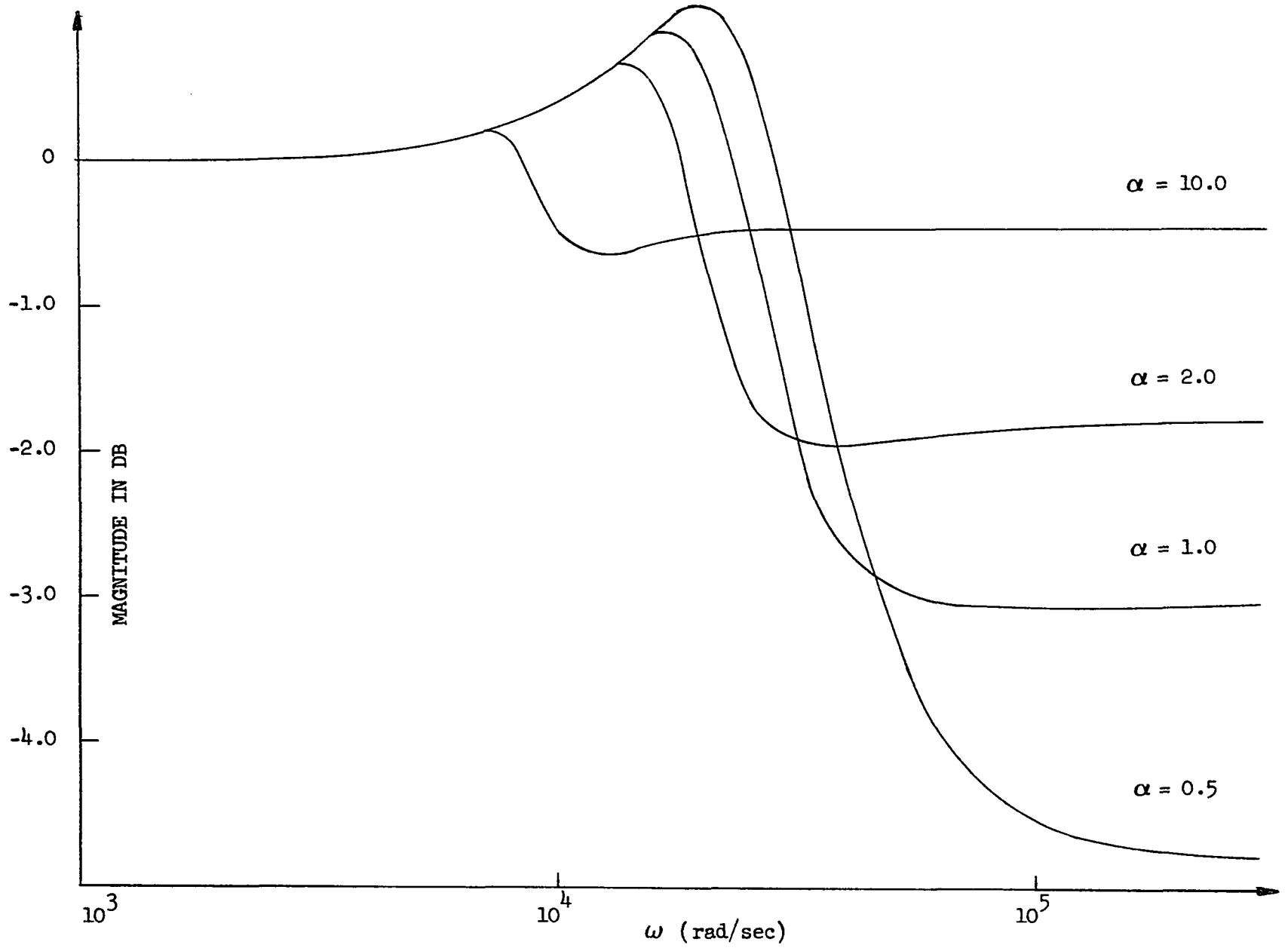

Fig. 2-8. Closed-loop magnitude response of the equivalent filter ERPLD (α = 0.5,1.0,2.0 and 10.0).

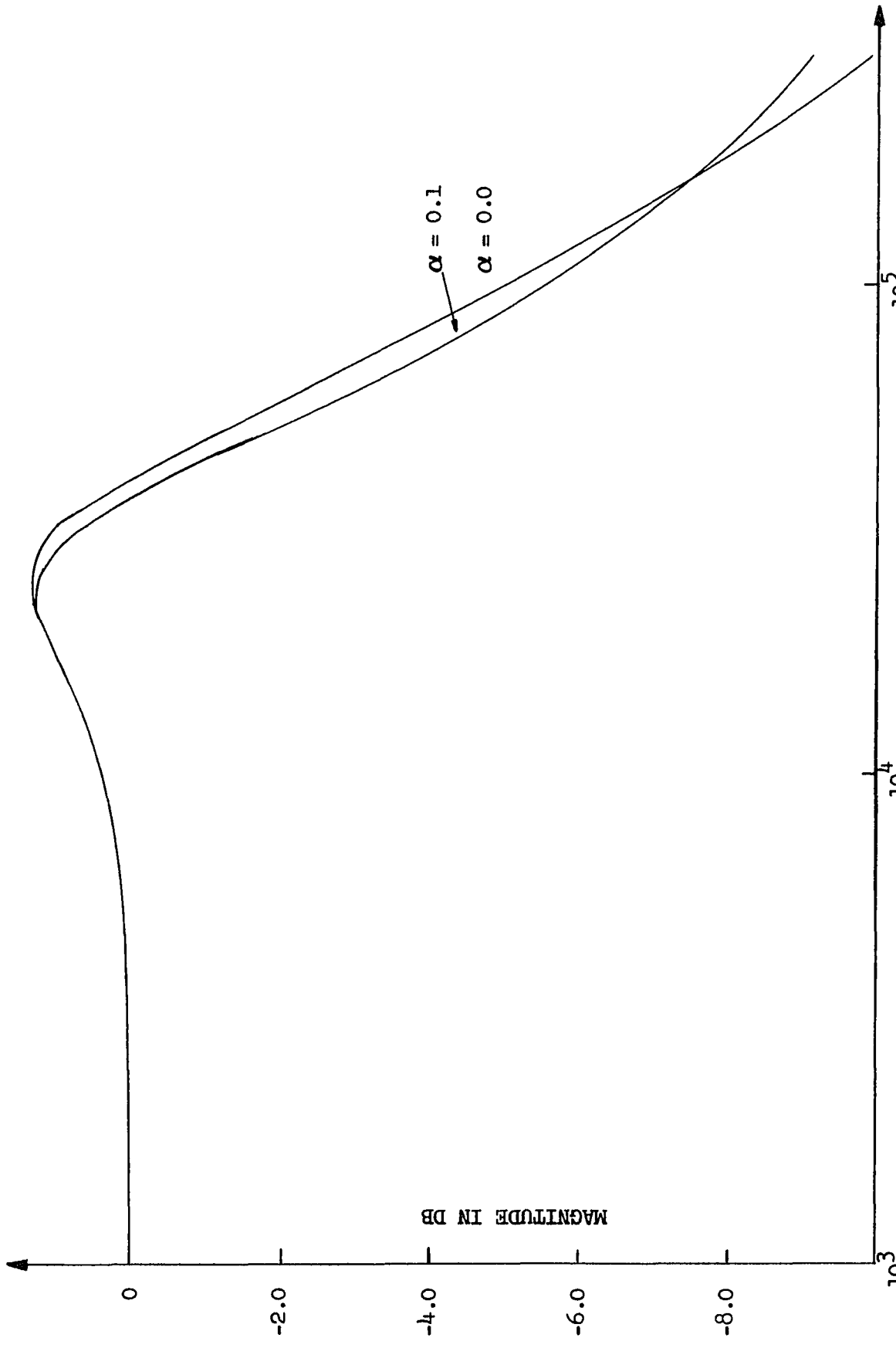

Fig. 2-9. Closed-loop magnitude response of the equivalent filter EKPID (α = 0.0 and 0.1).

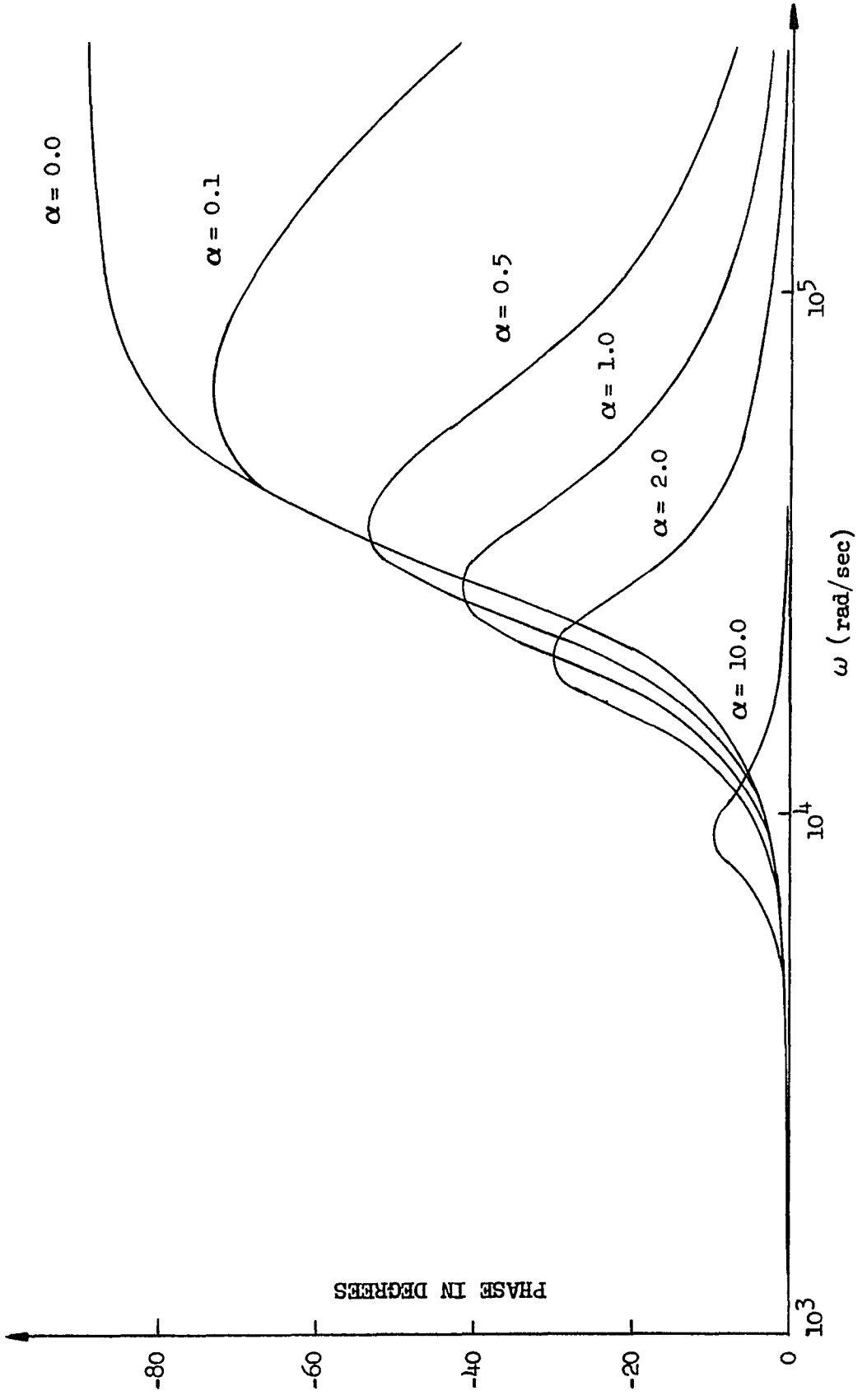

Fig. 2-10. Closed-loop phase angle response of the equivalent filter ERPID.

at DC and approaching -90° as the frequency becomes unbounded. For $\alpha>0$ the phase response changes markedly with the phase angle starting at 0° at DC but then peaking and again approaching 0° as the frequency becomes unbounded. Furthermore, as α is increased, the phase shift peak diminishes. Recall that in the Acampora and Newton case [Ref. 5] $\alpha = 1.0$. The computer programs used to generate the magnitude and phase response curves of the equivalent filter ERPLD are given in Appendix A.

Returning to the equivalent filter function of Eq. 2-16, it is noted that the coefficients of the various terms are not independent but rather interdependent. By making the coefficients independent it becomes a filter for what may be termed a "generalized second-order PLL."

2.3 The Generalized Second-Order PLL.

As discussed in the preceding section, the equivalent filter function of Eq. 2-16 leads directly to the generalized second-order filter function given by

$$F(s) = \frac{s^2/\beta + s/\gamma + 1}{s/b + 1} \qquad (2\text{-}17)$$

where the coefficients are now independent design parameters. Note that the response curves of Figs 2-8 through 2-10 are applicable to the generalized second-order PLL under the transformation

$$\left.\begin{aligned} \beta &= \frac{Kb}{\alpha} \\ \gamma &= \frac{1}{\frac{\alpha}{K} + \frac{1}{a}} \end{aligned}\right\} \qquad (2\text{-}18)$$

This generalized second-order PLL in which the loop filter contains a pair of complex zeros has been heretofore unexplored. The investigation and optimum design of this device forms the basis for this dissertation.

Fig 2-11 shows the root locus plot for the generalized second-order, type one PLL, using the equivalent Acampora and Newton parameters [Ref. 5] based on Eq. 2-18 and given by

$$\begin{aligned} \beta &= 8.836 \times 10^{8} \quad (\text{rad/sec})^2 \\ \gamma &= 2.767 \times 10^{4} \quad (\text{rad/sec}) \\ b &= 1.88 \times 10^{3} \quad (\text{rad/sec}) \\ K &= 4.7 \times 10^{5} \quad (\text{sec}^{-1}) \end{aligned}$$

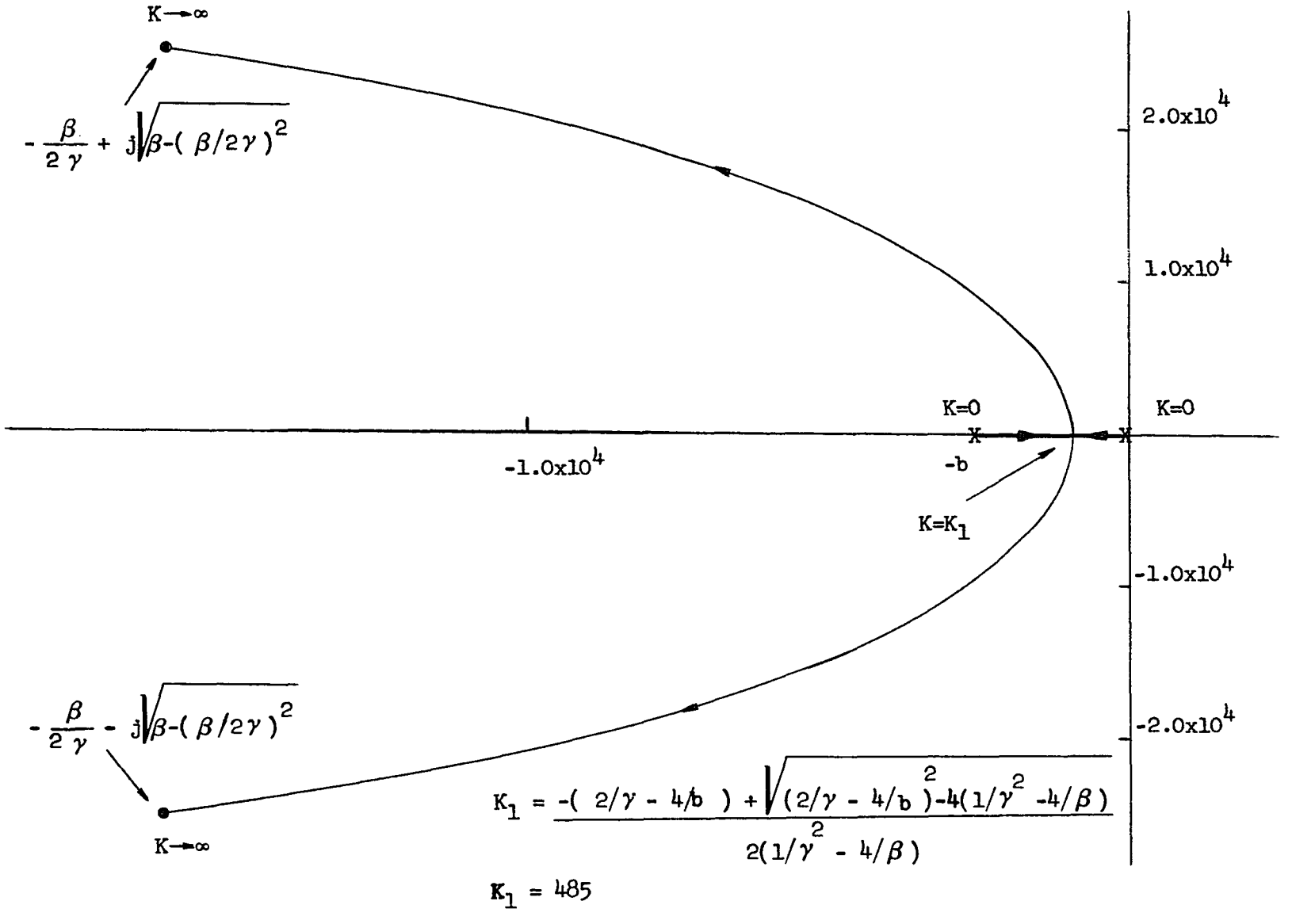

Fig. 2-11. Root locus for the generalized second-order, type one PLL (using Acampora and Newton parameters [Ref. 5]).

The figure is markedly different from that of the conventional second-order, type one PLL shown in Fig. 1-4, but retains the characteristic of being unconditionally stable. The computer program used to generate this root locus is given in Appendix A.

Fig. 2-12 shows a comparison of the asymptotic open loop amplitude responses for the conventional and generalized second-order, type one PLL. Again note that the amplitude response in the generalized PLL case does not drop off to zero with increasing frequency as it does in the conventional PLL case.

As a final item to be discussed, prior to the detailed analysis and optimum design of the generalized second-order PLL given in the subsequent chapters, consider a comparison of the design criterion for the equivalent filter ERPLD and the generalized second-order PLL. The question arises as to whether or not all of the possible designs of the generalized second-order PLL can be achieved with the equivalent filter ERPLD. First, note that there are four design parameters α, K, a and b for the equivalent filter ERPLD and the loop filter function is given by Eq. 2-16. Similarly, for the generalized second-order PLL there are four design parameters β , γ , b and K and its loop filter function is given by Eq. 2-17. In the generalized second-order PLL K is of course the loop gain and the remaining three parameters are those associated with the filter

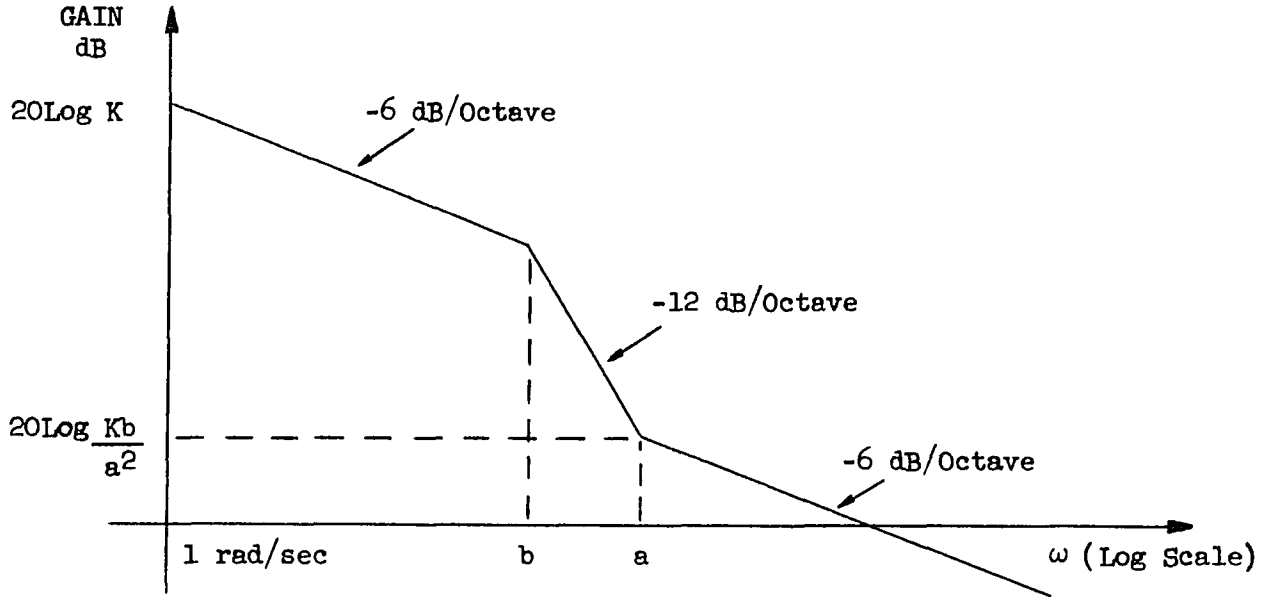

(a)

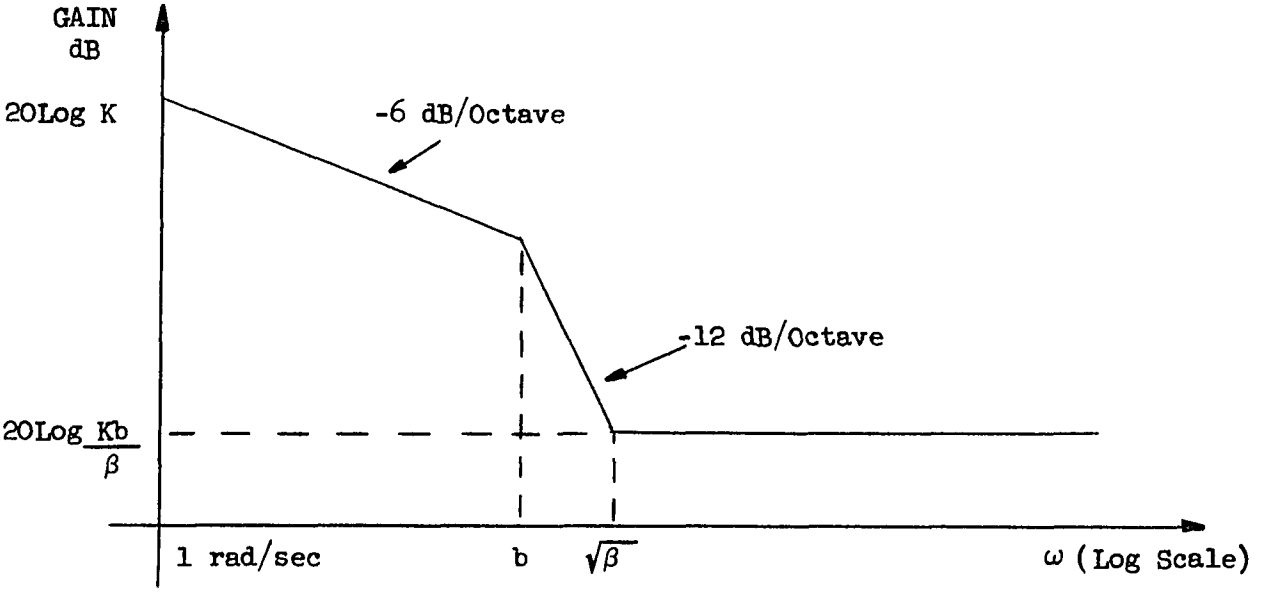

(b)

Fig. 2-12. Open-loop amplitude response (asymptotic). (a) Conventional second-order, type one PLL; (b) Generalized second-order, type one PLL (In conventional design $20 \log \frac{Kb}{a^2} = 20 \log \frac{Kb}{\beta} = 0$).

design which may be chosen independently. In the equivalent filter ERPLD K is again the loop gain but it also appears in the first two terms of the numerator in Eq. 2-16. The parameter b can be varied to adjust the coefficient in the first term of the denominator of Eq. 2-16 to a desired value. In the first term of the numerator of Eq. 2-16 even with K and b fixed α may be varied to achieve the desired co efficient value. This leaves only the second numerator term in Eq. 2-16 to be investigated. Even though the parameter "a" in this term can be varied independently at this point, the additive α/K factor does not permit the coefficient in the second numerator term of Eq. 2-16 to be independently adjusted. Strictly speaking then, the equivalent filter ERPLD cannot achieve all of the possible designs of the generalized second-order PLL. From a practical point of view, however, the picture changes. Consider, for example, the Acampora and Newton design [Ref. 5]. For those parameters, it is found that $1/a = 3.401 \times 10^{-5}$ and $\alpha/K = 2.128 \times 10^{-6}$ Thus in a typical design 1/a is more than an order of magnitude greater than α/K and so the second numerator term in Eq. 2-16 can also, for all intents and purposes, be varied independently.

References - Chapter 2

1. J. T. Frankle, "Threshold Performance of Analog FM Demodulators," RCA Review, vol. 27, No. 4, pp. 521-562, December 1966.

2. J. Klapper and J. Frankle, Phase-Locked and Frequency-Feedback Systems: Principles and Techniques, Academic Press, New York, 1972.

3. L. M. Robinson, "Tanlock: A Phase Lock Loop of Extended Tracking Capability," Proc. Nat. Conf. Military Electron., Los Angeles, California, pp. 396-421, February 1962.

4. J. J. Uhran and J. C. Lindenlaub, "Effects of a Class of Phase Comparators on the Threshold and Lock Range of Phase Lock Loop Systems," Int. Conf. Commun. 3rd, Minneapolis, Minnesota, June 1967; "Experimental Results for Phase-Lock Loop Systems Having a Modified nth-order Tanlock Phase Detector," IEEE Trans., COMM-16, No. 6, pp. 787-795, 1968.

5. A. Acampora and A. Newton, "Use of Phase Subtraction to Extend the Range of a Phase-Locked Demodulator," RCA Review, vol. 27, No. 3, pp. 577-599, December 1966.

6. J. Klapper and G. M. Veiga, "Threshold Performance of a PLL with Phase Feedback," Proc. Allerton Conf. on Circuit and System Theory, Monticello, Illinois, October 1971.

CHAPTER III

OPTIMUM DESIGN OF THE GENERALIZED SECOND-ORDER PHASE-LOCKED LOOP

3.1 Introduction.

In Chapter 2, the equivalent filter realization of the ERPLD was shown to lead to the generalized second-order PLL in which the loop filter contained complex zeros. In this chapter a method for determining an optimum design for the generalized second-order PLL for a practical class of input signals is developed.

3.2 Determination of Threshold Carrier-to-Noise Ratio (CNR).

3.2.1 General Description. The input modulation to a PLL tends to create a phase-error component which increases the total loop phase error both on an instantaneous and mean-square basis. For the linear model of the PLL with the noise and signal statistically independent, the modulation-induced phase error component $\phi_{es}(t)$ may be considered as an independent additive term which linearly increases the total mean-square phase error $\overline{\phi_e^2}(t)$. For the class of Gaussian noise type modulations including single-channel speech (FM), FDM-FM and FDM-PM, the modulation-induced phase error is Gaussian. This is also essentially true of the above-threshold noise-induced phase error. The total phase error thus has the same statistics with and without modulation, with the modulation

basically representing an increase in $\overline{\phi_e^2(t)}$. The threshold criterion for a PLL operating in the presence of Gaussian type modulations can be indicated as

$$\overline{\phi_{rn}^2(t)} + \overline{\phi_{es}^2(t)} = \overline{\phi_e^2(t)} \tag{3-1}$$

with $\overline{\phi_e^2(t)}$ set equal to the mean-square phase error at threshold [Ref 1, p. 136 and Ref. 2] . For modulations other than Gaussian, Eq. 3-1 generally becomes less realistic and each case should be treated on an individual basis. For example, Klapper and Frankle [Ref. 1, p. 136-137] have considered the threshold criterion for the test-tone modulation case.

For the case where the input to the PLL contains white Gaussian bandpass noise N(t) of power spectral density (PSD) η , the equivalent noise generator as discussed in Chapter 1 is also Gaussian, having the low-pass equivalent PSD of N(t) with height $2\eta/A^2$. Under these conditions, the noise-induced phase error component may be expressed as

$$\overline{\phi_{rn}^2(t)} = \frac{2\eta}{A^2} \int_0^{B_p/2} |H(j\omega)|^2 \, df \tag{3-2}$$

where it is recalled that B_p is the predetection bandwidth and H(s) is the closed-loop transfer function of the PLL. Referring to Fig. 3-1

$$H(s) = \frac{K \; F(s)}{s + K \; F(s)} \tag{3-3}$$

where

$$K = K_1 K_2 \delta \tag{3-4}$$

and the loop filter for the generalized second-order PLL case is given by

$$F(s) = \frac{s^2/\beta + s/\gamma + 1}{s/b + 1} \tag{3-5}$$

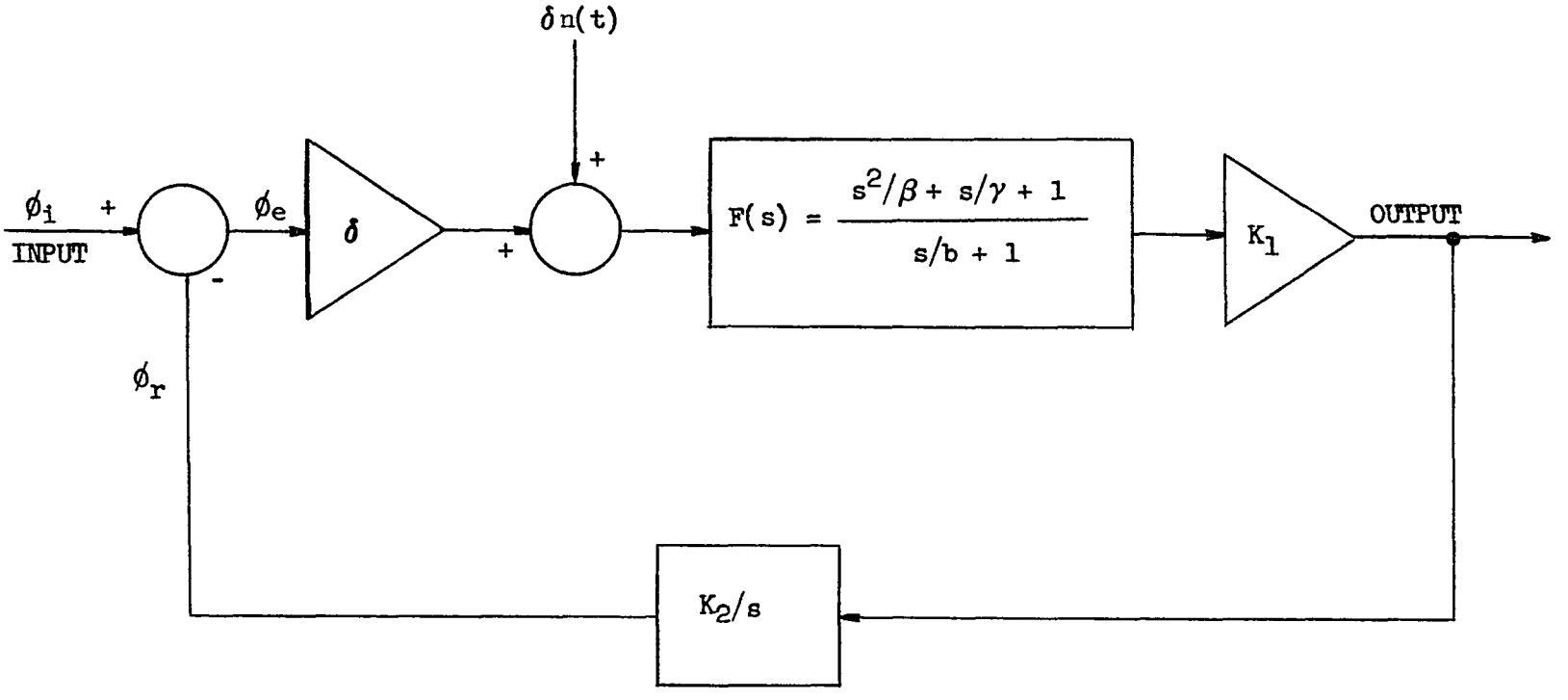

Fig. 3-1. Linear equivalent model of the generalized second-order PLL.

The expression for the signal-induced phase error component $\overline{\phi_{es}^2(t)}$ is dependent upon the type of modulation employed and may be expressed as

(3-6)

$$\overline{\phi_{es}^2(t)} = \int_0^{f_b} W_{\phi_i}(f) \left| 1 - H(j\omega) \right|^2 df$$

where W_{ϕ_i} is the one-sided PSD of the input phase modulation across the baseband range. The total mean-square phase error can then be expressed as

(3-7)

$$\overline{\phi_e^2(t)} = \int_0^{f_b} W_{\phi_i}(f) \left| 1 - H(j\omega) \right|^2 df + \frac{2\eta}{A^2} \int_0^{B_p/2} \left| H(j\omega) \right|^2 df$$

The threshold CNR with the noise measured in the IF bandwidth is given by

$$\left.\begin{aligned} (\mathrm{CNR}_{\mathrm{IF}})_{\mathrm{TH}} &= \left(\frac{A^2/2}{B_p \eta}\right)_{\mathrm{TH}} \\ \text{or} \\ \left(\frac{2\eta}{A^2}\right)_{\mathrm{TH}} &= \frac{1}{B_p\,(\mathrm{CNR}_{\mathrm{IF}})_{\mathrm{TH}}} \end{aligned}\right\} \qquad (3\text{-}8)$$

Defining the total mean-square error at threshold as

$$\left[\overline{\phi_e^2(t)}\right]_{\mathrm{TH}} \equiv \nu \qquad (3\text{-}9)$$

and substituting Eqs. 3-8 and 3-9 into Eq. 3-7 yields

$$(CNR_{IF})_{TH} = \frac{\int_0^{B_p/2} |H(j\omega)|^2 \, df}{B_p \left[\nu - \int_0^{f_b} W_{\phi_i}(f) \, |1 - H(j\omega)|^2 \, df \right]} \qquad (3\text{-}10)$$

In the above expression, with the previous assumptions that have been made, the only parameter which has any uncertainty associated with it is ν . Previous experimental and analytical evidence with conventional PLLs has indicated a range of values of ν between 0.20 and 0.25 as the region where the cycle slipping rate is such that the output signal-to-noise ratio is 1dB below that predicted by the above threshold formulation. The value of $\nu = 0.25$ has been derived exactly for the first-order PLL [Ref. 3] and is widely used in literature as the threshold criterion for the second-order PLL [Ref. 1, pp. 138-147, Ref. 2 and Ref. 4.] In this chapter, for the analysis which follows, a value of $\nu = 0.25$ is generally assumed for the generalized second-order PLL. In the subsequent chapter, a method is presented for determining ν by computer simulation of the non-linear model of the generalized second-order PLL.

This procedure indicates that 0.25 is a reasonable value to use for ν .

3.2.2 Voice Modulation Case. The first case to be considered is that of a single-channel FM speech signal. Before proceeding, it is necessary to settle on a suitable voice channel model. Previous analyses [Ref. 1, p. 339 and Ref. 2] have indicated success in using a speech channel which is modeled as follows:

(1) It is random with Gaussian statistics.

(2) It has a PSD that is nonzero between the frequencies fa and fb only, and within this band, the PSD varies inversely with f^2 .

This model may be represented by

$$W_{\phi_i} = \frac{\eta_m}{\omega^4} \qquad f_a \le f \le f_b \qquad (3\text{-}11)$$

$$= 0 \qquad \text{elsewhere}$$

where W_{ϕ_i} is the one-sided PSD of the input "phase" modulation and η_m is a modulation constant. It is convenient to reexpress η_m in terms of the mean-square frequency deviation $(\Delta\omega_{rms})^2$ of the signal. Recalling that multiplication by ω^2 changes the spectral density of phase to that of frequency and further, noting that

subsequent integration over the baseband gives the total power or the mean-square value, leads to the expression

(3-12)

$$(\Delta\omega_{rms})^2 = \int_{f_a}^{f_b} \omega^2 W_{\phi_i} \, df$$

This results in

(3-13)

$$\eta_m = \frac{(2\pi)^2 f_a f_b (\Delta\omega_{rms})^2}{f_a - f_b}$$

From Eq. 3-10, using the single-channel FM model of Eq. 3-11, yields

(3-14)

$$(CNR_{IF})_{TH} = \frac{\int_0^{B_p/2} |H(j\omega)|^2 \, df}{B_p \left[\nu - \eta_m \int_{f_a}^{f_b} \frac{1}{\omega^4} |1 - H(j\omega)|^2 \, df \right]}$$

Next, it is desired to express the integrals in Eq. 3-14 in terms of the generalized second-order PLL parameters. From Eqs. 3-3 and 3-5, the closed-loop transfer function may be expressed as

(3-15)

$$H(s) = \frac{s^2/\beta + s/\gamma + 1}{s^2\left(\frac{1}{Kb} + \frac{1}{\beta}\right) + s\left(\frac{1}{K} + \frac{1}{\gamma}\right) + 1}$$

Therefore

(3-16)

$$H(j\omega) = \frac{\left(1 - \omega^2/\beta\right) + j\left(\omega/\gamma\right)}{\left[1 - \omega^2\left(1/Kb + 1/\beta\right)\right] + j\left[\omega\left(1/K + 1/\gamma\right)\right]}$$

and

(3-17)

$$\left|H(j\omega)\right|^2 = \frac{\left(1 - \omega^2/\beta\right)^2 + \left(\omega/\gamma\right)^2}{\left[1 - \omega^2\left(1/Kb + 1/\beta\right)\right]^2 + \left[\omega\left(1/K + 1/\gamma\right)\right]^2}$$

Reexpressing $|H(j\omega)|^2$ as a ratio of polynomials in "ω" yields

(3-18)

$$|H(j\omega)|^2 = \frac{\omega^4\left(1/\beta^2\right) + \omega^2\left(1/\gamma^2 - 2/\beta\right) + 1}{\omega^4\left(1/Kb + 1/\beta\right)^2 + \omega^2\left[\left(1/K + 1/\gamma\right)^2 - 2\left(1/Kb + 1/\beta\right)\right] + 1}$$

In a similar manner

(3-19)

$$1 - H(s) = \frac{s^2/Kb + s/K}{s^2\left(1/Kb + 1/\beta\right) + s\left(1/K + 1/\gamma\right) + 1}$$

Therefore

(3-20)

$$1 - H(j\omega) =$$

$$\frac{\left(-\omega^2/Kb\right) + j\left(\omega/K\right)}{\left[1 - \omega^2\left(1/Kb + 1/\beta\right)\right] + j\left[\omega\left(1/K + 1/\gamma\right)\right]}$$

Expressing $|1 - H(j\omega)|^2$ as a ratio of polynomials in ω yields

(3-21)

$$|1 - H(j\omega)|^2 =$$

$$\frac{\omega^4\left(1/Kb\right)^2 + \omega^2\left(1/K\right)^2}{\omega^4\left(1/Kb + 1/\beta\right)^2 + \omega^2\left[\left(1/K + 1/\gamma\right)^2 - 2\left(1/Kb + 1/\beta\right)\right] + 1}$$

For convenience, the following definitions are made in Eqs. 3-18 and 3-21

(3-22)

$$A \equiv 1/\beta^2$$

$$B \equiv 1/\gamma^2 - 2/\beta$$

$$C \equiv \left(1/Kb + 1/\beta\right)^2$$

$$D \equiv \left(1/K + 1/\gamma\right)^2 - 2\left(1/Kb + 1/\beta\right)$$

$$A' \equiv \left(1/Kb\right)^2$$

$$B' \equiv 1/K^2$$

At this point it is well to reflect back to the original ERPLD configuration of Acampora and Newton [Ref. 5] discussed in Chapter 2 and realize again that the generalized second-order PLL reduces to the ERPLD under the conditions

(3-23)

$$\left.\begin{aligned} \beta &= \frac{K\,b}{\alpha} \\ \gamma &= \frac{1}{\frac{\alpha}{K} + \frac{1}{a}} \end{aligned}\right\}$$

The next task is the solution of the integrals in the numerator and denominator of Eq. 3-14. From Eqs. 3-18 and 3-22, the numerator of Eq. 3-14 may be expressed as

(3-24)

$$\int_0^{B_p/2} |H(j\omega)|^2 \, df = \frac{1}{2\pi} \int_0^{\pi B_p} \frac{A\omega^4 + B\omega^2 + 1}{C\omega^4 + D\omega^2 + 1} \, d\omega$$

Similarly the integral in the denominator of Eq. 3-14 may be expressed as

(3-25)

$$\int_{f_a}^{f_b} \frac{1}{\omega^4} \left| 1 - H(j\omega) \right|^2 \, df =$$

$$\frac{1}{2\pi} \int_{\omega_a}^{\omega_b} \frac{1}{\omega^4} \cdot \frac{A'\omega^4 + B'\omega^2}{C\,\omega^4 + D\,\omega^2 + 1} \, d\omega$$

Solution of the integrals in Eqs. 3-24 and 3-25 can be obtained, of course, by numerical integration techniques on the digital computer, and indeed this method will be used later in the chapter as a check on the alternate means of solution. It is desired, however, that a closed form solution of these integrals be obtained to facilitate the optimum design procedure for the generalized second-order PLL. As will be described in detail later in this chapter, the optimization algorithm requires evaluation of Eq. 3-14 during each iteration. The availability of a closed-form of Eq. 3-14 eliminates the necessity of performing a numerical integration evaluation of Eq. 3-14 during each iteration and thus greatly reduces the CPU time needed to determine

the optimum design. Indeed, as will be detailed later in this chapter, the use of the closed-form solution over numerical integration techniques in the optimization algorithm was shown to reduce the CPU time typically by a factor of 500 to 1 or more. In general, without having the closed-form solution at hand, the CPU time necessary to perform an optimization procedure would be prohibitive.

It should be noted that unlike definite integrals of the form

(3-26)

$$I = \int_0^\infty \frac{a_{n-1}\omega^{n-1} + \cdots\cdots + a_o}{b_n \omega^n + \cdots\cdots + b_o} df$$

which are encountered often in control theory applications and in PLL theory for determining equivalent noise bandwidths, and for

which tabulated results are readily available [Ref. 1, p. 21 and Ref. 6, p. 135] , solutions to integrals of the form of Eqs. 3-24 and 3-25 which have definite limits are considerably more complicated. The closed-form solutions of Eqs. 3-24 and 3-25 can fall into a number of different cases as dictated by the roots of the polynomial $C\omega^4 + D\omega^2 + 1$ which appears in the denominator of each of the integrals. Because the polynomial contains only even powers of ω , it follows directly that

(3-27)

$$\omega^2 = -\frac{D}{2C} \pm \sqrt{\left(\frac{D}{2C}\right)^2 - \frac{1}{C}}$$

From Eq. 3-22 it is apparent that C is always positive whereas D can be either positive or negative. Consider first the situation where the roots of Eq. 3-27 are complex. This leads to the first two cases to be considered. These are defined as follows

(3-28)

$$\left.\begin{array}{l} \dfrac{D^2}{4C} < 1 \\ \text{and} \\ D < 0 \end{array}\right\} \quad \text{CASE I}$$

(3-29)

$$\left.\begin{array}{l} \dfrac{D^2}{4C} < 1 \\ \text{and} \\ D > 0 \end{array}\right\} \quad \text{CASE II}$$

Detailed solutions of Eqs. 3-24 and 3-25 in closed form for these two cases are given in Appendix B with the results given as follows

(3-30)

$$\int_0^{B_p/2} |H(j\omega)|^2 \, df =$$

$$\frac{1}{2\pi C}\left\{\pi A B_p + \mathrm{Re}\left[\frac{1 - BG - A/C(\,1 - DG\,)}{J(\,G^* - G\,)} \ln\left(\frac{J - \pi B_p}{J + \pi B_p}\right)\right]\right\}$$

and

(3-31)

$$\eta_m \int_{f_a}^{f_b} \frac{1}{\omega^4} \cdot \left|1 - H(j\omega)\right|^2 \, df = \overline{\phi_{es}^2(t)} =$$

$$\frac{\omega_a \omega_b (\Delta\omega_{rms})^2}{\omega_b - \omega_a} \left\{ \frac{1}{C} Re\left[\frac{B' - A'G}{GJ\,(G - G^*)} \ln\left(\frac{\omega_b - J}{\omega_b + J} \cdot \frac{\omega_a + J}{\omega_a - J} \right) \right] \right.$$

$$\left. + \frac{B'}{CGG^*} \left(\frac{1}{\omega_a} - \frac{1}{\omega_b} \right) \right\}$$

where $\mathcal{Re}$ indicates that the real part of the bracketed term is to be taken and G and J are complex expressions given by

(3-32)

$$G = \frac{D}{2C} - j\sqrt{\frac{1}{C} - \left(\frac{D}{2C}\right)^2}$$

(3-33)

$$J = M \angle\theta$$

where

$$M = (1/C)^{1/4} \tag{3-34}$$

and

(3-35)

CASE I

$$\theta = \left\{ \frac{\tan^{-1}\left(\frac{-\sqrt{\frac{1}{C} - \left(\frac{D}{2C}\right)^2}}{\frac{D}{2C}} \right)}{2} \right\} + \pi$$

(3-36)

CASE II

$$\theta = \left\{ \frac{\tan^{-1}\left(\frac{-\sqrt{\frac{1}{C} - \left(\frac{D}{2C}\right)^2}}{\frac{D}{2C}} \right)}{2} \right\} + \frac{3\pi}{2}$$

and G* is the complex conjugate of G. Furthermore, the definitions of Eqs. 3-13 and 3-22 are used. Note also, that the principal value is to be used in the arctangent function and all angles are assumed to be in radians.

Next, consider the case where the roots of Eq. 3-27 are real. This immediately leads to a third case defined as follows

(3-37)

$$\left.\begin{aligned} \frac{D^2}{4C} &> 1 \\ \text{and} \\ D &> 0 \end{aligned}\right\} \quad \text{CASE III}$$

At this point it might be thought that another case that should be considered is

(3-38)

$$\left.\begin{array}{l} \dfrac{D^2}{4C} > 1 \\ \text{and} \\ D < 0 \end{array}\right\}$$

however from Eqs. 3-38 and 3-22 for this case to exist

(3-39)

$$\frac{\left[\left(1/K + 1/\gamma\right)^2 - 2\left(1/Kb + 1/\beta\right)\right]^2}{4\left(1/Kb + 1/\beta\right)^2} > 1$$

But the other necessary condition for this case to exist, is that $D<0$ which requires that

(3-40)

$$2\left(1/Kb + 1/\beta\right) > \left(1/K + 1/\gamma\right)^2$$

It is apparent that the conditions of Eqs. 3-39 and 3-40 cannot hold simultaneously and so the case postulated by Eq. 3-38 does not exist.

Detailed solutions of Eqs. 3-24 and 3-25 in closed form for Case III are given in Appendix B with the results given as follows

(3-41)

$$\int_0^{B_p/2} |H(j\omega)|^2 \, df =$$

$$\frac{1}{2\pi C}\left\{\left[\frac{1-BR_1^2}{R_2^2-R_1^2}\left(\frac{1}{R_1}\tan^{-1}\frac{\pi B_p}{R_1}\right)+\frac{1-BR_2^2}{R_1^2-R_2^2}\left(\frac{1}{R_2}\tan^{-1}\frac{\pi B_p}{R_2}\right)\right]\right.$$

$$-\frac{A}{C}\left[\frac{1-DR_1^2}{R_2^2-R_1^2}\left(\frac{1}{R_1}\tan^{-1}\frac{\pi B_p}{R_1}\right)+\frac{1-DR_2^2}{R_1^2-R_2^2}\left(\frac{1}{R_2}\tan^{-1}\frac{\pi B_p}{R_2}\right)\right]$$

$$\left.+A\pi B_p\right\}$$

and

(3-42)

$$\overline{\phi_{es}^{2}(t)} = \eta_m \int_{f_a}^{f_b} \frac{1}{\omega^4} \cdot |1 - H(j\omega)|^2 \, df =$$

$$\frac{\omega_a \omega_b (\Delta\omega_{rms})^2}{\omega_b - \omega_a} \left\{ \frac{A'}{C(R_1^2 - R_2^2)} \left[\frac{1}{R_2} \left(\tan^{-1} \frac{\omega_b}{R_2} - \tan^{-1} \frac{\omega_a}{R_2} \right) \right.\right.$$

$$\left. + \frac{1}{R_1} \left(\tan^{-1} \frac{\omega_a}{R_1} - \tan^{-1} \frac{\omega_b}{R_1} \right) \right] + \frac{B'}{C(R_1^2 - R_2^2)} \left[\frac{1}{R_1^3} \left(\tan^{-1} \frac{\omega_b}{R_1} \right.\right.$$

$$\left. \left. - \tan^{-1} \frac{\omega_a}{R_1} \right) + \frac{1}{R_2^3} \left(\tan^{-1} \frac{\omega_a}{R_2} - \tan^{-1} \frac{\omega_b}{R_2} \right) \right]$$

$$\left. + \frac{B'}{C R_1^2 R_2^2} \left(\frac{1}{\omega_a} - \frac{1}{\omega_b} \right) \right\}$$

where

(3-43)

$$\left.\begin{aligned} R_1 &\equiv \frac{D}{2C} + \sqrt{\left(\frac{D}{2C}\right)^2 - \frac{1}{C}} \\ R_2 &\equiv \frac{D}{2C} - \sqrt{\left(\frac{D}{2C}\right)^2 - \frac{1}{C}} \end{aligned}\right\}$$

The final case to be considered is that where the roots of Eq. 3-27 are real and repeated. This occurs when the following condition holds

(3-44)

$$\frac{D^2}{4C} = 1$$

causing the radical in Eq. 3-27 to become zero. Obviously, unlike the previous three cases, this condition is highly restrictive and should be considered a "special" case. From Eqs. 3-22 and 3-44, it follows that for this case to hold

(3-45)

$$\frac{\left[\left(1/K + 1/\gamma \right)^2 - 2\left(1/Kb + 1/\beta \right) \right]^2}{4\left(1/Kb + 1/\beta \right)^2} = 1$$

or

$$\left(1/K + 1/\gamma \right)^2 = 4 \left(1/Kb + 1/\beta \right)$$

From Eq. 3-45 it is seen that for the case under consideration, $D > 0$. Summarizing, the fourth and final case to be considered is given by

$$\left.\begin{aligned} \frac{D^2}{4C} &= 1 \\ \text{and} \qquad D &> 0 \end{aligned}\right\} \qquad \text{CASE IV} \tag{3-46}$$

Detailed solutions of Eqs. 3-24 and 3-25 in closed form for Case IV are given in Appendix B with the results given as follows

(3-47)

$$\int_0^{Bp/2} |H(j\omega)|^2 \, df =$$

$$\frac{1}{4\pi C}\left\{\left[\left(\frac{\pi Bp}{\pi^2 Bp^2 + R_0^2}\right)\left(\frac{1}{R_0^2} - B\right) + \left(\frac{1}{R_0} \tan^{-1}\frac{\pi Bp}{R_0}\right)\left(\frac{1}{R_0^2} + B\right)\right]\right.$$

$$-\frac{A}{C}\left[\left(\frac{\pi Bp}{\pi^2 Bp^2 + R_0^2}\right)\left(\frac{1}{R_0^2} - D\right) + \left(\frac{1}{R_0} \tan^{-1}\frac{\pi Bp}{R_0}\right)\left(\frac{1}{R_0^2} + D\right)\right]$$

$$\left. + 2A\pi Bp\right\}$$

and

(3-48)

$$\overline{\phi_{es}^2(t)} = \eta_m \int_{f_a}^{f_b} \frac{1}{\omega^4} \cdot |1 - H(j\omega)|^2 \, df = \frac{\omega_a \omega_b (\Delta\omega_{rms})^2}{\omega_b - \omega_a} \cdot$$

$$\left\{ \frac{A'}{2R_o^2 C} \left[\frac{\omega_b}{\omega_b^2 + R_o^2} - \frac{\omega_a}{\omega_a^2 + R_o^2} + \frac{1}{R_o} \left(\tan^{-1} \frac{\omega_b}{R_o} - \tan^{-1} \frac{\omega_a}{R_o} \right) \right] \right.$$

$$- \frac{B'}{2R_o^4 C} \left[\frac{\omega_b}{\omega_b^2 + R_o^2} - \frac{\omega_a}{\omega_a^2 + R_o^2} + \frac{3}{R_o} \left(\tan^{-1} \frac{\omega_b}{R_o} - \tan^{-1} \frac{\omega_a}{R_o} \right) \right]$$

$$\left. + \frac{B'}{R_o^4 C} \left(\frac{1}{\omega_a} - \frac{1}{\omega_b} \right) \right\}$$

where

$$R_o^2 = \frac{D}{2C} \tag{3-49}$$

At this point, it is well to reflect back to the impetus for considering the various cases that occur in the closed-form solution. In the optimum design procedure, to be discussed in detail shortly, an algorithm is used to determine a minimum for (CNRIF)TH. This algorithm involves a search technique which evaluates (CNRIF)TH during each iteration. The search can and generally does pass through more than one case before the minimum is found. If the various cases are not accounted for within the computer program, the search algorithm will stop prematurely if such a case is encountered.

In order to check the validity of the closed-form solutions of (CNRIF)TH for the various cases, a computer program was written to evaluate the integrals in Eqs. 3-24 and 3-25 by numerical integration techniques. A check was performed on each of the four cases which showed the two solutions to be in agreement to within an error of two percent or less. Even this small error is accounted for by the coarseness of the integration intervals in the numerical method, finer intervals bringing the two results into even closer agreement. The computer program used in this comparative check and additional discussion on the results are found in Appendix C.

Having determined the expression for (CNRIF)TH for the single-channel FM speech case for eventual use in the optimum design procedure, attention is next focused on another case of great interest.

3.2.3 FDM-FM Case. The next case to be considered is that of FDM-FM. Again, it is necessary to settle on a suitable model. Previous analysis [Ref. 1, p. 141 and p. 341] has indicated success in using an FDM-FM signal which is modeled as follows:

(1) It is random with Gaussian statistics.

(2) The PSD of the input "phase" modulation is nonzero between the baseband frequencies fa and fb only and is given by

(3-50)

$$W_{\phi_i} = \frac{\eta_m}{\omega^2} \quad , \qquad f_a \leq f \leq f_b$$

where again, the one-sided PSD is used and η_m is a modulation constant.

The modulation constant may be related to the mean-square frequency deviation using Eq. 3-12, resulting in

(3-51)

$$\eta_m = \frac{(\Delta \omega_{rms})^2}{f_b - f_a}$$

From Eq. 3-10, using the FDM-FM model of Eq. 3-31, yields

$$(CNR_{IF})_{TH} = \frac{\int_0^{B_p/2} |H(j\omega)|^2 \, df}{B_p\left[\nu - \eta_m \int_{f_a}^{f_b} \frac{1}{\omega^2} \cdot |1 - H(j\omega)|^2 \, df\right]} \qquad (3\text{-}52)$$

It should be noted that frequently when dealing with an FDM case, the performance is given in terms of noise power ratio (NPR) which is defined as the power ratio of signal-to-noise tested with a noise-like signal in a narrow FDM channel. In the method used here, as will be described in detail subsequently, the design is based on minimization of threshold carrier-to-noise ratio. This procedure takes into consideration the effects of the entire baseband as opposed to that of a single FDM channel.

Returning to Eq. 3-52, it is noted that the integral in the numerator has already been evaluated in closed form for all four cases in the previous section, the details of which have been presented in Appendix B. The remaining task is the evaluation of

the integral in the denominator of Eq. 3-52, i.e. $\overline{\phi_{es}^2(t)}$ (See alsoEq. 3-6), in closed form for each of the four cases. From Eqs. 3-6, 3-21, and 3-50, the signal-induced mean-square phase error component may be expressed as

(3-53)

$$\overline{\phi_{es}^2(t)} = \frac{(\Delta\omega_{rms})^2}{f_b - f_a}\int_{f_a}^{f_b} \frac{1}{\omega^2}\cdot\frac{A'\omega^4 + B'\omega^2}{C\omega^4 + D\omega^2 + 1}\,df$$

$$= \frac{(\Delta\omega_{rms})^2}{\omega_b - \omega_a}\int_{\omega_a}^{\omega_b} \frac{A'\omega^2 + B'}{C\omega^4 + D\omega^2 + 1}\,d\omega$$

where the coefficients of the integrand are defined by Eq. 3-22. A detailed solution of Eq. 3-53 in closed form for each of the four cases as defined in Eqs. 3-28, 3-29, 3-37 and 3-46, is given in Appendix D. Summarizing, the closed-form solution of (CNRIF)TH for FDM-FM Cases I and II may be expressed by Eq. 3-52 with the denominator term

(3-54)

$$\overline{\phi_{es}^2(t)} = \eta_m \int_{f_a}^{f_b} \frac{1}{\omega^2} \cdot \left| 1 - H(j\omega) \right|^2 df =$$

$$\frac{(\Delta\omega_{rms})^2}{\omega_b - \omega_a} \quad \frac{1}{C} \mathcal{R}e\left[\frac{B' - A'G}{J(G^* - G)} \ln\left(\frac{\omega_b - J}{\omega_b + J} \cdot \frac{\omega_a + J}{\omega_a - J} \right) \right]$$

and

(3-30)

$$\int_0^{B_p/2} |H(j\omega)|^2 \, df =$$

$$\frac{1}{2\pi C}\left\{\pi AB_p + \mathcal{R}e\left[\frac{1 - BG - A/C\,(1 - DG)}{J\,(G^* - G)} \cdot \ln\left(\frac{J - \pi B_p}{J + \pi B_p}\right)\right]\right\}$$

where G and J for each of these cases are as defined in Eqs. 3-32 through 3-36.

Next, Case III may be expressed by Eq. 3-52 with

(3-55)

$$\overline{\phi_{es}^2(t)} =$$

$$\frac{(\Delta\omega_{rms})^2}{\omega_b - \omega_a} \cdot \frac{1}{c(R_1^2 - R_2^2)} \left\{ \frac{B' - A'R_2^2}{R_2} \left(\tan^{-1}\frac{\omega_b}{R_2} - \tan^{-1}\frac{\omega_a}{R_2} \right) \right.$$

$$\left. + \frac{B' - A'R_1^2}{R_1} \left(\tan^{-1}\frac{\omega_a}{R_1} - \tan^{-1}\frac{\omega_b}{R_1} \right) \right\}$$

and

(3-41)

$$\int_0^{B_p/2} |H(j\omega)|^2 \, df =$$

$$\frac{1}{2\pi C}\left\{\left[\frac{1-BR_1^2}{R_2^2-R_1^2}\left(\frac{1}{R_1}\tan^{-1}\frac{\pi B_p}{R_1}\right)+\frac{1-BR_2^2}{R_1^2-R_2^2}\left(\frac{1}{R_2}\tan^{-1}\frac{\pi B_p}{R_2}\right)\right]\right.$$

$$-\frac{A}{C}\left[\frac{1-DR_1^2}{R_2^2-R_1^2}\left(\frac{1}{R_1}\tan^{-1}\frac{\pi B_p}{R_1}\right)+\frac{1-DR_2^2}{R_1^2-R_2^2}\left(\frac{1}{R_2}\tan^{-1}\frac{\pi B_p}{R_2}\right)\right]$$

$$\left.+\,A\pi B_p\right\}$$

where R_1 and R_2 are defined by Eq. 3-43.

Finally, Case IV may be expressed by Eq. 3-52 with

(3-56)

$$\overline{\phi_{es}^2(t)} = \frac{(\Delta\omega_{rms})^2}{\omega_b - \omega_a} \cdot \frac{1}{2C}\left[\left(\frac{B'}{R_o^2} - A'\right)\left(\frac{\omega_b}{\omega_b^2 + R_o^2} - \frac{\omega_a}{\omega_a^2 + R_o^2}\right)\right.$$

$$\left. + \left(\frac{B'}{R_o^2} + A'\right)\left(\frac{1}{R_o}\tan^{-1}\frac{\omega_b}{R_o} - \frac{1}{R_o}\tan^{-1}\frac{\omega_a}{R_o}\right)\right]$$

and

(3-47)

$$\int_0^{B_P/2} |H(j\omega)|^2 \, df =$$

$$\frac{1}{4\pi C}\left\{\left[\left(\frac{\pi B_P}{\pi^2 B_P^2 + R_0^2}\right)\left(\frac{1}{R_0^2} - B\right) + \left(\frac{1}{R_0} \tan^{-1}\frac{\pi B_P}{R_0}\right)\left(\frac{1}{R_0^2} + B\right)\right]\right.$$

$$-\frac{A}{C}\left[\left(\frac{\pi B_P}{\pi^2 B_P^2 + R_0^2}\right)\left(\frac{1}{R_0^2} - D\right) + \left(\frac{1}{R_0} \tan^{-1}\frac{\pi B_P}{R_0}\right)\left(\frac{1}{R_0^2} + D\right)\right]$$

$$\left. + 2A\pi B_P\right\}$$

where Ro is defined by Eq. 3-49.

These results will be used subsequently in the optimum design procedure. Attention will next be focused on the FDM-PM case.

3.2.4 FDM-PM Case. The next case to be considered is that of FDM-PM. Previous analysis [Ref. 1, p. 141 and p. 341] has indicated success in using an FDM-PM signal which is modeled as follows:

(1) It is random with Gaussian statistics.

(2) The PSD of the input "phase" modulation is nonzero between the baseband frequencies fa and fb only and is given by

$$W_{\phi_i} = \eta_m \quad , \quad f_a \leq f \leq f_b \tag{3-57}$$

where the one-sided PSD is used.

The modulation constant η_m may be related to the mean-square frequency deviation using Eq. 3-12, resulting in

$$\eta_m = \frac{3\,(\Delta\omega_{rms})^2}{(2\pi)^2(f_b^3 - f_a^3)} \tag{3-58}$$

From Eq. 3-10, using the FDM-PM model of Eq. 3-57 yields

(3-59)

$$(CNR_{IF})_{TH} =$$

$$\frac{\int_0^{B_p/2} |H(j\omega)|^2 \, df}{B_p\left[\nu - \eta_m \int_{f_a}^{f_b} |1 - H(j\omega)|^2 \, df\right]}$$

Again, the integral in the numerator of Eq. 3-59 has already been evaluated in closed form for each of the four cases. From Eqs. 3-6, 3-21 and 3-57, the signal-induced mean-square phase error component may be expressed as

(3-60)

$$\overline{\phi_{es}^2(t)} =$$

$$\frac{3\,(\Delta\omega_{rms})^2}{(2\pi)^2\,(f_b^3 - f_a^3)} \int_{f_a}^{f_b} \frac{A'\omega^4 + B'\omega^2}{C\,\omega^4 + D\,\omega^2 + 1}\, df =$$

$$\frac{3\,(\Delta\omega_{rms})^2}{\omega_b^3 - \omega_a^3} \int_{\omega_a}^{\omega_b} \frac{A'\omega^4 + B'\omega^2}{C\,\omega^4 + D\,\omega^2 + 1}\, d\omega$$

where the coefficients of the integrand are defined by Eq. 3-22. A detailed solution of Eq. 3-60 in closed form for each of the four cases is given in Appendix E. Summarizing, the closed-form solution of (CNRIF)TH for FDM-PM Cases I and II may be expressed by Eq. 3-59 with

(3-61)

$$\overline{\phi_{es}^2(t)} = \eta_m \int_{f_a}^{f_b} |1 - H(j\omega)|^2 \, df =$$

$$\frac{3\,(\Delta\omega_{rms})^2}{\omega_b^3 - \omega_a^3} \left\{ \frac{A'}{C}(\omega_b - \omega_a) - \frac{A'}{C^2} \mathrm{Re}\left[\frac{1 - (D - B'C/A')\,G}{J\,(G^* - G)} \cdot \ln\left(\frac{\omega_b - J}{\omega_b + J} \cdot \frac{\omega_a + J}{\omega_a - J} \right) \right] \right\}$$

and

(3-30)

$$\int_0^{B_p/2} |H(j\omega)|^2 \, df =$$

$$\frac{1}{2\pi C}\left\{ \pi A B_p + \mathrm{Re}\left[\frac{1 - BG - A/C\,(1 - DG)}{J\,(G^* - G)} \cdot \ln\left(\frac{J - \pi B_p}{J + \pi B_p} \right) \right] \right\}$$

where G and J for each of these cases are as defined in Eqs. 3-32 through 3-36.

Next, Case III may be expressed by Eq. 3-59 with

(3-62)

$$\overline{\phi_{es}^2(t)} = \frac{3(\Delta\omega_{rms})^2}{\omega_b^3 - \omega_a^3}\left\{\frac{A'}{C}(\omega_b - \omega_a)\right.$$

$$-\frac{A'}{(R_1^2 - R_2^2)C^2}\left[\frac{1-(D-B'C/A')R_2^2}{R_2}\left(\tan^{-1}\frac{\omega_b}{R_2} - \tan^{-1}\frac{\omega_a}{R_2}\right)\right.$$

$$\left.\left.+\frac{1-(D-B'C/A')R_1^2}{R_1}\left(\tan^{-1}\frac{\omega_a}{R_1} - \tan^{-1}\frac{\omega_b}{R_1}\right)\right]\right\}$$

and

(3-41)

$$\int_0^{Bp/2} |H(j\omega)|^2 \, df =$$

$$\frac{1}{2\pi C}\left\{\left[\frac{1-BR_1^2}{R_2^2-R_1^2}\left(\frac{1}{R_1}\tan^{-1}\frac{\pi Bp}{R_1}\right)+\frac{1-BR_2^2}{R_1^2-R_2^2}\left(\frac{1}{R_2}\tan^{-1}\frac{\pi Bp}{R_2}\right)\right]\right.$$

$$-\frac{A}{C}\left[\frac{1-DR_1^2}{R_2^2-R_1^2}\left(\frac{1}{R_1}\tan^{-1}\frac{\pi Bp}{R_1}\right)+\frac{1-DR_2^2}{R_1^2-R_2^2}\left(\frac{1}{R_2}\tan^{-1}\frac{\pi Bp}{R_2}\right)\right]$$

$$\left.+\pi A\,Bp\right\}$$

where R_1 and R_2 are defined by Eq. 3-43.

Finally, Case IV may be expressed by Eq. 3-59 with

(3-63)

$$\overline{\phi_{es}{}^2(t)} = \frac{3(\Delta\omega_{rms})^2}{\omega_b{}^3 - \omega_a{}^3}\left\{\frac{A'}{C}(\omega_b - \omega_a)\right.$$

$$-\frac{A'}{2C^2}\left[\left(\frac{1}{R_0{}^2} - D + \frac{B'C}{A'}\right)\left(\frac{\omega_b}{\omega_b{}^2 + R_0{}^2} - \frac{\omega_a}{\omega_a{}^2 + R_0{}^2}\right)\right.$$

$$\left.\left.+\left(\frac{1}{R_0{}^3} + \frac{D - B'C/A'}{R_0}\right)\left(\tan^{-1}\frac{\omega_b}{R_0} - \tan^{-1}\frac{\omega_a}{R_0}\right)\right]\right\}$$

and

(3-47)

$$\int_0^{B_p/2} |H(j\omega)|^2 \, df$$

$$\frac{1}{4\pi C}\left\{\left[\left(\frac{\pi B_p}{\pi^2 B_p^2 + R_0^2}\right)\left(\frac{1}{R_0^2} - B\right) + \left(\frac{1}{R_0} \tan^{-1}\frac{\pi B_p}{R_0}\right)\left(\frac{1}{R_0^2} + B\right)\right]\right.$$

$$-\frac{A}{C}\left[\left(\frac{\pi B_p}{\pi^2 B_p^2 + R_0^2}\right)\left(\frac{1}{R_0^2} - D\right) + \left(\frac{1}{R_0} \tan^{-1}\frac{\pi B_p}{R_0}\right)\left(\frac{1}{R_0^2} + D\right)\right]$$

$$\left. + 2A\pi B_p\right\}$$

where Ro is defined by Eq. 3-49.

3.2.5 Test-Tone Case. As indicated previously, Eq. 3-1 holds for Gaussian type modulations such as those covered in the preceding sections. For modulations other than Gaussian the expression generally becomes less realistic. It is of interest, however, to investigate how well this threshold criterion holds for the case of test-tone modulation, since the results can be compared against the experimental findings of Acampora and Newton [Ref. 5] . Panter [Ref 7, pp. 501-503] has also found this criterion useful in the test-tone case. For the case at hand, the input signal phase modulation may be expressed as

(3-64)

$$\phi_i(t) = \frac{\Delta\omega}{\omega_{TT}} \cos \omega_{TT} t = \beta \cos \omega_{TT} t$$

where

$\Delta\omega$ $\equiv$ peak frequency deviation (rad/sec)

ω_{TT} $\equiv$ test-tone frequency (rad/sec)

β $\equiv$ modulation index

The PSD of the input phase modulation is then given by

(3-65)

$$W_{\phi_i} = \frac{\beta^2}{2} \delta(f - f_{TT})$$

From Eq. 3-6, the expression for the signal-induced phase error component may be expressed as

(3-66)

$$\overline{\phi_{es}^2(t)} = \int_0^{f_b} \frac{\beta^2}{2} \delta(f - f_{TT}) \left| 1 - H(j\omega) \right|^2 df$$

The expression for $|1 - H(j\omega)|^2$ is given by Eq. 3-21. It is desirable, however, to reduce this expression, which is given in terms of the generalized second-order PLL parameters, to the original ERPLD parameters since that is the configuration actually under consideration here. This may be accomplished simply by using Eq. 3-23. From Eqs. 3-21, 3-23, and 3-66, using the sifting property of the delta function, yields the expression

(3-67)

$$\overline{\phi_{es}^2(t)} =$$

$$\frac{\beta^2}{2}\left\{\frac{\omega_{TT}^4\left(\frac{1}{Kb}\right)^2 + \omega_{TT}^2\left(\frac{1}{K}\right)^2}{\omega_{TT}^4\left(\frac{1+\alpha}{Kb}\right)^2 + \omega_{TT}^2\left[\left(\frac{1+\alpha}{K} + \frac{1}{a}\right)^2 - 2\left(\frac{1+\alpha}{Kb}\right)\right] + 1}\right\}$$

Again, for the original ERPLD configuration

$$\int_0^{B_p/2} |H(j\omega)|^2 \, df = \tag{3-24}$$

$$\frac{1}{2\pi} \int_0^{\pi B_p} \frac{A\omega^4 + B\omega^2 + 1}{C\omega^4 + D\omega^2 + 1} \, d\omega$$

where

$$A = \left(\frac{\alpha}{Kb}\right)^2$$

$$B = \left(\frac{\alpha}{K} + \frac{1}{a}\right)^2 - \frac{2\alpha}{Kb} \tag{3-68}$$

$$C = \left(\frac{1+\alpha}{Kb}\right)^2$$

$$D = \left(\frac{1+\alpha}{K} + \frac{1}{a}\right)^2 - 2\left(\frac{1+\alpha}{Kb}\right)$$

The expression for (CNRIF)TH is then given by

(3-69)

$$(CNR_{IF})_{TH} =$$

$$\frac{\int_0^{B_p/2} |H(j\omega)|^2 \, df}{B_p \left[\nu - \overline{\phi_{es}^2(t)} \right]}$$

Eq. 3-69 was evaluated using the parameters of the Acampora and Newton ERPLD [Ref. 5] . The computer program used to accomplish this, is given in Appendix F. Again, it is important to realize that the ERPLD was designed to detect voice modulation but was tested with a 1kHz tone. The result obtained from the computer program in Appendix F was

$$(CNRIF)TH = 2.94 \quad dB$$

The experimental results of Acampora and Newton [Ref. 5] indicate that threshold occurs for CNRIF between approximately 2.5 to 3 dB using the same definition of threshold used throughout this chapter, i.e., the point where the output signal-to-noise ratio is 1 dB below that predicted by the above threshold formulation. Summarizing, the threshold criterion of Eq. 3-1 applied to the case of test-tone modulation yields results which are in close agreement with those obtained experimentally.

3.3 Optimum Design Procedure.

3.3.1 General Description. In the preceding section, closed-form solutions for (CNRIF)TH for a number of practical basebands were developed for the generalized second-order PLL. In this section, an optimization algorithm is applied to the closed-form solutions to achieve an optimum design. By optimum design it is meant one which achieves the minimum threshold carrier-to-noise ratio.

The algorithm chosen for this procedure is known as Powell's Method [Ref. 8] . The chief advantage of this method is that it does not necessitate the calculation of partial derivatives. The mathematical rigor associated with this method is available from a number of sources [Ref. 9, pp. 392-396, Ref. 10, pp. 60-71 and Ref. 11, pp. 48-55] ; however, the basis for the method is easily understood as follows: assuming that the function has been minimized once in each of the coordinate directions and then in the associated pattern direction, as shown in Fig. 3-2, one of the coordinated directions is discarded in favor of the pattern direction for inclusion in the next set of minimizations, since this is likely to be a better direction than the coordinate direction which was discarded. Following the next cycle of minimizations, a new pattern direction is generated which again replaces one of the coordinate directions. Theoretically, somewhat more is involved to make the method efficient; however, the basic idea is as presented above.

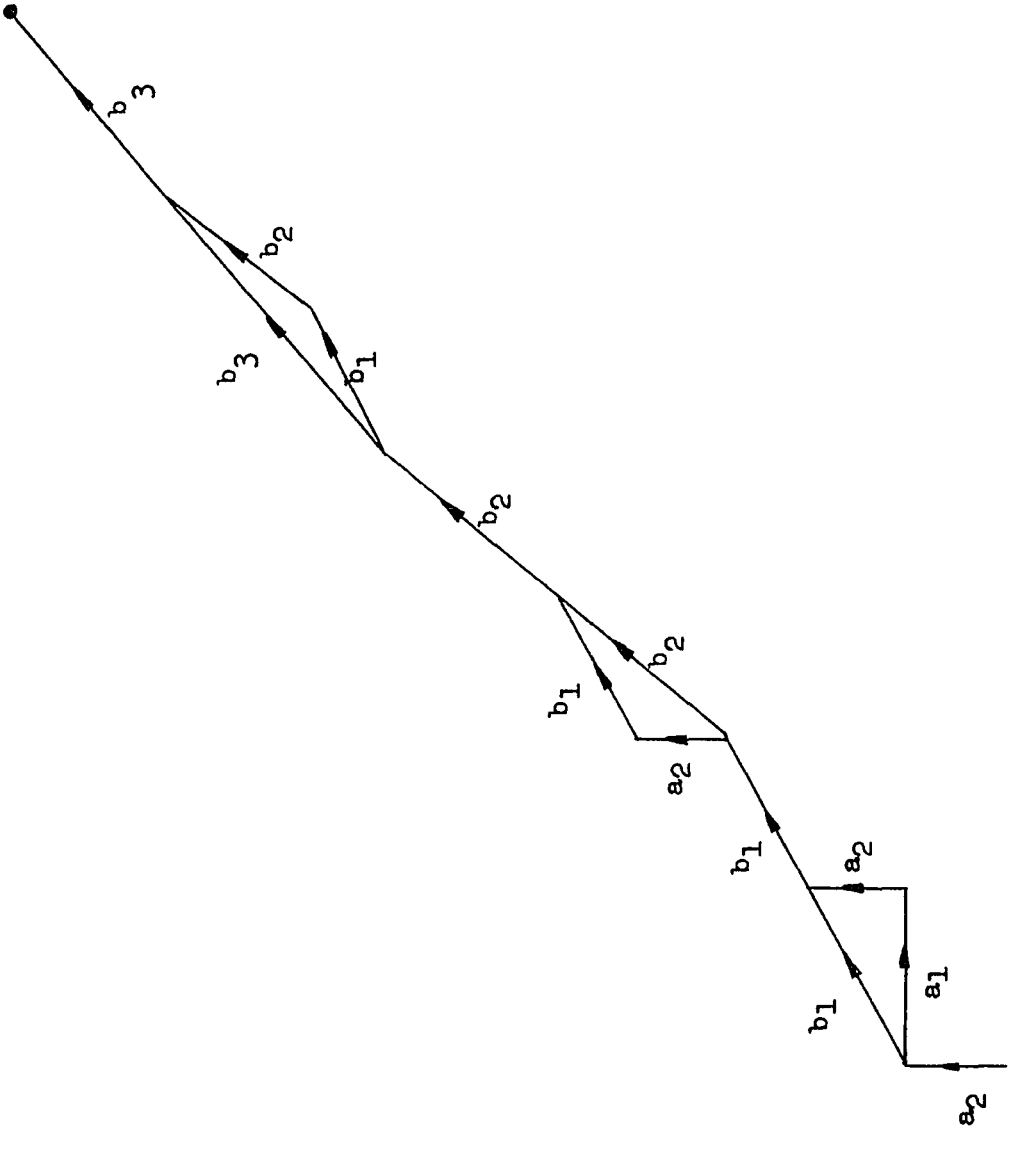

Fig. 3-2. Powell's Method illustrated in two dimensions.

A computer program was written to implement Powell's method with the aid of Dr. J. Marowitz, formerly of the Department of Electrical Engineering, Newark College of Engineering. The basic program is given in Appendix G, along with the subprograms used for each of the cases studied. In the sections which follow, a number of examples are given which illustrate the use of the optimum design procedure along with amplifying remarks.

3.3.2 Voice Modulation Case. The first design example considered is for the voice modulation case using the generalized second-order PLL. The voice channel parameters chosen for this example are the same as those used in the Acampora and Newton ERPLD [Ref. 5] so that comparisons can be made to its performance. These parameters are given by

Baseband Voice Channel : 300-3300 Hz

Peak-to-RMS Amplitude Ratio: 10dB

RMS Deviation: $\pm \sqrt{10}$ kHz

IF Bandwidth: 35 kHz

Using the above optimization program; along with the subprogram for the generalized second-order PLL; voice modulation case as given in Appendix G, the following optimum design was found

$$\beta = 1.34\times10^{9} \quad (\text{rad/sec})^2$$

$$\gamma = 3.49\times10^{4} \quad (\text{rad/sec})$$

$$b = 5.98\times10^{3} \quad (\text{rad/sec})$$

$$K = 1.62\times10^{5} \quad (\text{sec}^{-1})$$

yielding

$$(\overset{\sim}{\text{CNRIF}})\text{TH} = 0.378 \text{ dB}$$

In order to determine whether the above design does indeed yield a true minimum for (CNRIF)TH, each of the parameters was varied about its optimum value while holding the other three parameters at their optimum values. The results, shown in Figs. 3-3 through 3-6, indicate that the value of (CNRIF)TH above is indeed a true minimum. It should be noted that the optimization program requires initial starting points for β , γ , b and K from which the search proceeds. In this case, the original Acampora and Newton parameters [Ref. 5] translated into generalized second-order PLL parameters through Eq. 3-23 were used as a starting point. In general, however, as was subsequently done in this case as a check, several different starting points should be used since the function may have more than one local minimum whereas the global minimum is normally desired. In addition, it was found that some starting points led to forbidden regions where one or more of the parameters became negative.

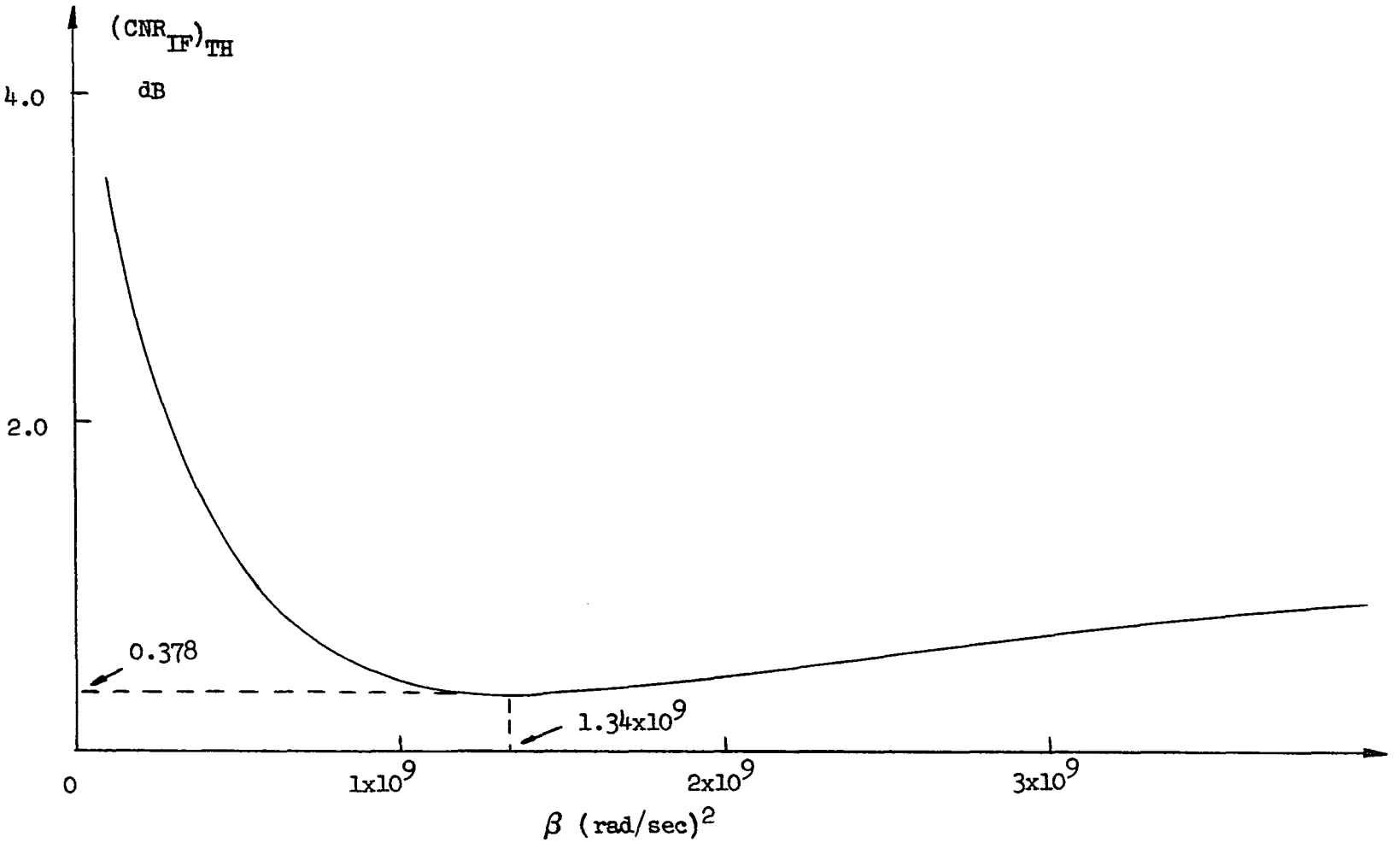

Fig. 3-3. $(CNR_{IF})_{TH}$ vs β using optimum values of γ, b and K for the generalized second-order PLL; voice modulation case.

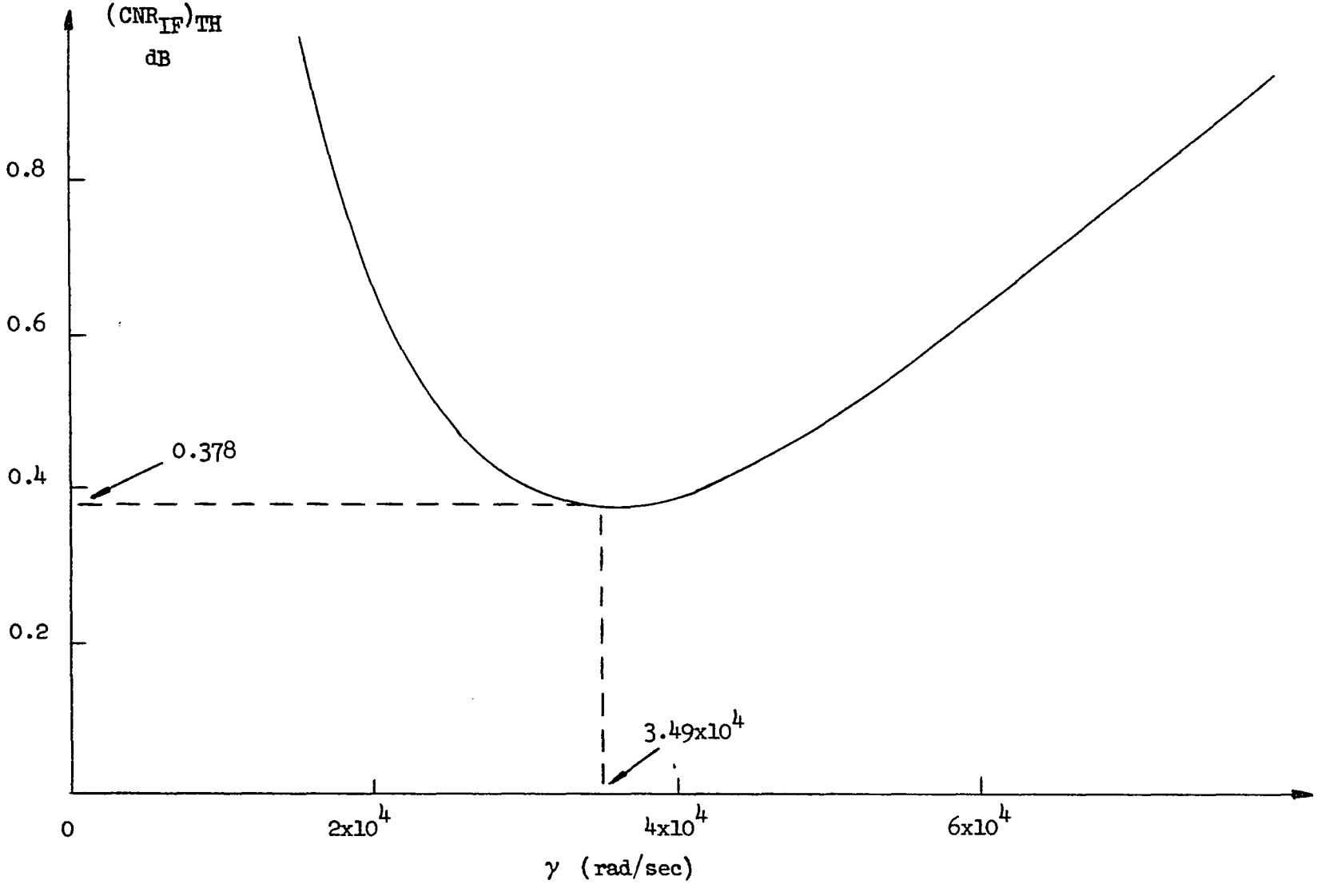

Fig. 3-4. $(CNR_{IF})_{TH}$ vs γ using optimum values of β, b and K for the generalized second-order PLL; voice modulation case.

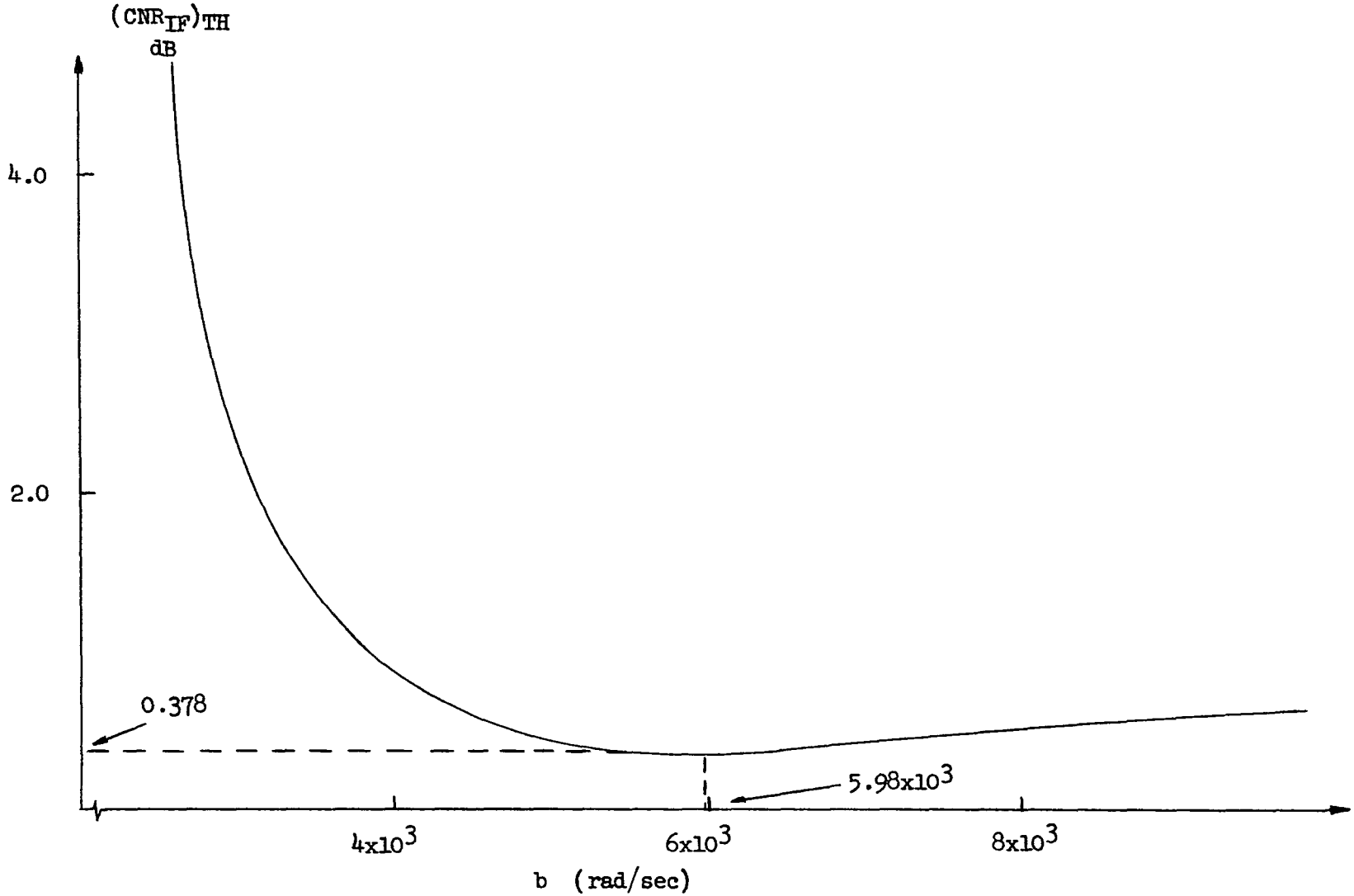

Fig. 3-5. $(CNR_{IF})_{TH}$ vs b using optimum values of β, γ and K for the generalized second-order PLL;voice modulation case.

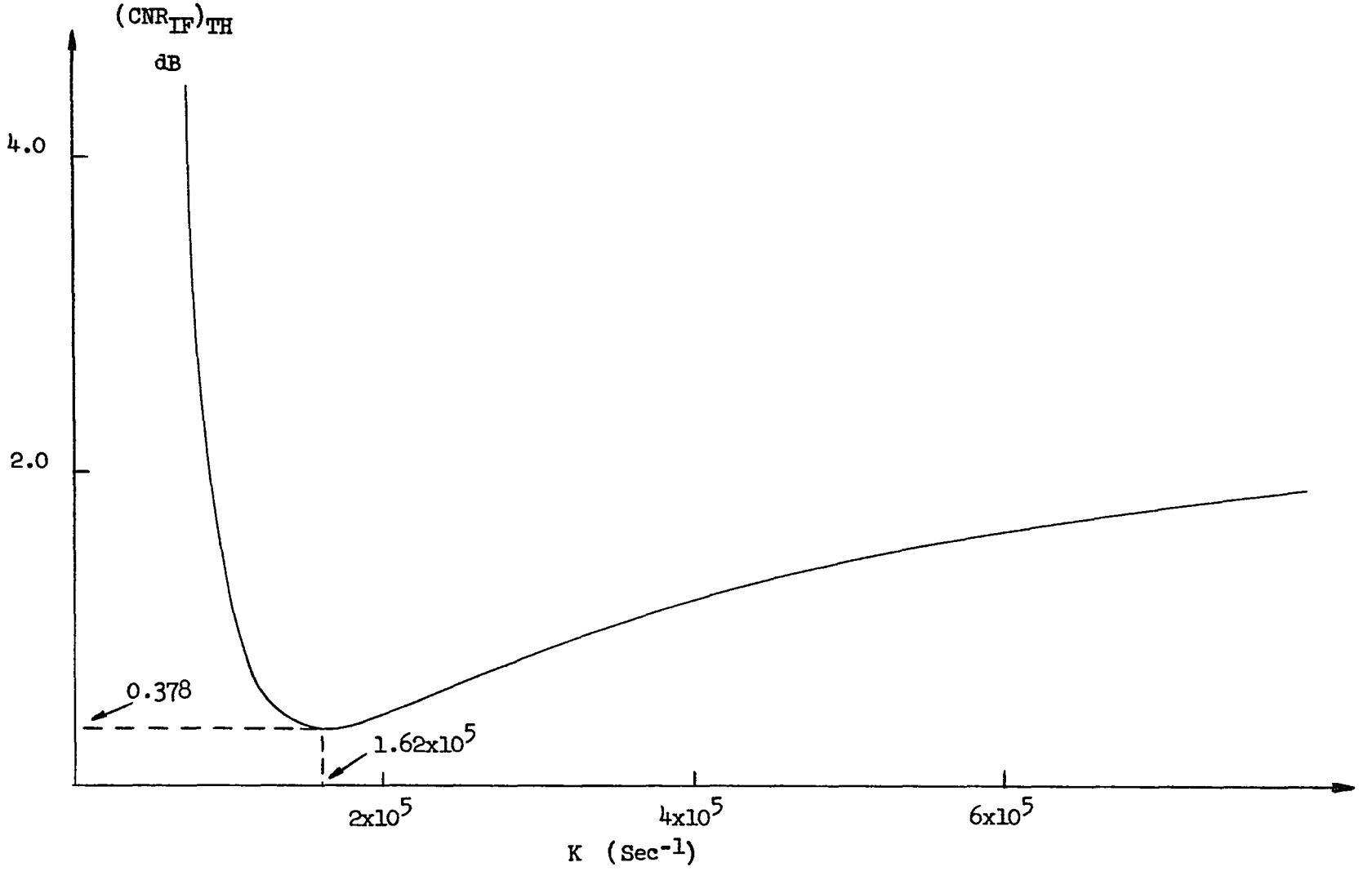

Fig. 3-6. $(CNR_{IF})_{TH}$ vs K using optimum values of β , γ and b for the generalized second-order PLL; voice modulation case.

Reflecting back to Eq. 3-10, which formed the foundation for the optimum design procedure, it is recalled that the only parameter which has any uncertainty associated with it is ν , the mean-square phase error at threshold. In order to determine how variation of ν affects the design, a sensitivity study was performed for the preceding case in which the optimization program was run for a range of values of ν . The results are shown in Figs. 3-7 through 3-11. For the range of ν normally cited in literature, i.e., ν between 0.20 and 0.25, it is found that although (CNRIF)TH changes considerably over this range, the design parameters β , γ , b and K vary very little. These results, then, give added strength to the design procedure. Nevertheless, it is still desirable to have a firm fix on ν . In the next chapter a method is presented using computer simulation of the non-linear model of the generalized second-order PLL which enables the determination of ν .

Finally, an optimization procedure was performed on the original Acampora and Newton configuration by reducing the generalized second-order PLL to the ERPLD through Eq. 3-23. The resultant optimum design was

$\alpha = 0.72$

$a = 4.15 \times 10^4$ (rad/sec)

$b = 5.98 \times 10^3$ (rad/sec)

$K = 1.62 \times 10^5$ (sec^{-1})

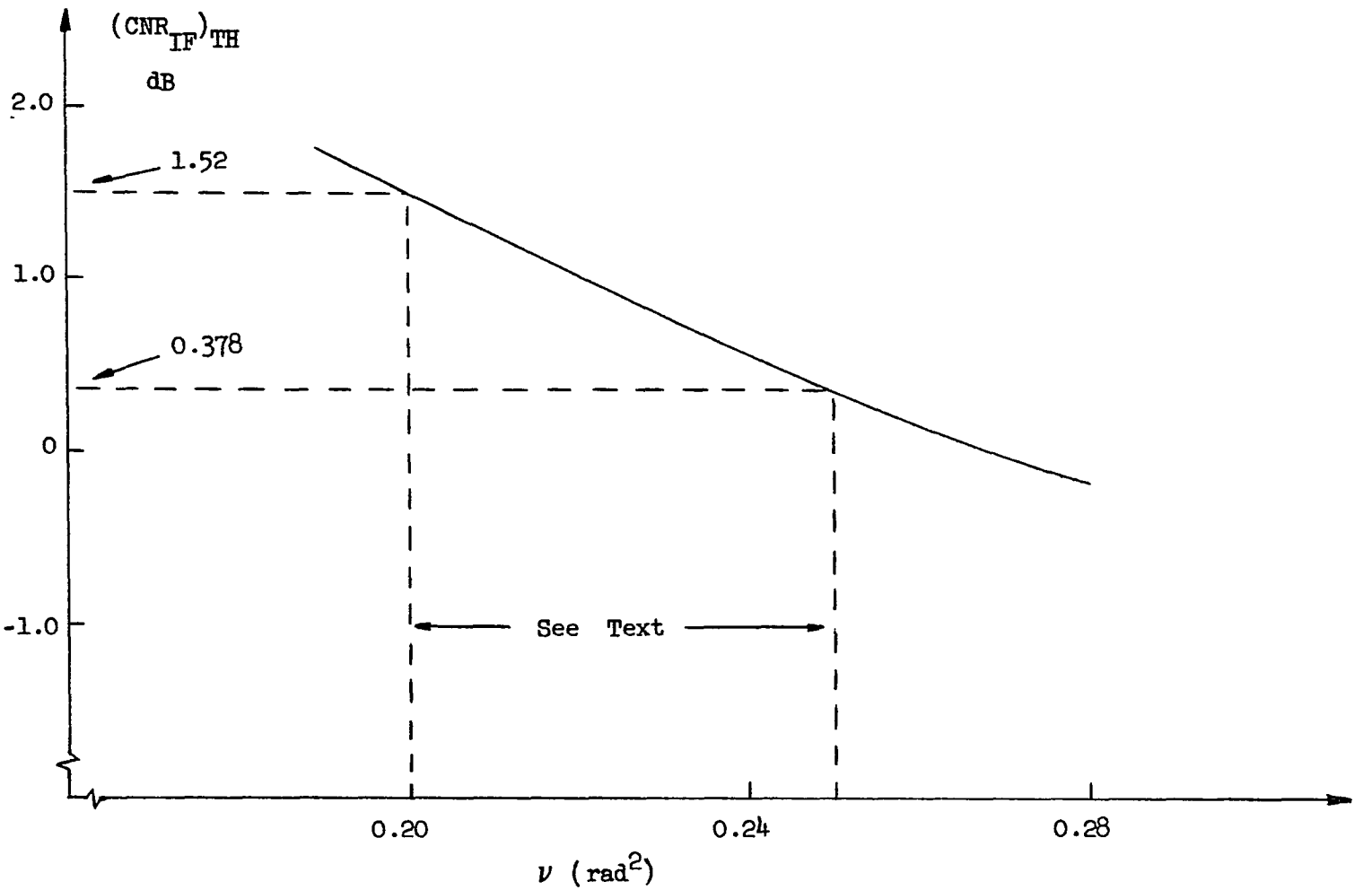

Fig. 3-7. Optimum $(CNR_{IF})_{TH}$ vs ν for the generalized second-order PLL; voice modulation case.

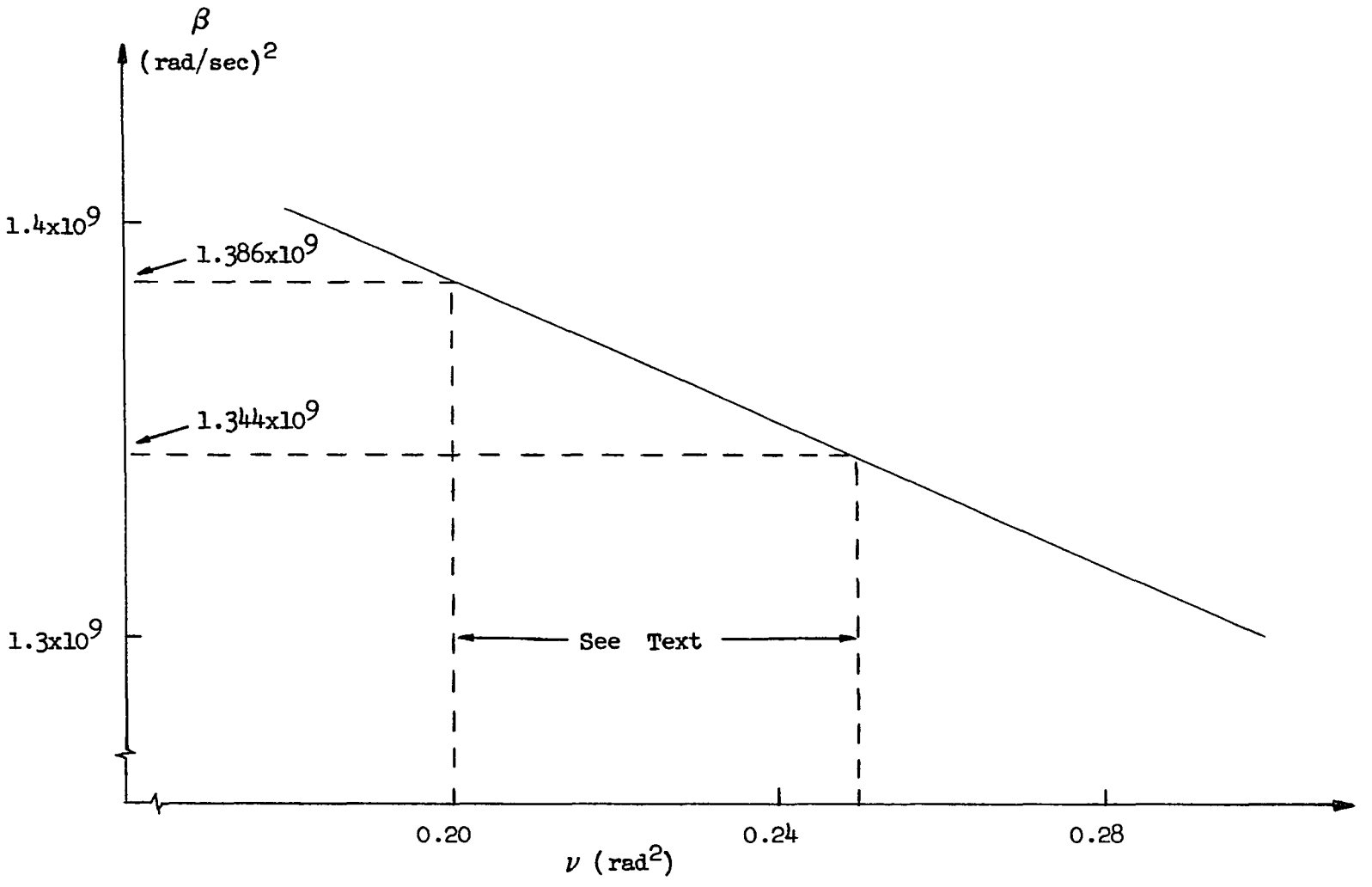

Fig. 3-8. Optimum value of β vs ν for the generalized second-order PLL; voice modulation case.

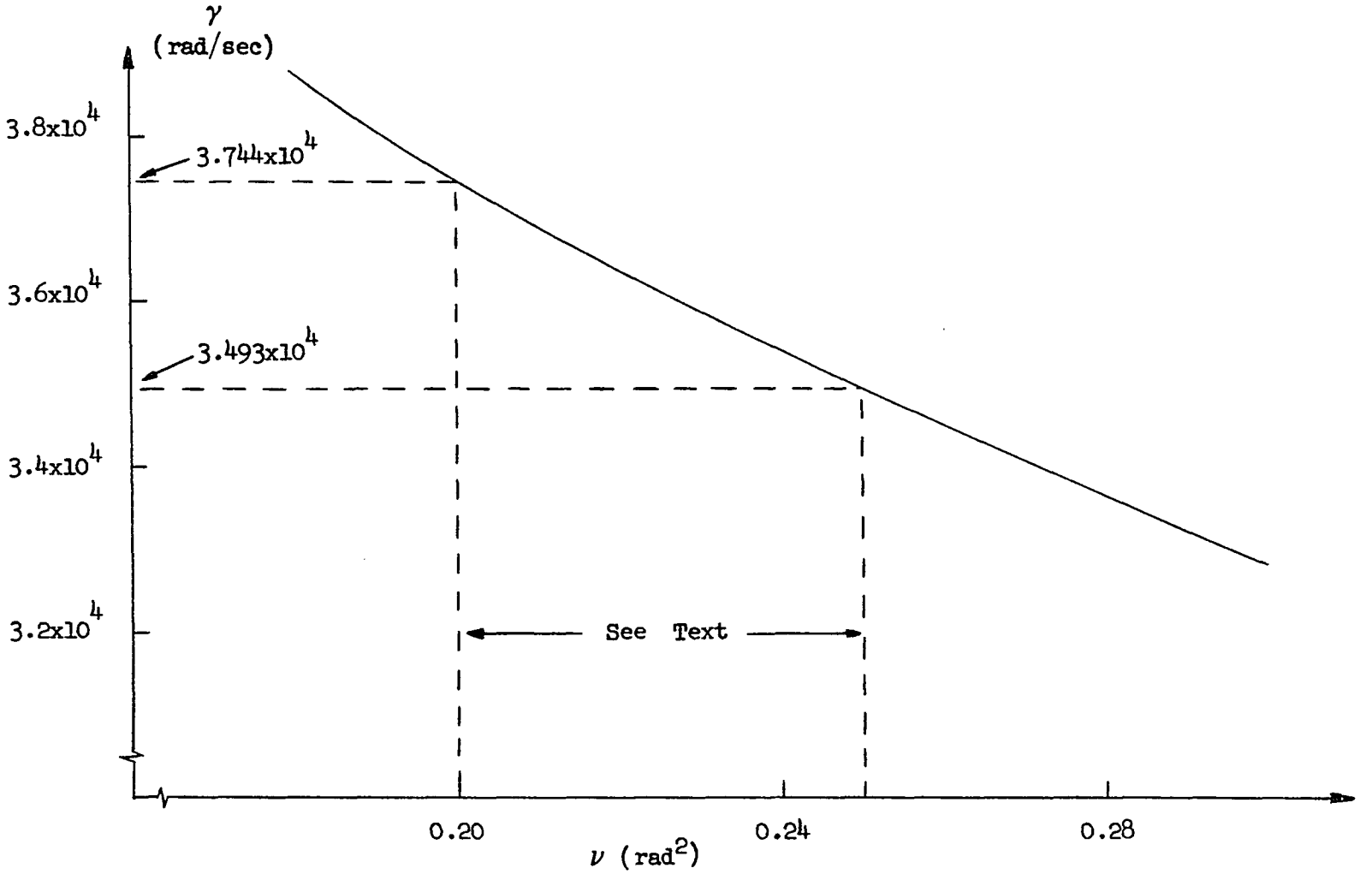

Fig. 3-9. Optimum value of γ vs ν for the generalized second-order PLL; voice modulation case.

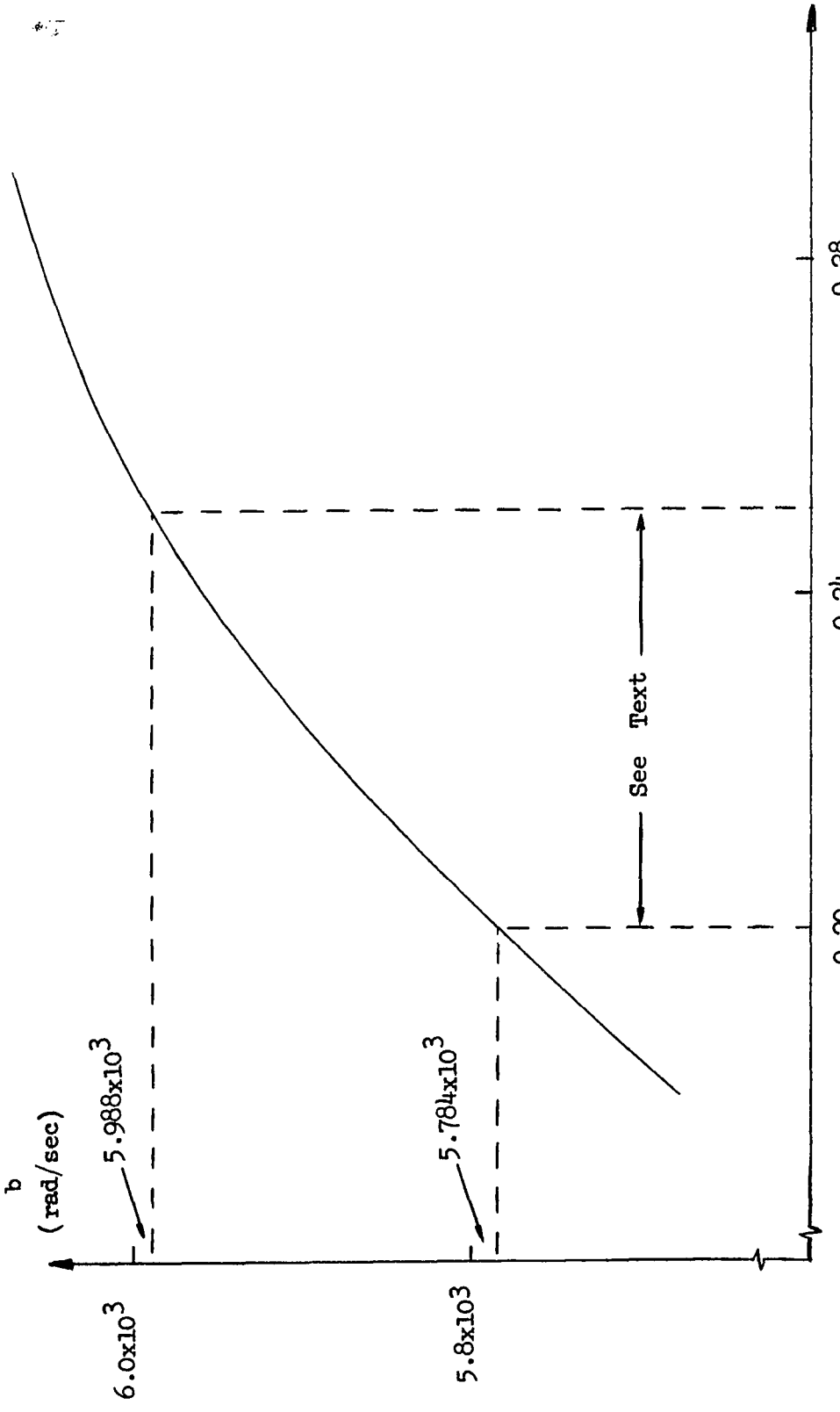

Fig. 3-10. Optimum value of b vs ν for the generalized second-order PLL; voice modulation case.

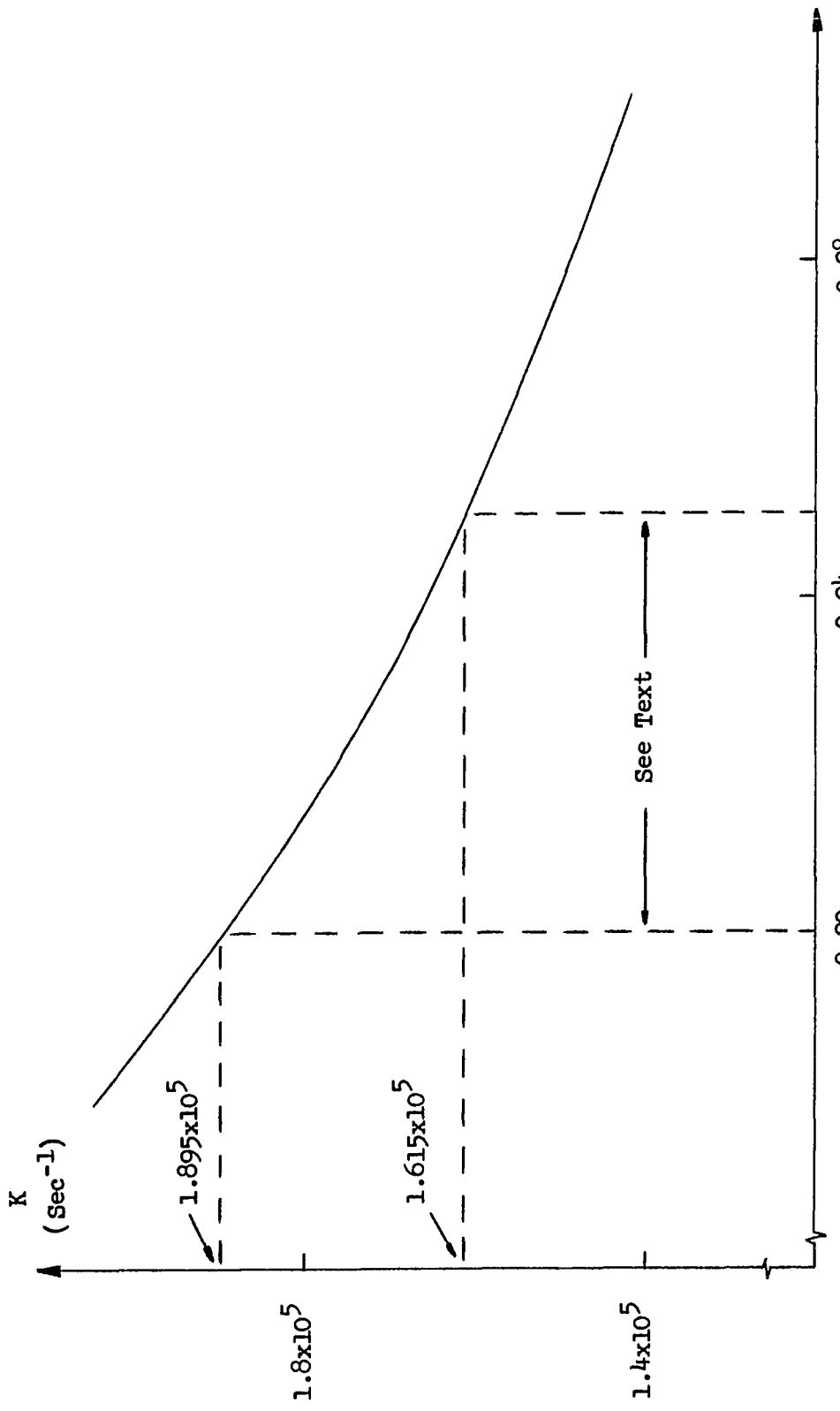

Fig. 3-11. Optimum value of K vs ν for the generalized second-order PLL; voice modulation case.

yielding

$$(CNRIF)TH = 0.378 \text{ dB}$$

Again, using Eq. 3-23, it is seen that the ERPLD and generalized second-order PLL have the equivalent optimum design. This bares out the development in Chapter 2 in which it was shown that for practical cases the ERPLD can generally achieve the same designs as the generalized second-order PLL. It is also significant to note that the original Acampora and Newton design parameters [Ref. 5] were very close to optimum yielding by the closed-form solution of the voice modulation case

$$(CNRIF)TH = 0.573 \text{ dB}$$

3.3.3 FDM-FM Case. The next design example is for the FDM-FM case using the generalized second-order PLL. The parameters chosen for this example are given by

Modulation: 600-channel FDM-FM (4kHz bandwidth/channel)

Baseband: 60kHz to 2.54MHz

Peak to RMS Amplitude Ratio: 10dB

RMS Deviation: 7.1 MHz

IF Bandwidth: 50MHz

Using the basic optimization program along with the subprogram for the generalized second-order PLL; FDM-FM case as given in Appendix G, the following optimum design was found

$$\beta = 2.83\times10^{15} \quad (\text{rad/sec})^2$$

$$\gamma = 6.75\times10^{7} \quad (\text{rad/sec})$$

$$\mathbf{b} = 6.38\times10^{6} \quad (\text{rad/sec})$$

$$\mathbf{K} = 4.75\times10^{8} \quad (\text{sec}^{-1})$$

yielding

$$(\text{CNRIF})\text{TH} = 0.976 \text{ dB}$$

Again, in order to determine whether the above design yields a true minimum for (CNRIF)TH, each of the parameters was varied about its optimum value, while holding the other three parameters at their optimum values. The results shown in Figs. 3-12 through 3-15 indicate the value of (CNRIF)TH above is indeed a minimum.

It is of interest to note that if the generalized second-order PLL parameters are reduced to those of the ERPLD thtorugh Eq. 3-23, the value of α is 1.07 consistant with Acampora and Newton's findings [Ref. 5] that a value of α of approximately unity yields the best design.

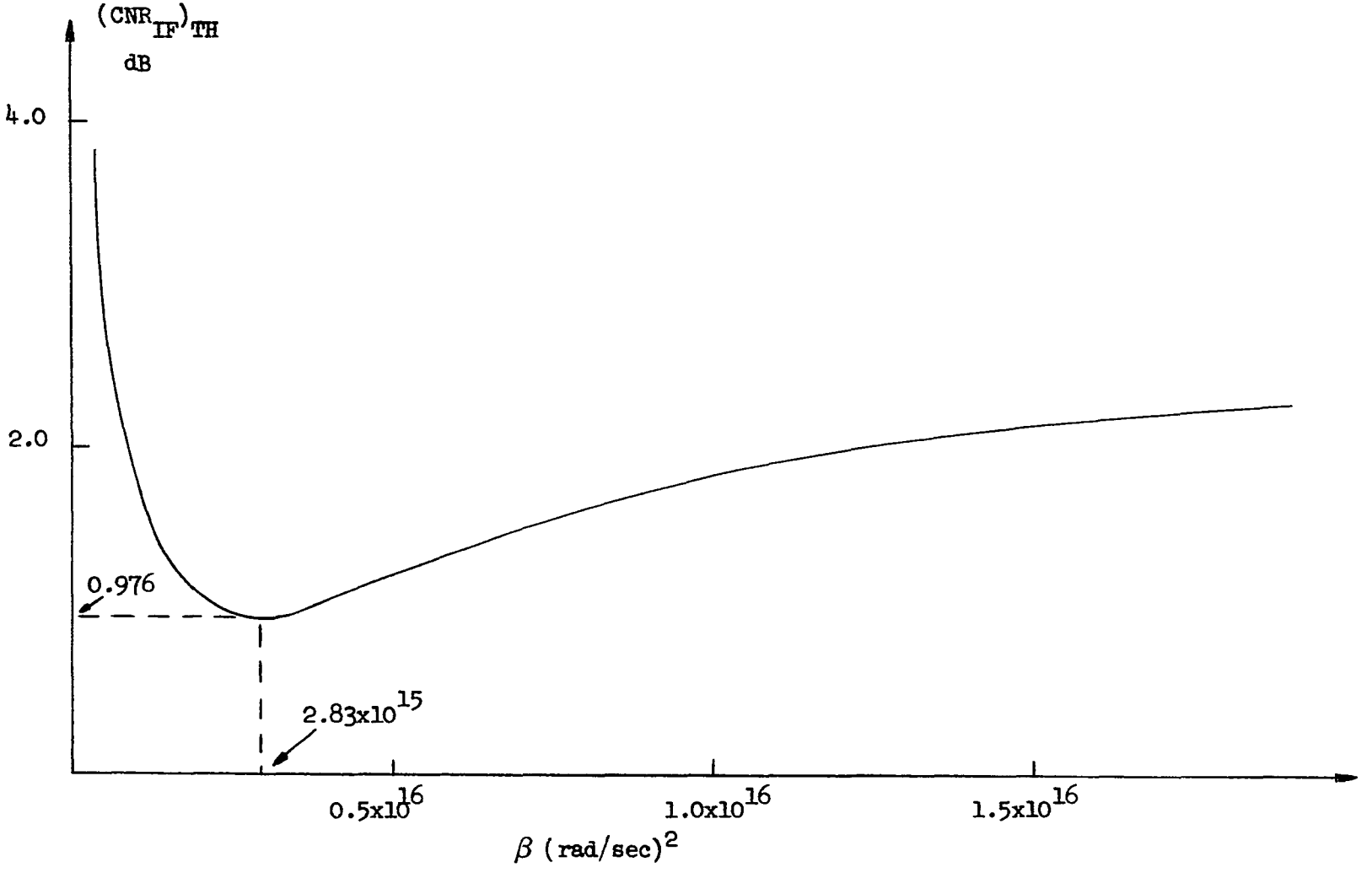

Fig. 3-12. $(CNR_{IF})_{TH}$ vs β using optimum values of γ, b and K for the generalized second-order PLL; FDM-FM case.

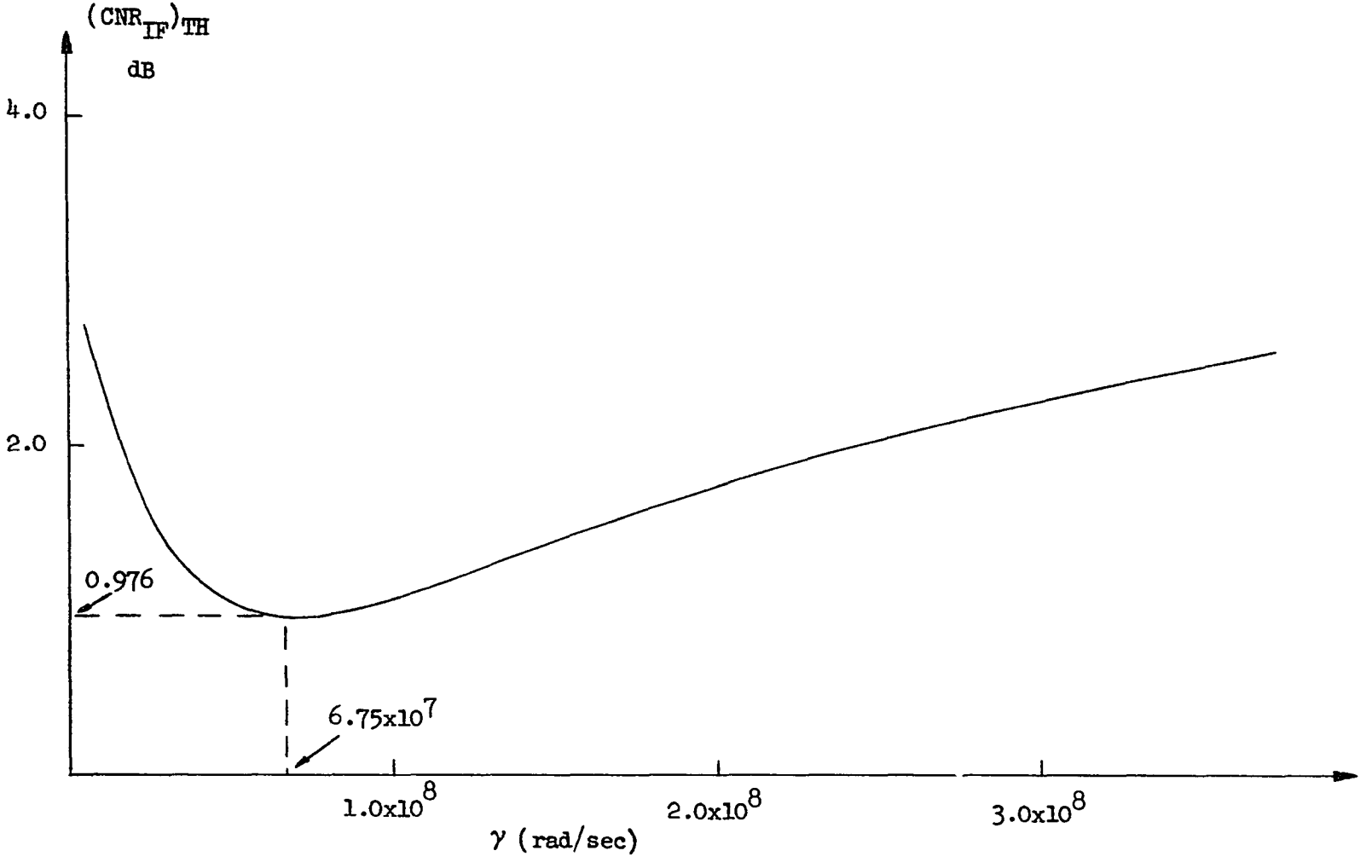

Fig. 3-13. $(CNR_{IF})_{TH}$ vs γ using optimum values of β, b and K for the generalized second-order PLL; FDM-FM case.

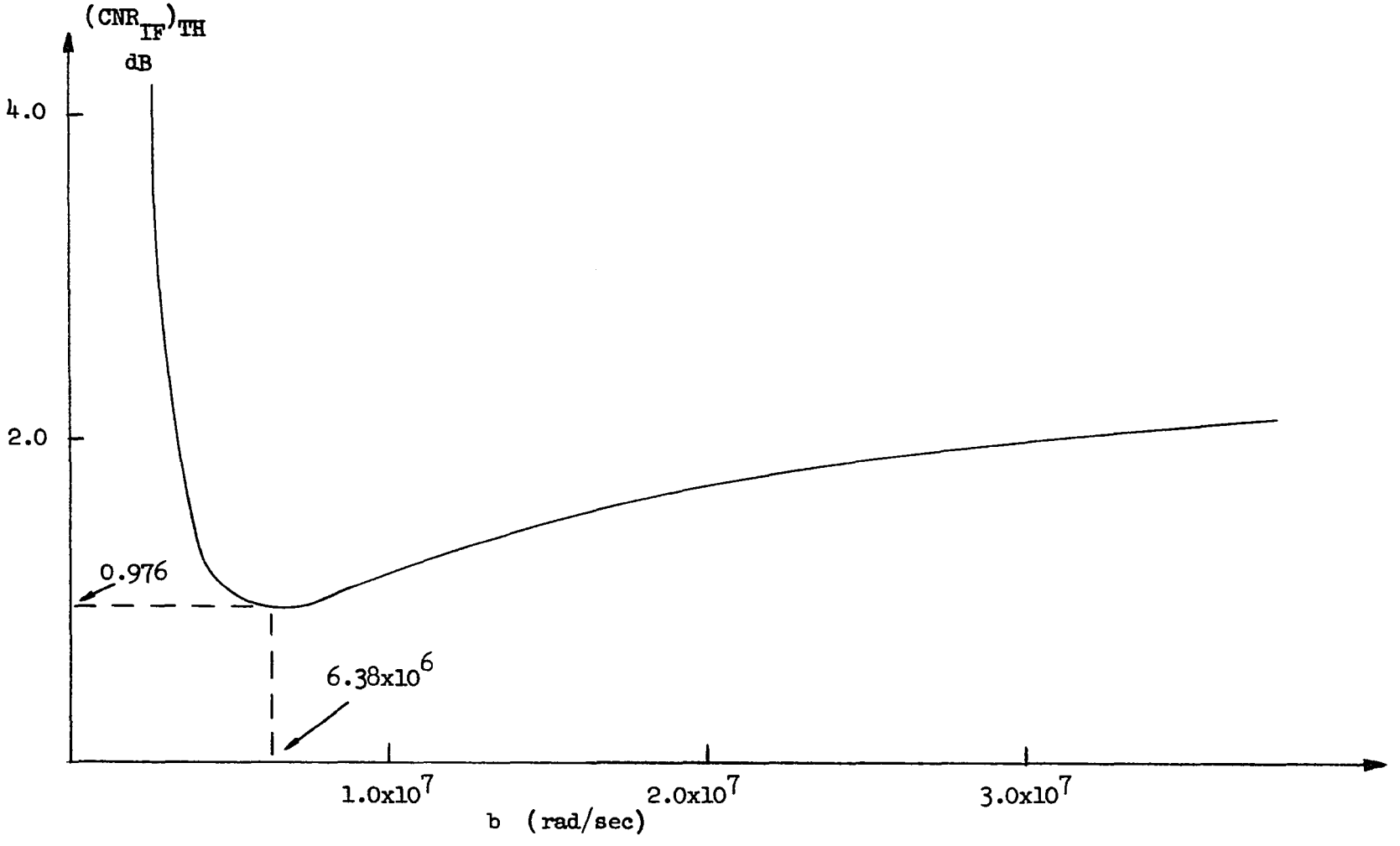

Fig. 3-14. $(CNR_{IF})_{TH}$ vs b using optimum values of β , γ and K for the generalized second-order PLL; FDM-FM case.

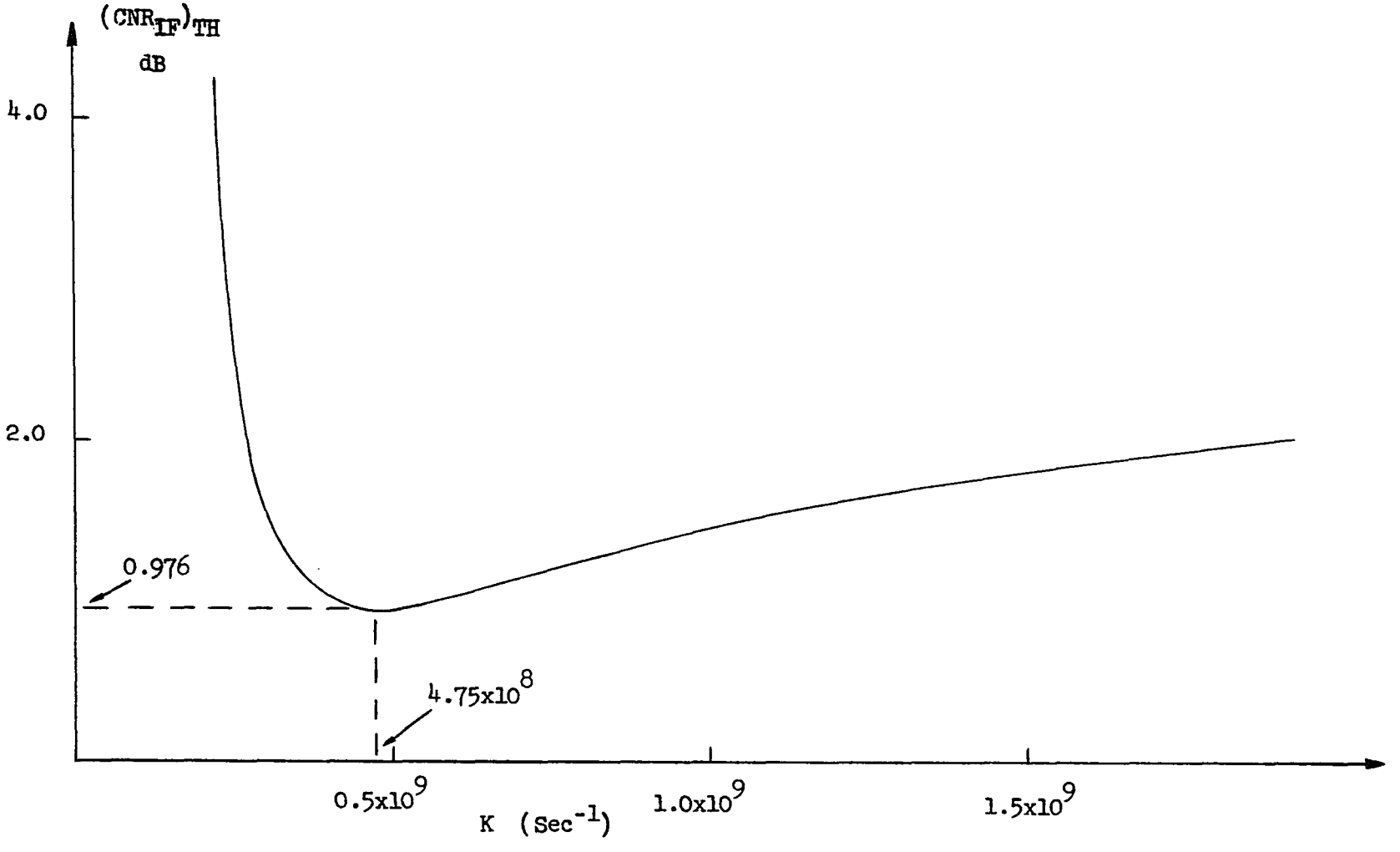

Fig.3-15. $(CNR_{IF})_{TH}$ vs K using optimum values of β , γ and b for the generalized second-order PLL; FDM-FM case.

References - Chapter 3

1. J. Klapper and J. Frankle, Phase-Locked and Frequency-Feedback Systems: Principles and Techniques, Academic Press, New York, 1972.

2. J. Frankle, "Threshold Performance of Analog FM Demodulators," RCA Review 27, No. 4, pp. 521-562, 1966.

3. A. Viterbi, "Phase-Locked Loop Dynamics in the Presence of Noise by Fokker-Planck Techniques," Proc. IEEE, Vol. 51, pp. 1737-1753, December 1963. Also in J. Klapper, ed., Selected Papers on Frequency Modulation, Dover, 1970.

4. R. E. Heitzman, "A Study of the Threshold Power Requirements of FMFB Receivers," IRE Trans. SET-8, pp. 249-256, 1962.

5. A. Acampora and A. Newton, "Use of Phase Subtraction to Extend the Range of a Phase-Locked Demodulator," RCA Review, Vol. 27, No. 3, pp. 577-599, December 1966.

6. W. C. Lindsey, Synchronization Systems in Communication and Control, Prentice Hall Inc., Englewood Cliffs, New Jersey, 1972.

7. P. F. Panter, Modulation, Noise and Spectral Analysis, McGraw-Hill, New York, 1965.

8. M. J. Powell, "An Efficient Method for Finding the Minimum of a Function of Several Variables without Calculating Derivatives, Computer J., No. 7, p. 155, 1964.

9. G. S. Beveridge and R. S. Schechter, Optimization Theory and Practice, McGraw-Hill, New York, 1970.

10. R. L. Fox, Optimization Methods for Engineering Design, Addison-Wesley, Reading, Massachusetts, 1971.

11. J. Kowalik and M. Osborne, Methods for Unconstrained Optimization Problems, Elseiver, New York, 1968.

CHAPTER IV

COMPUTER SIMULATION OF THE GENERALIZED SECOND-ORDER PHASE-LOCKED LOOP

4.1 Introduction

In the preceding chapter, a method was presented for achieving an optimum design for the generalized second-order PLL for several useful modulation types. It was indicated that the only parameter in the analysis with uncertainty associated with it was ν the mean-square phase error at threshold. In this chapter, using the Continuous System Modeling Program (CSMP), a non-linear model of the generalized second-order PLL was simulated for the representative cases of test-tone modulation and a single-channel FM voice signal. By comparing the results obtained from the non-linear model against those predicted from the linear formulation, a measure of the mean-square phase error at threshold was obtained. The methods used in this procedure are shown to be directly applicable to the FDM-FM and FDM-PM cases as well.

4.2 Basic Digital Computer Model in the Absence of Noise.

4.2.1 General Description of the CSMP. The CSMP allows the solution of a wide variety of problems expressed in either analog block diagram form or a system of ordinary differential equations. It provides 34 functional blocks, including those normally associated with analog computers such as integrators and relays

plus a number of special purpose functions such as limiters and time delays. In addition, a number of signal sources are available such as pulse generators and noise (random number) generators. These functional blocks may be combined with FORTRAN algebraic statements allowing the solution of highly complex non-linear problems. Complete information may be obtained from the associated IBM user's manuals [Ref. 1, Ref. 2 and Ref. 3] ; however, additional descriptive information on pertinent aspects of CSMP will be interspersed within the text where it is felt necessary.

4.2.2 Second-Order Type One PLL. Before proceeding directly to the generalized second-order PLL, the standard second-order type one PLL was simulated to gain familiarity with the CSMP package. Fig. 4-1 shows the model used to simulate the second-order PLL in the absence of noise. Fig. 4-2 shows the program used in the simulation for the case of a frequency step input $\Delta\omega_i$. The structural segmentation of CSMP consists of three parts [Ref. 1, pp. 17-19] . The INITIAL portion is generally used for computation of initial conditions, expressing parameters in terms of more basic parameters or simply to insert constants. The DYNAMIC portion is analogous to block diagram or ordinary differential equation representation of the system dynamics and represents the heart of the CSMP package. This segment normally consists of a combination of CSMP and FORTRAN

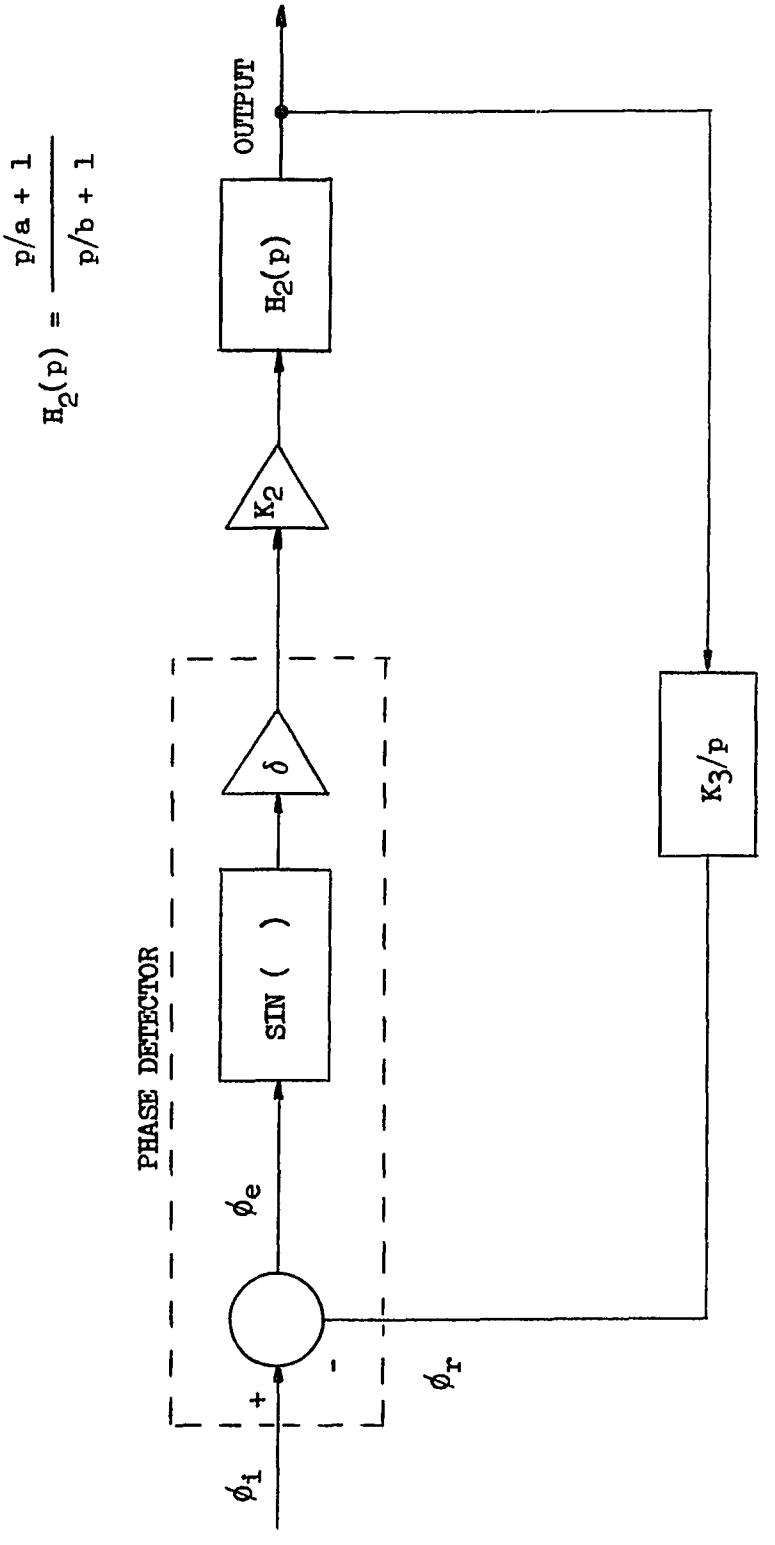

Fig. 4-1. Model of the second-order, type one PLL in the absence of noise.

```
TITLE SECOND ORDER TYPE ONE PLL STEP FREQUENCY RESPONSE
INITIAL
 CONSTANT A=2.94E4,B=1.88E3
          APRIM=1.0/A
          APRIM=1.0/A
          BPRIM=1.0/B
CONSTANT XK2=0.293,XK3=1.6E6
CONSTANT DELOMG=(6.28E2,6.28E3,6.28E4)
DYNAMIC
          ERROR=XINPUT-RETSIG
          PHDEOT=SIN(ERROR)
          XNEW1=LEDLAG(APRIM,BPRIM,PHDEOT)
          OUTPUT=XNEW1*XK2
          XNEW2=INTGRL(0.0,OUTPUT)
          RETSIG=XNEW2*XK3
          XNEW3=RAMP(0.0)
          XINPUT=XNEW3*DELOMG
TIMER DELT=0.0000001,FINTIM=0.001
PRINT XINPUT,ERROR,PHDEOT,OUTPUT,RETSIG
PRTPLOT XINPUT
LABEL INPUT VS TIME
PRTPLOT ERROR
LABEL PHASE ERROR VS TIME
PRLTPLOT PHDEOT
LABEL PHASE DETECTOR OUTPUT VS TIME
PRLTPLOT OUTPUT
LABEL SECOND ORDER TYPE ONE PLL OUTPUT VS TIME
PRTPLOT RETSIG
LABEL RETURN SIGNAL VS TIME
METHOD RKS
END
STOP
```

Fig. 4-2. CSMP program for second-order, type one PLL with a frequency step input.

statements. Finally, the TERMINAL portion, not used in the program of Fig. 4-2, allows computations which are desired after the completion of each run, such as incorporation of an optimization algorithm to modify parameters for the next run. The DYNAMIC segment in Fig. 4-2 follows the model of Fig. 4-1 with the following explanations being in order. The baseband filter is simulated using the CSMP LEDLAG function which is defined as follows

$$Y = \text{LEDLAG}\ (P_1\ ,\ P_2\ ,X) \tag{4-1}$$

where P_1 and P_2 are the parameter arguments and X is the input expression. The LEDLAG function is used to solve the equation

$$P_2\ \dot{Y} + Y\ = P_1\ \dot{X} + X \tag{4-2}$$

with the equivalent Laplace Transform

$$Y(s) = \frac{P_1\ S + 1}{P_2\ S + 1}\quad X(s) \tag{4-3}$$

It should be noted that CSMP functions such as LEDLAG are essentially a convenience factor and in actuality, they are composed of more fundamental operations. Fig. 4-3 shows the actual implementation of LEDLAG [Ref. 3, p. 160] .

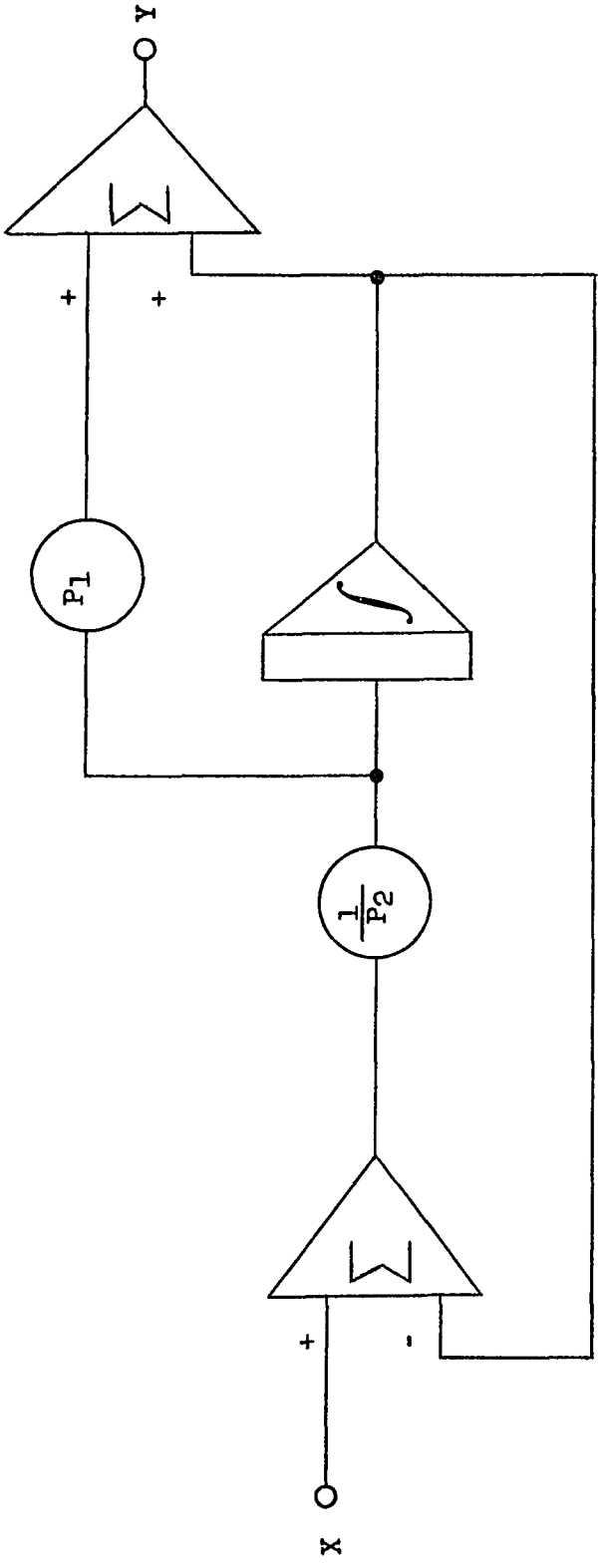

Fig. 4-3. CSMP implementation of the LEDLAG function.

Returning to Fig. 4-2, it is noted that the CSMP INTGRL function is used to represent the VCO. The INTGRL function represents the fundamental operation of integration and is defined as follows

$$Y = \text{INTGRL (IC, X)} \tag{4-4}$$

which is used to solve the equation

$$Y = \int_0^t X \quad t + IC \tag{4-5}$$

The input in this example is a frequency step or equivalently a ramp in phase. This is implemented using the CSMP RAMP function which is defined as

$$Y = \text{RAMP (P)} \tag{4-6}$$

and represents the function

$$\left.\begin{array}{ll} Y = 0 & t < P \\ Y = t - P & t \geq P \end{array}\right\} \tag{4-7}$$

Following the DYNAMIC segment in Fig. 4-2, is the TIMER statement. In its simplest form the TIMER specifies the integration interval

or step size of the independent variable designated as DELT, and FINTIM the maximum simulation value for the independent variable. The PRINT statement allows the desired system variables to be printed. In addition, any system variable may be plotted as a function of the independent variable using the PRTPLOT statement. The METHOD statement allows for the choice of integration method. Several different integration methods are available with CSMP including both fixed and variable integration step-size routines [Ref. 1, pp. 64-65] . The two variable step-size routines are fifth-order Milne predictor-corrector and fourth-order Runge-Kutta. The fixed-step routines, in order of decreasing complexity, are fourth-order Runge-Kutta, Simpson's, trapezoidal, second-order Adams, and rectangular. In addition, the option exists for implementing a user-supplied integration method. Finally, returning to Fig. 4-2, it is noted that multiple runs with different values of frequency step input $\Delta\omega_i$ are achievable simply by separating each of the desired values by a comma and enclosing them within parentheses in the defining equation for $\Delta\omega_i$ designated DELOMG.

The CSMP program of Fig. 4-2 was run with various integration methods over a range of values of integration interval to gain familiarity with the CSMP. The results obtained were in agreement with those theoretically predicted for the second-order, type one PLL [Ref. 4, p. 84] . In particular, the steady-

state tracking error followed the expression

$$\phi_e = \sin^{-1} \left(\Delta\omega_i / K \right) \qquad (4\text{-}8)$$

where K is the total loop gain. In addition to the step frequency input, a 1kHz test-tone input was also run again to develop facility with the CSMP package. Again, the results were in agreement with their theoretical prediction. Furthermore, the integration method and integration interval, over a range of approximately 10^{-6} to 10^{-7} seconds, were found not to critically affect the response. As will be detailed later in this chapter, the inclusion of noise in the simulation makes the choice of integration method and integration interval critical, if one is to achieve quantitatively viable results.

4.2.3 Generalized Second-Order PLL. Next, consider the CSMP implementation of the generalized second-order PLL in the absence of noise. First, from Chapter 2, it is recalled that the equivalent filter ERPLD in the absence of noise is as shown in Fig. 4-4. Also, recall that the equivalent filter realization leads directly to the generalized second-order PLL filter given by

$$F(P) = \frac{P^2/\beta + P/\gamma + 1}{P/b + 1} \qquad (4\text{-}9)$$

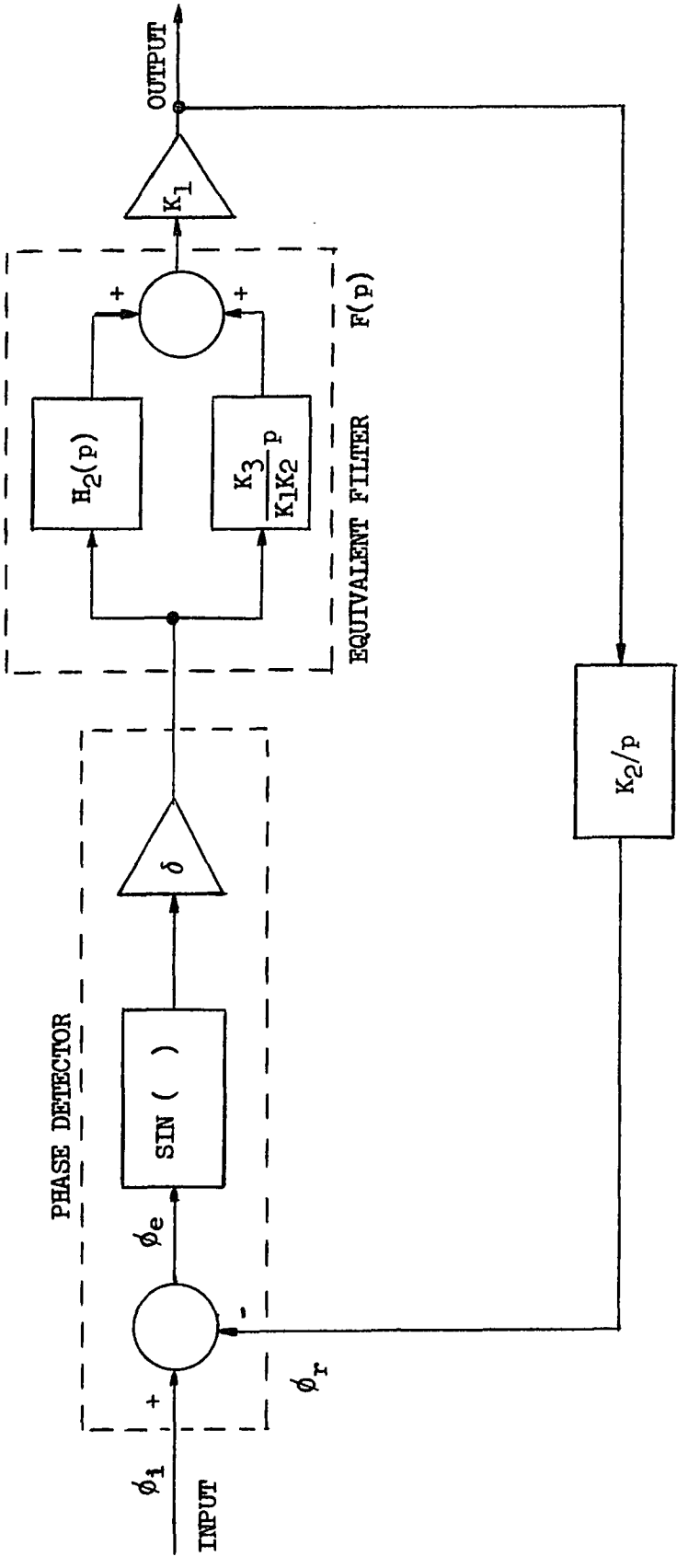

Fig. 4-4. Model of the equivalent filter EKPLD in the absence of noise.

This filter transfer function may be realized with CSMP as shown in Fig. 4-5 using conventional analog computer techniques [Ref. 5, pp. 80-86] . Alternately, the implementation shown in Fig. 4-6 can be used to simulate this filter.

When attempts were made to run the model of Fig. 4-4 with F(P) in either the equivalent filter or generalized filter configuration, for the sinusoidal test-tone case, the results were erroneous. Even when the sinusoidal function was removed, reducing the model to a linear circuit, the output waveform was observed to be non-sinusoidal in contradiction to the basic principle of linear theory. The cause of this problem can best be explained as follows. Unlike a true analog computer in which the simulated parameters are continuous, CSMP being a digital computer program must handle the parameters as discrete variables. Therefore, in Fig. 4-4 even though in the test-tone case ϕ_i is theoretically a sinusoidal waveform, in actuality, a discrete representation is used with samples separated by the integration interval. Then, if for example a 1KHz test-tone is used, instead of the spectrum consisting of a only single line at 1KHz, it consists of this line plus additional spectral component pairs centered about multiples of the sampling frequency $1/\Delta t$ and separated from this frequency by 1KHz. This is shown in Fig. 4-7.

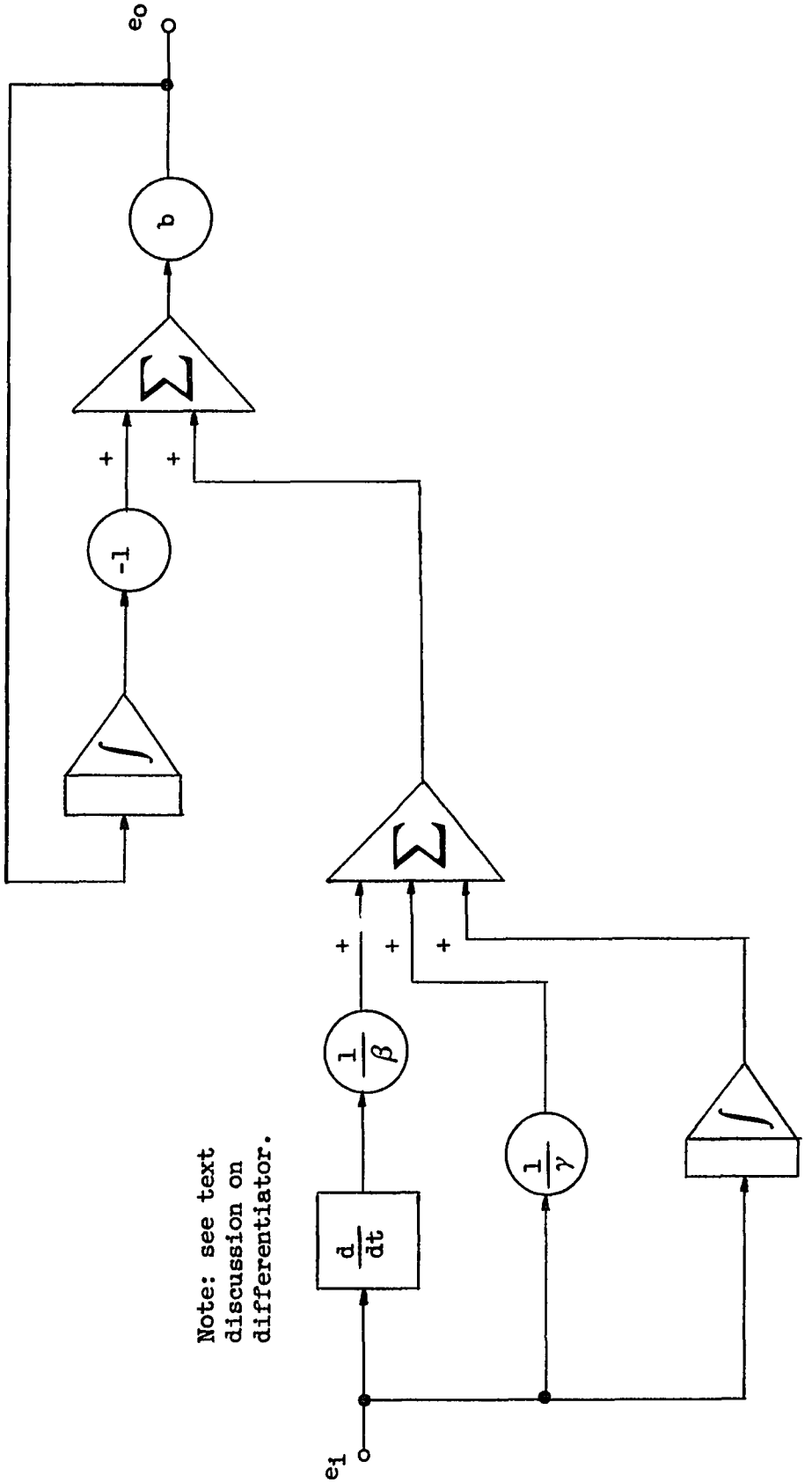

Fig. 4-5. CSMP implementation of the generalized second-order PLL filter.

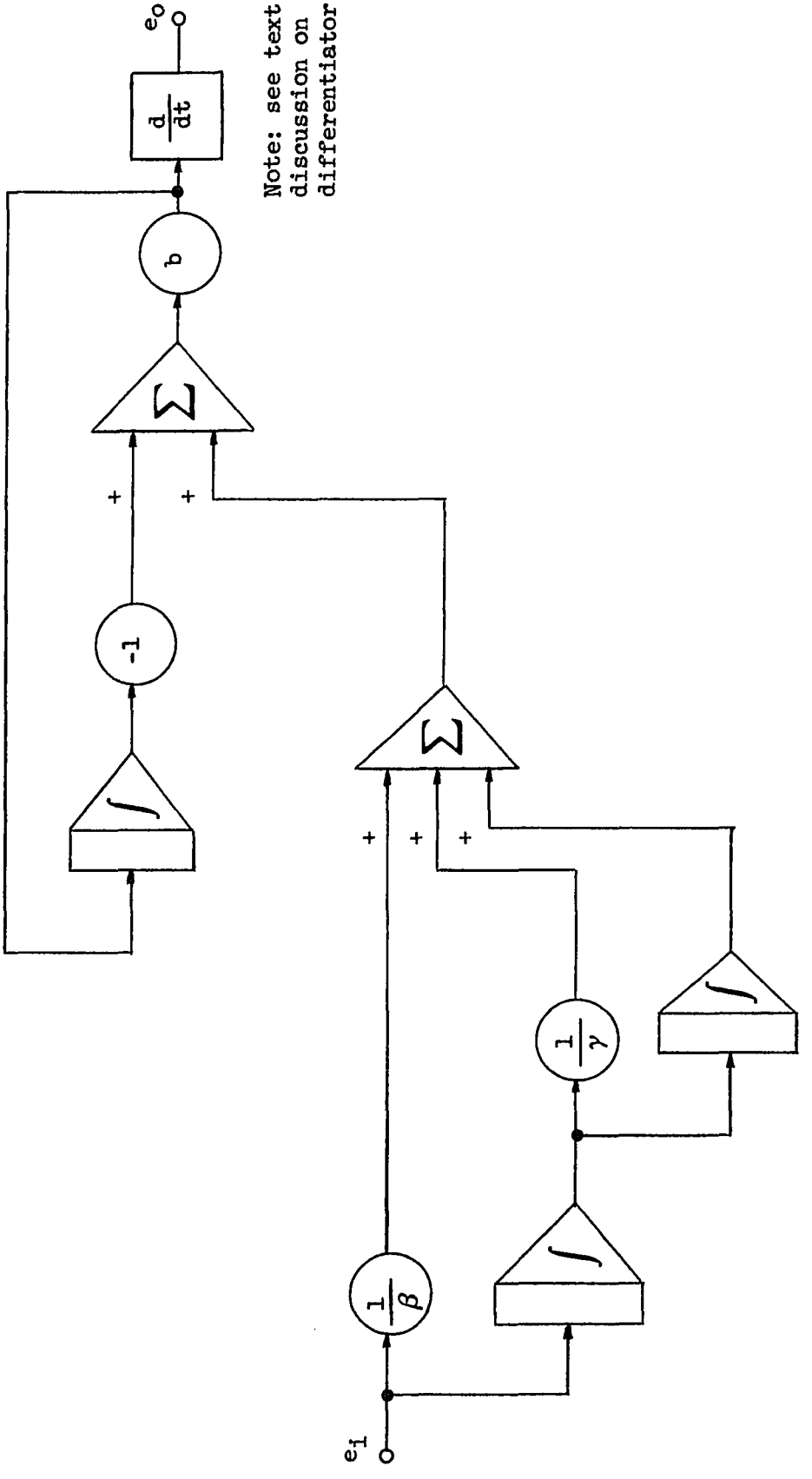

Fig. 4-6. Alternate CSMP implementation of the generalized second-order PLL filter.

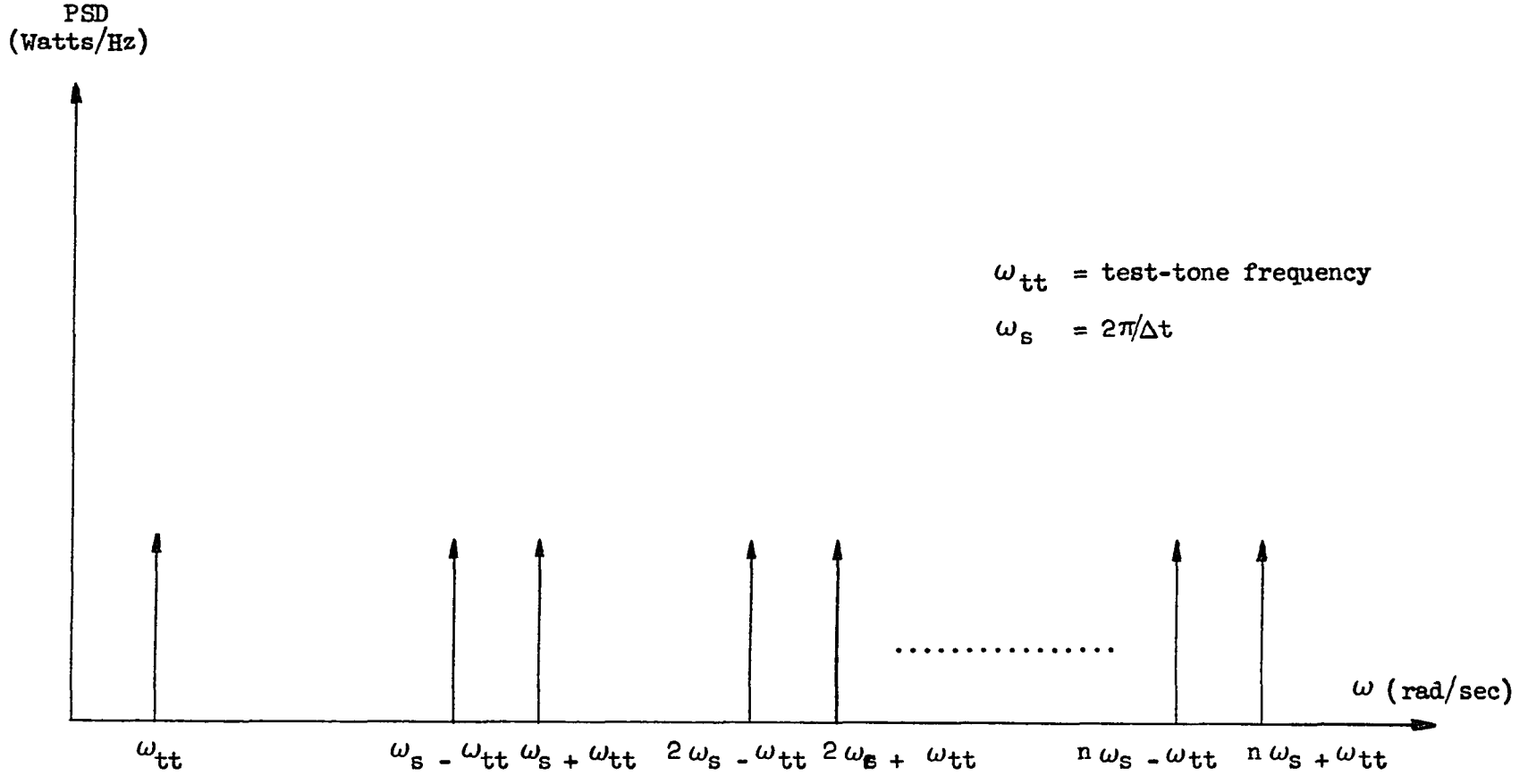

Fig. 4-7. Spectral components associated with test-tone implementation on CSMP (see also Appendix H).

A more detailed discussion of this analysis is given in Appendix H. Returning to the diagnosis, it is noted that in each of the filter representations of Fig. 4-4 through Fig. 4-6, a differentiator is required. Since the differentiator emphasizes higher frequencies, the additional spectral components caused by the discrete nature of the simulation resulted in the difficulties discussed earlier.

In order to remedy this problem, an imperfect differentiator was used in place of the theoretically perfect differentiator available with CSMP. The imperfect differentiator was achieved by following the DERIV function by a CSMP REALPL function [Ref. 1, p. 10] which is defined as follows

$$Y = \text{REALPL (IC, P, X)} \tag{4-10}$$

where IC is the initial condition, P is the parameter argument and X is the input expression. The REALPL function is used to solve the equation

$$X = P\,\dot{Y} + Y \tag{4-11}$$

with the equivalent Laplace Transform

$$Y(s) = \frac{1}{PS + 1}\,X(s) \tag{4-12}$$

Fig. 4-8 shows the CSMP implementation of the imperfect differentiator along with the Bode plot. To achieve the desired results, the cutoff frequency for the imperfect differentiator must be chosen high enough to act like a true differentiator for all frequencies of interest within the model, but low enough so that the undesired frequencies associated with the discrete nature of the waveforms are negligible. This factor will be of increasing importance when noise is added to the simulation later in this chapter.

After substituting the imperfect differentiator for the ideal differentiator in the loop filters shown in Figs. 4-4 through 4-6, the CSMP programs for the equivalent filter ERPLD and the generalized second-order PLL were again run, this time without the erroneous results encountered in the original programs. As a check on the validity of the new model, an analysis was performed on the linear model of the generalized second-order PLL again for the test-tone case, using Laplace transform techniques. This was compared against the results obtained in the CSMP simulation of the same linear model. The comparison showed both results to be precisely the same. The CSMP programs for the equivalent filter ERPLD and the generalized second-order PLL along with the linear analysis described above is given in Appendix I.

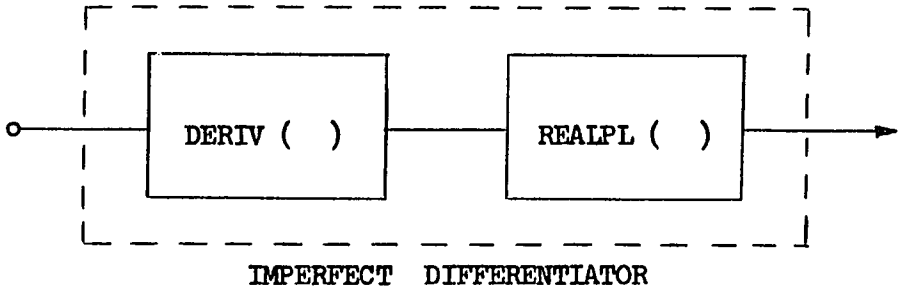

(a)

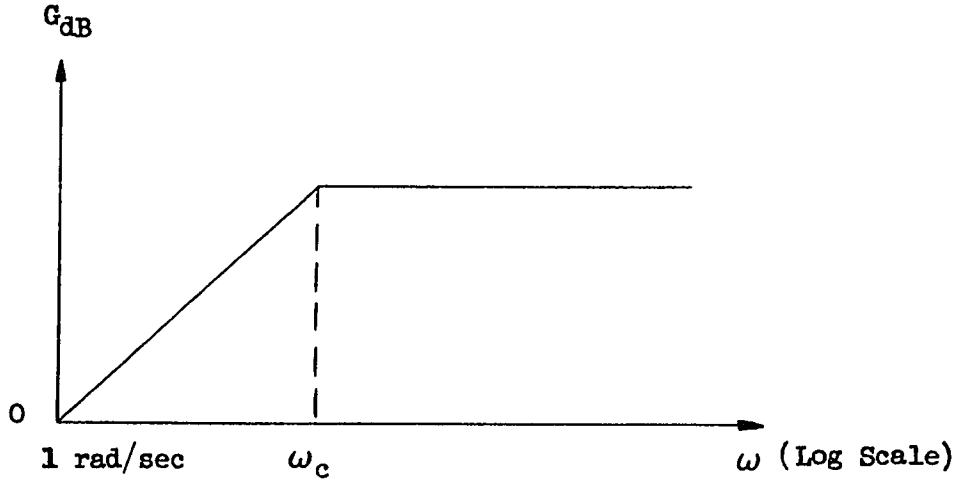

(b)

Fig. 4-8. CSMP implementation of the imperfect differentiator.
(a) Block diagram; (b) Bode plot.

4.2.4 Acampora and Newton ERPLD. The final simulation which was performed before introducing noise into the models was the original ERPLD configuration of Acampora and Newton [Ref. 6]. The model used in this simulation is shown in Fig. 4-9. When an attempt is made to run the CSMP program obtained from this model, an immediate problem is encountered. Unlike the equivalent filter ERPLD and the generalized second-order PLL discussed earlier, the configuration in Fig. 4-9 contains an algebraic loop around the phase detector, phase modulator path. An algebraic loop is one containing no memory functions. In so far as the CSMP package is concerned, the memory functions are integrators and delay functions. When such an algebraic loop is encountered in the simulation, the program will fail to run and a diagnostic message will be provided.

In order to resolve the difficulties associated with the algebraic loop, the CSMP IMPL function can be used. This function is defined as follows [Ref. 1, p. 9 and 44]

$$Y = \text{IMPL} \quad (\text{IC}, \text{P}, \text{FUNCT}) \tag{4-13}$$

where IC is the first estimate of the output Y , P is the desired accuracy and FUNCT is the output name of the last statement in the algebraic loop, definition. The IMPL or implicit function directs the system to perform a subiteration within the implicit

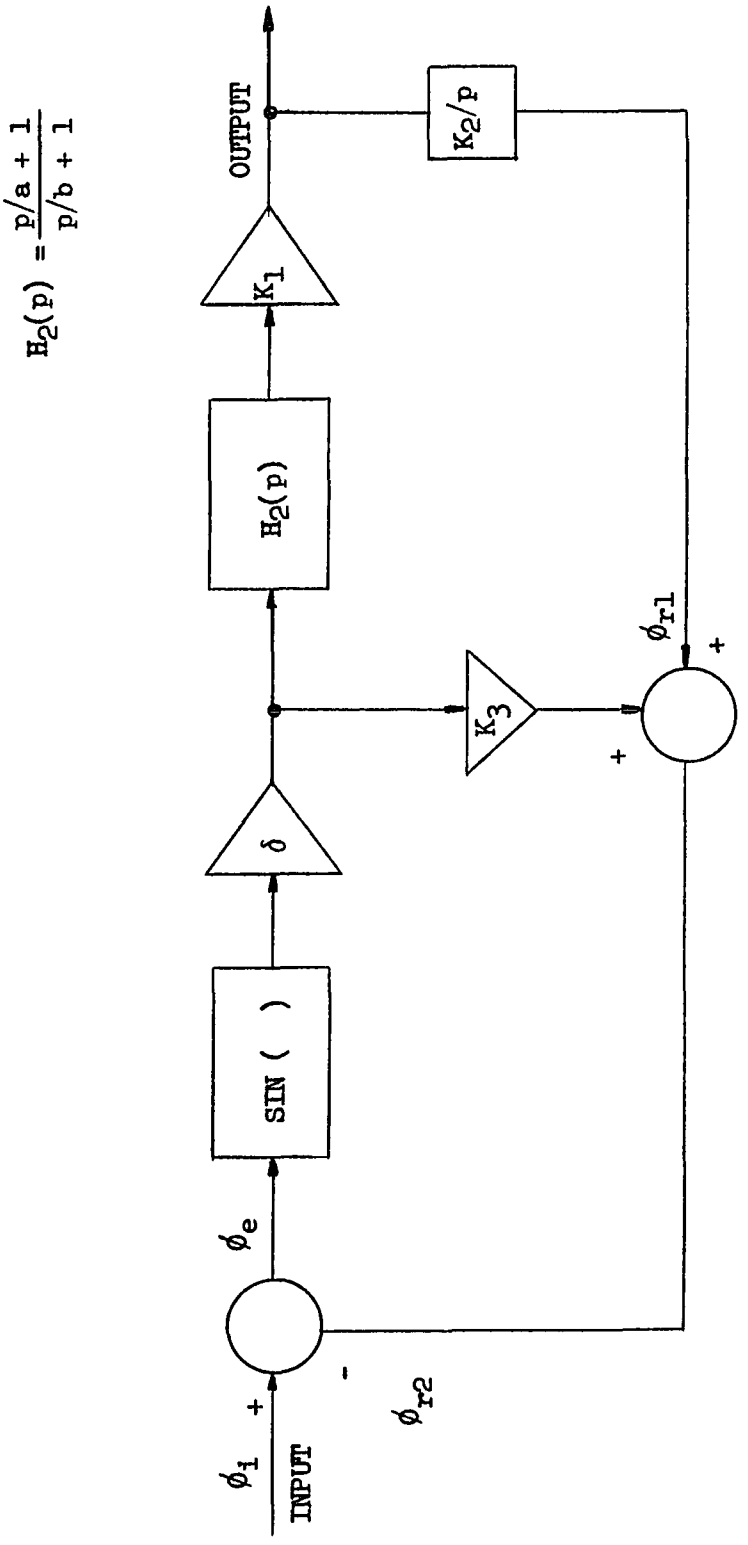

Fig. 4-9. Model of the Acampora and Newton ERPLD in the absence of noise.

loop at each instant of time, until the algebraic relationship is satisfied. Fig. 4-10 shows the CSMP program for the Acampora and Newton ERPLD test-tone case with the IMPL function used to resolve the algebraic loop. Note that the original Acampora and Newton parameters were used in the simulation [Ref. 6]. The results, as anticipated, were the same as those for the equivalent filter ERPLD and the generalized second-order PLL using the equivalent loop parameters (see Appendix I). The only difficulty encountered in using the IMPL function was a two to three fold increase in CPU time.

4.3 Addition of Noise to the Simulation.

4.3.1 General. In the preceding section the computer simulation of the generalized second-order PLL, the equivalent filter ERPLD, and the original Acampora and Newton ERPLD in the absence of noise was presented. It was found that choice of integration method and integration interval within wide limits did not critically effect the results. In this section the addition of noise to the simulation is considered. It will be shown that under these conditions, the choice of integration method and integration interval is indeed critical.

```
TITLE ERPLD ORIGINAL DOUBLE LOOP CONFIGURATION

INITIAL
CONSTANT        A = 2.94E4, B = 1.88E3
                APRIM = 1.0/A
                BPRIM = 1.0/B

DYNAMIC
                XNEW1 = IMPL (0.0, 0.0001, DUMVAR)
                ERROR = XINPUT - RETSIG
                PHDEOT = SIN (ERROR)
                XNEW2 = LEDLAG (APRIM, BPRIM, XNEW1)
                OUTPUT = XNEW2 * 2.94E-1
                XNEW3 = OUTPUT * 1.6E6
                XNEW4 = INTGRL (0.0, XNEW3)
                RETSIG = XNEW1 + XNEW4
                XNEW5 = SINE (0.0, 6.283E3, 0.0)
                XINPUT = 10.0 * XNEW5
                DUMVAR = PHEDEOT
TIMER DELT = 1.0E-7, FINTIM = 5.0E-2
PRTPLOT ERROR
LABEL PHASE ERROR VS TIME
PRTPLOT OUTPUT
LABEL ERPLD OUTPUT VS TIME
METHOD RECT
END
STOP
```

Fig. 4-10. CSMP program for the original Acampora and Newton ERPLD configuration; test-tone, no noise.

4.3.2 Effects of the PLL Model Due to Noise. In this section, as has been assumed in the previous chapters, the representative case of signal corruption by bandpass Gaussian noise will be considered. The input to the PLL having passed through a pre-detection filter may expressed as

$$a(t) = A \cos \left[\omega_i t + \phi_i(t) \right] + N(t) \qquad (4\text{-}14)$$

where the bandpass noise may be written as

$$N(t) = x(t) \cos \omega_i t - y(t) \sin \omega_i t \qquad (4\text{-}15)$$

On the assumption that N(t) is Gaussian with zero mean, having a PSD W(f), with arithmetic symmetry about ω_i, then x(t) and y(t) are also Gaussian with zero mean values. In addition, x(t) and y(t) are statistically independent and have spectra which have the lowpass equivalent shape of W(f) with twice the amplitude. Recall from Chapter 1 that the effect of this noise can be conveniently incorporated into the PLL simulation through the equivalent noise input term n(t) expressed by

$$n(t) = -\left[x(t)/A\right] \sin \phi_r + \left[y(t)/A\right] \cos \phi_r \qquad (4\text{-}16)$$

Fig. 4-11 shows the generalized second-order PLL with the equivalent noise input incorporated into the model. In order to make use of this model, n(t) as given by Eq.4-16 must be simulated.

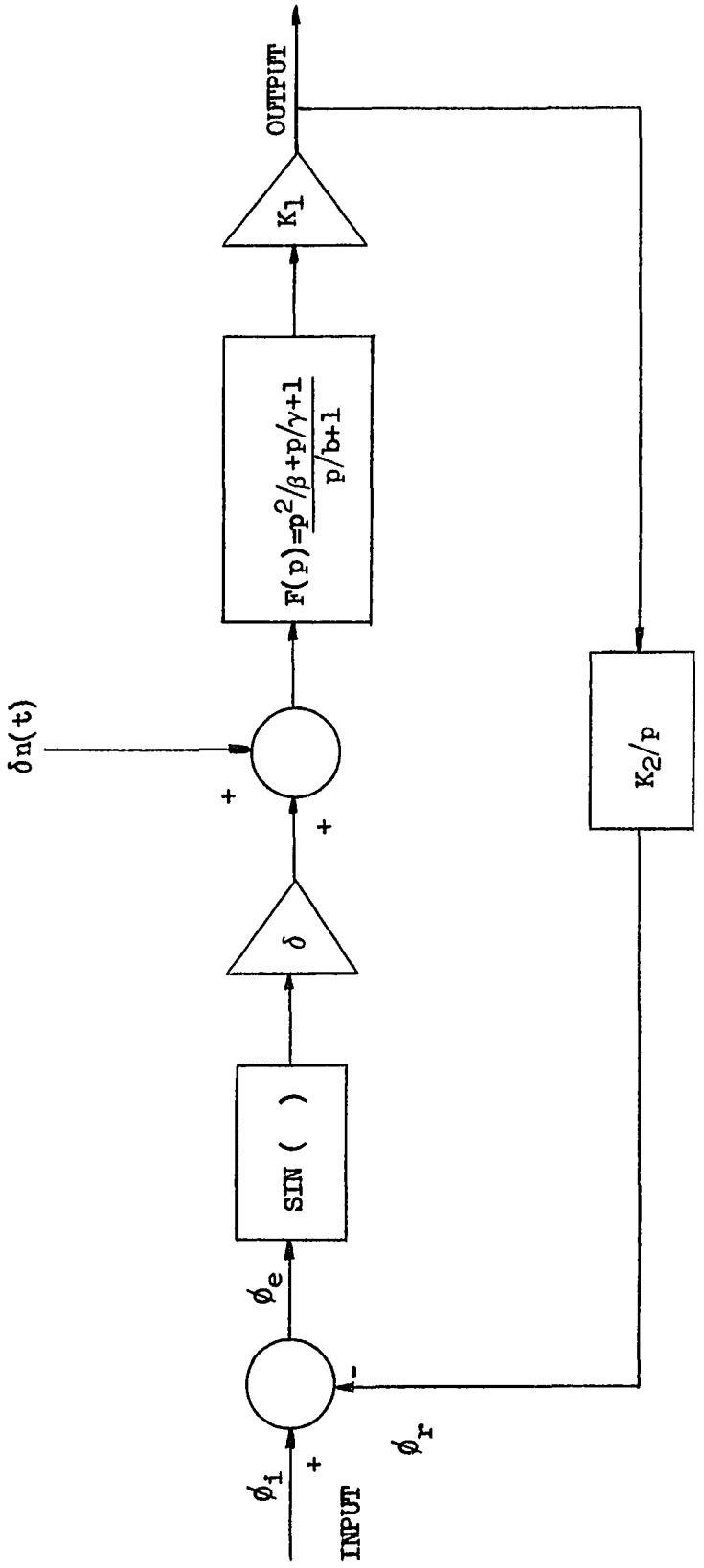

Fig. 4-11. Model of the generalized second-order PLL with the equivalent noise input.

Prior to simulating this exact expression, it is of interest to consider a frequently used simplification. It has been shown [Ref. 7, pp. 28-34] that for the case where N(t) has a symmetrical bandpass spectral density which is much wider than the bandwidth of $\phi_r(t)$, then n(t) is essentially the lowpass analog of N(t) with appropriate scaling. Thus, for example, if the input noise is assumed to be white with density η then the PSD of n(t) is also white with value $2\eta/A^2$ as shown in Fig. 4-12. In the next section, the simulation of the approximate equivalent noise input will be presented and it will be shown how these results can be directly applied to the simulation of the exact expression in Eq. 4-16.

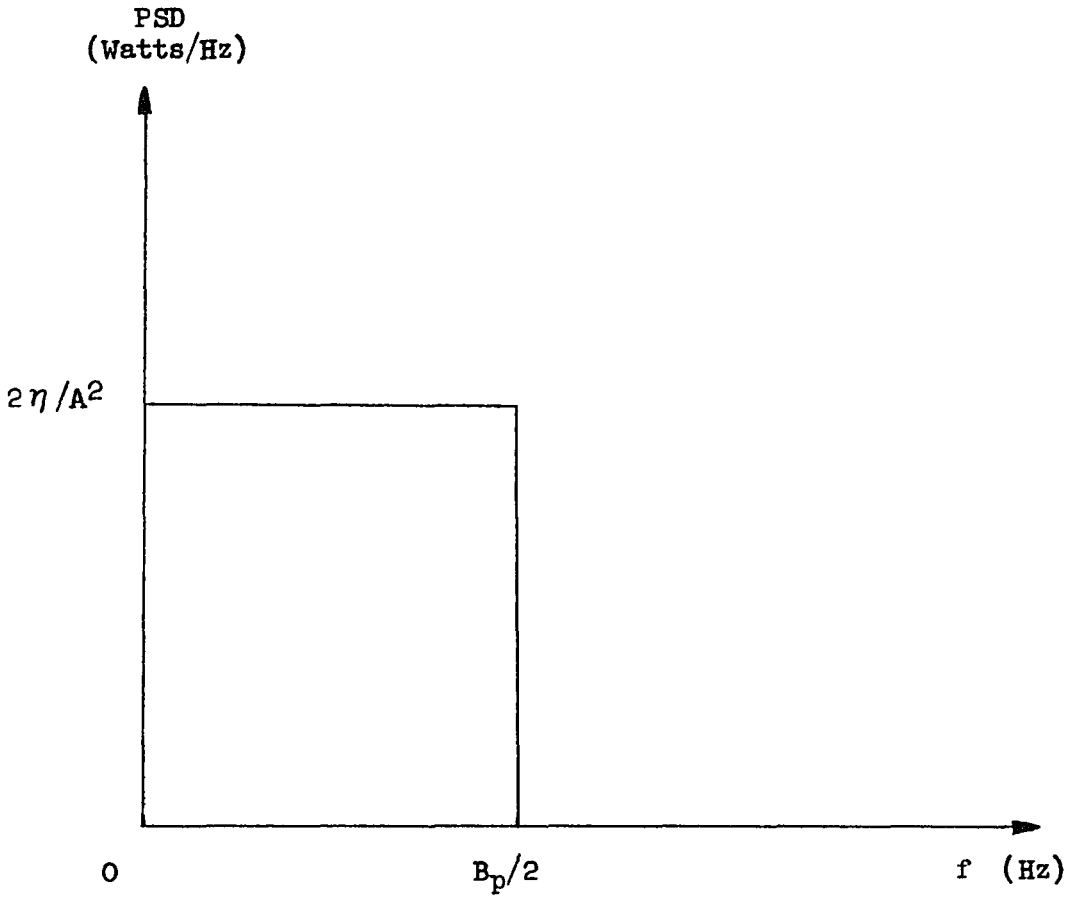

Fig. 4-12. Approximate equivalent noise input PSD.

4.3.3 Simulation of the Approximate Equivalent Noise Input. The fundamental applicable noise source available on CSMP is the GAUSS function [Ref. 1, p. 13 and Ref. 3, p. 154] which is defined as follows

$$Y = \text{GAUSS}\ (N,\ P_1\ ,\ P_2\ ) \tag{4-17}$$

where N is a seed for the random number generator, which may be any odd integer, P_1 is the required mean and P_2 is the required standard deviation. This function produces a normally distributed random number with a specified mean and standard deviation. Furthermore, different random number sequences may be obtained using different seeds. It is significant to realize that a major advantage of CSMP over conventional analog computers is the repeatability of the noise source. If a given set of parameters are set into the GAUSS function, the associated program may be run repeatedly with the insurance that the same random number sequence will be generated each time. Thus, for example, the response of a system with different sets of design parameters could be tested with the identical strip of noise. MacLaren et al. [Ref. 8] have detailed the mechanisms by which random numbers are generated on the digital computer.

When an attempt is made to use the GAUSS function to simulate the equivalent noise input, a problem is immediately encountered; that is, what is the PSD associated with the use of the GAUSS function. The answer to this question is not so simple, since the spectral properties of this source are seen to vary greatly depending upon the integration method and integration interval chosen. CSMP, as indicated previously, has a number of integration techniques available most of which are relatively complicated, having predictor and/or corrector expressions associated with them [Ref. 1, pp. 64-65] . Determination of the associated PSD for these methods is in general difficult and is an area which deserves future investigation. However, for the case of simple rectangular integration, the PSD has been shown to be given by [Ref. 9, pp. 26-14-15, Ref. 10, pp. 433-436 and Ref. 11, pp. 145-146]

$$W_o(f) = 2\sigma_G^2 \quad \Delta t \left[\frac{\sin \pi f \Delta t}{\pi f \Delta t} \right]^2 \qquad (4\text{-}18)$$

where σ_G is the standard deviation set into the GAUSS function, Δt is the integration interval, a mean of zero is assumed and the one-sided PSD is used. This expression is plotted in Fig. 4-13 (a).

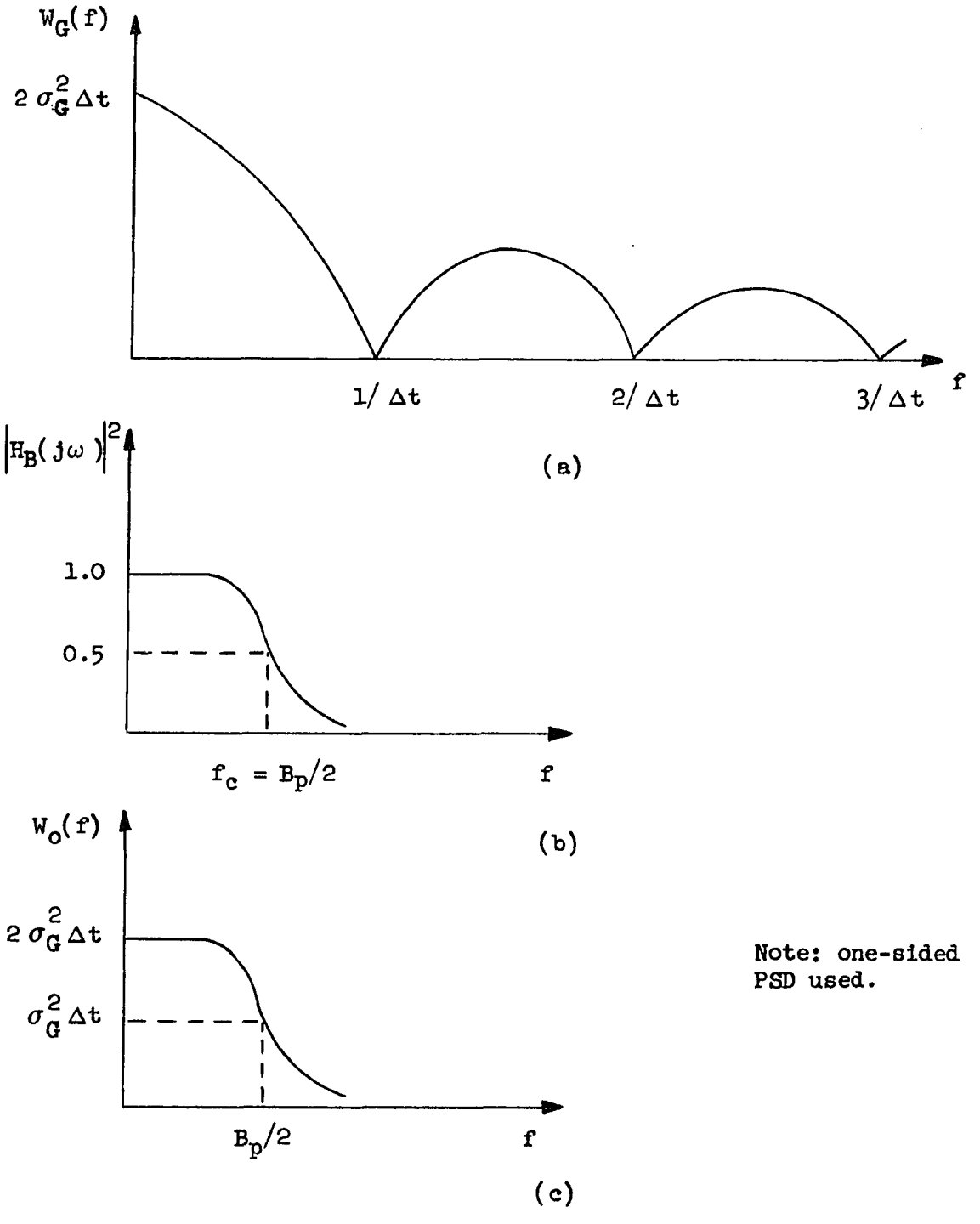

Fig. 4-13. Stages in the synthesis of the approximate equivalent noise input. (a) PSD of the GAUSS source using rectangular integration; (b) Butterworth filter characteristic; (c) Desired lowpass PSD.

Obviously, the PSD generated by the GAUSS function using the rectangular integration method is far from the desired lowpass shape ideally shown in Fig. 4-12. In order to achieve the desired shape the output of the GAUSS function may be passed through a lowpass Butterworth filter. A Butterworth configuration was used because of its maximally flat property and the fact that it is relatively straightforward to implement using CSMP. The use of the Butterworth function is available from a number of sources [Ref. 12, pp. 344-349 and Ref. 13, pp. 588-592] with the basic function given by

$$\left|H_B\,(j\omega)\right|^2 = \frac{1}{1 + (\omega/\omega_c)^{2n}} \qquad (4\text{-}19)$$

where n is the Butterworth filter order and ω_c is the 3dB cutoff frequency of the filter. The PSD obtained by passing the GAUSS function through a Butterworth filter is then given by

$$W_O(f) = 2\sigma_G^2 \Delta t \left[\frac{\text{Sin } \pi f \Delta t}{\pi f \Delta t}\right]^2 \left[\frac{1}{1 + \left(\frac{f}{f_c}\right)^{2n}}\right] \qquad (4\text{-}20)$$

In order to achieve the desired PSD, fc is first chosen equal to Bp/2. Next, Δt must be small enough such that the sinc function in Eq. 4-20 is essentially unity out to the frequency Bp/2. Table 4-1 shows the variation of the square of the sinc

Table 4-1. $\mathrm{Sinc}^2(\pi f \Delta t)$ evaluated over a range of Δt at f = 17.5 kHz.

Δt (Sec)	$\mathrm{Sinc}^2 (\pi f \Delta t)$
10^{-5}	0.903222
10^{-6}	0.998993
10^{-7}	0.999989
10^{-8}	0.999999

function for a range of values of Δt at a frequency of 17.5 kHZ. This point was chosen corresponding to a predetection bandwidth of 35KHZ which will be used in the single-channel FM voice case to be simulated subsequently. From this table it can be seen that a value of Δt of approximately 10^{-6} or smaller, meets the unity amplitude requirement previously discussed. Next the filter order n must be chosen to give the desired sharpness in the PSD characteristic being simulated. A practical note is in order here concerning this choice. Since in the actual case, the predetection filter used with a PLL would typically be a 6th order Butterworth, this would be a realistic choice for n. Fig. 4-13 shows the various stages in the synthesis of the approximate form of the equivalent noise input n(t). Finally, the amplitude of the PSD must be chosen properly corresponding to the desired carrier-to-noise ratio to be simulated. The amplitude of the desired PSD (see Fig. 4-12) may be expressed in terms of the predetection bandwidth and the carrier-to-noise ratio measured in the predection bandwidth as follows

$$\frac{2\eta}{A^2} = \frac{1}{B_p \, CNR_{IF}} \qquad (4\text{-}21)$$

The amplitude of the PSD in Fig. 4-13(c) is then equated to the above expression yielding

$$2\,\sigma_G^2 \Delta t = \frac{1}{B_P\ CNR_{IF}} \qquad (4\text{-}22)$$

or

$$\sigma_G = \sqrt{\frac{1}{2\Delta t\ B_P\ CNR_{IF}}} \qquad (4\text{-}23)$$

Therefore, for a given simulation with fixed values for Δt and B_P , the carrier-to-noise ratio being simulated is achieved by setting the value of the standard deviation obtained in Eq. 4-23 into the GAUSS function. Note that when dealing with Butterworth filters, expressions are normally given in terms of 3dB bandwidths whereas when discussing power spectral densities noise bandwidths are used. For the values of Butterworth filter order used in the subsequent simulations, the difference between these two bandwidths is generally negligibly small.

Having developed the basic theory for implementing the approximate form of the equivalent noise input, the next step is to write the CSMP program for the model and test it. A detailed analysis of the Butterworth implementation is given in Appendix J with the highlights presented here. The transfer function for a sixth-order Butterworth filter with a 3dB cutoff frequency of 17.5 kHz is given by

$$H_B(s) = \frac{1.772\times10^{30}}{(s^2 + 5.698\times10^4 s + 1.21\times10^{10})(s^2 + 1.555\times10^5 s + 1.21\times10^{10})} \cdot \frac{1}{(s^2 + 2.125\times10^5 s + 1.21\times10^{10})} \quad (4\text{-}24)$$

Each section of the Butterworth filter may be implemented using the CSMP CMPXPL function which is defined as follows

$$Y = CMPXPL\ (IC_1,\ IC_2\ ,\ P_1\ ,\ P_2\ ,\ X) \quad (4\text{-}25)$$

where IC_1 , and IC_2 are intital conditions, P_1 and P_2 are parameter arguments and X is the input expression. The CMPXPL function is used to solve the equation

$$\ddot{Y} = 2P_1\ P_2\ \dot{Y} + P_2^2\ Y = X \quad (4\text{-}26)$$

with the equivalent Laplace Transform

$$Y(s) = \frac{1}{S^2 + 2\ P_1\ P_2\ S + P_2^2}\ X(s) \quad (4\text{-}27)$$

The block diagram showing the complete CSMP implementation of the approximate equivalent noise input is shown in Fig. 4-14. The next

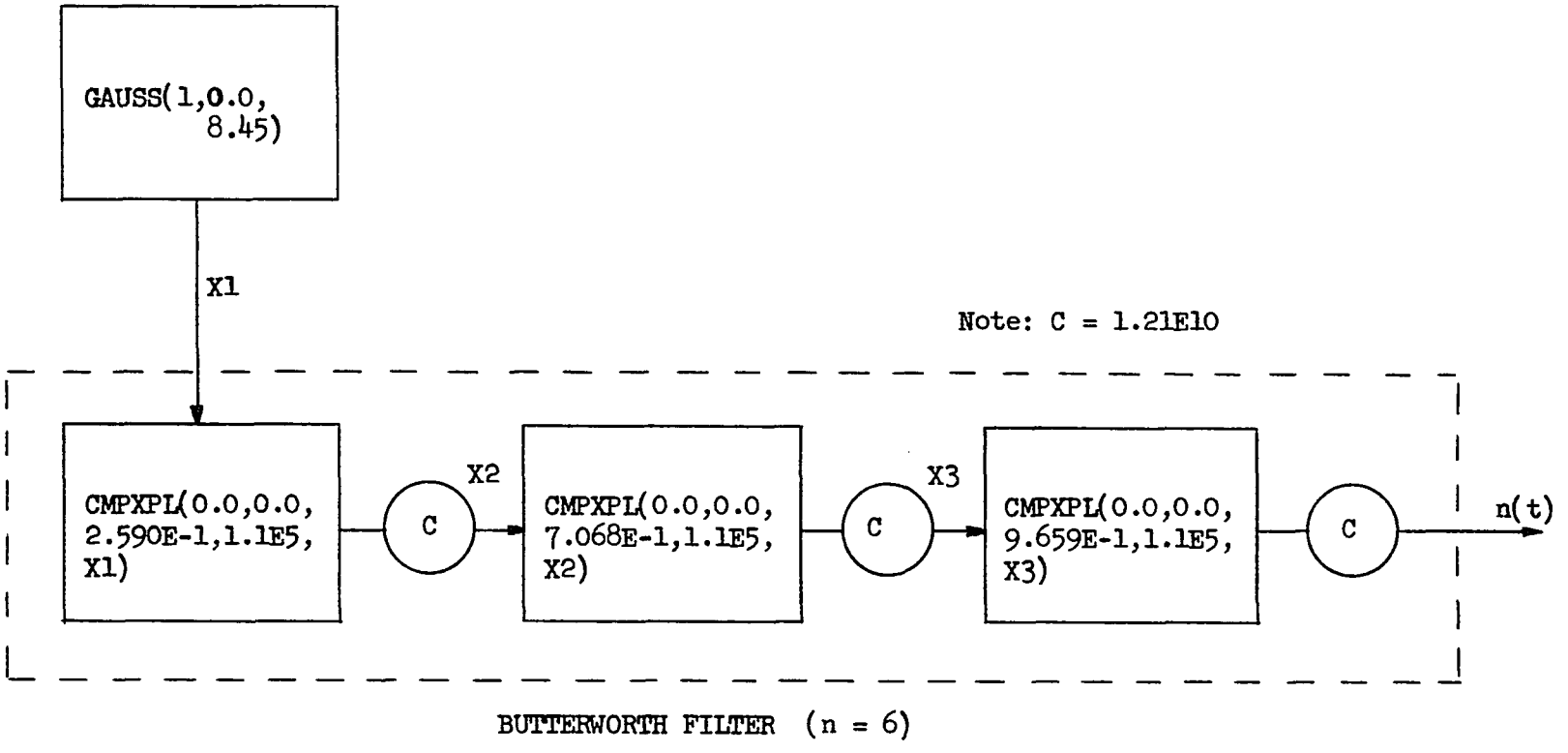

Fig. 4-14. CSMP implementation of the approximate equivalent noise input.

step is to test the approximate equivalent noise input by comparing the simulation results against those predicted by theory. The definition of the mean-square value of a random noise voltage n(t) is given by

$$\overline{n^2(t)} = \lim_{T\to\infty} \frac{1}{2T}\int_{-T}^{T} n^2(t)dt \qquad (4\text{-}28)$$

Since in the case under consideration, a digital computer is being used to simulate the noise, only a finite sample of the noise is available and therefore the mean-square value of the noise must be approximated by

$$\overline{n^2(t)} \cong \frac{1}{T}\int_{0}^{T} n^2(t)\,dt \qquad (4\text{-}29)$$

The PSD represents average power per cycle of bandwidth (watts per hertz) and when integrated over all frequencies yields the mean-square value (or average power) of the waveform therefore

$$\int_0^\infty W(f)df = \overline{n^2(t)} \qquad (4\text{-}30)$$

A series of test runs were made for the approximate equivalent noise input in which the mean-square value of the source was determined. The CSMP program used to accomplish this is shown in Fig. 4-15. In this analysis a strip of noise of 0.05 seconds duration, corresponding to about 875 independent samples from the Butterworth filter, was used. In addition, a value of CNR_{IF} equal to 3dB was chosen as a representative value in testing the approximate equivalent noise input.

Eq. 4-30 represents the basic criteria used in the test, i.e., the mean-square value of noise was compared against the area under the PSD curve. This area, shown in Fig. 4-13(c), can be determined as follows. Starting with Eq. 4-20 and recalling that for Δt equal to about 10^{-6} seconds or less the sinc function is essentially unity, Wo(f) is then given by

$$W_o(f) = 2\,\sigma_G^2\,\Delta t \left[\frac{1}{1 + \left(\frac{f}{f_c}\right)^{2n}}\right] \qquad (4\text{-}31)$$

Then

$$\int_0^\infty W_o(f)\,df = \int_0^\infty 2\,\sigma_G^2\Delta t \cdot \frac{df}{1 + \left(f/f_c\right)^{2n}} \qquad (4\text{-}32)$$

The integral on the right side of Eq. 4-32 can be evaluated from

```
TITLE APPROX. EQUIVALENT NOISE SOURCE TEST PROG.

DYNAMIC
                XNEW1 = GAUSS (5, 0.0, 5.35)
                XNEW2 = CMPXPL (0.0, 0.0, 2.590E-1, 1.1E5, XNEW1)
                XNEW3 = XNEW2 * 1.21E10
                XNEW4 = CMPXPL (0.0, 0.0, 7.068E-1, 1.1E5,XNEW3)
                XNEW5 = XNEW4 * 1.21E10
                XNEW6 = CMPXPL (0.0, 0.0, 9.659E-1, 1.1E5, XNEW5)
                EQNOIN = XNEW6 * 1.21E10
                XNEW7 = EQNOIN**2
                XNEW8 = INTGRL (0.0,XNEW7)
                XNEW9 = RAMP (0.0)
                XMSQ = XNEW8/XNEW9
TIMER DELT = 2.5E-7, OUTDEL = 1.0E-4, FINTIM = 5.0E-2
PRTPLOT XMSQ
LABEL MEAN-SQUARE VALUE OF NOISE SOURCE
METHOD RECT
END
STOP
```

Fig. 4-15. CSMP program to determine mean-square value of approximate equivalent noise input.

standard tables of definite integrals [Ref. 14, p. 454] with the result

$$\int_0^\infty W_o(f)\, df = 2\,\sigma_G^2\,\Delta t\, f_c \left[\frac{\pi}{2n\ \mathrm{Sin}\ \frac{\pi}{2n}}\right] \qquad (4\text{-}33)$$

where it is recalled that fc was chosen equal to B_p /2. The bracketed term in Eq. 4-33 actually represents the correction factor between using the 3dB bandwidth and the noise bandwidth in the Butterworth filter characteristic, as discussed earlier. This factor evaluated for a range of values of n is given in Table 4-2. From this table it can be seen that there is a very small difference (about one percent) between the 3dB and noise bandwidths for a sixth order Butterworth lowpass filter characteristic.

Returning to the program of Fig. 4-15, it is noted that since the noise source is statistical in nature, simply taking the mean-square value of a strip of noise 0.05 seconds in duration from this source is less than desirable. Rather, it is more meaningful to make a number of runs, 0.05 seconds in duration, with different seeds in the GAUSS function, thereby obtaining a set of values of mean-square value of the noise source. By using this data for purposes of comparison with the theoretically predicted value, additional confidence in the results is obtained. This technique

Table 4-2. Correction factor between 3 dB and noise bandwidths for lowpass Butterworth filter.

Butterworth Filter Order n	1.0/Sinc($\pi/2n$)
2	1.1107
4	1.0261
6	1.0115
8	1.0064
10	1.0041

was used to obtain the results shown in Fig. 4-16. This figure shows the results of the mean-square value of the noise source as a function of integration interval Δt. For each value of Δt, the standard deviation in the GAUSS function was adjusted to correspond to the same test point (CNRIF equal to 3dB) according to Eq. 4-23. In addition, each of the points was arrived at by maing three separate runs of 0.05 seconds duration with different seeds and averaging the results. For purposes of comparison, the results for an approximate equivalent noise input using a tenth-order Butterworth filter are shown.

The significance of this set of curves is the deviation of the curves from the theoretical value as larger and larger values of Δt are used. The greater deviation of the tenth-order Butterworth from the theoretical value than the sixth-order results, particularly at the smaller values of Δt may be due to a cumulative error caused by the additional tandem filter sections required in the higher order filter. Fig. 4-17 shows the economic aspect of the approximate equivalent noise input simulation. The curves show the amount of CPU time required for the simulation of 0.05 seconds of the noise source as a function of the integration interval used. Again, both sixth and tenth-order Butterworth filter results are shown for comparison. It must be emphasized that the CPU time shown is for the noise source only and does not include that associated with the

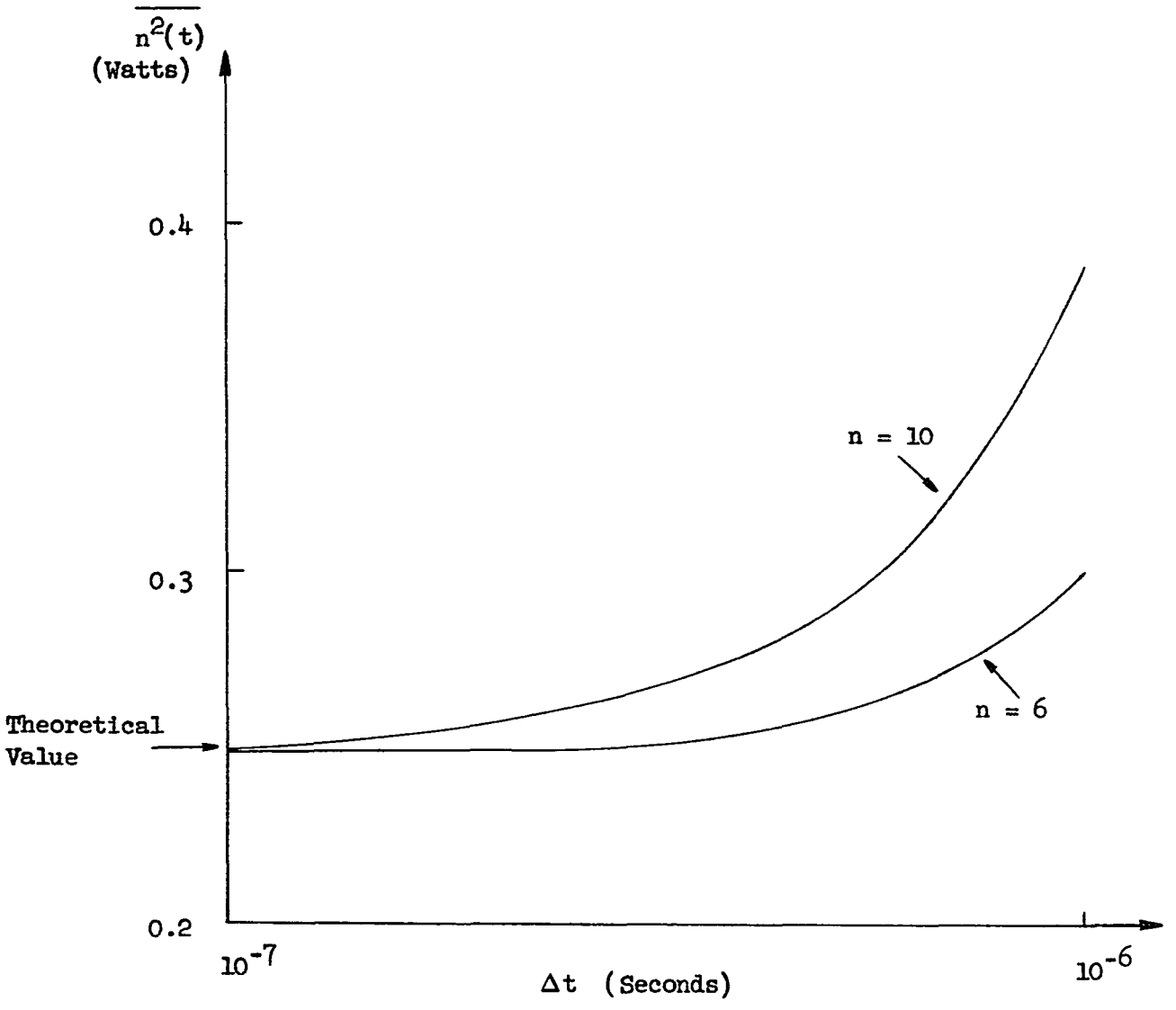

Fig. 4-16. Results of approximate equivalent noise input test program.

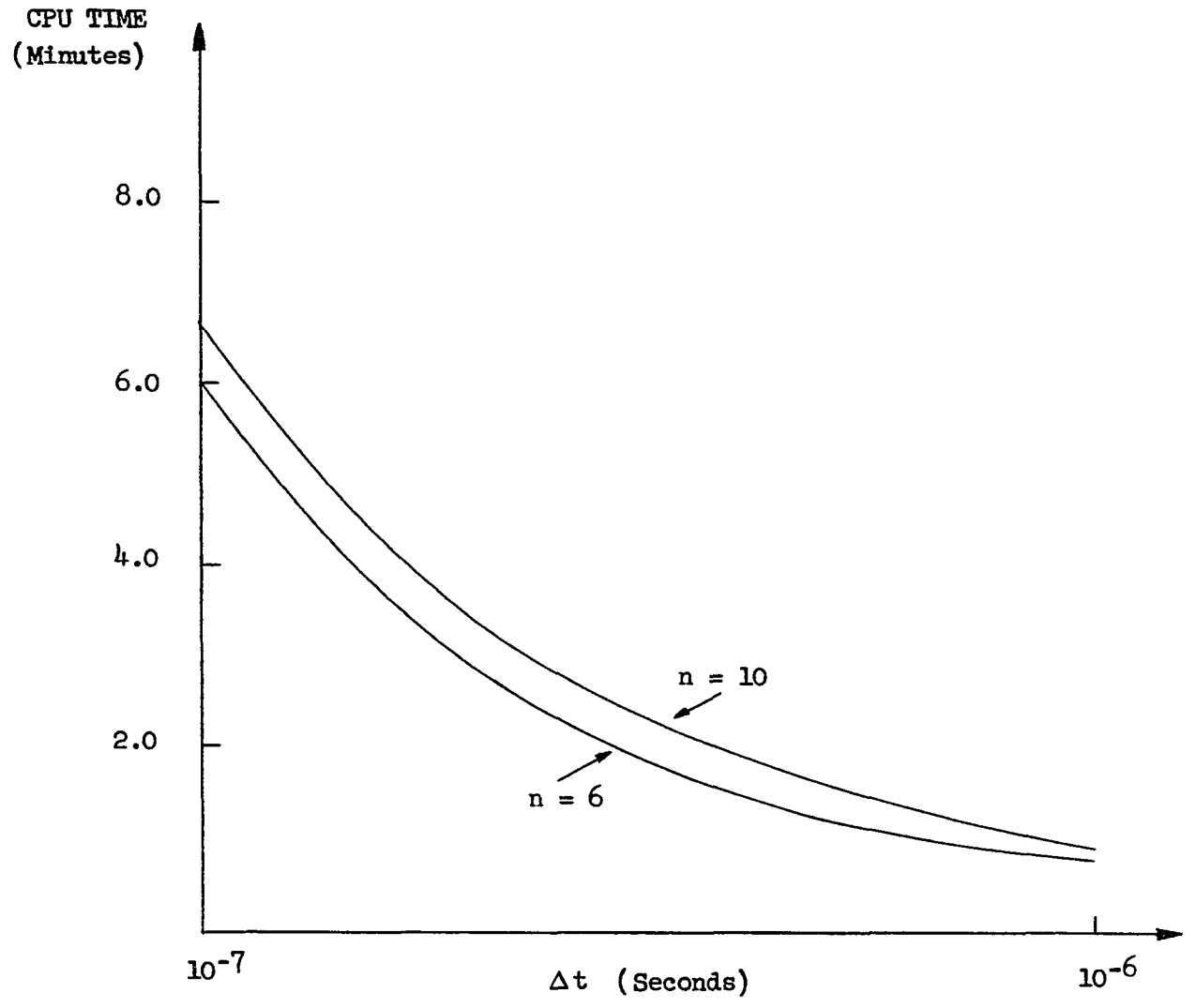

Fig. 4-17. CPU time requirements for simulation of 0.05 seconds of approximate equivalent noise input.

remainder of the PLL. From Figs. 4-16 and 4-17, a trade-off in the PLL simulation in the presence of noise becomes readily apparent. The integration interval must be chosen small enough to achieve quantitatively viable results, yet if Δt is too small, prohibitively high CPU times result. For the case where the noise source incorporates a sixth-order Butterworth filter, which shall be true in the subsequent simulations, a Δt in the range of approximately 1.0×10^{-7} to 5.0×10^{-7} seconds appears appropriate.

4.3.4 Simulation of the Exact Equivalent Noise Input. As indicated earlier, the results of the preceding section can be directly applied to the simulation of the exact equivalent noise input as expressed by Eq. 4-16. Referring back to this equation, it is recalled that x(t) and y(t) are both Gaussian with zero mean values. Furthermore, x(t) and y(t) are statistically independent and have PSD's which have the lowpass equivalent shape of the input noise PSD with twice the amplitude. The PSD of x(t)/A and y(t)/A are then the same as that shown in Fig. 4-12 for the case of white input noise with perfect predetection filtering.

The first step in simulating the exact equivalent noise input is the generation of two statistically independent lowpass spectra of the type discussed in the previous section. One

possible approach is to simply set up two noise sources of the type given in Fig. 4-15 and use different seeds in the GAUSS functions. From the point of view of statistical independence, a more desirable approach is one in which a single GAUSS function is used and the noise samples are alternately channeled into two lowpass Butterworth filters. A block diagram of the CSMP implementation of the exact equivalent noise input using this method is shown in Fig. 4-18. Fig. 4-19 shows the segment of a CSMP program used to simulate this noise source for the illustrative case of Δt equal to 2.5×10^{-7} seconds. The operation of this noise source can be explained with the aid of Fig. 4-20 which shows the various steps in the synthesis of the desired noise waveform. The fundamental strip of noise is generated by the GAUSS as shown in Fig. 4-20 (a). The output of the GAUSS function is then multiplied by the CSMP IMPULS function [Ref. 1, p. 10] which is defined as follows

$$Y = \text{IMPULS}\ (P_1\ ,\ P_2\ ) \qquad (4\text{-}34)$$

This function generates a train of impulses of unity height beginning at time P_1 and separated by P_2 seconds. The impulse train used is shown in Fig. 4-20(b) with the result of the multiplication shown in (c). This procedure, then, selects every other sample from the GAUSS source. Next, the CSMP ZHOLD function is used [Ref. 1, p. 6 and Ref. 3, p. 180] to hold each of these samples for an additional iteration as shown

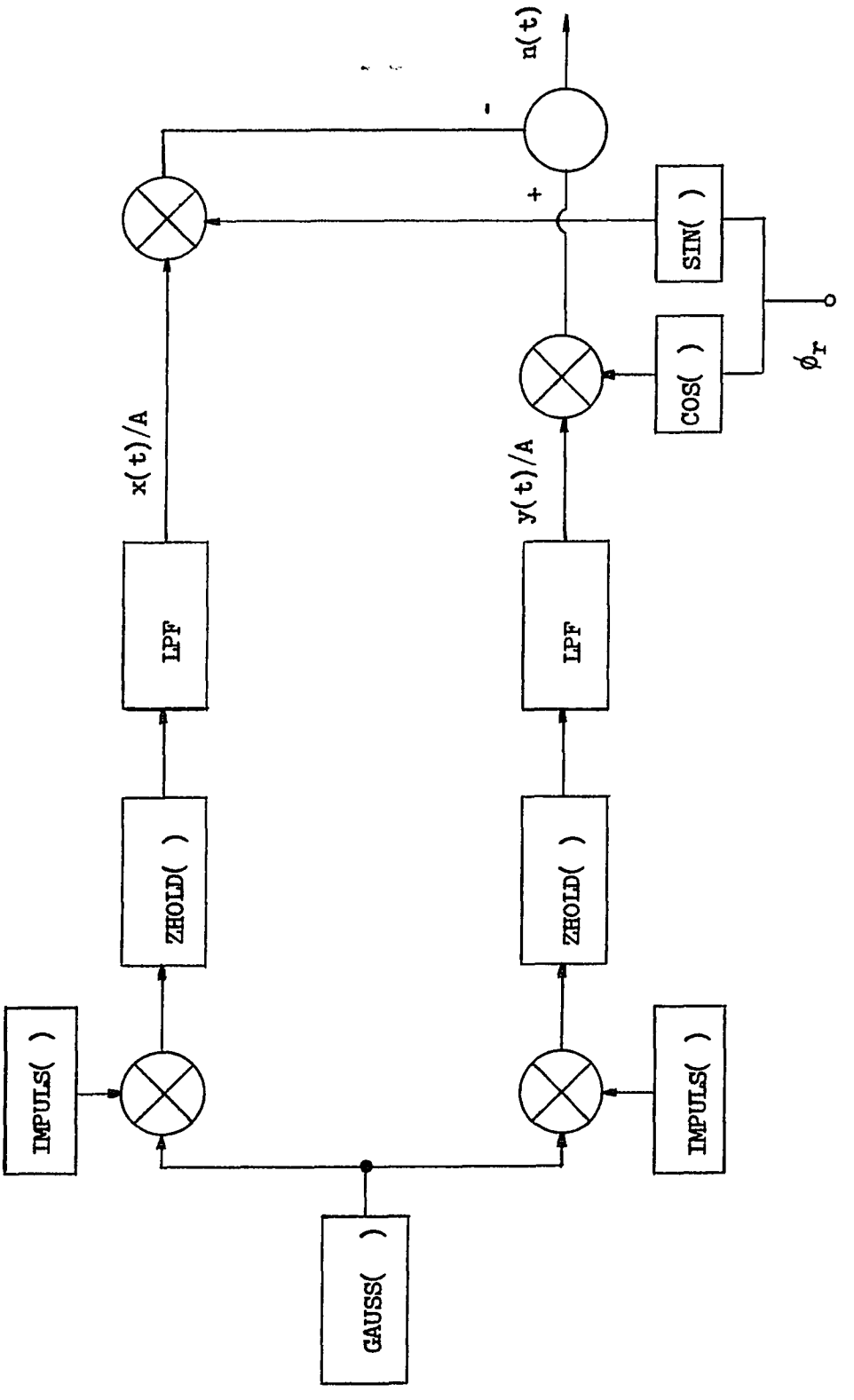

Fig. 4-18. CSMP implementation of the exact equivalent noise input.

```
. . . . . .

XNEWA=GAUSS(5.0.0,3.779)
XNEWB=IMPULS(0.0,5.0E-7)
XNEWC=XNEWA*XNEWB
XNEWD=XNEWC**2
EQNOA=ZHOLD(XNEWD,XNEWC)
XNEWE=CMPXPL(0.0,0.0,2.590E-1,1.1E5,EQNOA)
XNEWF=XNEWE*1.21E10
XNEWG=CMPXPL(0.0,0.0,7.068E-1,1.1E5,XNEWF)
XNEWH=XNEWG*1.21E10
XNEWI=CMPXPL(0.0,0.0,9.659E-1,1.1E5,XNEWH)
EQNO1=XNEWI*1.21E10
XNEWJ=IMPULS(2.5E-7,5.0E-7)
XNEWK=XNEWA*XNEWJ
XNEWL=XNEWK**2
EQNOB=ZHOLD(XNEWL,XNEWK)
XNEWM=CMPLPL(0.0,0.0,2.590E-1,1.1E5,EQNOB)
XNEWN=XNEWM*1.21E10
XNEWO=CMPXPL(0.0,0.0,7.068E-1,1.1E5,XNEWN)
XNEWP=XNEWO*1.21E10
XNEWQ=CMPXPL(0.0,0.0,9.659E-1,1.1E5,XNEWP)
EQNO2=XNEWQ*1.21E10
YNEWA=SIN(RETSIG)
YNEWB=COS(RETSIG)
YNEWC=EQNO1*YNEWA
YNEWD=EQNO2*YNEWB
EQNOIN=YNEWD-YNEWC

. . . . . .
```

Fig. 4-19. Segment of CSMP program used to simulate exact equivalent noise input.

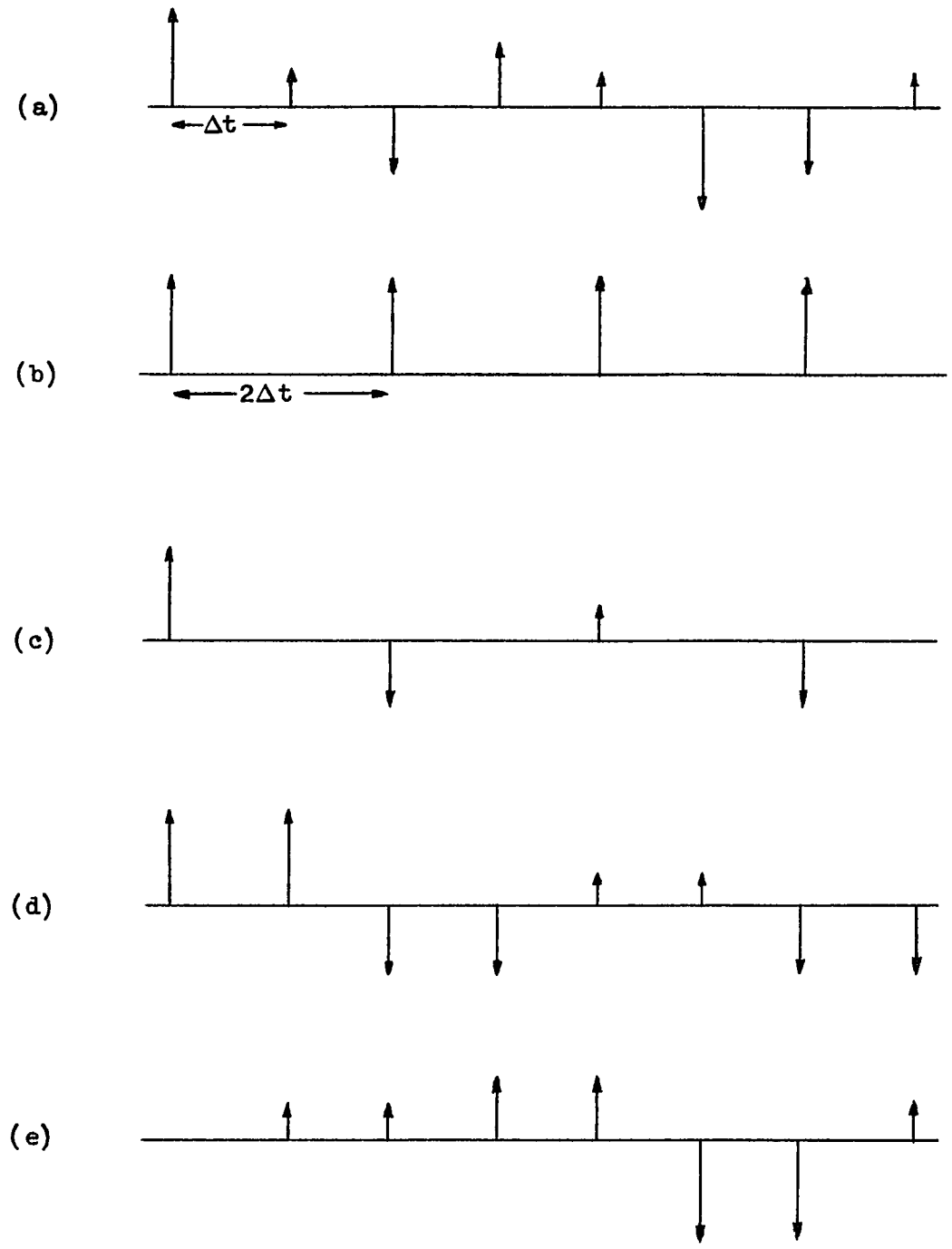

Fig. 4-20. Synthesis of statistically independent noise source pair. (a) GAUSS output; (b) Impulse train used to sift GAUSS output; (c) Sifted output; (d) Sifted output after applying zero-order hold; (e) Second source.

in Fig. 4-20(d). The ZHOLD function is defined as

$$Y = \text{ZHOLD}\ (X_1\ ,\ X_2\ ) \tag{4-35}$$

where

$$\left.\begin{aligned} Y &= X_2 \qquad \text{for} \qquad X_1 > 0 \\ Y &= \text{LAST OUTPUT for} \qquad X_1 \leq 0 \end{aligned}\right\} \tag{4-36}$$

By using a second IMPULS function shifted Δt seconds from the first, the in-between samples from the GAUSS function are used to create the second noise source shown in Fig. 4-20(e).

At this point, it is important to realize that the expression for the PSD of the noise sources obtained by the procedure just described is no longer given by Eq. 4-18. Rather, because of the effects of the zero-order hold function, it is necessary to substitute $2\Delta t$ for Δt in the equation to obtain the correct expression, again assuming rectangular integration is used. Returning to Fig. 4-18 it is noted that after the statistically independent sources are synthesized, they are each passed through a sixth-order lowpass Butterworth filter. Subsequently, the filtered noise sources are multiplied by the sine and cosine of the PLL return signal $\phi_r(t)$, respectively, and finally they are

subtracted to form the exact equivalent noise input n(t). It is significant to realize that unlike the approximate equivalent noise input, the exact expression is far more complex; $\phi_r(t)$ is in part derived from n(t) and in part determines n(t).

4.3.5 Simulation Results for the Test-Tone Case with Noise. Several computer runs were made for the generalized second-order PLL in the presence of noise for the test-tone case. In addition, runs were made for the generalized second-order PLL reduced to a standard second-order PLL. The next several figures show portions of the simulations of particular interest. Fig. 4-21 shows the characteristic 2π shifting of the phase error response observed in the generalized second-order PLL. Fig. 4-22 shows the output of the PLL during the same time period when the 2π transition occurred. Although the output has not been passed through a post-detection filter, the characteristic "click" is apparent. Fig. 4-23 shows a segment of a phase error response in which a positive 2π transition is observed. In addition to the preceding, phase transitions which were multiples of 2π were also encountered.

Fig. 4-24 shows a plot of the mean-square phase error as a function of noise-to-carrier ratio with the noise measured in the IF bandwidth for the generalized second-order PLL. Both the results for the non-linear model of Fig. 4-11 and the linear model with the sinusoidal function in the phase detector removed are shown for comparison. These results are considered only rough

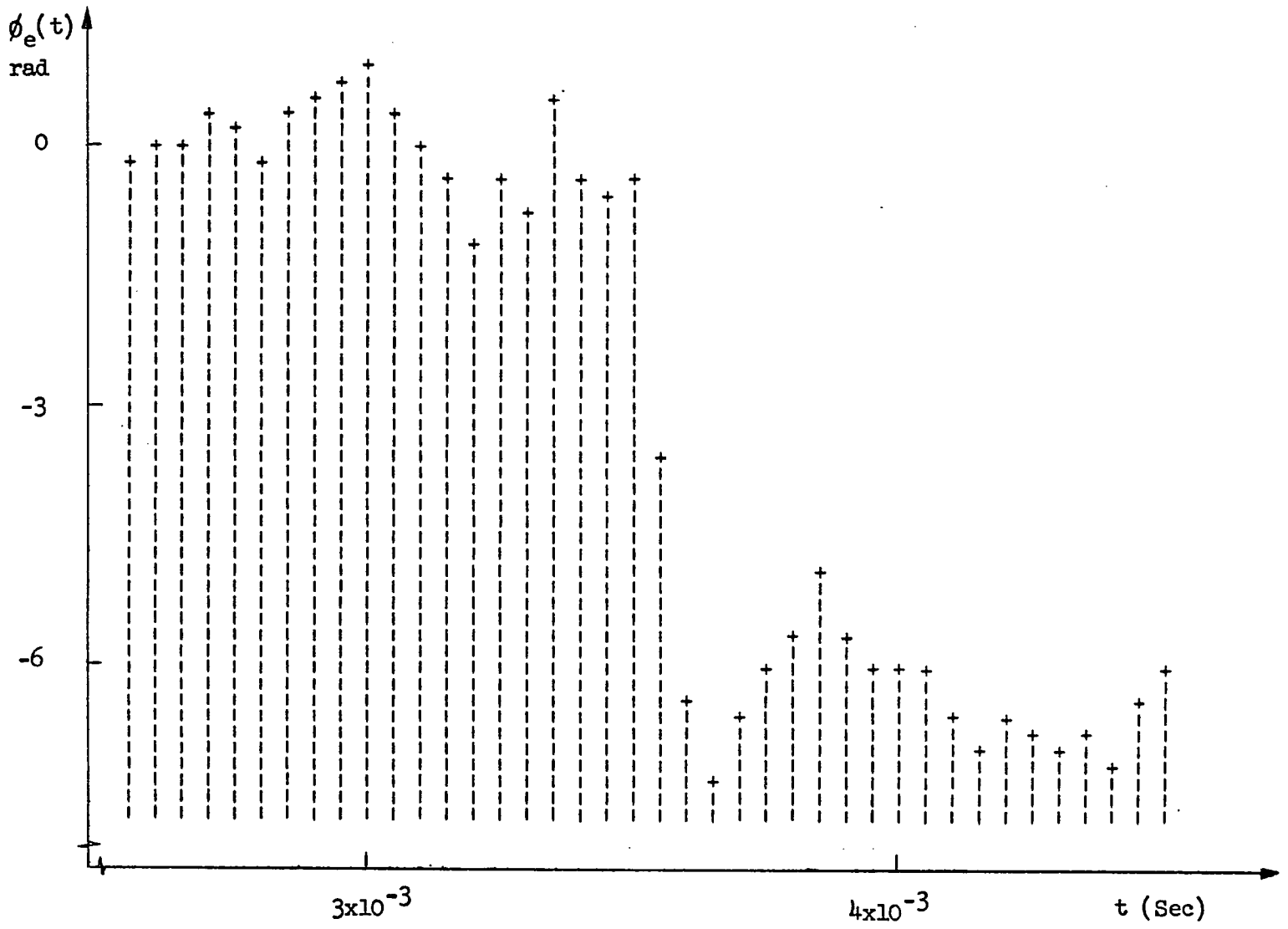

Fig. 4-21. Segment of phase error for generalized second-order PLL showing negative 2π transition.

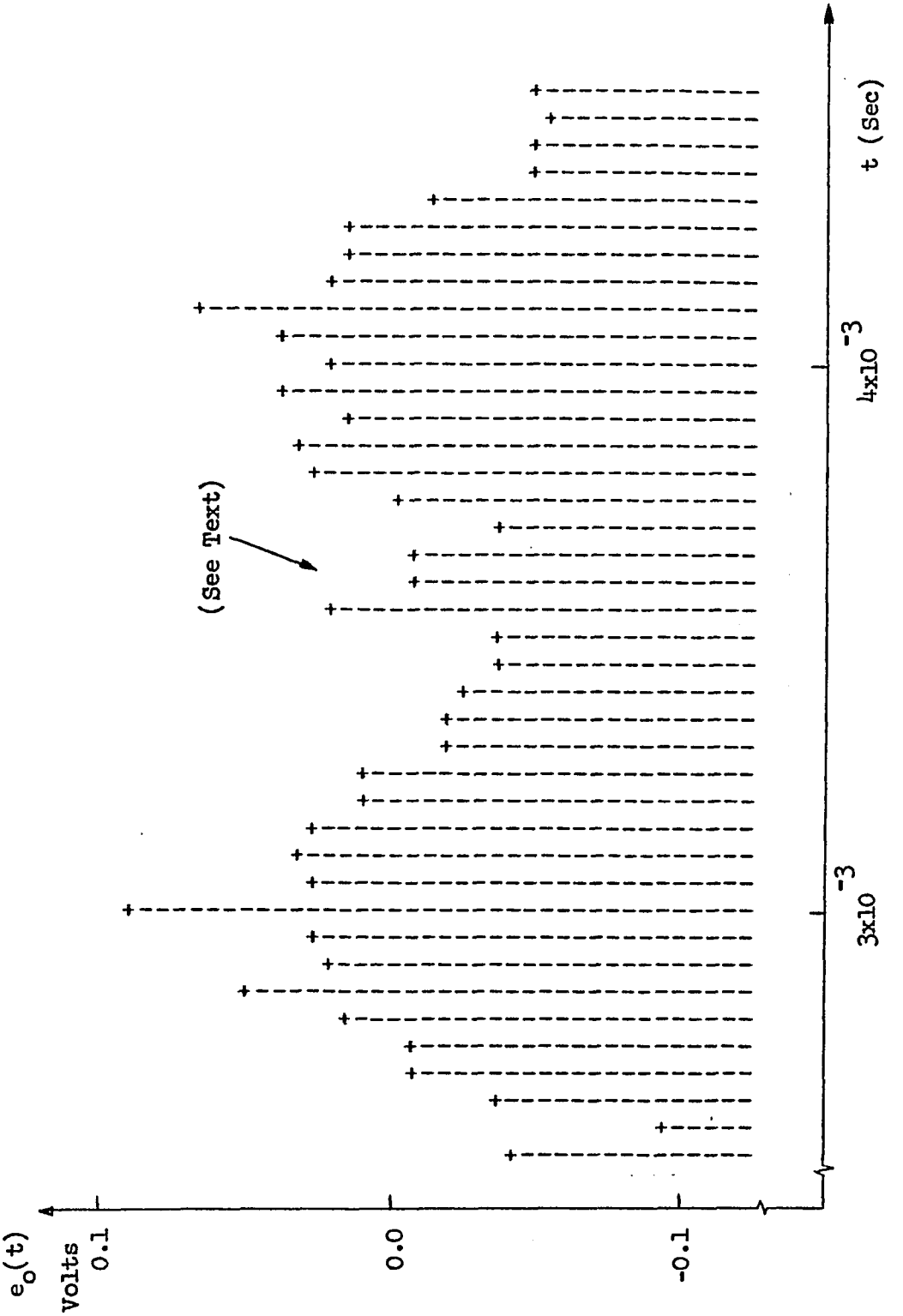

Fig. 4-22. Segment of output response for generalized second-order PLL during 2π phase transition.

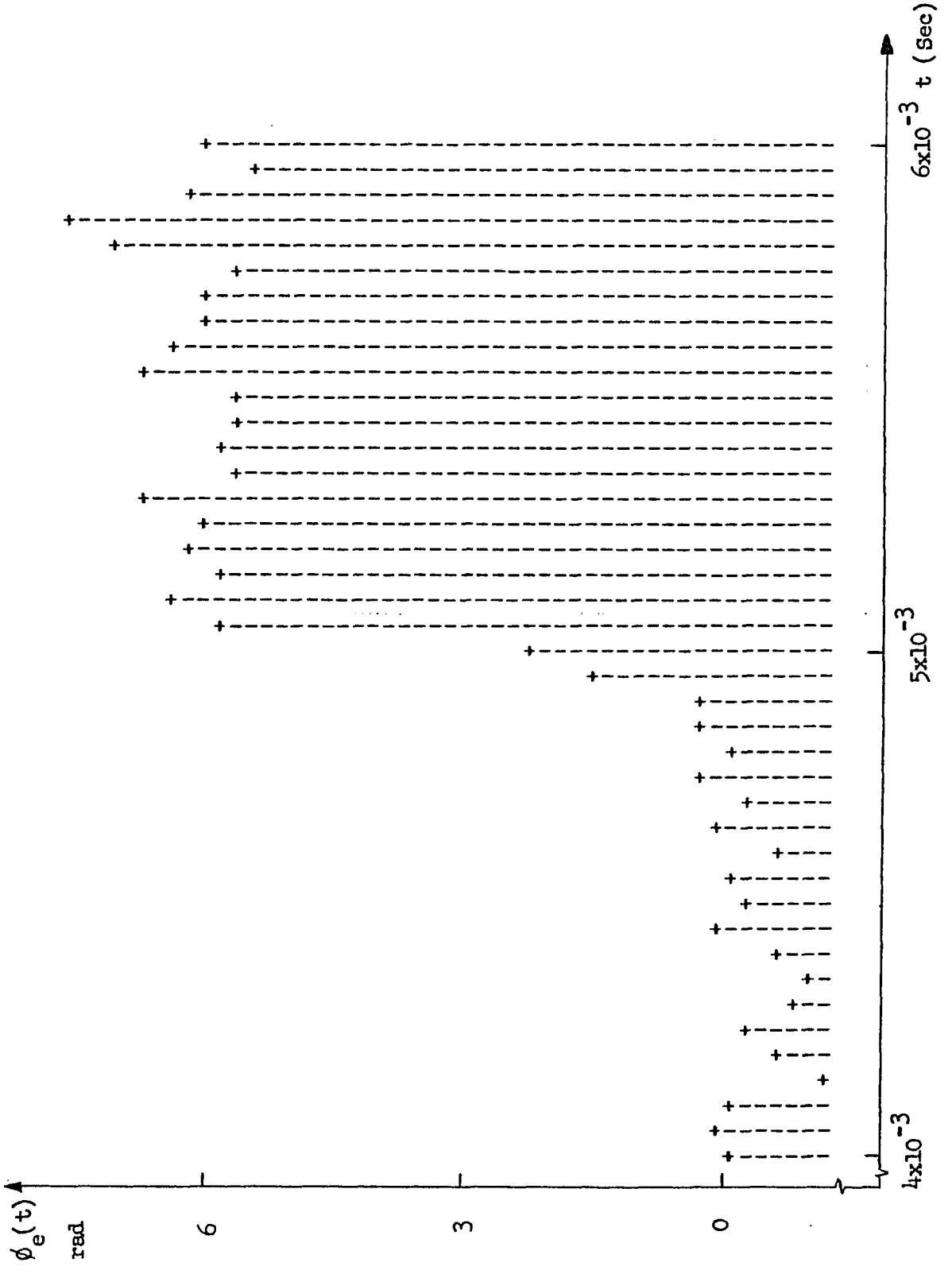

Fig. 4-23. Segment of phase error response showing 2π transition.

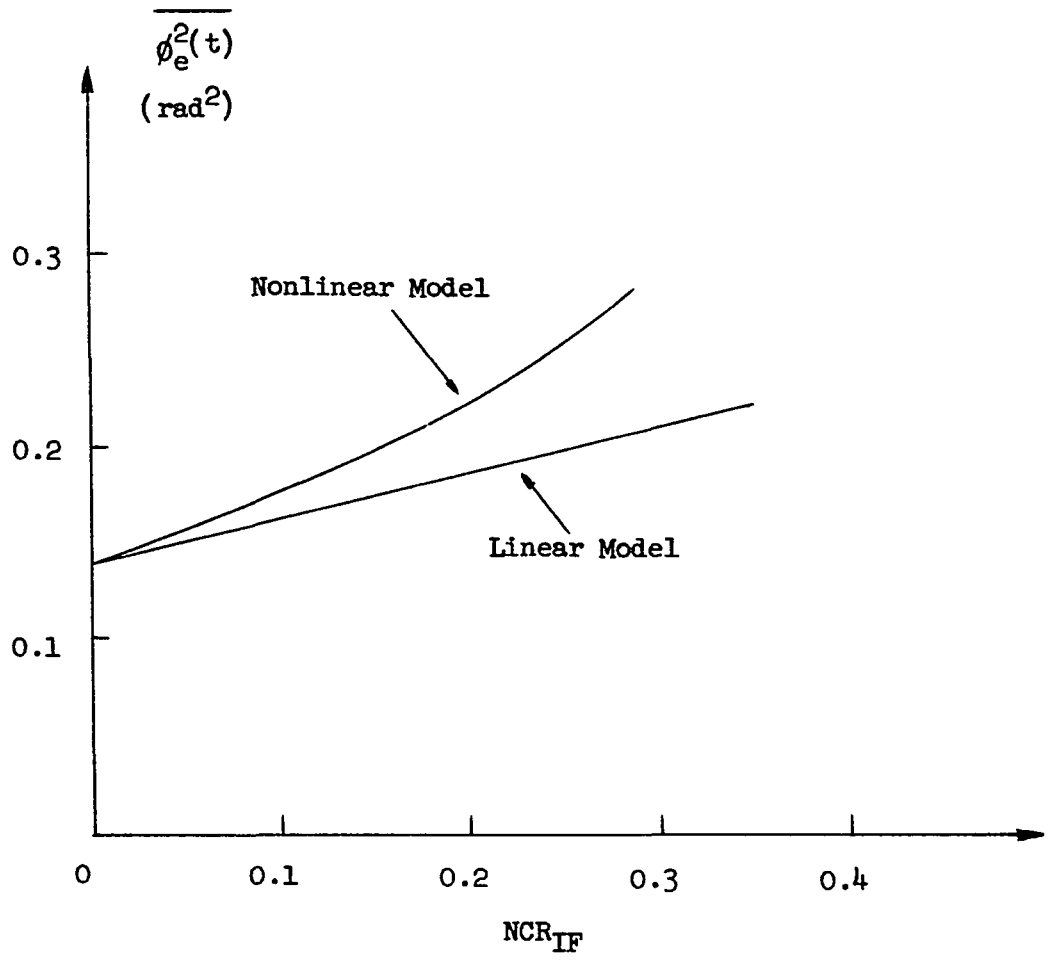

Fig. 4-24. Mean-square phase error as a function of noise-to-carrier ratio for the generalized second-order PLL.

and preliminary. Due to a lack of available computer time each point in these curves was limited to a single run with a FINTIM of only 0.01 seconds. It is necessary to make several runs with different seeds in the GAUSS function with a FINTIM of at least 0.05 seconds for each point in the curve to achieve the desired confidence in the results. A monitoring of the equivalent noise source during the 0.01 second runs used to obtain Fig. 4-24 indicates the results are pessimistic. Fig. 4-24 can be used to illustrate a number of important concepts. One criterion which has been used [Ref. 15, p. 549] as the threshold condition is the point where the actual mean-square phase error has increased 1dB over that predicted by the linear model. The mean-square phase error in the linear model that is indicative of the point where threshold occurs, it is recalled, was a parameter required in the optimum design procedure of Chapter 3. In Fig. 4-24, for example, this parameter is approximately 0.28. Note in Fig. 4-24 that the mean-square phase error corresponding to the point where NCR_{IF} is equal to zero is caused totally by the signal.

4.4 Non-deterministic Signal Source Simulation.

4.4.1 General. In the previous sections of this chapter, methods for simulating the generalized second-order PLL, the original Acampora and Newton ERPLD, and the standard second-order PLL were discussed. In addition, the procedure for accounting for noise in the simulation was presented. This analysis, however, was

limited to deterministic signal sources, such as test-tones and frequency steps. In this section a procedure is presented which enables the simulation of a useful class of non-deterministic signal sources. Included in this group are voice modulation, FDM-FM and FDM-PM.

4.4.2 Voice Modulation Case. The first case to be considered is that of a single-channel FM speech signal. The voice channel model to be used is the same as that employed in Chapter 3 (see Section 3.2.2) in which Gaussian statistics were assumed and the one-sided PSD of the input "phase" modulation was given by

$$W_{\phi_i} = \frac{\eta_m}{\omega^4} \quad , \quad f_a \leq f \leq f_b \tag{4-37}$$

The frequencies fa and fb will be taken as 1kHz and 4kHz respectively based on success with this model in previous analyses [Ref. 4, p. 339 and Ref. 15] . As with the equivalent noise input simulation, the fundamental applicable CSMP function to be used in the voice modulation case is the GAUSS function. Recall from the previous section that the PSD associated with the GAUSS function when rectangular integration is used is given by Eq. 4-18 and shown in Fig. 4-13(a). Before synthesizing the desired PSD associated with the voice signal, it is again necessary to insure that the sinc function in Eq. 4-18 is essentially unity over the

frequency range from 1kHz to 4kHz for the value of Δt used in the simulation. This in effect has already been shown previously in Table 4-1. Since the desired upper cutoff frequency of 4kHz is considerably below the 17.5 kHz given in the table, it can be seen that the unity amplitude requirement is again met for Δt equal to 10^{-6} or smaller.

The next task is to achieve the proper pass band in the PSD. Again, because of the maximally flat property and the ease of implementation on the CSMP, Butterworth filters were used in the analysis which follows. Two alternatives immediately are apparent. A bandpass filter could be used or high-pass and low-pass filter pair in tandem. Because the bandpass Butterworth realization is based on the use of a center frequency which is the geometric average of the two cutoff frequencies, this method does not afford as much control over the shape of the transfer function and was avoided in favor of the second method.

The expression for the total power response of the tandem filter pair is given by

$$\left|H_1(j\omega)\right|^2 = \frac{\left(\frac{\omega}{\omega_a}\right)^{2n_1}}{1 + \left(\frac{\omega}{\omega_a}\right)^{2n_1}} \cdot \frac{1}{1 + \left(\frac{\omega}{\omega_b}\right)^{2n_2}} \qquad (4\text{-}38)$$

where ω_a is the 3dB cutoff frequency for the high-pass filter of order n_1 and ω_b is the cutoff frequency for the low-pass filter of order n_2 . The next problem is to introduce the $1/\omega^4$ weighting factor into the bandpass PSD. This can be achieved by using a double integration which has a transfer function given by

$$H_I(s) = 1/s^2 \tag{4-39}$$

and a power response expressed by

$$\left|H_I(j\omega)\right|^2 = 1/\omega^4 \tag{4-40}$$

Finally, the modulation constant η_m must be accounted for. As will be subsequently shown, this factor will be introduced in the simulation by proper choice of the GAUSS PSD height $2\sigma_G^2\Delta t$ shown in Fig. 4-13 (a). Combining factors yields the expression for the PSD of the input "phase" modulation to be realized with CSMP as

$$W_{\phi_1 s} = \frac{\left(\frac{\omega}{\omega_a}\right)^{2n_1}}{1 + \left(\frac{\omega}{\omega_a}\right)^{2n_1}} \cdot \frac{1}{1 + \left(\frac{\omega}{\omega_b}\right)^{2n_2}} \cdot \frac{\eta_m}{\omega^4} \tag{4-41}$$

Before preceeding, it is desirable to take a closer look at Eq. 4-41. The low-pass term, of course, was inserted to fix the upper end of the passband at the desired cutoff frequency of 4kHz. The $1/\omega^4$ term, however, diminishes the PSD so rapidly that any effects of the low-pass filter are far overshadowed. This can be seen from Eq. 4-37 by comparing the PSD amplitudes at the upper and lower ends of the passband. At 4kHz the PSD characteristic has dropped to less than one percent of its maximum at 1kHz. The low-pass filter can then be eliminated leaving the PSD to be simulated as

$$W_{\phi_{is}} = \frac{\left(\frac{\omega}{\omega_a}\right)^{2n_1}}{1 + \left(\frac{\omega}{\omega_a}\right)^{2n_1}} \cdot \frac{\eta_m}{\omega^4} \tag{4-42}$$

Before testing the model using CSMP, it is necessary to choose a suitable set of parameters to insert in Eq. 4-42. The upper and lower cutoff frequencies have already been fixed at 4kHz and 1kHz respectively. As was shown in Sec. 3.2.2, the modulation constant may be expressed for the voice modulation case as follows

$$\eta_m = \frac{(2\pi)^2 \; f_a \, f_b \; (\Delta\omega_{rms})^2}{f_b - f_a} \tag{4-43}$$

The value chosen for the mean-square frequency deviation $(\Delta \omega_{rms})^2$ was $4\pi^2 \times 10^{-7}$ (rad/sec)^2 . This is based on a voice signal with a $\pm$10kHz peak deviation with the peak-to-rms ratio for voice assumed to be 10dB. This is the same value used in the original Acampora and Newton voice channel [Ref. 6] . The value of η_m from Eq. 4-43 is then 2.078×10^{13} . The final parameter to be chosen is the high-pass Butterworth filter of order n_1 . Fig. 4-25 shows a comparison between the voice model of Eq. 4-37 and the approximations to the model achievable with CSMP using 6th and 10th order filters. Of course as n_1 is increased the approximations becomes closer to the theoretical model. There is a tradeoff, however, since an increase in n_1 rapidly increases the CPU time requirements for the simulation. Indeed, there is little point in using very large values of n_1 to better approximate a model which itself is only approaches the true PSD of voice.

As discussed earlier, the modulation constant η_m can be accounted for within the CSMP model by proper choice of the GAUSS PSD height. The basic condition which must be met then is given by

$$2 \sigma_G^2 \Delta t = \eta_m \qquad (4\text{-}44)$$

The standard deviation that must be set into the GAUSS function is therefore

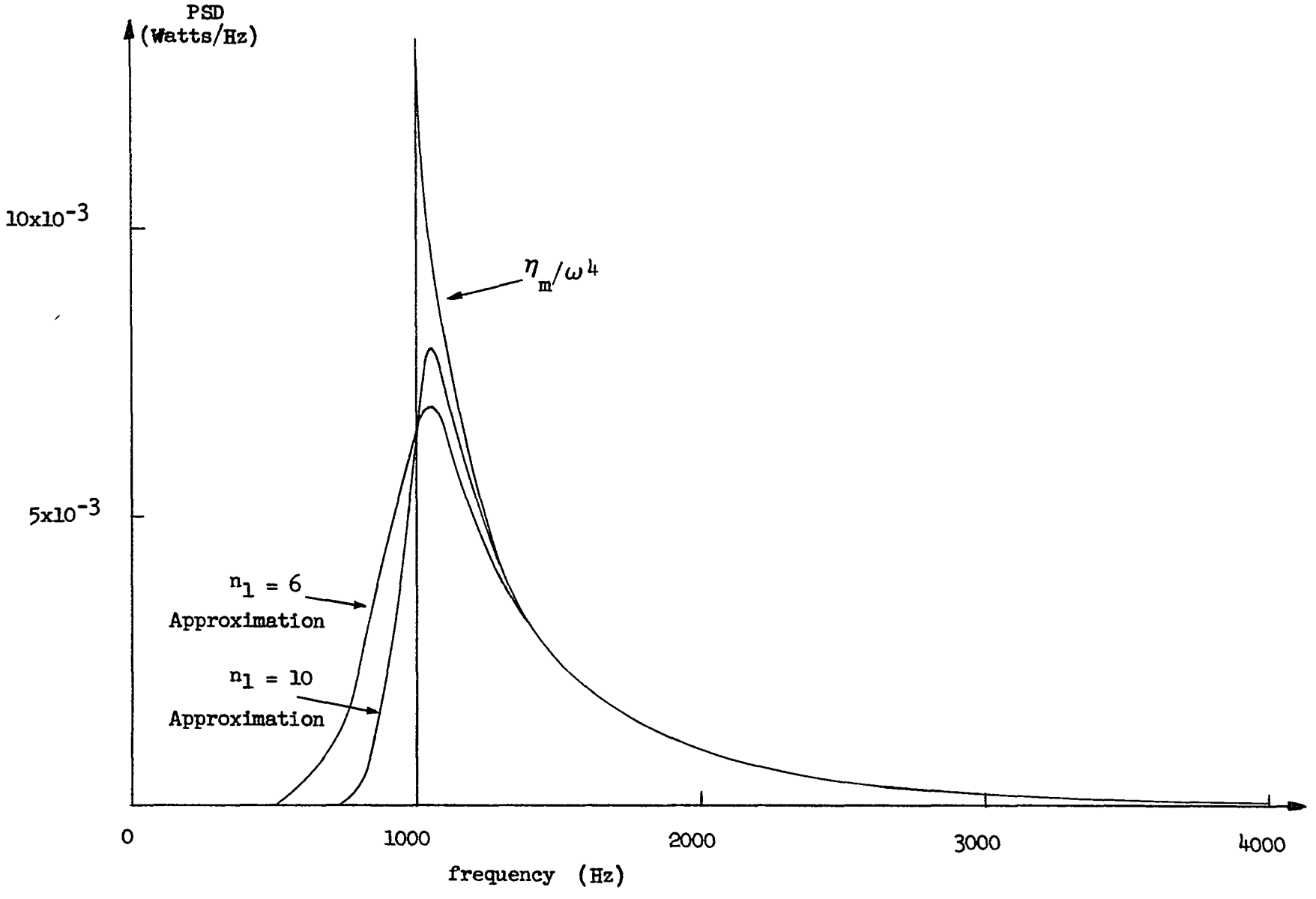

Fig. 4-25. PSD of voice modulation model along with approximations used in computer simulations.

$$\sigma_G = \sqrt{\frac{\eta_m}{2\Delta t}} \tag{4-45}$$

There is an additional factor that must be taken into consideration in the CSMP model. Referring back to Fig. 4-25, it is noted that the area under the PSD curve is the mean-square value of input phase modulation. This area for the original model and the two approximations is given as follows

$$\overline{\theta_i^2(t)} = 4.375 \text{ (original model)}$$

$$\overline{\theta_i^2(t)} = 4.578 \ (n_1 = 10 \text{ approximation}) \tag{4-46}$$

$$\overline{\theta_i^2(t)} = 4.900 \ (n_1 = 6 \text{ approximation})$$

It is therefore necessary to apply a correction factor to adjust the mean-square value of the approximation to that of the original model. This may be accomplished by simply making a proportional adjustment in the modulation constant. For example, using the n_1 equal to 6 approximation, the corrected modulation constant

is given by

$$\eta_{mc} = 2.078\text{x}10^{13} \cdot \frac{4.375}{4.900} = 1.855\text{x}10^{13} \quad (4\text{-}47)$$

This corrected modulation constant may be used in Eq. 4-45 to determine the standard deviation required for the simulation.

Having developed the basic theory for implementing the voice modulation case, the next step is to write the CSMP program for the model and test it. A detailed analysis of the implementation using the Butterworth high-pass filter is given in Appendix J with the highlights presented here for the example of n_1 equal to 6. The transfer function for a sixth-order high-pass Butterworth filter with a cutoff frequency at 1kHz is given by

$$H_B(s) = \quad (4\text{-}48)$$

$$\frac{s^6}{(s^2 + 3.255\text{x}10^3 s + 3.948\text{x}10^7)(s^2 + 8.884\text{x}10^3 s + 3.948\text{x}10^7)} \cdot \frac{1}{(s^2 + 1.214\text{x}10^4 s + 3.948\text{x}10^7)}$$

The double integration required to obtain the $1/\omega^4$ variation in the PSD simply reduces the numerator in Eq. 4-48 to s^4 . Fig. 4-26 shows the CSMP implementation of the voice PSD simulator and Fig. 4-27 shows the CSMP program used to determine the mean-square value of the simulator output. Table 4-3 shows the results of tests performed on the voice PSD simulator. As with the tests on the equivalent noise input, for each value of Δt three separate runs were made with different seeds. The third column in Table 4-3 shows the average value of $\overline{\theta_i^2(t)}$ for the three runs and the last column shows the associated standard deviation for the three runs. The table shows an increasing accuracy compared to the theoretical value as Δt is decreased until an integration interval on the order of 1.5×10^{-7} seconds is reached. For this and smaller values of Δt the simulations produced erroneous results. The probable cause of this difficulty is computer round-off [Ref. 16, p.7] . The differentiator is particularly susceptible to this problem as can be seen by the following explanation. Recall that the derivative is defined as follows

$$\frac{dx}{dt} = \lim_{\Delta t \to 0} \frac{x(t) - x(t-\Delta t)}{\Delta t} \qquad (4\text{-}49)$$

If Δt is chosen so small that the difference between $x(t)$ and $x(t-\Delta t)$ occurs in the 11th significant digit, for example, the computer will evaluate the derivative as zero, when in actuality it is not. The fact that the voice PSD simulator, for the example

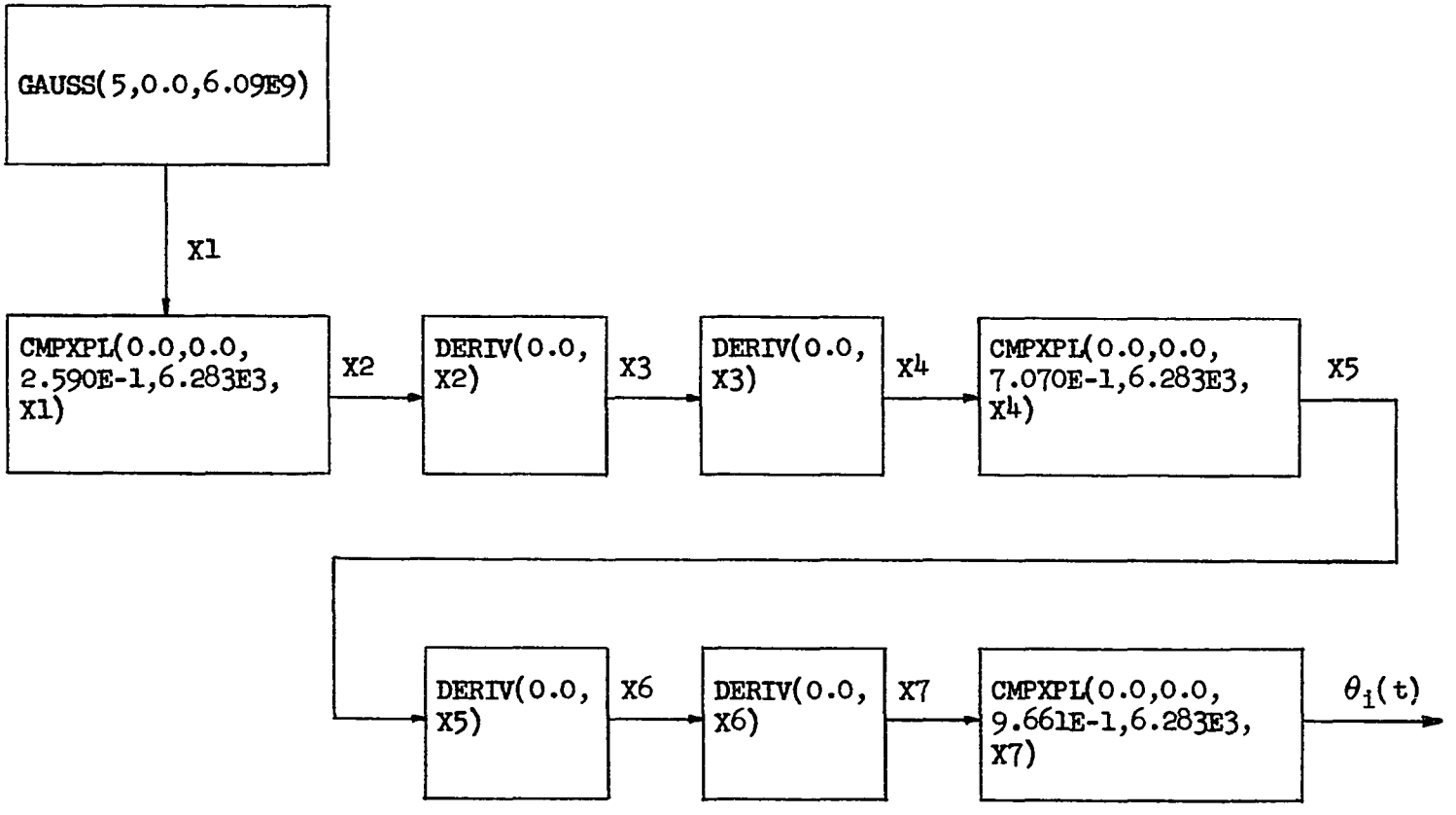

Fig. 4-26. CSMP implementation of the voice PSD simulator ($n_1 = 6$).

```
TITLE VOICE PSD SIMULATOR TEST PROGRAM
DYNAMIC
            XNEW11=GAUSS(5,0.0,6.091E9)
            XNEW12=CMPXPL(0.0,0.0,2.590E-1,6.283E3,XNEW11)
            XNEW13=DERIV(0.0,XNEW12)
            XNEW14=DERIV(0.0,XNEW13)
            XNEW15=CMPXPL(0.0,0.0,7.070E-1,6.283E3,XNEW14)
            XNEW16=DERIV(0.0,XNEW15)
            XNEW17=DERIV(0.0,XNEW16)
            XNEW18=CMPXPL(0.0,0.0,9.661E-1,6.283E3,XNEW17)
            VOIPSD=XNEW18
            XNEW19=VOIPSD**2
            XNEW20=INTGRL(0.0,XNEW19)
            XNEW21=RAMP(0.0)
            XMSQVL=XNEW20/XNEW21
TIMER DELT=2.5E-7,PRDEL=2.0E-5,OUTDEL=2.0E-5,FINTIM=2.5E-2
PRTPLOT XMSQVL
LABEL MEAN SQUARE VALUE OF VOICE SIGNAL
PRTPLOT VOIPSD
LABEL VOICE SIGNAL VS TIME
METHOD RECT
END
STOP
```

Fig. 4-27. CSMP program used to test the voice PSD simulator.

Table 4-3. Test results for voice PSD simulator.

Δt	$\overline{\theta_i^2(t)}$	$\overline{\theta_i^2(t)}$	Standard Deviation
Sec.	Theoretical	Avg. Using 3 Seeds	Based on 3 Runs
1.0×10^{-6}	4.375	4.506	6.799×10^{-1}
5.0×10^{-7}	4.375	4.334	4.004×10^{-1}
2.5×10^{-7}	4.375	4.389	2.655×10^{-1}
1.5×10^{-7}	4.375	*	_____
1.0×10^{-7}	4.375	*	_____

* see text

under consideration has four differentiators, compounds the problem. The useful range of Δt for the voice PSD simulator does, however, fall within that for the equivalent noise source and so a value of Δt between approximately 2.5×10^{-7} and 5.0×10^{-7} is appropriate for the PLL simulation in the presence of noise for the voice modulation case.

A final consideration is in order for the complete simulation of the voice modulation case. Since the voice PSD simulator requires a GAUSS source which is statistically independent of those used for the equivalent noise source, a procedure similar to that illustrated in Fig. 4-20 can be used. Every third sample can be used for the voice PSD simulator while the first two samples are used for the exact equivalent noise source representation.

4.4.3 FDM-FM Case. The next case which shall be commented on is that of FDM-FM. The model to be used in this discussion is the same as that employed in Chapter 3 (see Section 3.2.3) in which Gaussian statistics were assumed and the one-sided PSD of the input "phase" modulation was given by

$$W_{\phi_i} = \frac{\eta_m}{\omega^2} \quad , \quad fa \leq f \leq fb \qquad (4\text{-}50)$$

As with the voice modulation, the basic bandpass shape can be achieved with a Butterworth low-pass and high-pass filter pair in tandem. The $1/\omega^2$ weighting factor can be achieved using a single integrator. Again, the modulation constant η_m can be accounted for by proper choice of the GAUSS PSD height $2\ \sigma_G^2\ \Delta t$ shown in Fig. 4-13(a). Finally, it is necessary to insure that the sinc function in Eq. 4-18 is essentially unity over the frequency range from fa to fb for the value of Δt used in the simulation. This is much more of a problem than in the voice modulation case, since the upper baseband frequency for FDM-FM is typically on the order of 10^5 to 10^6 Hz, and the Δt required is proportionally smaller. The expression for the PSD of the input "phase" modulation realizable with CSMP is then given by

$$W_{\phi_{is}} = \frac{\left(\frac{\omega}{\omega_a}\right)^{2n_1}}{1 + \left(\frac{\omega}{\omega_a}\right)^{2n_1}} \cdot \frac{1}{1 + \left(\frac{\omega}{\omega_b}\right)^{2n_2}} \cdot \frac{\eta_m}{\omega^2} \qquad (4\text{-}51)$$

Whether or not the expression in Eq. 4-51 can be simplified by removal of the low-pass filter, as was done in the previous section, depends of course on the values of fa and fb, and each case should be considered on an individual basis. Because the PSD diminishes only as $1/\omega^2$, however, the use of this simplification is considerably more restrictive than in the voice modulation case.

4.4.4 FDM-PM Case. The final case which shall be commented on is that of FDM-PM. The model to be used in this discussion is the same as that employed in Chapter 3 (Section 3.2.4) in which Gaussian statistics were assumed and the one-sided PSD of the input "phase" modulation was given by

$$W_{\phi_{is}} = \eta_m \quad , \quad f_a \leq f \leq f_b \tag{4-52}$$

The desired bandpass shape can again be achieved with a Butterworth low-pass and high-pass filter pair in tandem. The modulation constant η_m m can once more be accounted for by proper choice of the GAUSS PSD height. The comments in the previous section on the unity amplitude requirement of the sinc function in Eq. 4-18 also holdsfor the FDM-PM case. The expression for the PSD of the input "phase" modulation realizable with CSMP is then given by

$$W_{\phi_{is}} = \frac{\left(\frac{\omega}{\omega_a}\right)^{2n_1}}{1 + \left(\frac{\omega}{\omega_a}\right)^{2n_1}} \cdot \frac{\eta_m}{1 + \left(\frac{\omega}{\omega_b}\right)^{2n_2}} \tag{4-53}$$

References - Chapter 4

1. IBM Application Program, "System/360 Continuous System Modeling Program User's Manual", GH20-0367-4.

2. IBM Application Program, "System/360 Continuous System Modeling Program Application Description", GH20-0240-3.

3. IBM Application Program, "System/360 Continuous System Modeling Program System Manual", GY20-0111-0.

4. J. Klapper and J. Frankle, Phase-Locked and Frequency-Feedback Systems: Principles and Techniques, Academic Press, New York, NY, 1972.

5. C. L. Johnson, Analog Computer Techniques, McGraw Hill Book Co., New York, 1963.

6. A. Acampora and A. Newton, "Use of Phase Subtraction to Extend the Range of a Phase-Locked Demodulator", RCA Review, vol. 27, No. 3, pp. 577-599, December 1966.

7. A. Viterbi, Principles of Coherent Communication, McGraw Hill Book Co., New York, 1966.

8. M. MacLaren, M. Donald, and G. Marsaglia, "Uniform Random Number Generators", Journal of ACM, vol. 12, No., 1, pp. 83-89.

9. E. Grabbe, S. Ramo and D. Wooldridge, Handbook of Automation Computation and Control, vol. 2, John Wiley and Sons, New York, 1959.

10. R. Kochenburger, Computer Simulation of Dynamic Systems, Prentice Hall Inc., Englewood Cliffs, New Jersey, 1972.

11. G. A. Korn, Random-Process Simulation and Measurements, McGraw Hill Book Co., New York, 1966.

12. S. Karni, Network Theory: Analysis and Synthesis, Allyn and Bacon Inc., Boston, Massachusetts, 1966.

13. E. A. Guillemin, Synthesis of Passive Networks, John Wiley and Sons, New York, 1957.

14. S. M. Selby, editor, Standard Mathematical Tables, 17th Edition, The Chemical Rubber Co., Cleveland, Ohio, 1969.

15. J. Frankle, "Threshold Performance of Analog FM Demodulators", RCA Review 27, No. 4, pp. 521-562, 1966.

16. D. D. McCracken, A Guide to FORTRAN IV Programming, John Wiley and Sons, New York, 1965.

CHAPTER V

ACQUISITION AND TRACKING BEHAVIOR OF THE GENERALIZED SECOND-ORDER PHASE-LOCKED LOOP

5.1 Introduction

In this chapter additional insight into the operation of the generalized second-order PLL is gained through investigation of its acquisition and tracking behavior. This is accomplished using phase plane techniques to study the non-linear differential equation which governs the loop operation. These results are compared against those of the standard second-order PLL.

5.2 The Basic Differential Equation

The fundamental differential equation that specifies the behavior of a PLL in the absence of noise is given by [Ref. 1, p. 96 and Ref. 2, p. 585-586]

$$\dot{\phi}_e(t) = \dot{\phi}_i(t) - K\,F(p)\,\mathrm{Sin}\,\phi_e(t) \tag{5-1}$$

where ϕ_e is the loop phase error, ϕ_i is the input signal phase process, K is the total loop gain and F(p) is the loop filter function. Recall that the expression for the generalized second-order PLL loop filter is given by

(5-2)

$$F(p) = \frac{p^2/\beta + p/\gamma + 1}{p/b + 1}$$

Substituting Eq. 5-2 into Eq. 5-1 yields

$$\dot{\phi}_e(t) = \dot{\phi}_i(t) - K\left[\frac{p^2/\beta + p/\gamma + 1}{p/b + 1}\right]\text{Sin}\,\phi_e(t) \qquad (5\text{-}3)$$

Although Eq. 5-3 is the differential equation governing the operation of the generalized second-order PLL, it is not in standard form. By carrying out the indicated operations of the differential operator "p", Eq. 5-3 becomes

$$\ddot{\phi}_e = \qquad (5\text{-}4)$$

$$\frac{\ddot{\phi}_i + b\dot{\phi}_i - Kb\,\text{Sin}\phi_e - \left(b + \frac{Kb}{\gamma}\text{Cos}\phi_e\right)\dot{\phi}_e + \frac{Kb}{\beta}\dot{\phi}_e^2\,\text{Sin}\phi_e}{1 + \frac{Kb}{\beta}\text{Cos}\phi_e}$$

The details of the derivation of Eq. 5-4 are given in Appendix L. The differential equation governing the response of the Acampora and Newton ERPLD [Ref. 3] and the equivalent filter ERPLD can be determined by making the substitutions

(5-5)

$$\left.\begin{aligned} \beta &= \frac{K\,b}{\alpha} \\ \text{and} \\ \gamma &= \frac{1}{\frac{\alpha}{K} + \frac{1}{a}} \end{aligned}\right\}$$

into Eq. 5-4 yielding

$$\ddot{\phi}_e = \frac{\ddot{\phi}_i + b\dot{\phi}_i - Kb\,\mathrm{Sin}\phi_e - \left(b + \left[\alpha b + \frac{Kb}{a}\right]\mathrm{Cos}\,\phi_e\right)\dot{\phi}_e + \alpha\dot{\phi}_e^2\,\mathrm{Sin}\,\phi_e}{1 + \alpha\,\mathrm{Cos}\,\phi_e} \tag{5-6}$$

It should be recalled that, as was shown in Chapter 2, for practical cases, designs achievable with the generalized second-order PLL can also be achieved with the ERPLD or equivalent filter ERPLD. In the analysis which follows Eq. 5-6 will be used. The purpose for using this equation is two-fold. Firstly, the Acampora and Newton design [Ref. 3] will be the basic set of parameters around which the analysis is to be performed. Secondly, it is of great interest to consider intermediate cases between the standard second-order PLL and the Acampora and Newton ERPLD. This can easily be accomplished by varying α between zero and unity in Eq. 5-6. It is of great importance, however, to realize that the results achieved, for all intents and purposes apply directly to the generalized second-order PLL through the change in variables of Eq. 5-5. The case of primary interest is that of an input signal which has a frequency offset $\Delta\omega_i$ from the VCO frequency at time t = o. For this case, Eq. 5-6 reduces to

$$\ddot{\phi}_e = \frac{b\Delta\omega_i - N \sin\phi_e - \left(M\cos\phi_e + b\right)\dot{\phi}_e + \alpha\dot{\phi}_e^2 \sin\phi_e}{1 + \alpha\cos\phi_e} \qquad (5\text{-}7)$$

where

(5-8)

$$\left.\begin{aligned} M &= \alpha b + \frac{Kb}{a} \\ \text{and} \\ N &= Kb \end{aligned}\right\}$$

Eq. 5-7 is a nonlinear differential equation to which a general analytic solution is not available. However, using phase plane analysis, a number of important properties of the response can be obtained. Before continuing, it is desirable to put Eq. 5-7 in a more convenient form for phase plane analysis. Let

$$\phi_e \equiv x \tag{5-9}$$

and

$$\dot{\phi}_e \equiv y \tag{5-10}$$

Then

(5-11)

$$\ddot{\phi}_e = \frac{d\dot{\phi}_e}{dt} = \frac{d\dot{\phi}_e}{d\phi_e} \cdot \frac{d\phi_e}{dt} = \frac{dy}{dx} \cdot y$$

Substituting Eq. 5-9 through Eq. 5-11 into Eq. 5-7 yields

$$\frac{dy}{dx} = \frac{b\Delta\omega_i - N \operatorname{Sin} x - (b + M \operatorname{Cos} x)\, y + \alpha y^2 \operatorname{Sin} x}{y\,(1 + \alpha \operatorname{Cos} x)} \tag{5-12}$$

The plot of "y" as a function of "x" (i.e. $\dot{\phi}_e$ versus ϕ_e)is termed the phase plane portrait for the differential equation under consideration.

5.3 Phase Plane Analysis

5.3.1 General Description. Consider the second-order system described by the nonlinear differential equation given in Eq. 5-7. The time solution of this system can be illustrated using a plot of $\phi_e(t)$ versus "t." Alternately, the solution can be illustrated by plotting $\dot{\phi}_e$ versus ϕ_e with time as a parameter. If $\dot{\phi}_e$ and ϕ_e are taken as the coordinates of a plane, then for each state of the system there corresponds a point in this plane. As "t" varies this point describes a curve in the ϕ_e-$\dot{\phi}_e$ plane called a trajectory. A family of these trajectories is termed a phase plane portrait.

The initial conditions determine the starting point on a trajectory and as time increases the point moves along the trajectory. The phase plane response depicts all possible states of the system and thus shows the nature of the response of the system. One and only one trajectory can pass through a given

point in the phase plane unless it happens to be a singular point. The behavior of the phase plane in the region about a singular point is extremely important and warrants special attention to be given subsequently.

Finally, it should be noted that phase plane analysis is normally limited to second-order systems. For third order systems, it is usually difficult to construct or visualize trajectories. For higher order systems, it is virtually impossible to visualize trajectories. Of course, a phase space of "n" dimensions can be conceived for an nth order system, but the method loses the simplicity and convenience associated with its use with a second-order system.

5.3.2 Preliminary Investigation of the Differential Equation. Before proceeding with the techniques for generating phase plane portraits for Eq. 5-12 it is useful to perform a preliminary investigation of the differential equation.

First, it is noted that Eq. 5-12 is periodic in x with a period of 2π. Thus, the slope of the trajectories at (x_o, y_o) is the same as it is at $(x_o+2n\pi, y_o)$ where n is a positive or negative integer. It is therefore necessary only to plot the trajectories for $-\pi < x \leq \pi$ in order to describe the complete behavior of the system.

Next, consider Eq. 5-12 for large y, which corresponds to large frequency error. Under this condition the differential equation reduces to

$$\frac{dy}{dx} \approx \frac{\alpha y \, \text{Sin } x}{1 + \alpha \, \text{Cos } x} \tag{5-13}$$

Rearranging terms to put Eq. 5-13 in convenient form for solution yields

$$\frac{dy}{y} = \frac{\alpha \, \text{Sin } x}{1 + \alpha \, \text{Cos } x} dx \tag{5-14}$$

Fortunately, this differential equation can be evaluated in closed form using standard techniques. Integrating both sides of Eq. 5-14 [Ref. 4, p. 90] yields the result

$$\ell n \, y = - \ell n \left(1 + \alpha \, \text{Cos } x\right) + C \tag{5-15}$$

Reexpressing the integration constant as

$$C = \ell_n K \tag{5-16}$$

results in the solution to Eq. 5-14 given as follows

$$y = \frac{K}{1 + \alpha \cos x} \tag{5-17}$$

Figs. 5-1 through 5-6 show a plot of Eq. 5-17 over a range of α between 0.1 and 10.0. For α equal to 0.1, the trajectories look essentially sinusoidal. As α increases towards unity the trajectories develop an increased peakedness at $\pm\pi$. At α equal to unity the trajectories change rather dramatically, and develop a discontinuity at a phase error of $\pm\pi$. As α is increased even further, the discontinuities more inward from $\pm\pi$ towards $\pm\pi/2$ in the limit as α approaches infinity. It is important to realize that although Eq. 5-17 was derived for the Acampora and Newton ERPLD or the equivalent filter ERPLD it is also seen to hold for the generalized second-order PLL by simply replacing α with Kb/β.

It is of interest to compare the results obtained in Eq. 5-17 with that of the standard second-order PLL. This may be accomplished by first setting α equal to zero in Eq. 5-12 yielding

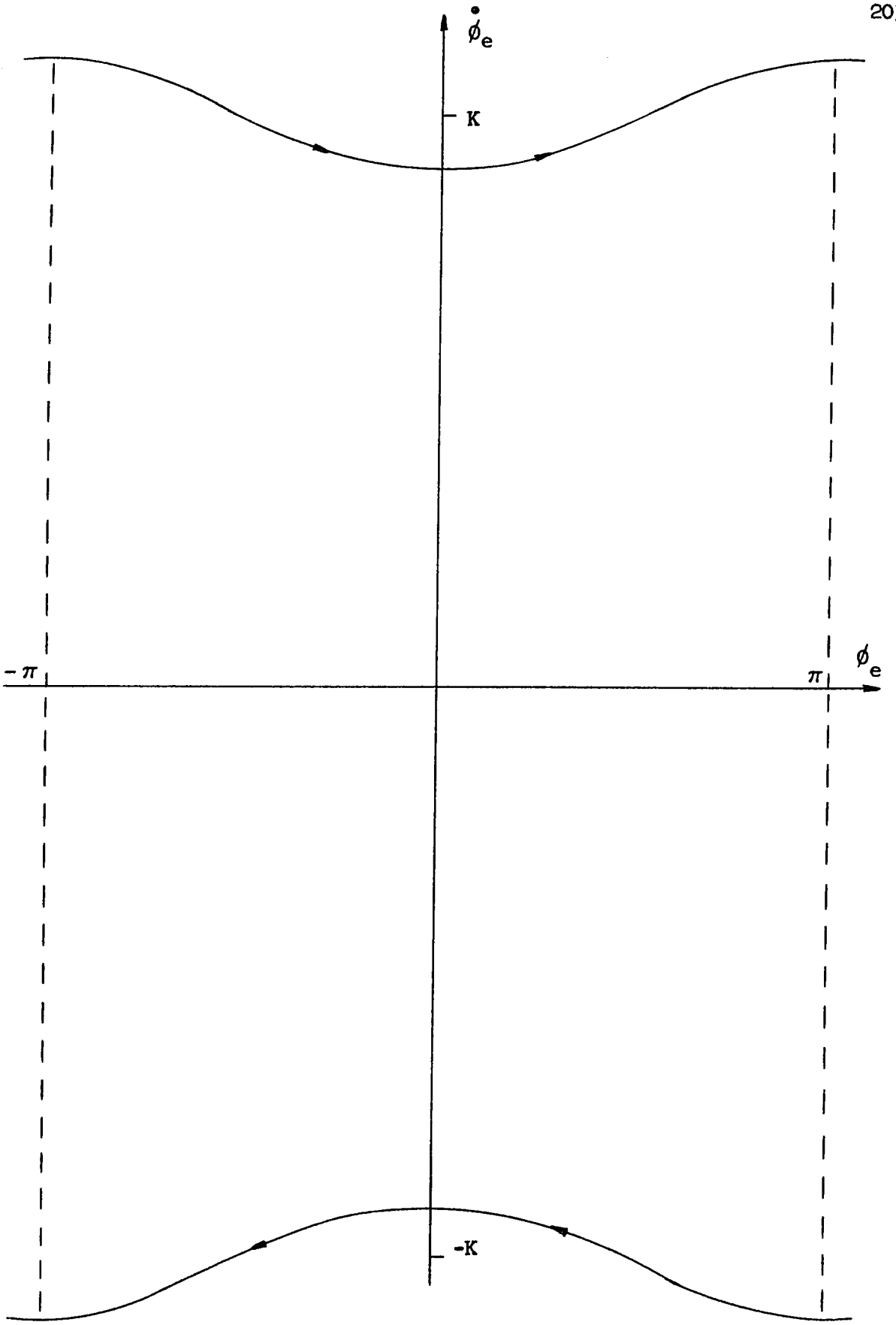

Fig. 5-1. Phase plane trajectories for large frequency error; $\alpha = 0.1$.

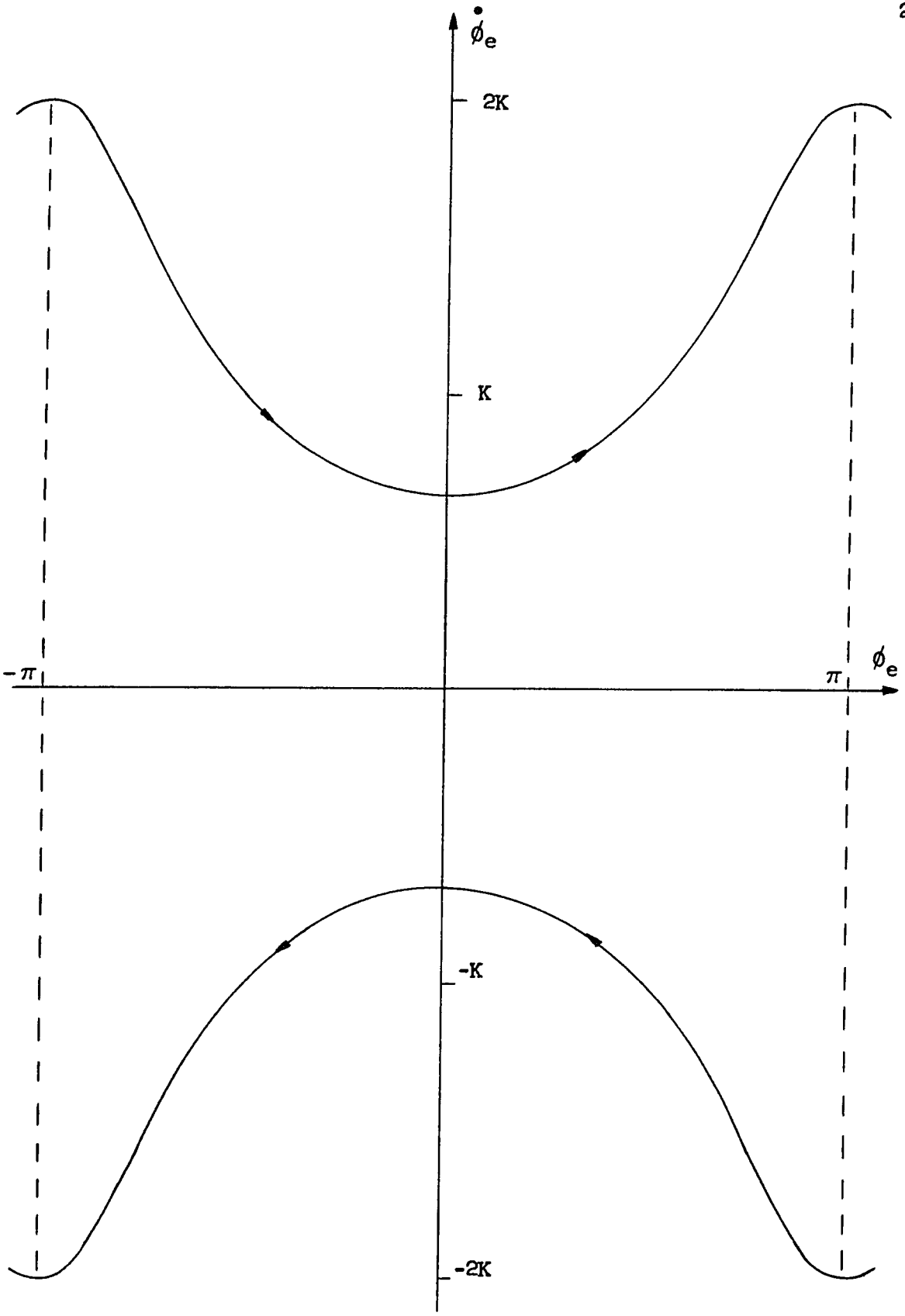

Fig. 5-2. Phase plane trajectories for large frequency error; $\alpha = 0.5$.

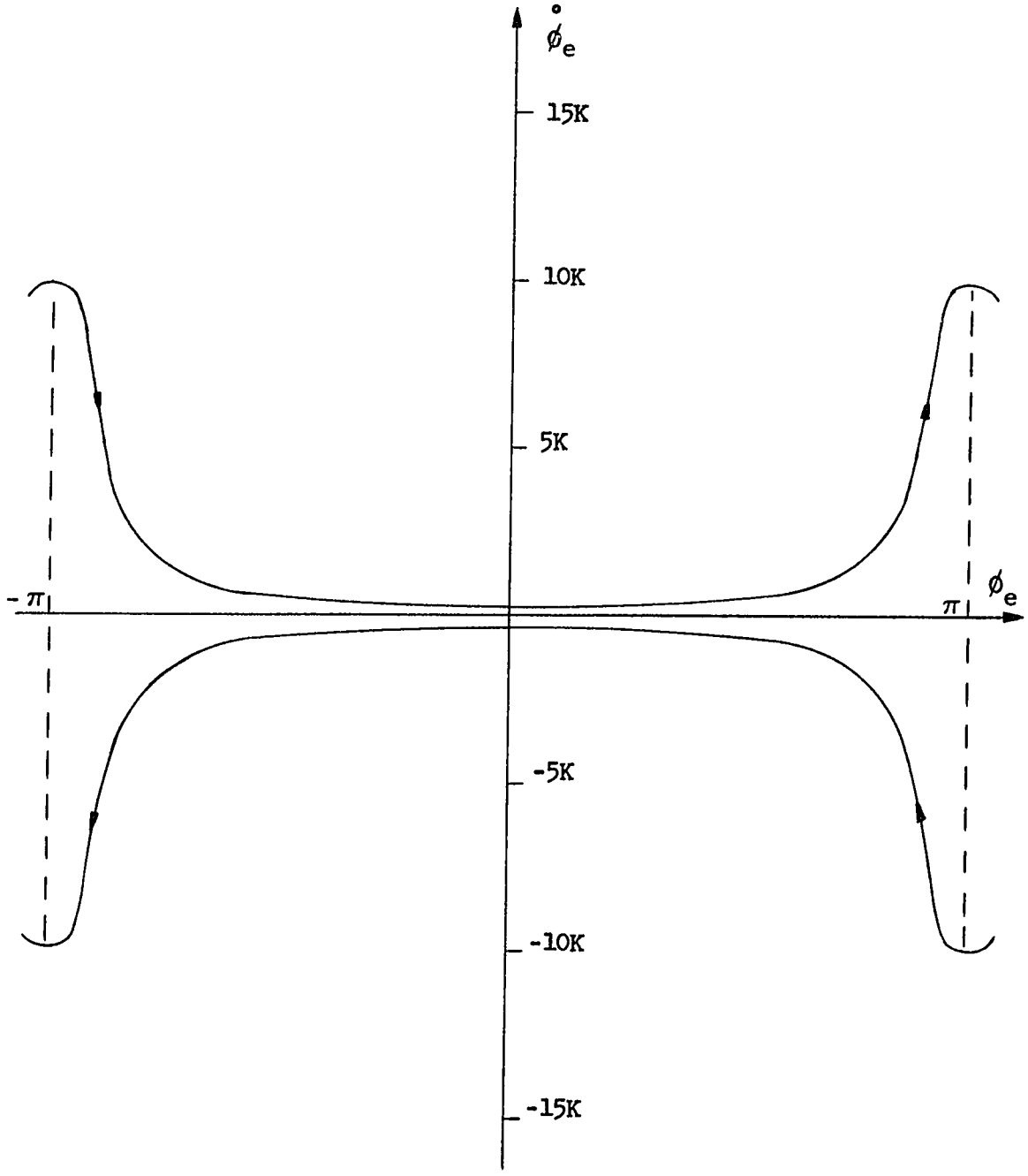

Fig. 5-3. Phase plane trajectories for large frequency error; $\alpha = 0.9$.

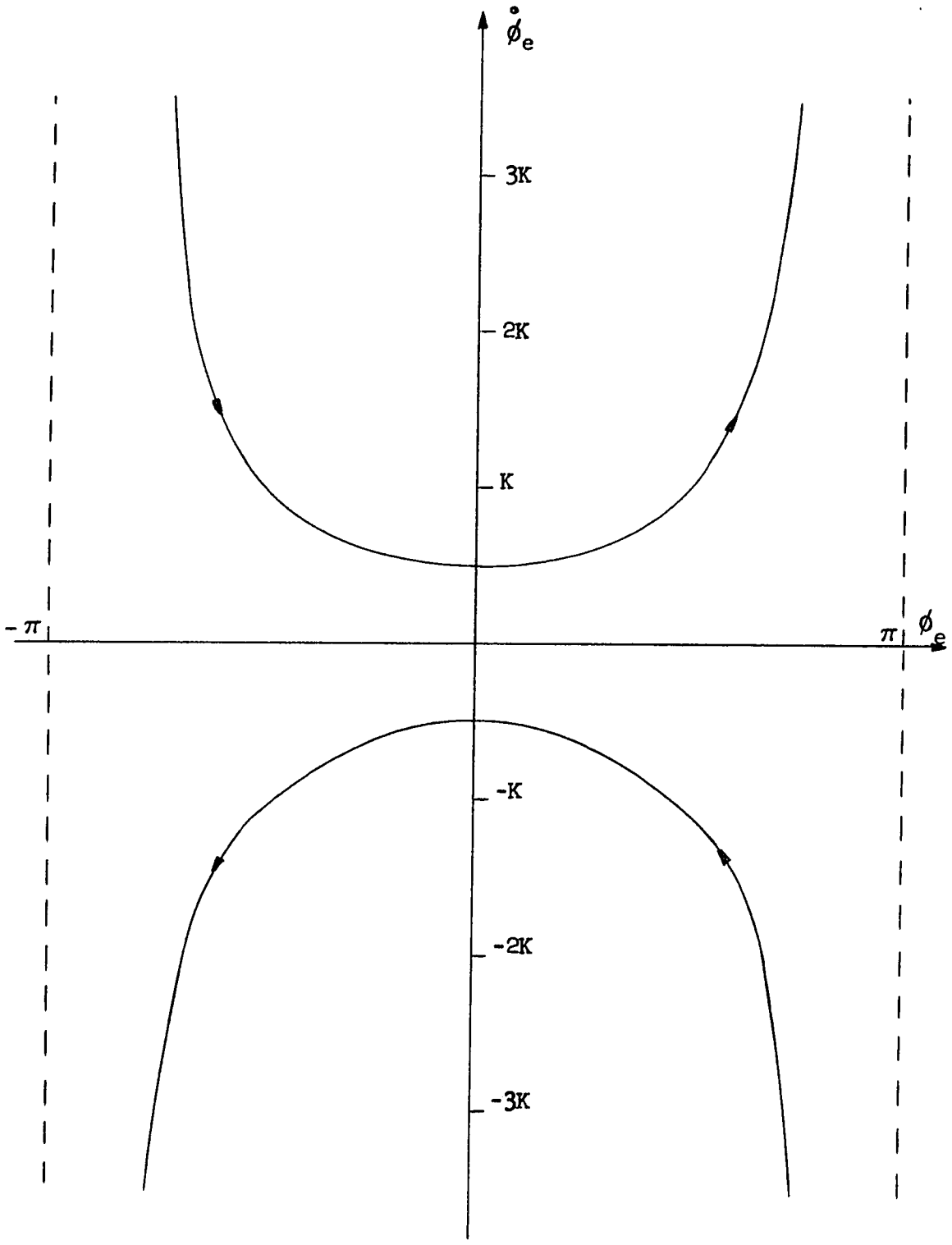

Fig. 5-4. Phase plane trajectories for large frequency error; $\alpha = 1.0$.

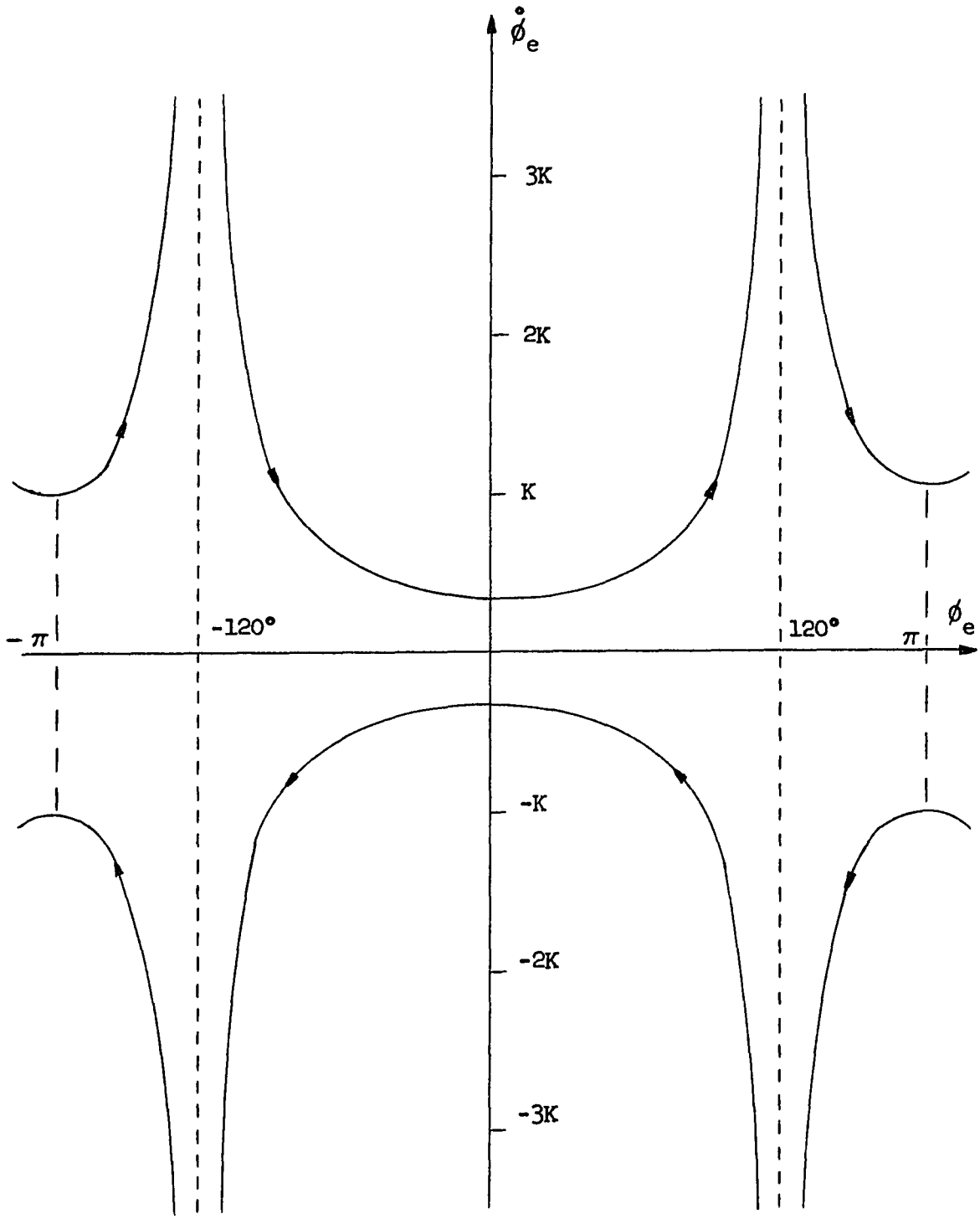

Fig.5-5. Phase plane trajectories for large frequency error; $\alpha = 2.0$.

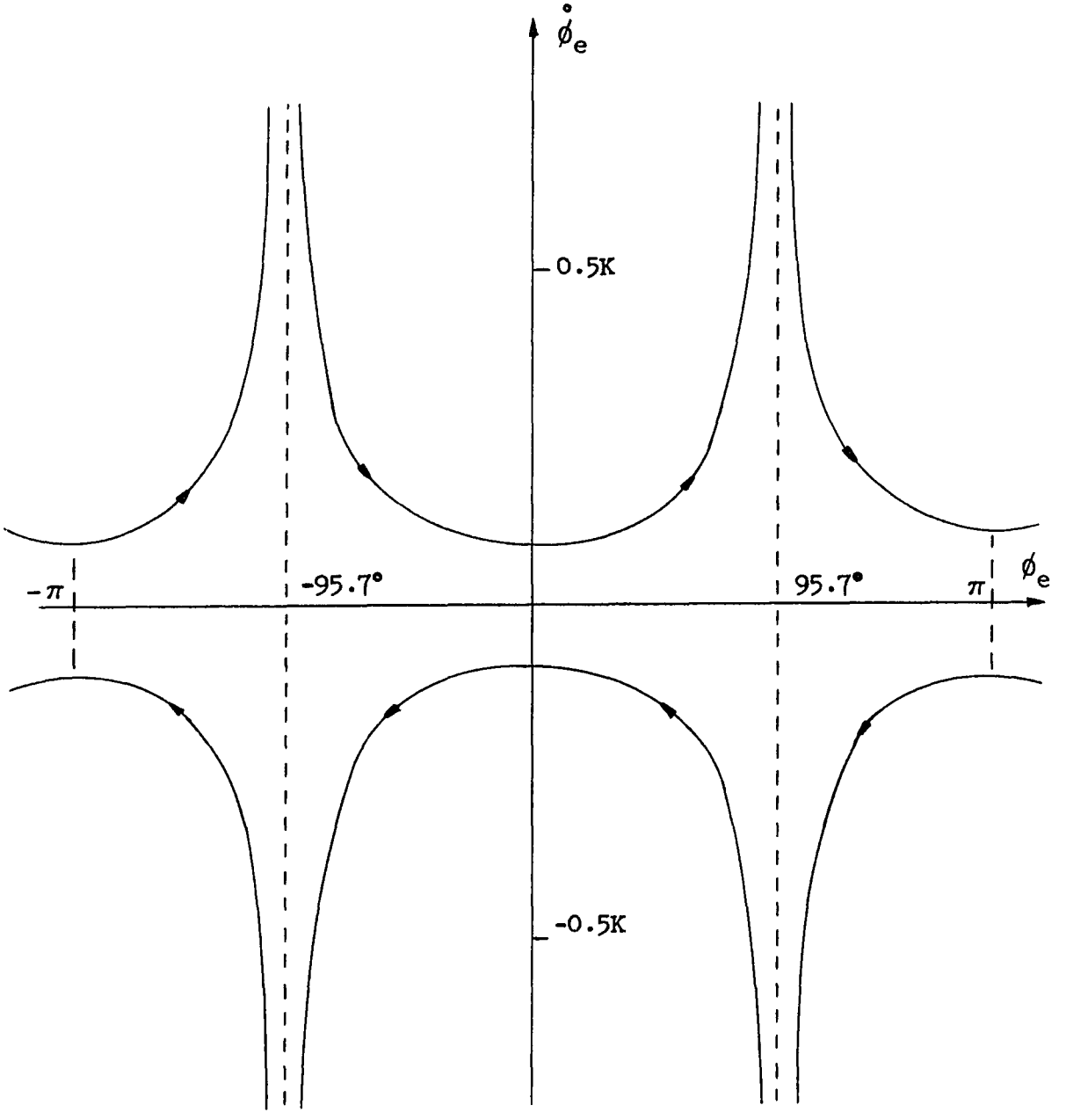

Fig. 5-6. Phase plane trajectories for large frequency error; $\alpha = 10.0$.

$$\frac{dy}{dx} = \frac{b\Delta\omega_1 - Kb \sin x - \left(b + \frac{Kb}{a}\cos x\right) y}{y} \tag{5-18}$$

For large y, Eq. 5-18 reduces to

$$\frac{dy}{dx} = -b + \frac{Kb}{a}\cos x \tag{5-19}$$

Solution of the differential equation in Eq. 5-19 readily yields

$$y = -bx - \frac{Kb}{a}\sin x + C \tag{5-20}$$

For typical design parameters these trajectories are seen to be nearly sinusoidal with a slight amount of skew, such as those shown in Fig. 5-7. A comparison of the results in Eqs. 5-17 and 5-20, then, show significant differences which shall be investigated in greater detail subsequently.

This section has served to give some initial insight into the phase plane portraits for the generalized second-order PLL and the ERPLD, prior to using computer techniques for generating

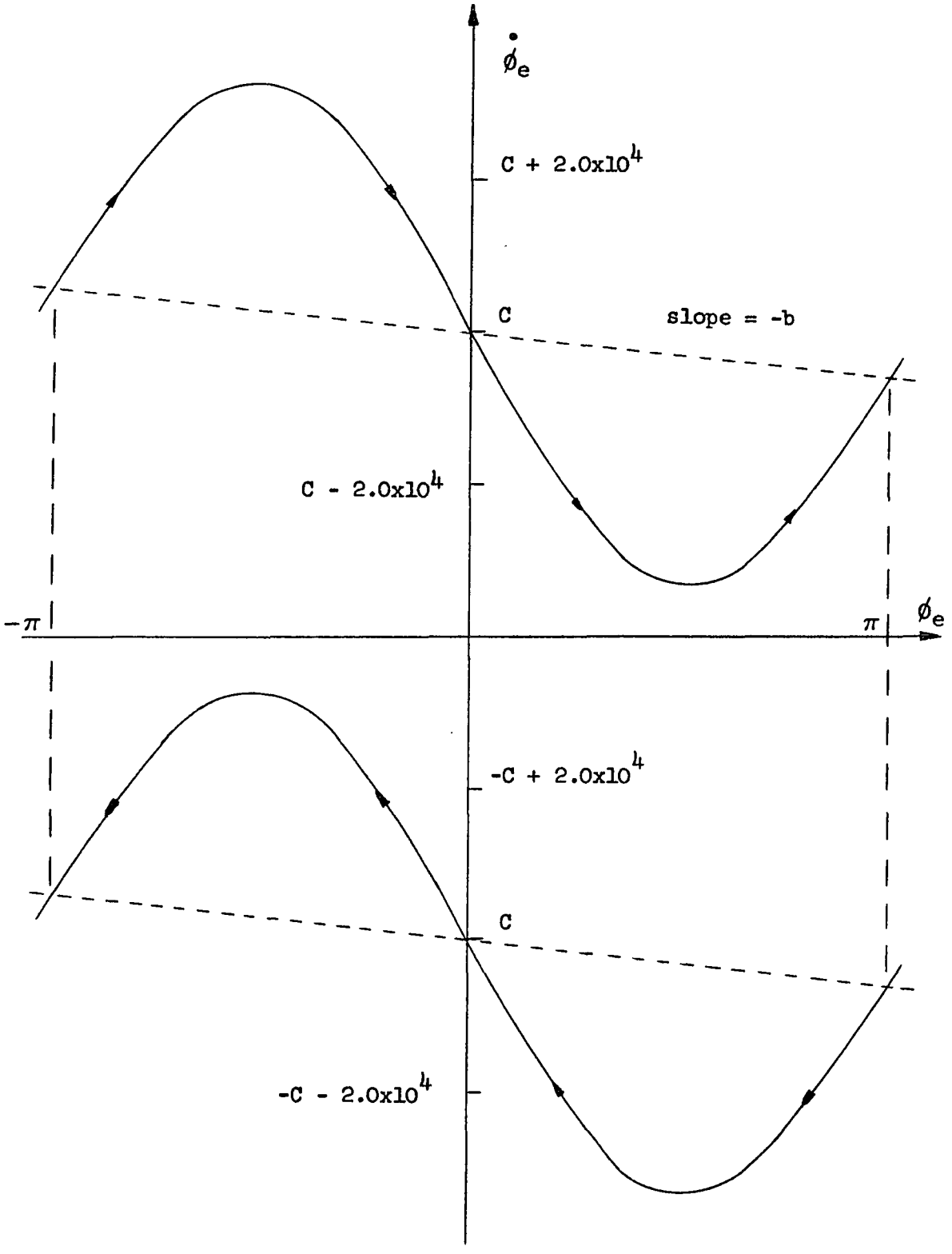

Fig. 5-7. Typical phase plane trajectories for large frequency error for a standard second-order, type one PLL.

such portraits. In addition, these results will serve as an additional check on the computer analysis.

5.3.3 Determination of Singular Points. The singular points of a differential equation are critical in determining the properties of its solution. Through the study of the singularities, considerable insight into the qualitative aspects of the solution as well as some quantitative properties can be obtained. Insofar as the phase plane portrait is concerned, the determination and classification of the singularities is an extremely important procedure to be performed prior to determining the actual trajectories.

Consider the differential equation under investigation given by Eq. 5-12. This equation may be expressed in the form

$$\frac{dy}{dx} = \frac{Q(x,y)}{P(x,y)} \tag{5-21}$$

where Q(x,y) and P(x,y) are nonlinear functions of x and y. The singularities of Eq. 5-21 are defined as those values of x and y for which P and Q are simultaneously equal to zero [Ref. 5, p. 86 and Ref. 6, p. 76]. In general, the singular points may found by plotting Q(x,y)=0 and P(x,y)=0 and locating the points at which the two curves intersect. For the case at hand, however, the forms

of Q and P are such that the singularities can be found more directly. As will be shown subsequently, it is still desirable to plot $Q(x,y) = 0$ and $P(x,y) = 0$ since this information will give added insight into the phase plane construction. Returning to Eq. 5-12 it is first noted that the singularity search may be divided into two distinct categories. Firstly, for $\alpha < 1$ the singular points are seen to occur at

$$\left.\begin{aligned} x &= \sin^{-1} \frac{\Delta\omega_i}{K} \\ \text{and} \\ y &= 0 \end{aligned}\right\} \qquad (5\text{-}22)$$

Next, for $\alpha \geq 1$, singular points also occur as given by Eq. 5-22; however, additional singularities are seen to exist at

$$x = \text{Cos}^{-1}\left(-\frac{1}{\alpha}\right) \qquad (5\text{-}23)$$

with y given by the solution to the quadratic equation

$$y^2(\alpha \,\text{Sin}\, x) - y(b + M \,\text{Cos}\, x) + (b\Delta\omega_i - N \,\text{Sin}\, x) = 0 \qquad (5\text{-}24)$$

after substitution of the value of x given by Eq. 5-23. It should be noted that Eq. 5-22 and Eq. 5-23 are indicative of an infinite number of singularities because of the multi-valued nature of the arc functions; however, as indicated earlier, the principal values are the only ones of concern. Finally, in Eq. 5-22, note that the singularities exist only for $\Delta\omega_i \leq K$.

In the analysis which follows, the basic Acampora and Newton values will again be used [Ref. 3]. Values of $\Delta\omega_i/K$ of 0.4, 0.6, 0.9, and 1.1 will be investigated for a range of α from 0.1 to 10.0. Consider first Figs. 5-8 through 5-13 which show the determination of singular points for $\Delta\omega_i \leq 0.4$ over a range of α from 0.1 to 10.0. Referring to Eq 5-21 it is noted that these figures represent plots of Q(x,y) = 0 and P(x,y) = 0. Starting with Fig. 5-8, Q(x,y) = 0 is the multi-valued function given by Eq. 5-24. P(x,y) = 0 for this case only when y = 0 which is of course represented by the x-axis. Thus the intersections of the Q(x,y) = 0 curves and the x-axis yield the singular points at (0.412,0.0) and (2.730,0.0). Fig. 5-9 and Fig. 5-10 (note scale change) show a change in the Q(x,y) = 0 curve, but the identical singularities as expected. Fig. 5-11 again shows the two previous singularities, but in addition P(x,y) = 0 is also satisfied by $x = \pm\pi$ and so new singularities appear as shown. In addition to the new singularities at $(\pm\pi, -1.176\text{x}10^{4})$ theoretically two other singularities exist at the intersection of Q(x,y) = 0 and

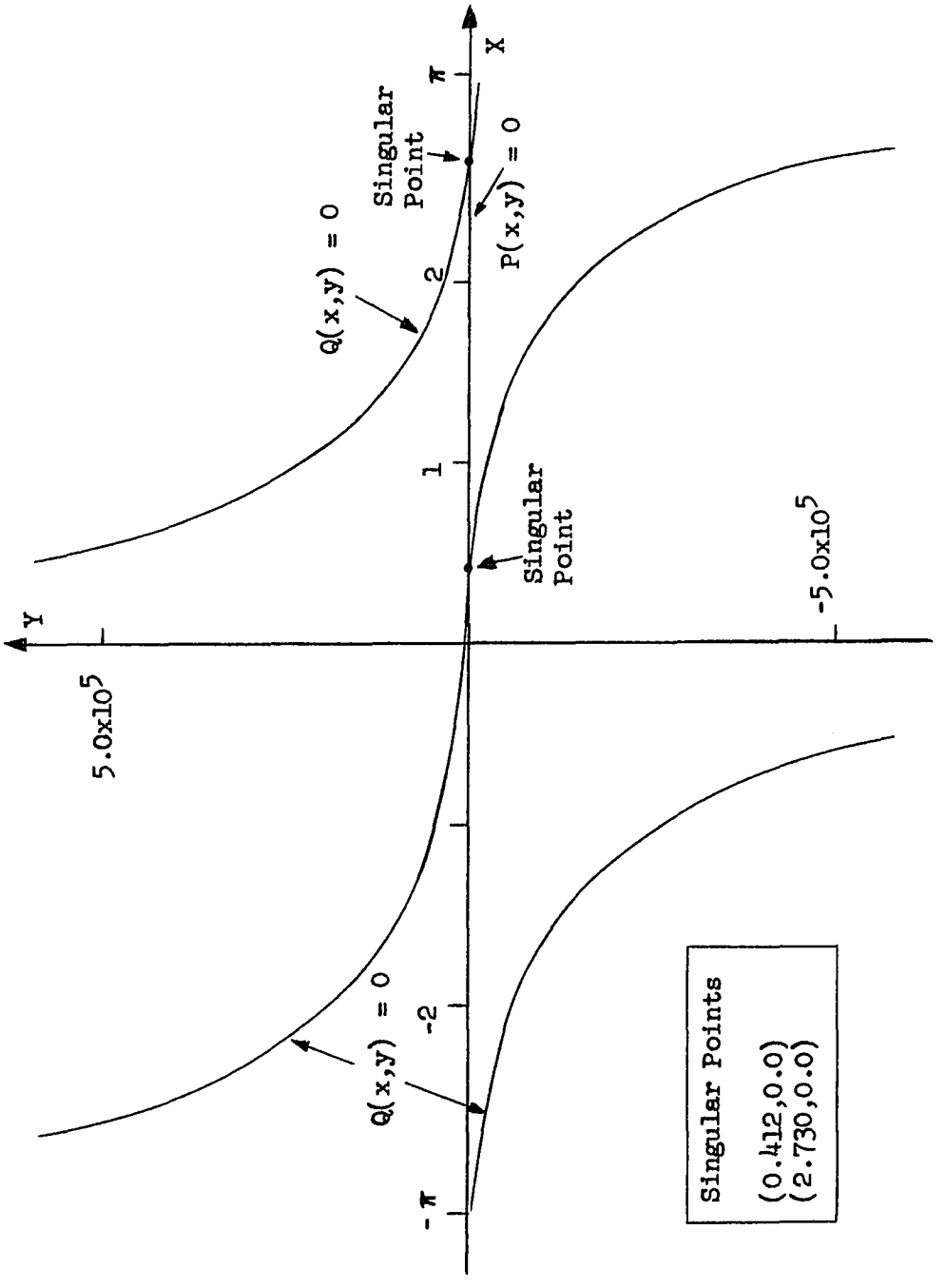

Fig. 5-8. Singular points for $\Delta\omega_1/K = 0.4$ and $\alpha = 0.1$.

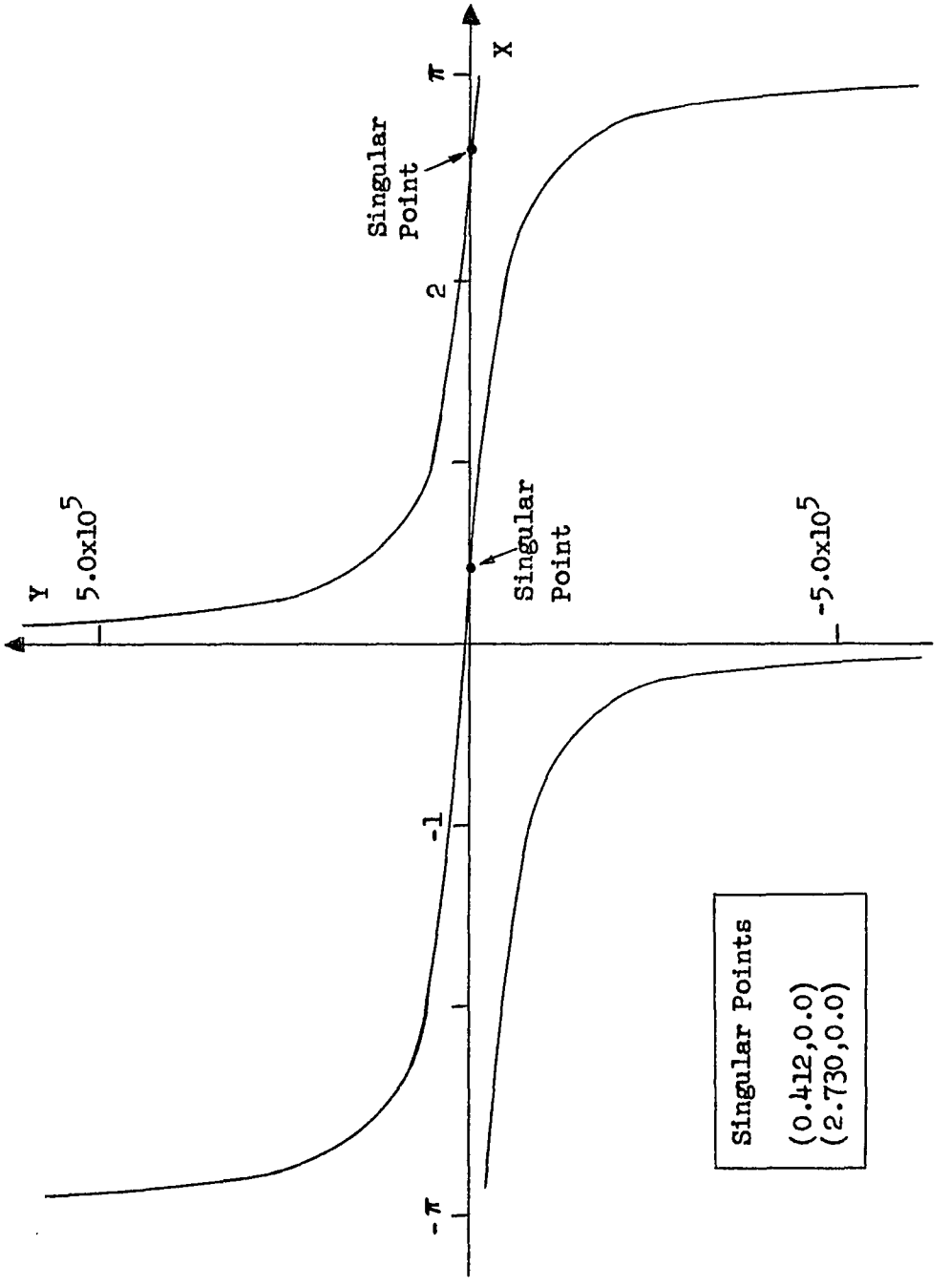

Fig. 5-9. Singular points for $\Delta\omega_1/K = 0.4$ and $\alpha = 0.5$.

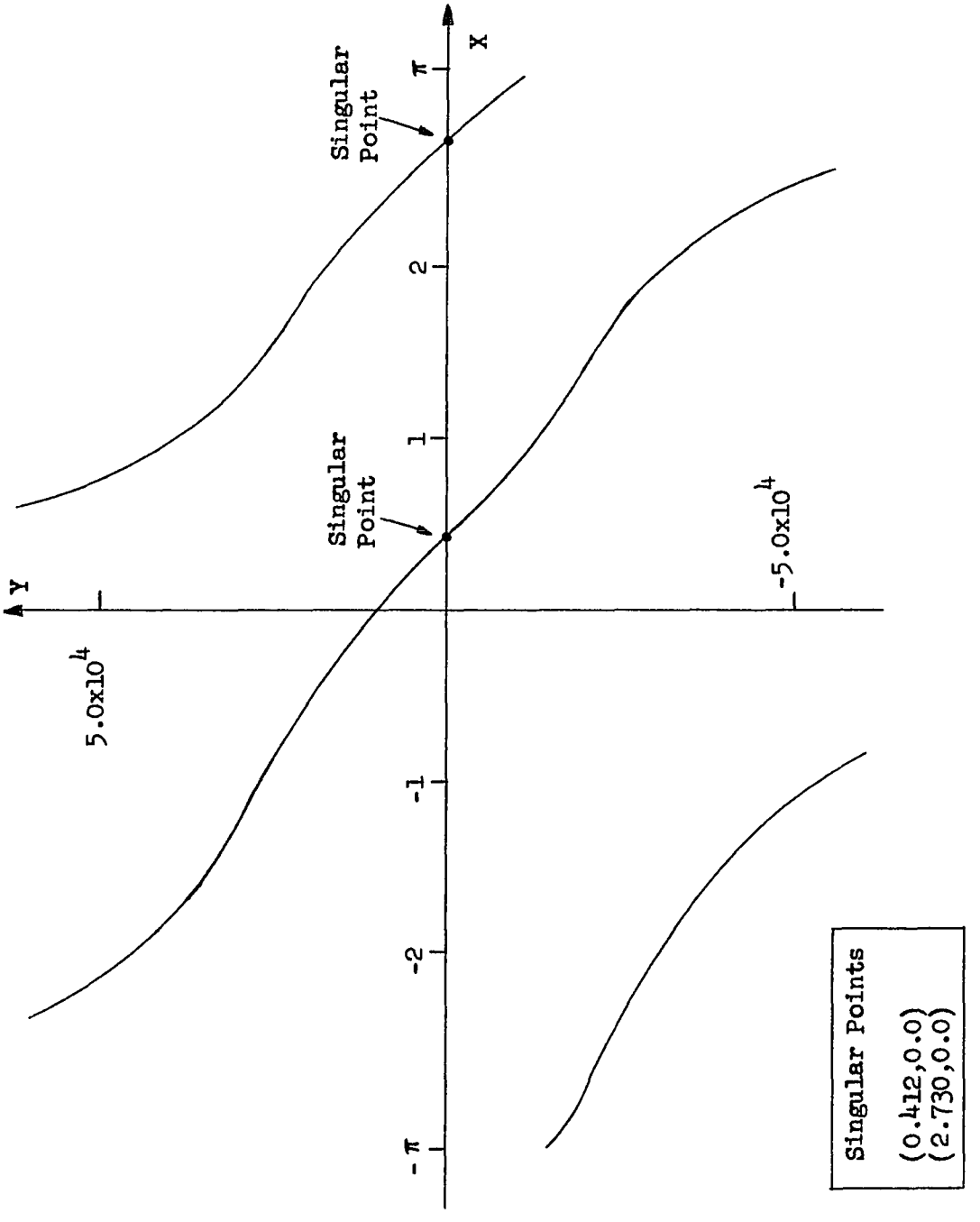

Fig. 5-10. Singular points for $\Delta\omega_1/K = 0.4$ and $\alpha = 0.9$.

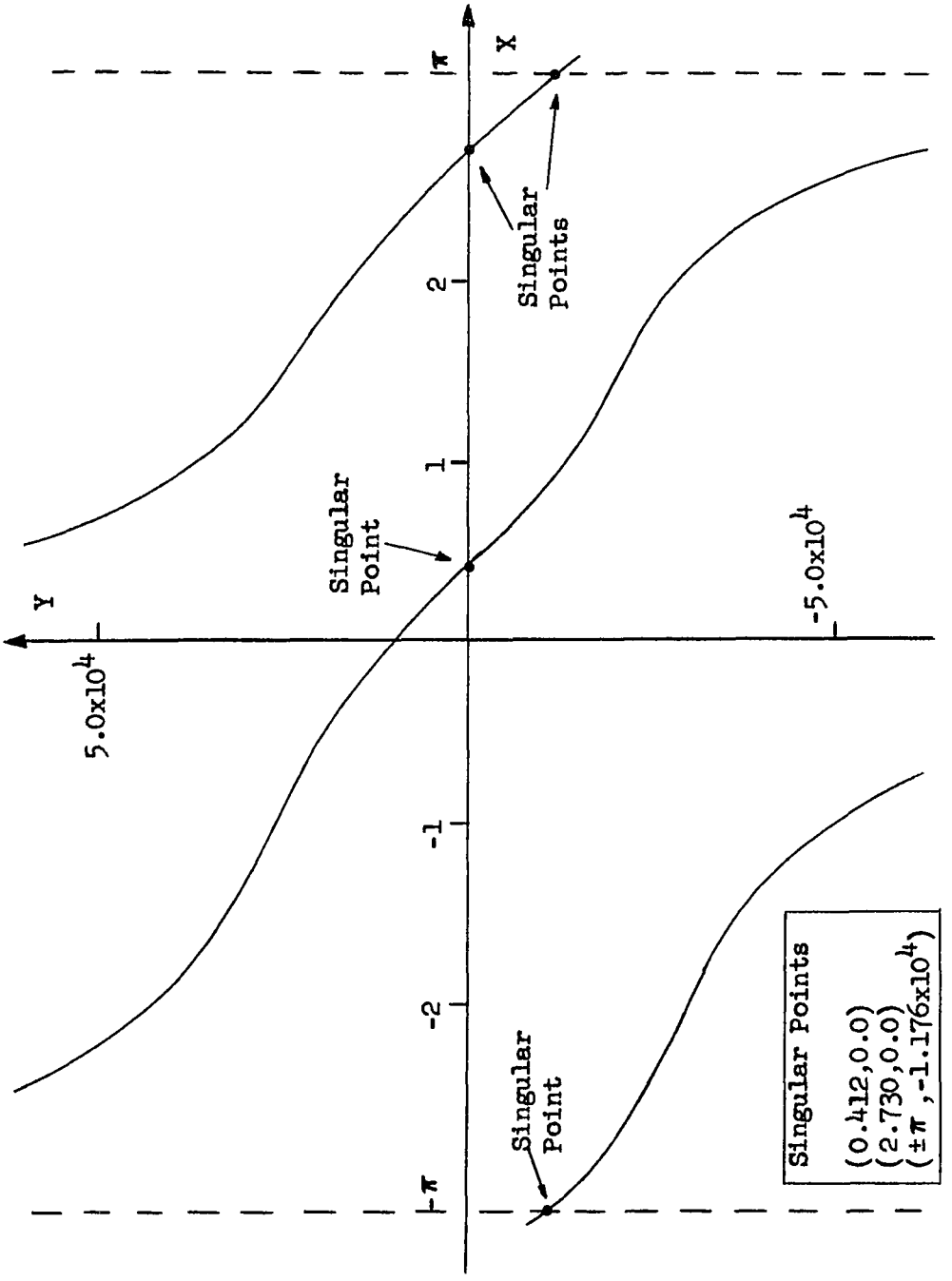

Fig. 5-11. Singular points for $\Delta\omega_1/K = 0.4$ and $\alpha = 1.0$.

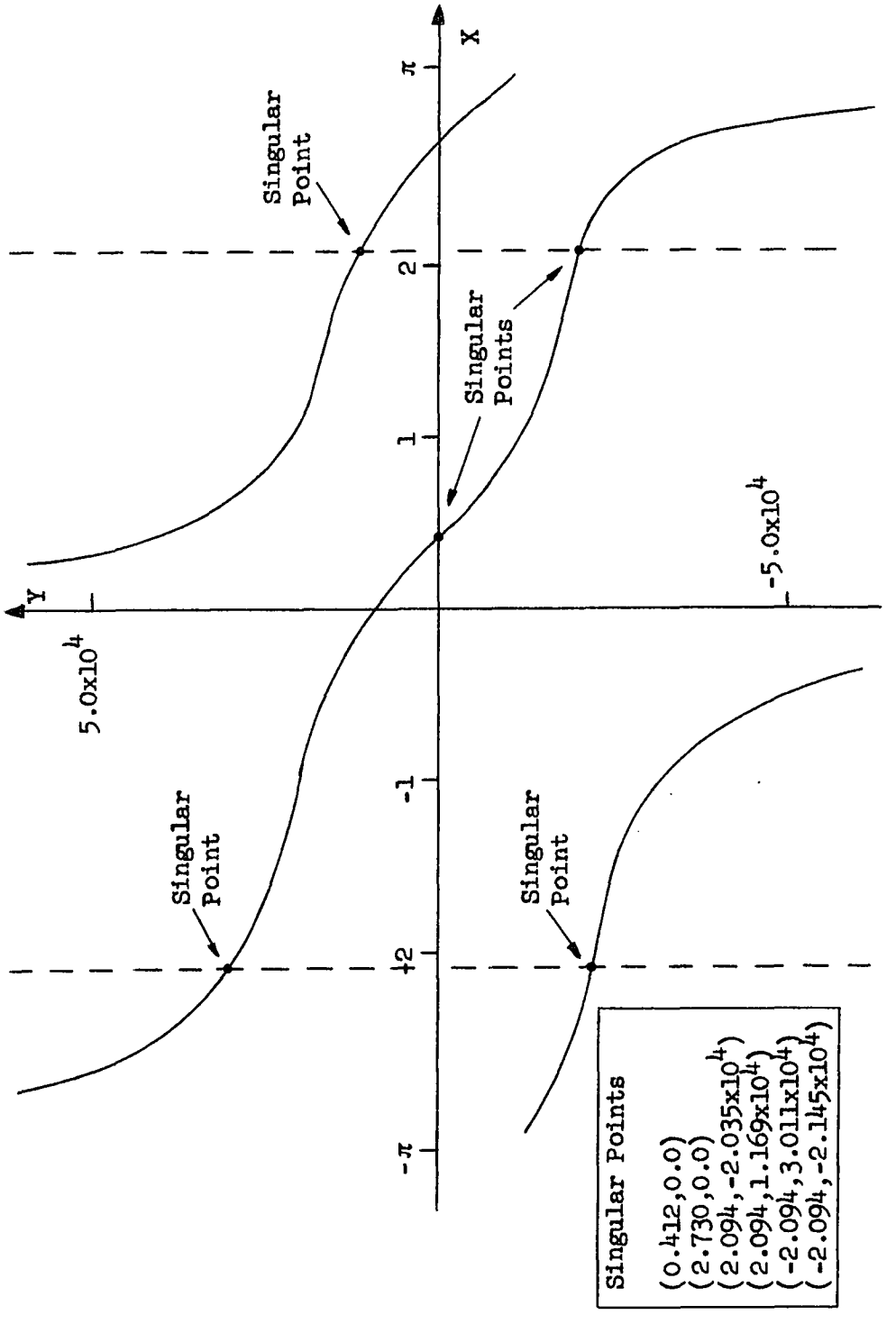

Fig.5-12. Singular points for $\Delta\omega_i/K = 0.4$ and $\alpha = 2.0$.

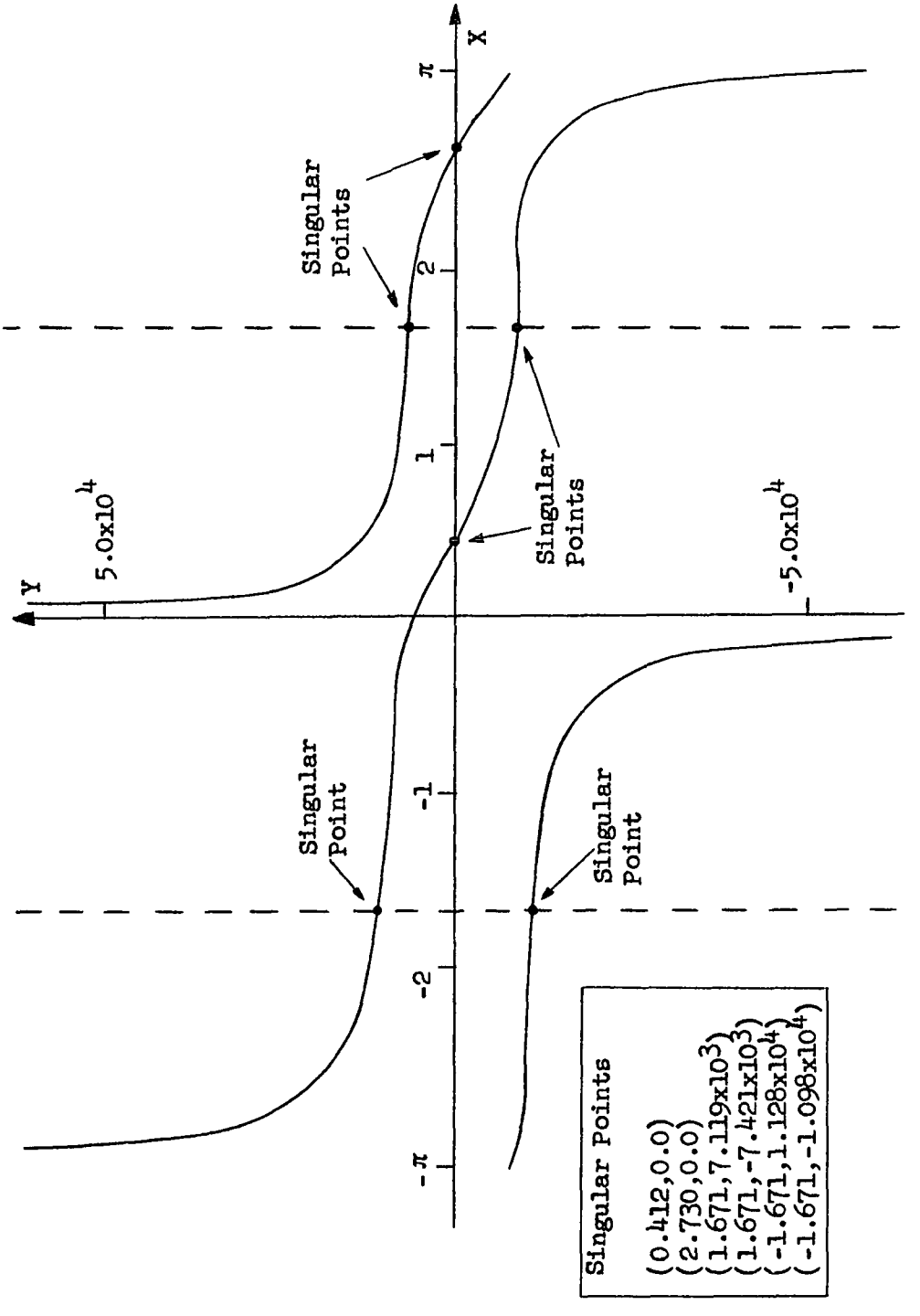

Fig. 5-13. Singular points for $\Delta\omega_i/K = 0.4$ and $\alpha = 10.0$.

$x = \pm\pi$ at infinity. Fig. 5-12 and 5-13 again show the two original singularities at (0.412,0.0) and (2.730, 0.0) along with the two new sets of singularities which move closer to the $x = \pm\pi$ limit as α increases. Besides graphically illustrating the determination of the singularity points, these figures serve another very important function in the determination of the phase plane portraits as indicated in the following discussion.

One popular method for the construction of phase plane portraits is the "method of isoclines" [Ref. 6, pp. 68-70, Ref. 7, pp. 238-241 and Ref. 8, pp. 570-574]. From Eq. 5-21 it is noted that $dy/dx = m$ is the slope of the trajectory on the phase plane. If a specific numerical value of $m = m_1$ is chosen, then

$$\frac{Q(x,y)}{P(x,y)} = m_1 \tag{5-25}$$

defines a curve on the x-y plane which has the property of being the locus of all points for which the slope of trajectories is m_1. This curve is termed an "isocline." If a number of values of m are chosen and the associated isoclines plotted, then the trajectory from a given initial condition may be constructed by using straight-line segments directed according to the slopes associated with the isoclines. By using a sufficient number of isoclines

extremely accurate trajectories can be achieved. Returning to Figs. 5-8 through 5-13 it is noted that the $Q(x,y) = 0$ curves given by Eq. 5-24 are in actuality, isoclines for $m = 0$. Furthermore, the $P(x,y) = 0$ lines given by Eq. 5-23 and $y = 0$ are the isoclines for $m = \infty$. Thus although the isocline method was not specifically used to generate the phase plane portraits given later in this chapter, figures such as Fig. 5-8 serve as an excellent check on the computer generated trajectories. Furthermore, the $m = 0$ and $m = \infty$ isoclines even by themselves yielded a great amount of information on the phase plane behavior. Finally, note that these isoclines check the results shown in Figs. 5-1 through 5-6.

Figs. 5-14 through 5-16 show the singular point determination for $\Delta\omega_i/K = 0.6$ again over a range of α from 0.1 to 10.0. Fig. 5-16 shows an interesting phenomenon, in that a portion of the $m = 0$ isocline has broken away and formed a closed contour. Figs. 5-17 through 5-19 show the singular point determination for $\frac{\Delta\omega_i}{K} = 0.9$ over a range of α from 0.1 to 10.0. These figures in addition, show the breaking off of the closed contour which occurs when values of x are encountered such that the quadratic equation in y given by Eq. 5-24 yields complex roots.

Consider next, the occurrence of singularities for $\Delta\omega_i/K > 1$ Fig. 5-20 shows an example for $\alpha < 1$. The $Q(x,y) = 0$ curve never crosses the x-axis and so no singularities occur. Fig. 5-21 shows

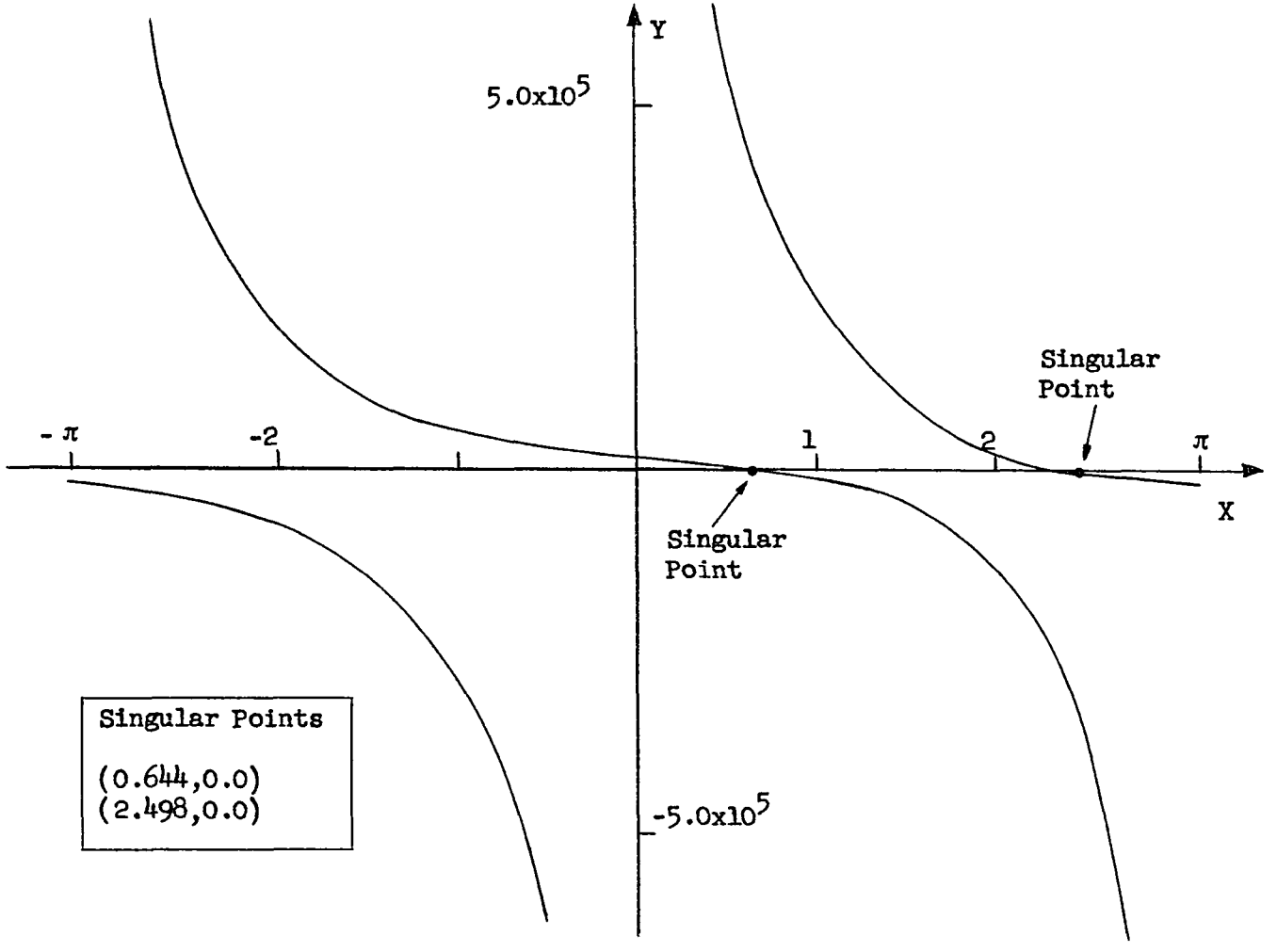

Fig. 5-14. Singular points for $\Delta\omega_1/K = 0.6$ and $\alpha = 0.1$.

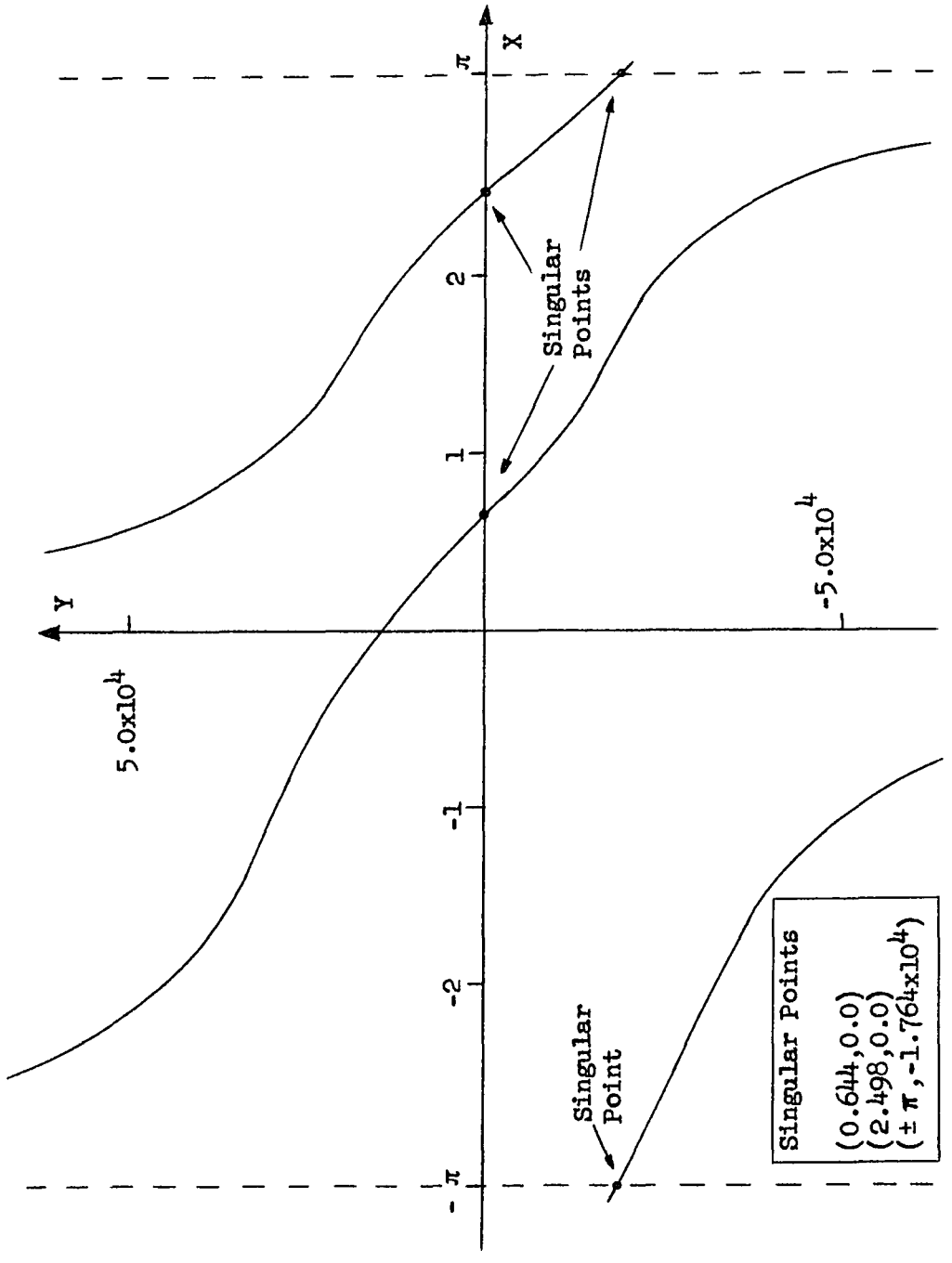

Fig. 5-15. Singular points for $\Delta\omega_i/K = 0.6$ and $\alpha = 1.0$.

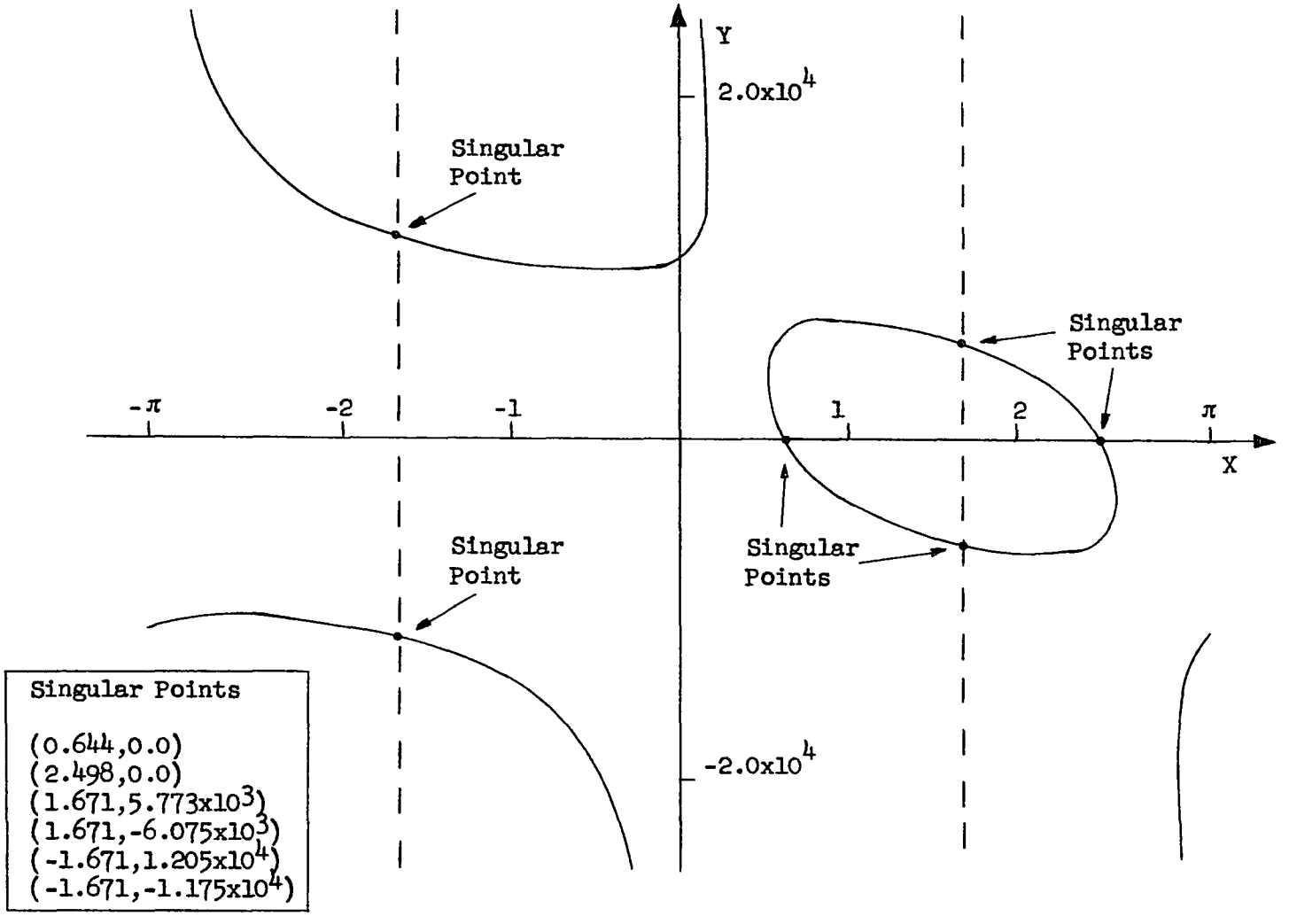

Fig. 5-16. Singular points for $\Delta\omega_i/K = 0.6$ and $\alpha = 10.0$.

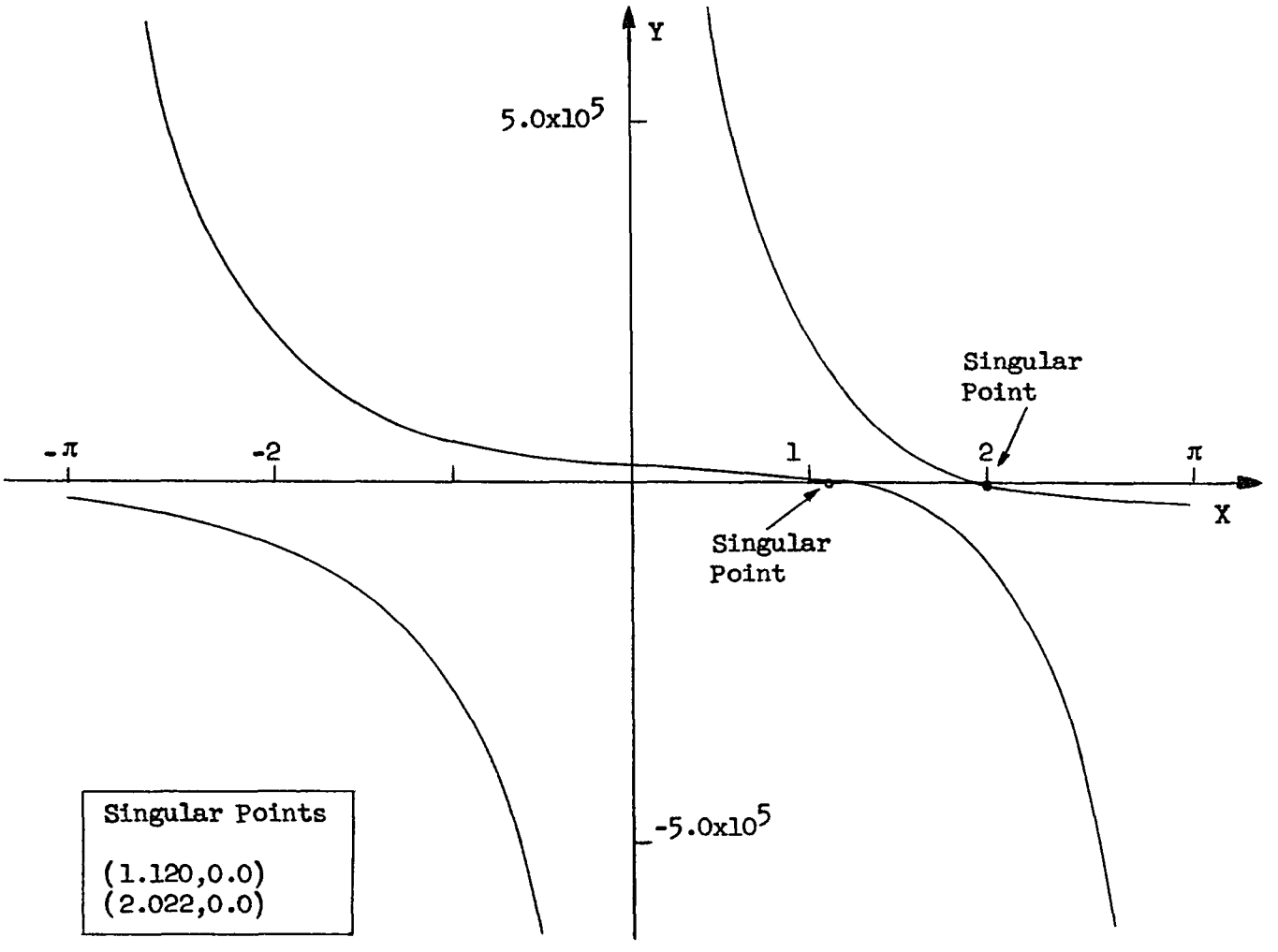

Fig. 5-17. Singular points for $\Delta\omega_i/K = 0.9$ and $\alpha = 0.1$.

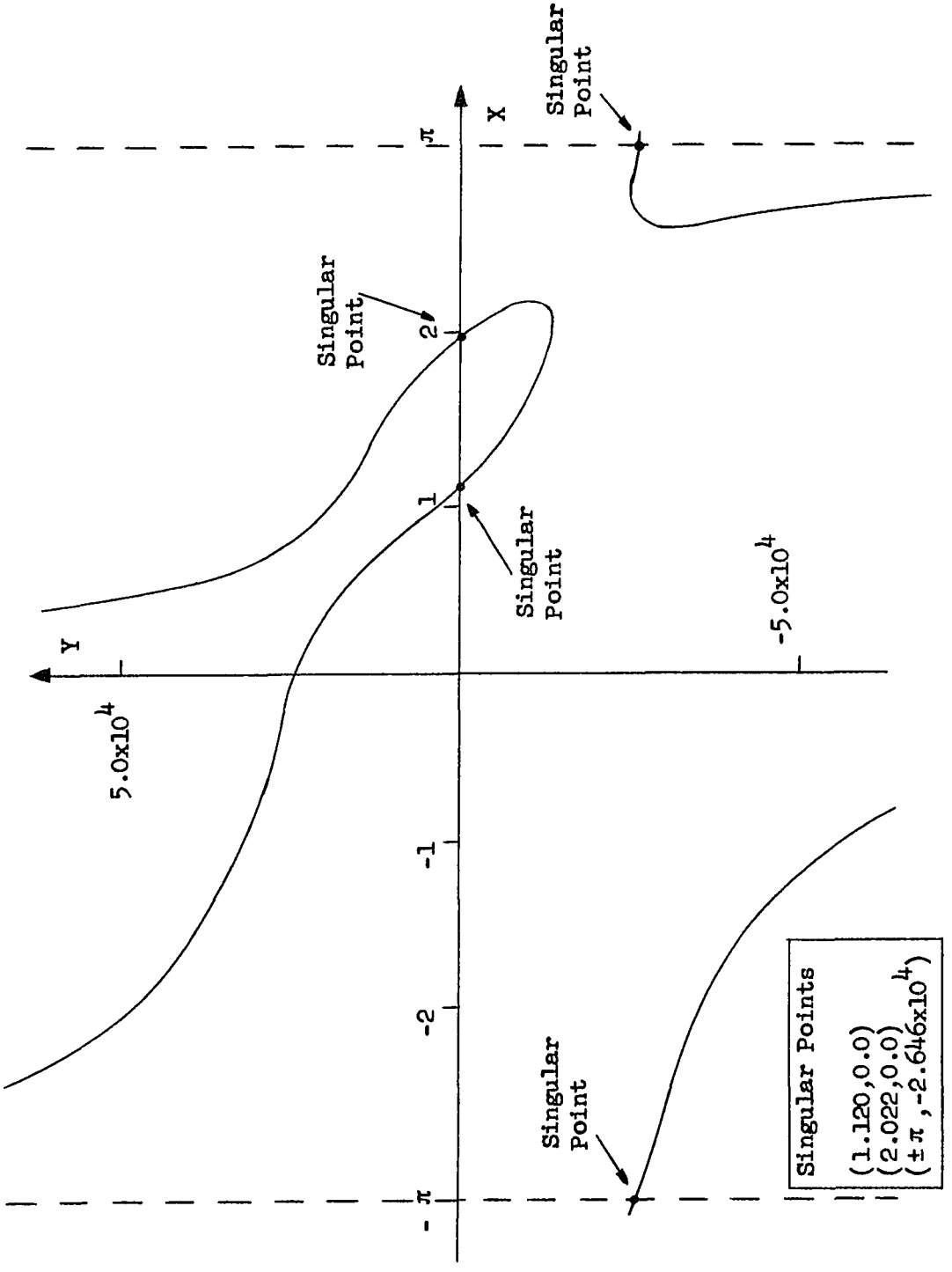

Fig. 5-18. Singular points for $\Delta\omega_1/K = 0.9$ and $\alpha = 1.0$.

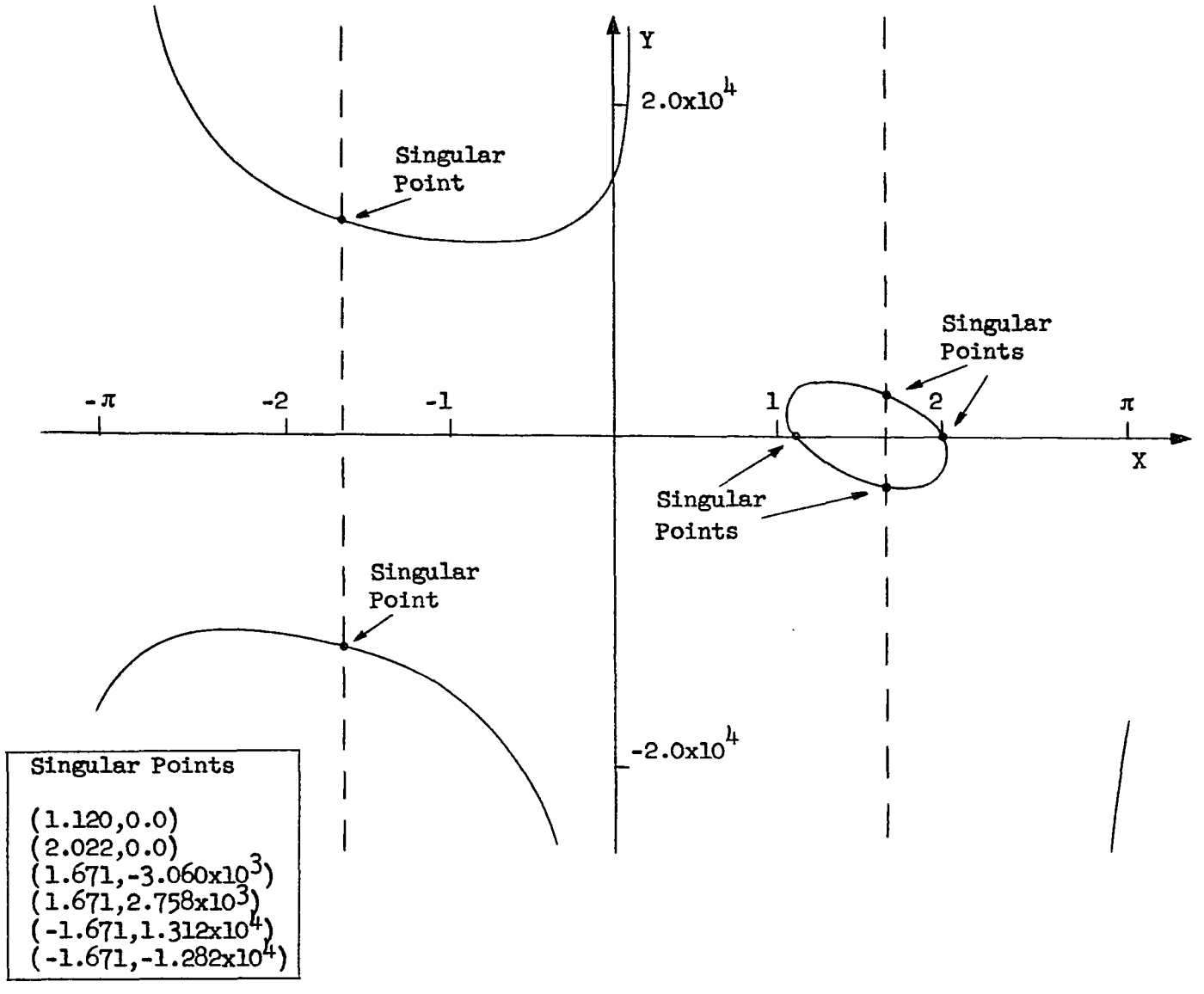

Fig. 5-19. Singular points for $\Delta\omega_i/K = 0.9$ and $\alpha = 10.0$.

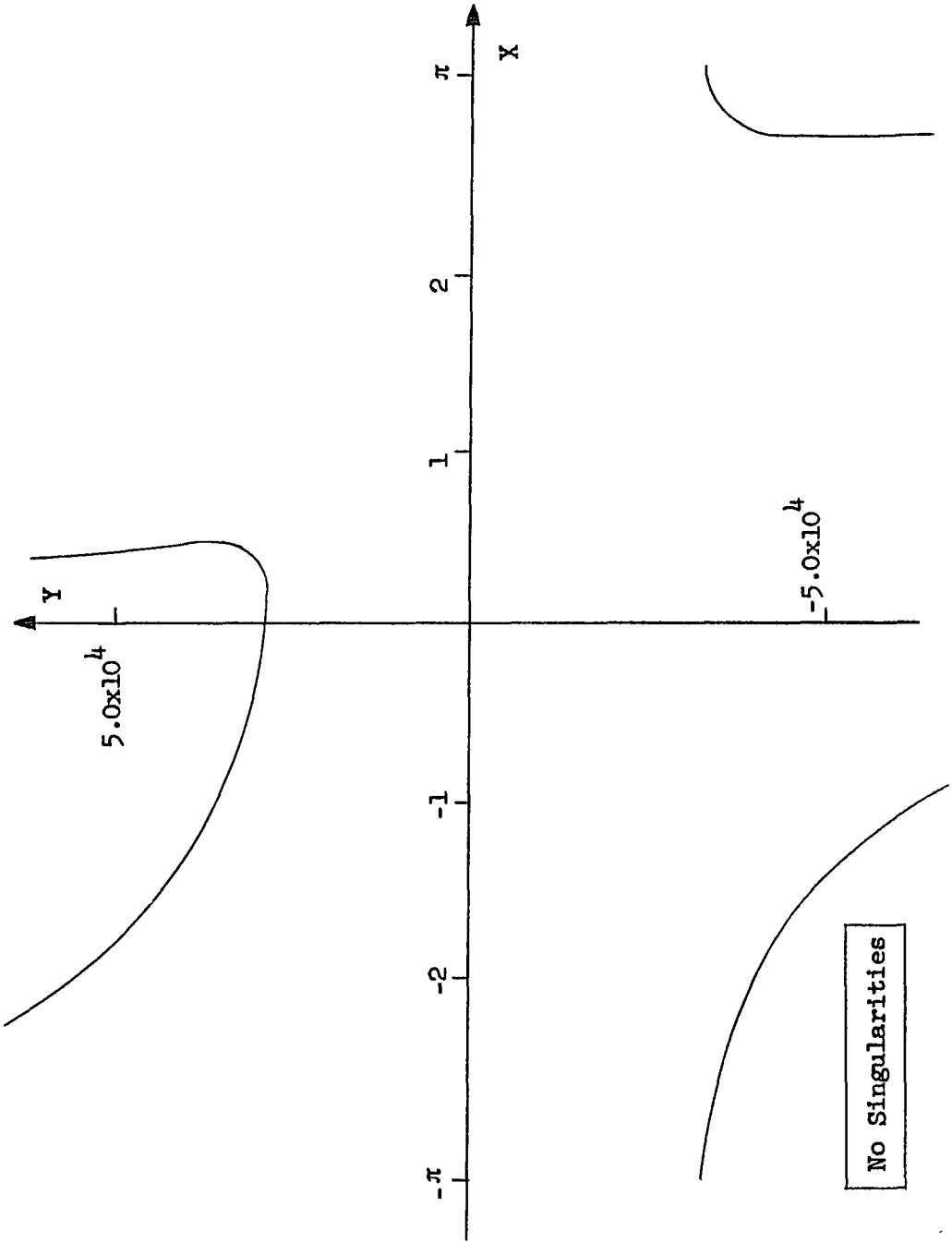

Fig. 5-20. Singular points for $\Delta\omega_1/K = 1.1$ and $\alpha = 0.9$.

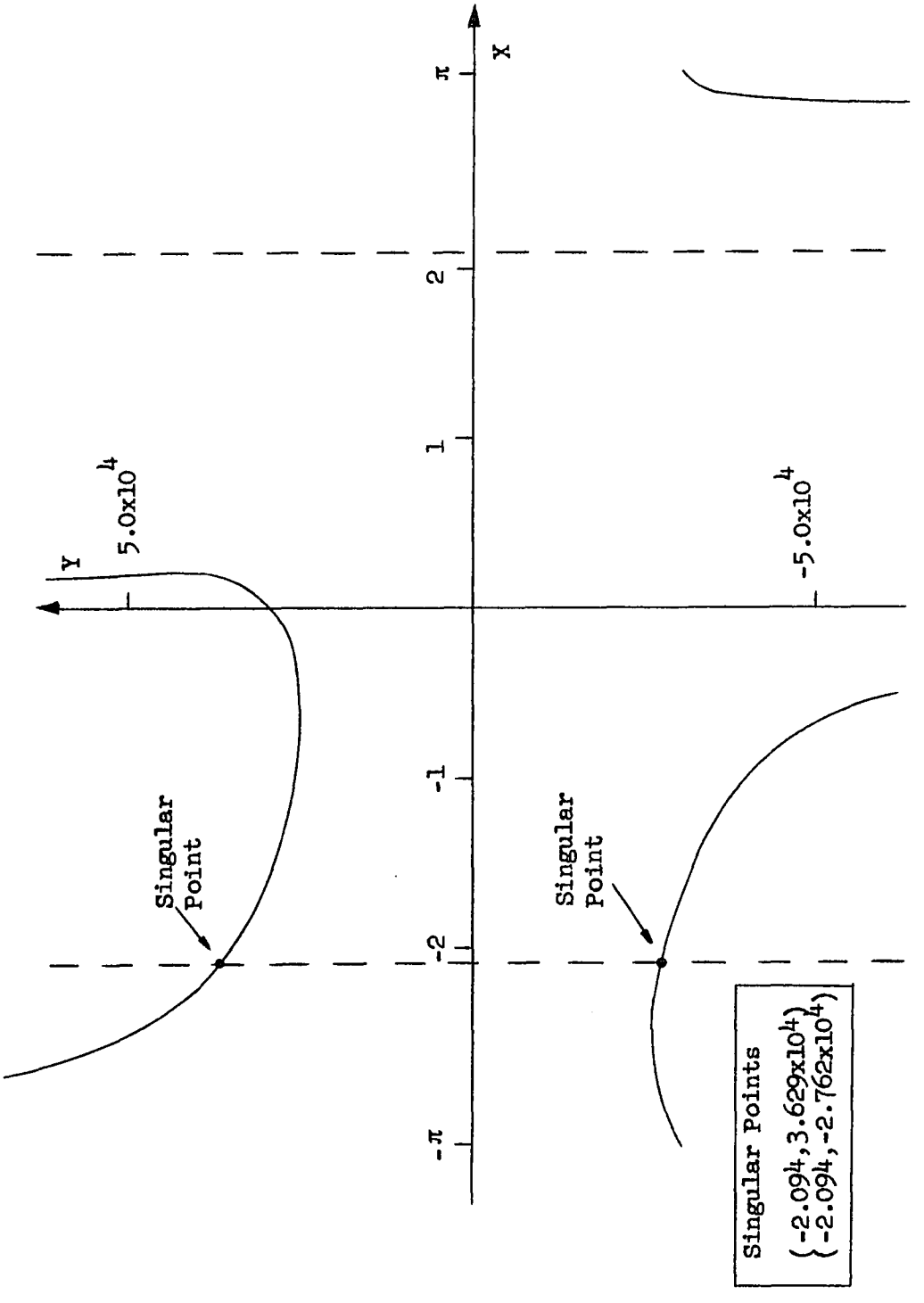

Fig. 5-21. Singular points for $\Delta\omega_1/K = 1.1$ and $\alpha = 2.0$.

an example for $\alpha > 1$. Again no singularities occur along the x-axis; however, from the condition of Eq. 5-23 it is noted that a pair of singularities occur along the x = -2.094 line. In this case no singular points occur along the x = 2.094 line since no intersections with the Q(x,y) = 0 curve exist.

Finally, it is again of interest to compare the preceding results with that for the standard second-order PLL. From Eq. 5-18 the singularities can occur only at

$$\left.\begin{aligned} x &= \sin^{-1} \frac{\Delta\omega_i}{K} \\ \text{and} \\ y &= 0 \end{aligned}\right\} \qquad (5\text{-}26)$$

In this case, it is necessary that $\Delta\omega_i \leq K$ for any singularities to occur. Fig 5-22 shows the singular point determination for a typical second-order PLL design (voice modulation) with $\Delta\omega_i / K = 0.4$.

5.3.4 Classification of Singular Points. Having determined the position of the singularities on the phase plane, the next task is to determine their classification. The analysis of

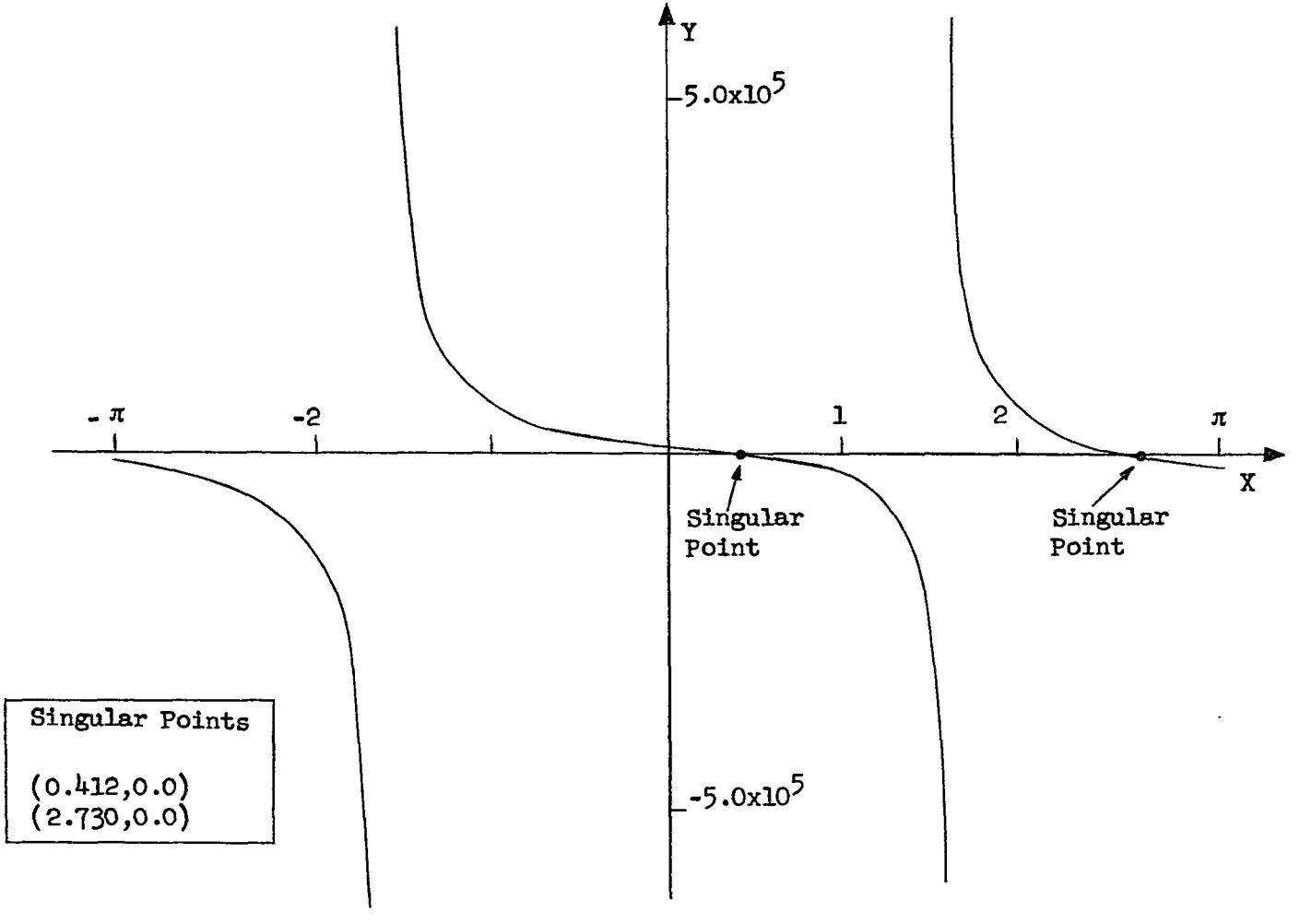

Fig. 5-22. Singular points for standard second-order, type one PLL; $\Delta\omega_i/K = 0.4$.

singular points for a nonlinear system is accomplished by a process of linearization as will be subsequently shown. Recall that the general form of the phase plane equation is given by Eq. 5-21, where Q(x,y) and P(x,y) may be linear or nonlinear. The first step in determining the classification of the singularity is to translate the origin to a selected singular point. This may be accomplished by making the substitution

$$\left.\begin{aligned} x &= X + x_s \\ \text{and} \\ y &= Y + y_s \end{aligned}\right\} \qquad (5\text{-}27)$$

where (x_s, y_s) is the singular point under consideration. After translation, Eq. 5-21 may be expanded into the form

$$\frac{dY}{dX} = \frac{cX + dY + Q'(X,Y)}{aX + bY + P'(X,Y)} \qquad (5\text{-}28)$$

where $Q'(x,y)$ and $P'(x,y)$ contain neither constant terms nor linear terms in x and y [Ref. 5, p. 86, Ref. 6, pp. 81-82 and Ref. 9, p. 114]. The system may be linearized at the singular point by discarding $Q'(x,y)$ and $P'(x,y)$ since near the singularity the linear terms dominate. The linearized equation then becomes

$$\frac{dY}{dX} = \frac{cX + dY}{aX + bY} \tag{5-29}$$

The characteristic equation associated with Eq. 5-29 is given by [Ref. 5, p. 91 and Ref. 9, p. 115]

$$\lambda^2 - (a + d)\lambda + (ad - bc) = 0 \tag{5-30}$$

The location of the roots λ_1 and λ_2 of the characteristic equation in the complex plane then determine the classification of the singular point. It can be seen that six possible cases exist:

1. λ_1 and λ_2 are complex conjugates in the left-half plane.
2. λ_1 and λ_2 are complex conjugates in the right-half plane.
3. λ_1 and λ_2 are purely imaginary.
4. λ_1 and λ_2 are real and negative.
5. λ_1 and λ_2 are real and positive.
6. λ_1 and λ_2 are real and opposite in sign.

Each of these cases along with the corresponding singularity classification, are shown in Fig. 5-23. The sketches of the singular points in this figure are only meant to exemplify typical singularities. The actual trajectories about a given singular point can differ significantly from those shown.

The next task is to apply the preceding theory to the results of the previous section. Consider the two singular points shown in Fig. 5-8. Taking first the point (0.412,0.0), it is noted that in Eq 5-27 only the translation in the x-direction is required. Making the required substitution into Eq. 5-12 yields

$$\frac{dY}{dX} = \frac{b\,\Delta\omega_1 - N\,\mathrm{Sin}\left[X+0.412\right] - \left(b + M\,\mathrm{Cos}\left[X+0.412\right]\right)Y + \alpha\,Y^2\,\mathrm{Sin}\left[X+0.412\right]}{Y\left(1 + \alpha\,\mathrm{Cos}\left[X+0.412\right]\right)} \tag{5-31}$$

In order to put Eq. 5-31 into the proper form, it is first necessary to express the sine and cosine terms as follows

$$\left.\begin{aligned} \sin\left[x+0.412\right] &= \sin x \cos 0.412 + \cos x \sin 0.412 \\ \cos\left[x+0.412\right] &= \cos x \cos 0.412 - \sin x \sin 0.412 \end{aligned}\right\} \tag{5-32}$$

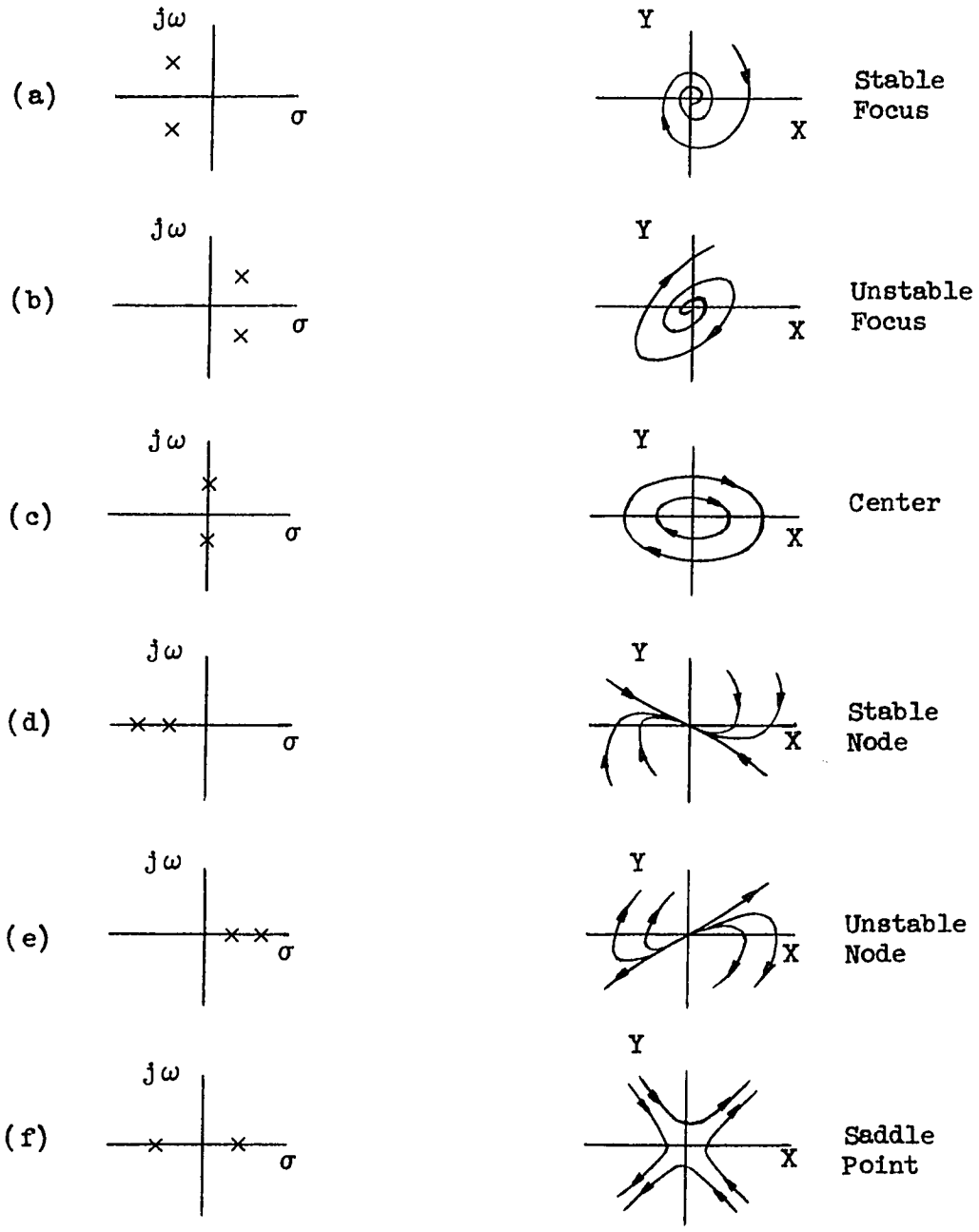

Fig. 5-23. Classification of singular points.

Next, the series representation of sinx and cosx must be substituted into Eq. 5-32. After carrying through the indicated multiplications and substituting the parameter values, Eq. 5-31 may be expressed as

$$\frac{dY}{dX} = \frac{-8.094\times10^{8}\,X - 2.958\times10^{4}\,Y + Q'(X,Y)}{1.092\,Y + P'(X,Y)} \tag{5-33}$$

where again Q'(x,y) and P'(x,y) contain neither constants nor linear terms in x and y. The characteristic equation is then given by

$$\lambda^2 + 2.958\times10^{4}\lambda + 8.839\times10^{8} = 0 \tag{5-34}$$

with the corresponding roots

$$\lambda_1,\lambda_2 = -1.479\times10^{4} \pm j\ 2.579\times10^{4} \tag{5-35}$$

This corresponds to the case shown in Fig. 5-23(a) and so the singularity is a "stable focus."

Next, consider the second singularity located at (2.730,0.0). Following the same procedure used in the previous example yields

$$\frac{dY}{dX} = \frac{8.094\text{x}10^{8}\,X + 2.582\text{x}10^{4}\,Y + Q'(X,Y)}{0.908\,Y + P'(X,Y)} \tag{5-36}$$

The corresponding characteristic equation is given by

$$\lambda^2 - 2.582\text{x}10^{4}\,\lambda - 7.353\text{x}10^{8} = 0 \tag{5-37}$$

which has the roots

$$\lambda_1,\lambda_2 = 4.294\text{x}10^{4}\ ,\ -1.712\text{x}10^{4} \tag{5-38}$$

This corresponds to the case shown in Fig. 5-23(f) and so the singularity is a "saddle point." Although, the previous examples were based on the parameters of Fig. 5-8, it can readily be shown that the singularity pairs on the x-axis in Fig. 5-9 through Fig. 5-19 fall into the same classifications i.e a stable focus and a saddle point. In addition, the singularity pair associated with the standard second-order PLL in Fig. 5-22 are found to be a stable focus at (0.412,0.0) and a saddle point at (2.730, 0.0).

Finally, consider the additional singularities which occur along the lines defined by Eq. 5-23 when $\alpha \geq 1$. The illustrative example chosen is the singular point (2.094, 1.169 x 10^4) in Fig. 5-12. In this case both a translation in the x and y direction are required. Making the required substitutions into Eq. 5-12 yields

$$\frac{dY}{dX} = \frac{b\,\Delta\omega_i - N\,\mathrm{Sin}\left[X+2.094\right] - \left(b + M\,\mathrm{Cos}\left[X+2.094\right]\right)\left(Y + 1.169\times10^4\right)}{\left(Y + 1.169\times10^4\right)\left(1 + \alpha\,\mathrm{Cos}\left[X+2.094\right]\right)} \quad (5\text{-}39)$$

$$+ \frac{\alpha\left(Y + 1.169\times10^4\right)^2\,\mathrm{Sin}\left[X+2.094\right]}{\left(Y + 1.169\times10^4\right)\left(1 + \alpha\,\mathrm{Cos}\left[X+2.094\right]\right)}$$

which may be expressed as

$$\frac{dY}{dX} = \frac{9.208\times10^8\,X + 5.553\times10^4\,Y + Q'(X,Y)}{-\,2.025\times10^4\,X + P'(X,Y)} \quad (5\text{-}40)$$

The corresponding characteristic equation is given by

$$\lambda^2 - 3.528\times10^4\,\lambda - 1.124\times10^9 = 0 \quad (5\text{-}41)$$

which has the roots

$$\lambda_1, \lambda_2 = 5.552\times10^4\ ,\ -\,2.024\times10^4 \quad (5\text{-}42)$$

Again, this corresponds to the case shown in Fig. 5-23(f) and so the singularity is a "saddle point." It can readily be shown that the other singular points located on the lines $x = \pm 2.094$ in Fig. 5-12 are also saddle points. Indeed, in each of the Figs. 5-11 through 5-19, for which $\alpha \geq 1$, the singularities on the lines given by Eq. 5-23 are seen to be saddle points.

5.3.5 Computer Generation of Phase Plane Portraits. In the previous sections, a number of key properties of the phase plane were analyzed including location and classification of singular points, phase plane behavior for large frequency error and the isocline method. It remains to generate a series of trajectories over the range of parameters of interest and interpret the results in order to complete the phase plane analysis. Again, the results are presented in terms of the basic Acampora and Newton ERPLD or equivalent filter ERPLD parameters [Ref. 3] in order that the transition from the standard second-order PLL to these more complex devices be shown more clearly. For all intents and purposes, however, these results apply directly to the generalized second-order PLL through the change of variables given in Eq. 5-5. Values of $\Delta\omega_i / K$ of 0.4, 0.6 and 0.9 were investigated for a range of α from 0.1 to 0.9 with again the primary thought in mind being to determine how the phase plane portrait changes in the transition from the standard to the generalized second-order PLL over a range of frequency offsets $\Delta\omega_i$. In addition, a phase plane portrait for $\alpha = 1$ was

generated for comparison purposes.

The phase plane trajectories were determined by the solution of Eq. 5-7 on the digital computer using the Continuous System Modeling Program (CSMP). Details on the use of CSMP were presented in the previous chapter. Fig. 5-24 shows an example of a CSMP program used to generate a typical phase plane trajectory.

Figs. 5-25 through 5-28 show pertinent phase plane trajectories for $\Delta\omega_i / K = 0.4$ and $\alpha = 0.1$. Note that the trajectory motion as a function of time is always from left to right in the upper half plane and right to left in the lower half plane. Fig. 5-25 indicates that for a small negative frequency error, the trajectory moves to the region of the stable focus and achieves lock-in without skipping cycles. It should be noted that theoretically it requires an infinite amount of time to actually reach the lock-in point at (0.412,0.0); however, it is normally assumed that lock-in has occurred at time t_o such that $|\phi_e(t_o) - \phi_e(\infty)| < \delta$ where δ is some small allowed error [Ref 1, p. 99]. As the initial frequency error is increased further and further in the negative direction, the system begins to skip cycles before lock-in occurs. For example, in Fig. 5-27, three cycles are skipped prior to lock-in. For positive initial frequency error, lock-in occurs for some initial conditions but not for others. In particular, there is a limit cycle at 1.66×10^5 below which the trajectories tend to

```
TITLE PHASE PLANE TRAJECTORY GENERATION

INITIAL
CONSTANT DELOMG=4.23E5
CONSTANT ALPHA=0.5
CONSTANT A=2.94E4
CONSTANT B=1.88E3
CONSTANT XK=4.7E5
         XM=ALPHA*B+XK*B/A
         XN=XK*B
DYNAMIC
         PHI1=INTGRL(-1.0E4,PHI2)
          PHI=INTGRL(3.1415927,PHI1)
        XNEW2=SIN(PHI)
        XNEW3=COS(PHI)
        XNEW4=B*DELOMG
        XNEW5=(-XN)*XNEW2
        XNEW6=(XM*XNEW3+B)*(-PHI1)
        XNEW7=(PHI1**2)*ALPHA*XNEW2
        XNEW8=1.0+ALPHA*XNEW3
         PHI2=(XNEW4+XNEW5+XNEW6+XNEW7)/XNEW8
TIMER DELT=1.0E-7,PRDEL=1.0E-6,FINTIM=2.5E-3
PRINT PHI,PHI1
METHOD RECT
END
STOP
```

Fig. 5-24. CSMP program used to generate a typical phase plane trajectory.

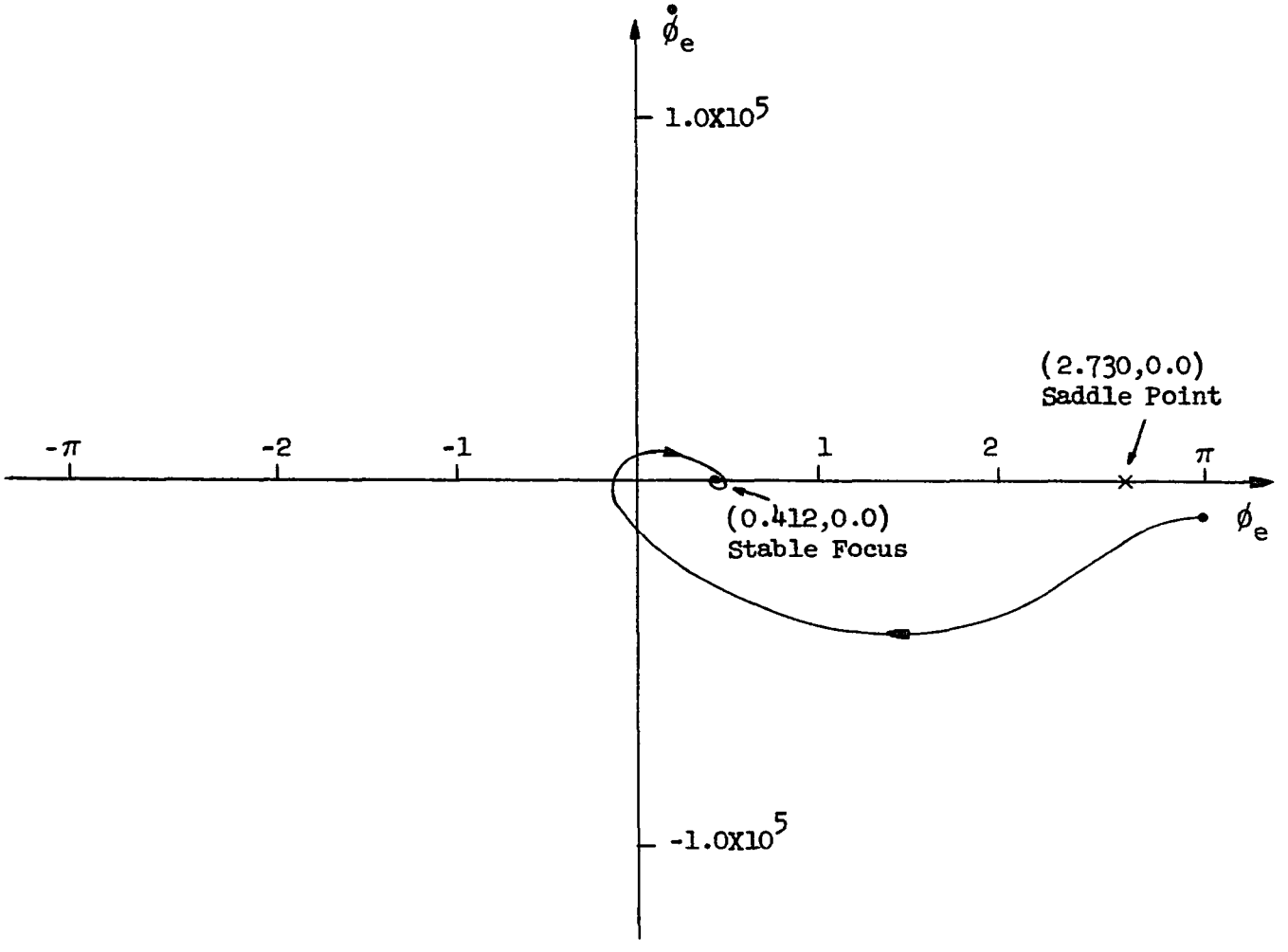

Fig. 5-25. Phase plane trajectory for $\Delta\omega_i/K = 0.4$, $\alpha = 0.1$, $\dot{\phi}_e(0) = -1.0\text{x}10^4$ and $\phi_e(0) = \pi$.

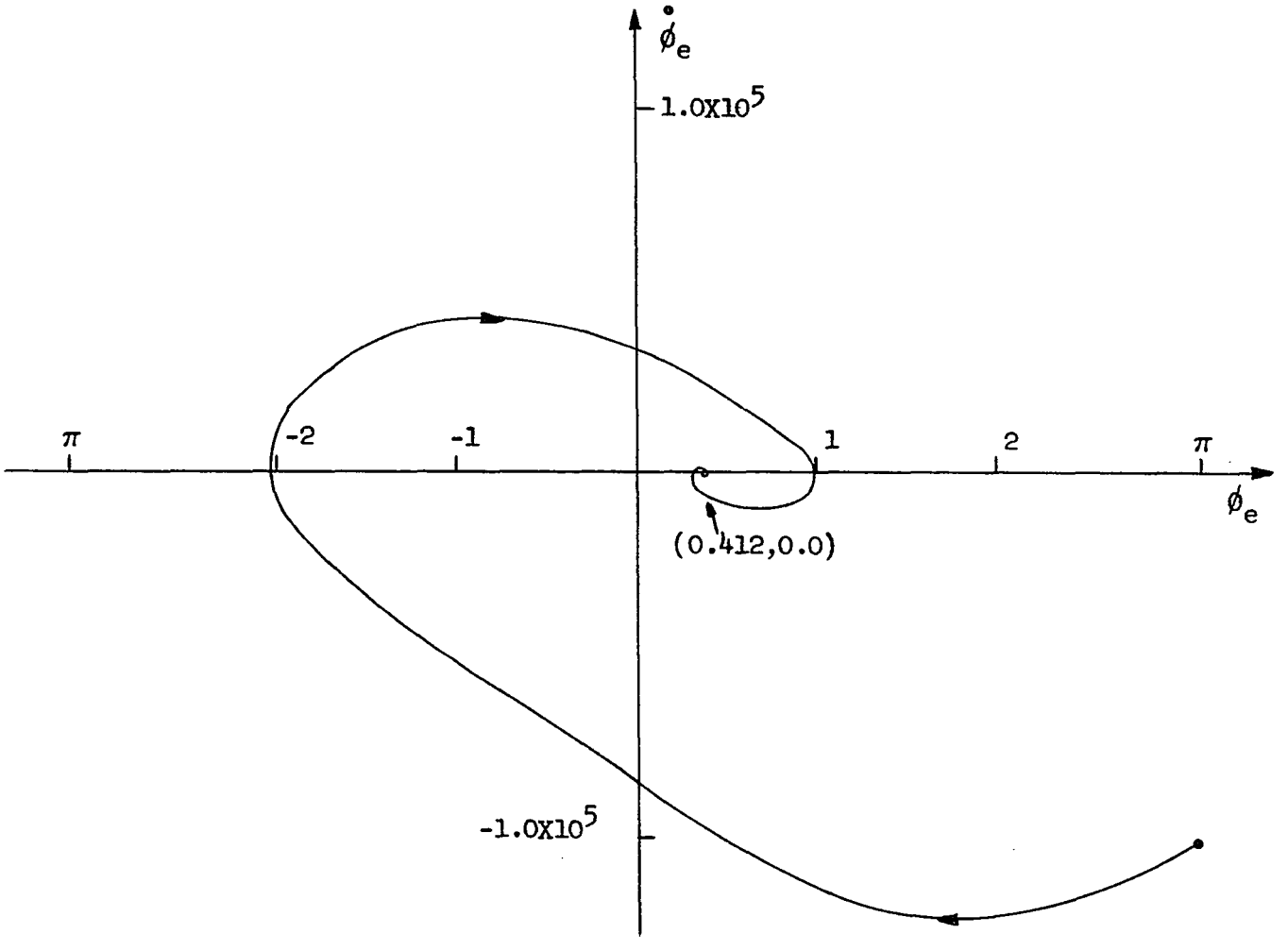

Fig. 5-26. Phase plane trajectory for $\Delta\omega_i/K = 0.4$, $\alpha = 0.1$, $\dot{\phi}_e(0) = -1.0\text{x}10^5$ and $\phi_e(0) = \pi$.

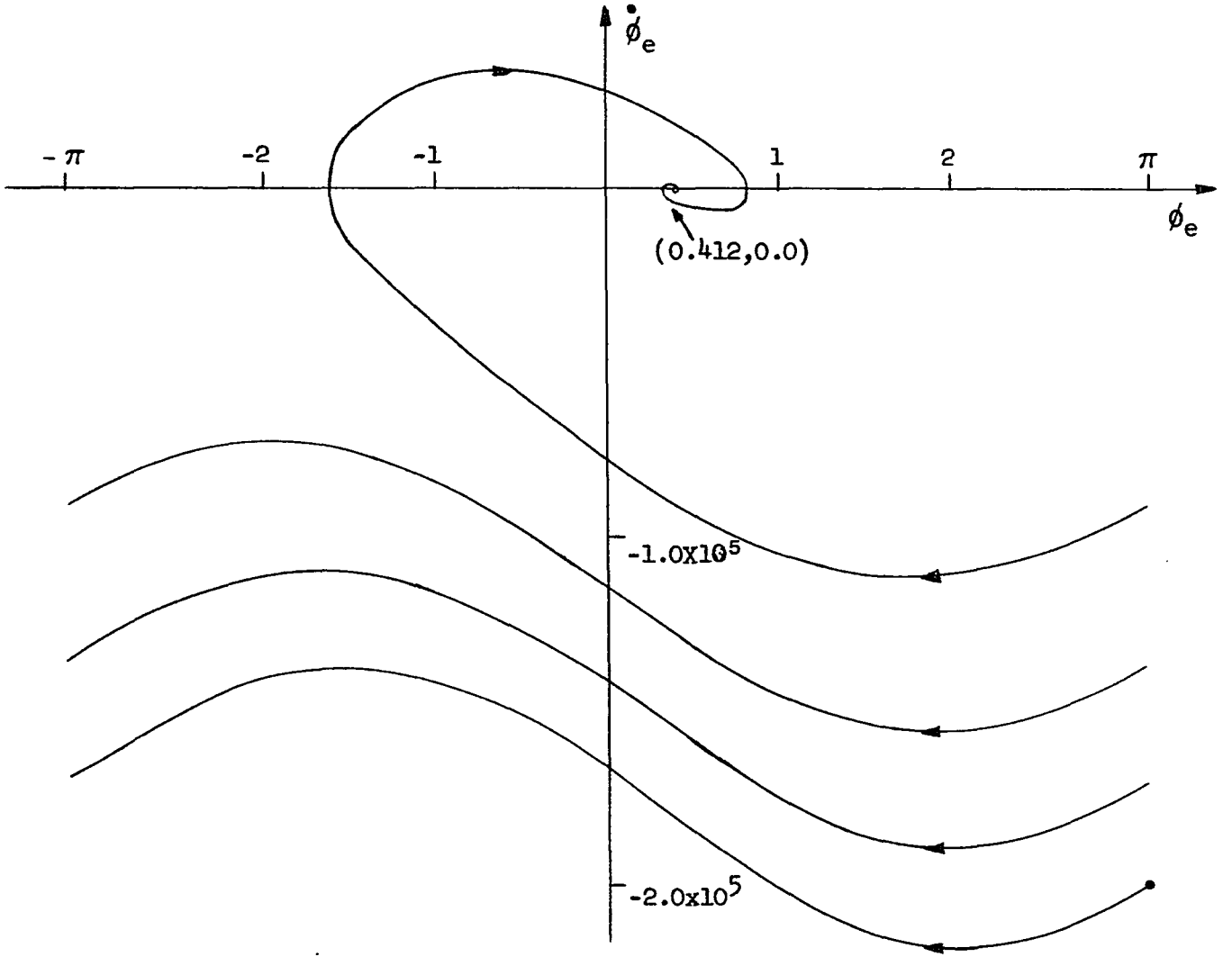

Fig. 5-27. Phase plane trajectory for $\Delta\omega_i/K = 0.4$, $\alpha = 0.1$, $\dot{\phi}_e(0) = -2.0\times10^5$ and $\phi_e(0) = \pi$.

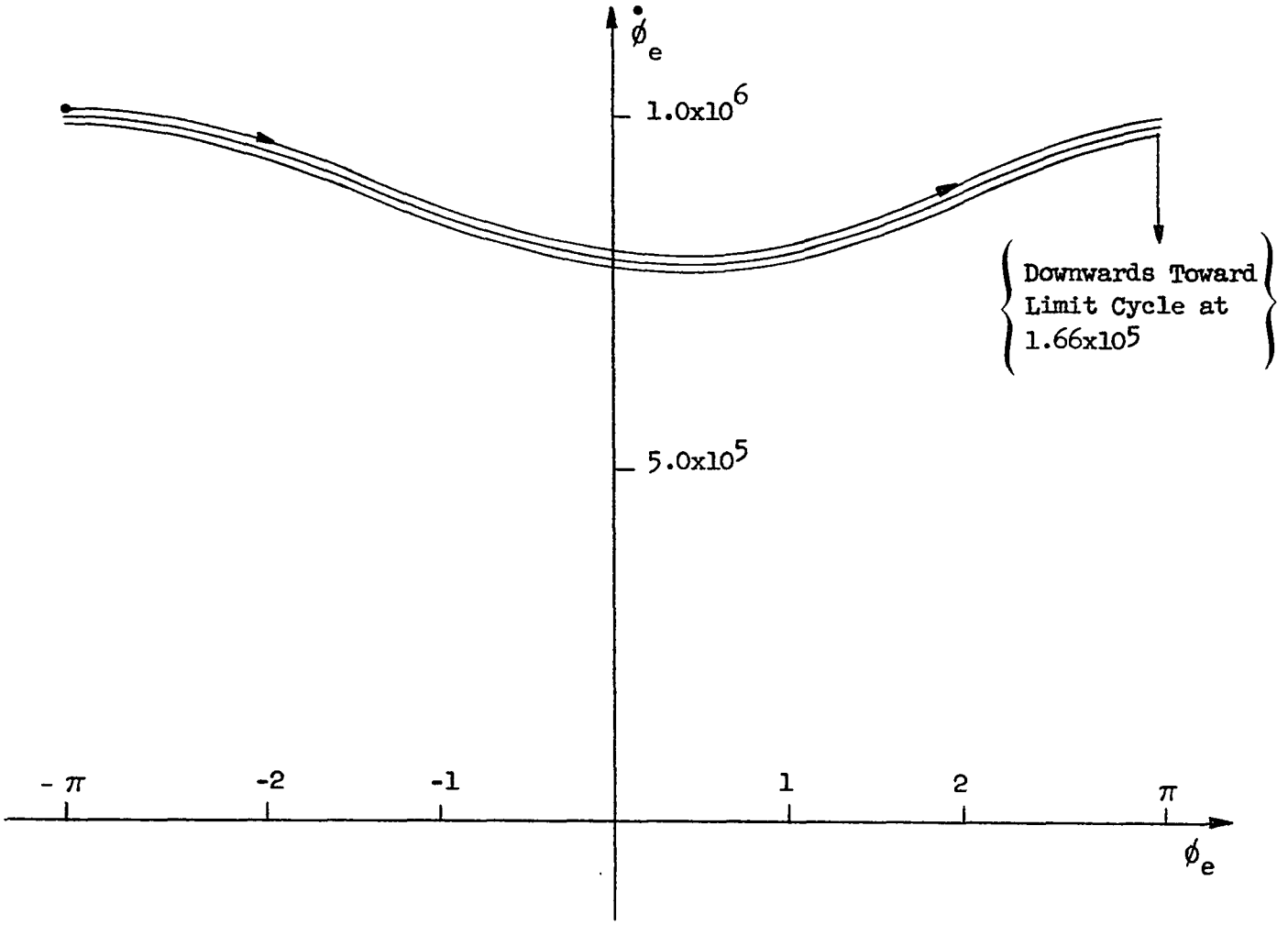

Fig.5-28. Phase plane trajectory for $\Delta\omega_i/K = 0.4$, $\alpha = 0.1$, $\dot{\phi}_e(0) = 1.0x10^6$ and $\phi_e(0) = -\pi$.

move upwards toward this oscillation region and above which the trajectories move downwards towards the oscillation region. Fig. 5-28 shows an initial condition which results in cycle slipping trajectories moving downwards towards the limit cycle. It is significant to note that the trajectories shown in Fig. 5-28 are for relatively large values of frequency error. As such, they should approximately be given by Eq. 5-17. Fig 5-1 shows this to indeed be the case. Some additional comments are in order concerning the saddle point at (2.730,0.0). There is a pair of curves passing through a saddle point called separatrices. These curves separate the phase plane into regions in which the phase trajectories have different topological characteristics. For the case at hand, the separatrices divide the phase plane into regions where trajectories tending towards lock-in occur and those tending towards the oscillatory limit cycle are found. This property will become more evident in subsequent phase plane portraits.

A comparison of the preceding results with that found for the standard second-order, type one PLL [Ref. 1, p. 103, Ref. 2, pp. 600-602 and Ref. 10, pp. 20-21] show them to be quite similar in many respects as expected for $\alpha = 0.1$. In the region of relatively small frequency error, the characteristics of the trajectories are found to be virtually the same. For relatively large values of frequency error, a 90° phase difference in the trajectories for the $\alpha = 0.1$ case and the standard second-order PLL is found (see also Figs. 5-1 and 5-7).

Consider next how the phase plane portraits change as α is increased towards unity. Figs. 5-29 through 5-31 show a group of trajectories again for $\Delta\omega_i/K = 0.4$ but with $\alpha = 0.5$. Similarly, Figs. 5-32 through 5-35 show trajectories for $\Delta\omega_i/K = 0.4$ with $\alpha = 0.9$. A comparison of Figs. 5-25, 5-29, and 5-32, all of which have the same initial conditions, show little change in the trajectory until $\alpha = 0.9$ is reached. At this point, the trajectory changes rather dramatically showing a more pronounced effect due to the saddle point. Next, consider Figs. 5-26, 5-30 and 5-33, which again have the same initial conditions. In this sequence, it is noted that an increase in α causes the trajectory to become increasingly peaked. Consider next Figs. 5-27, 5-31 and 5-34. In this sequence it is noted that with the same set of initial conditions, as α is increased the system skips fewer and fewer cycles before lock-in. In Fig. 5-34, for $\alpha = 0.9$, no cycles are skipped and in fact the initial frequency error must be made substantially more negative before cycles are skipped, as shown in Fig. 5-35. It is also noted (in data not shown here) that as α is increased, the limit cycle in the upper half plane moves to a greater frequency error.

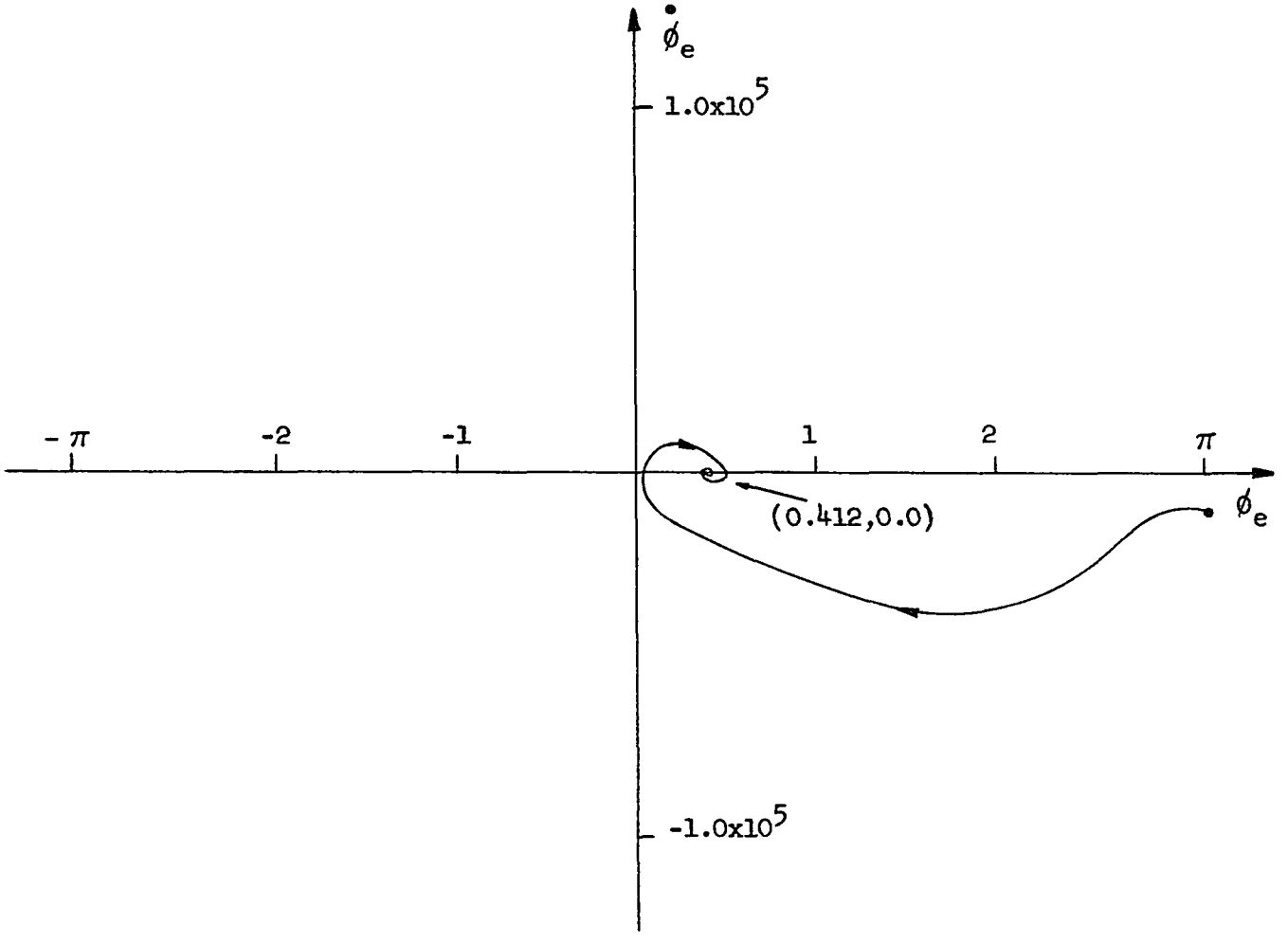

Fig. 5-29. Phase plane trajectory for $\Delta\omega_i/K = 0.4$, $\alpha = 0.5$, $\dot{\phi}_e(0) = -1.0\text{x}10^4$ and $\phi_e(0) = \pi$.

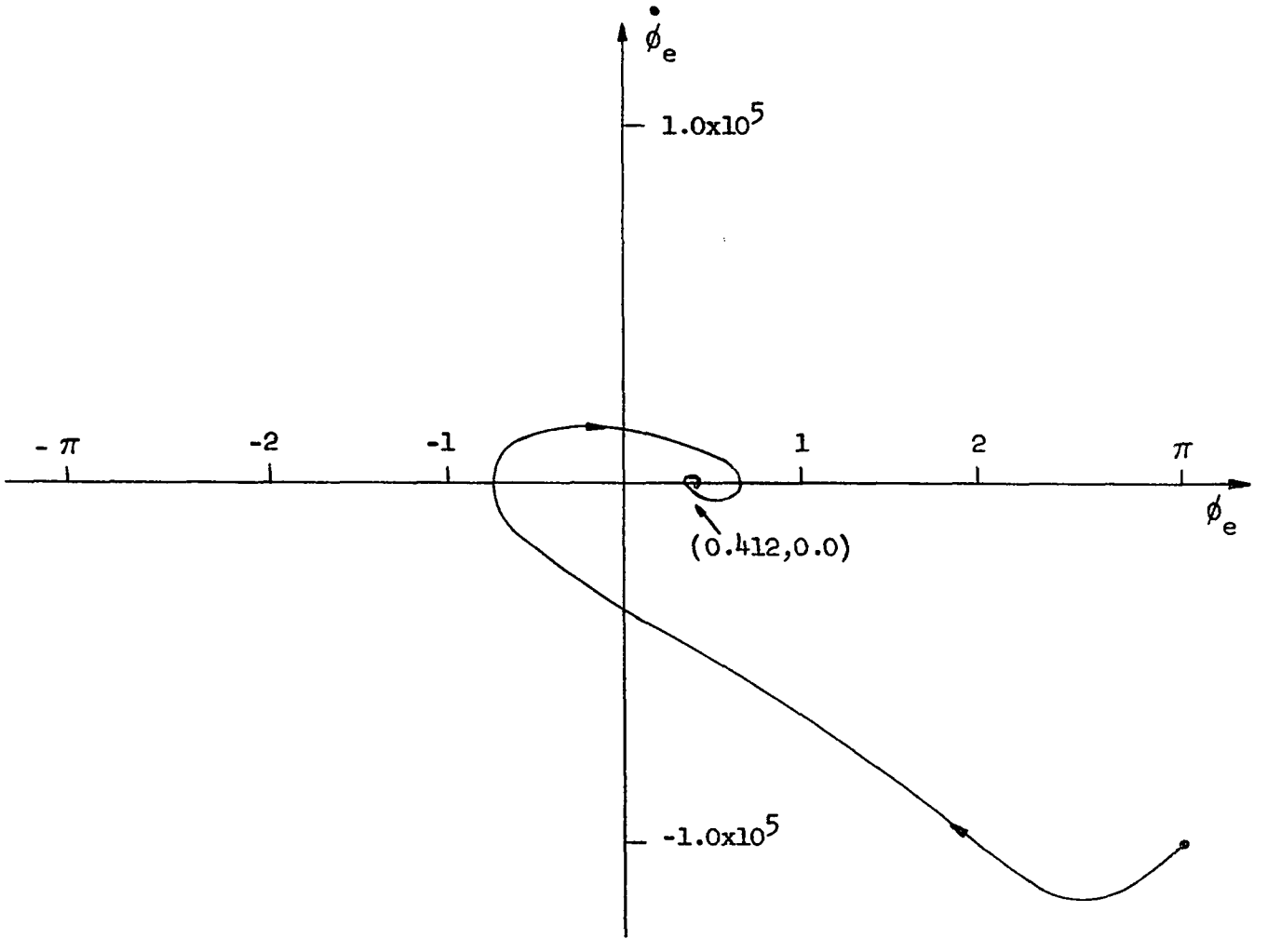

Fig. 5-30. Phase plane trajectory for $\Delta\omega_i/K = 0.4$, $\alpha = 0.5$, $\dot{\phi}_e(0) = -1.0\text{x}10^5$ and $\phi_e(0) = \pi$.

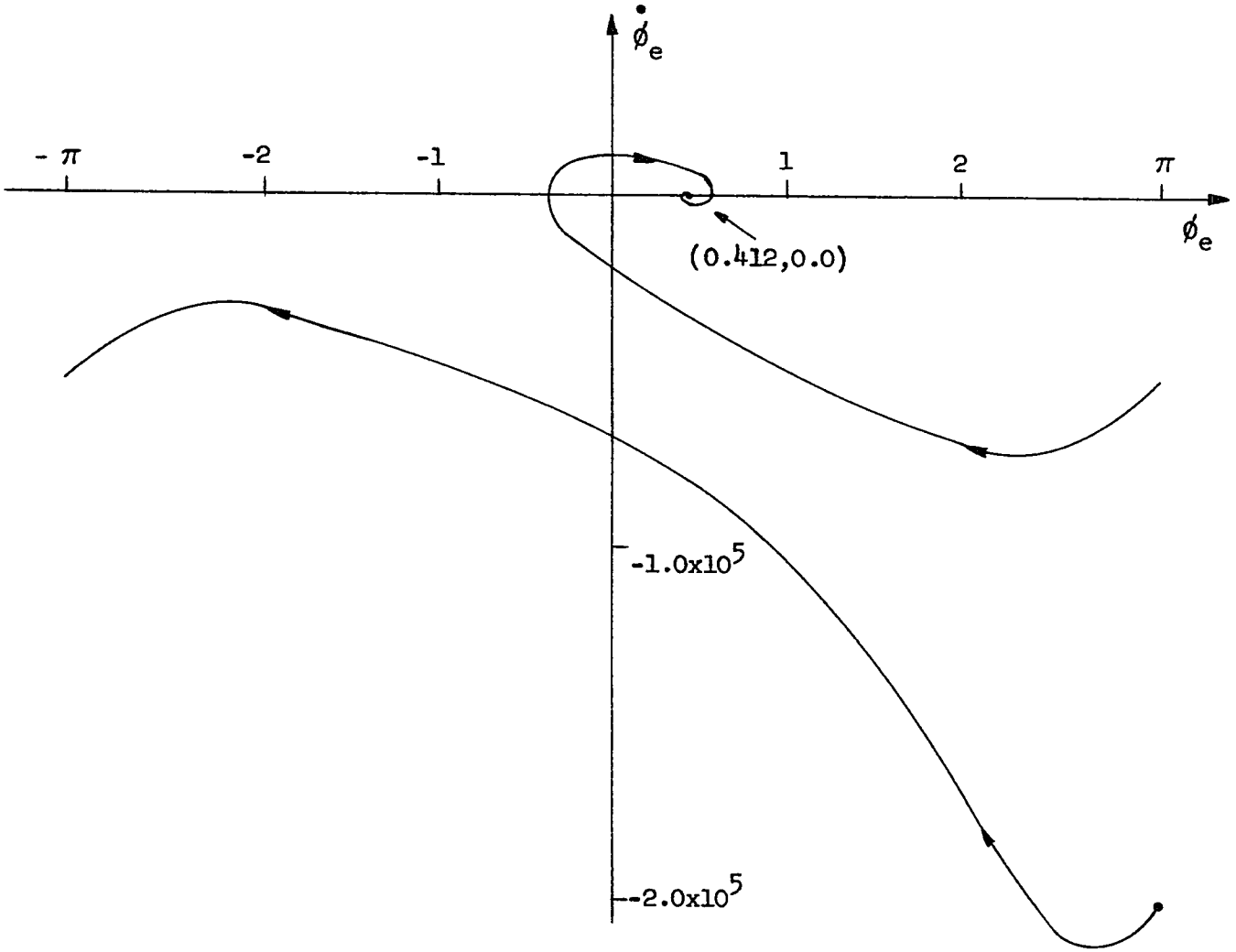

Fig. 5-31. Phase plane trajectory for $\Delta\omega_i/K = 0.4$, $\alpha = 0.5$, $\dot{\phi}_e(0) = -2.0x10^5$ and $\phi_e(0) = \pi$.

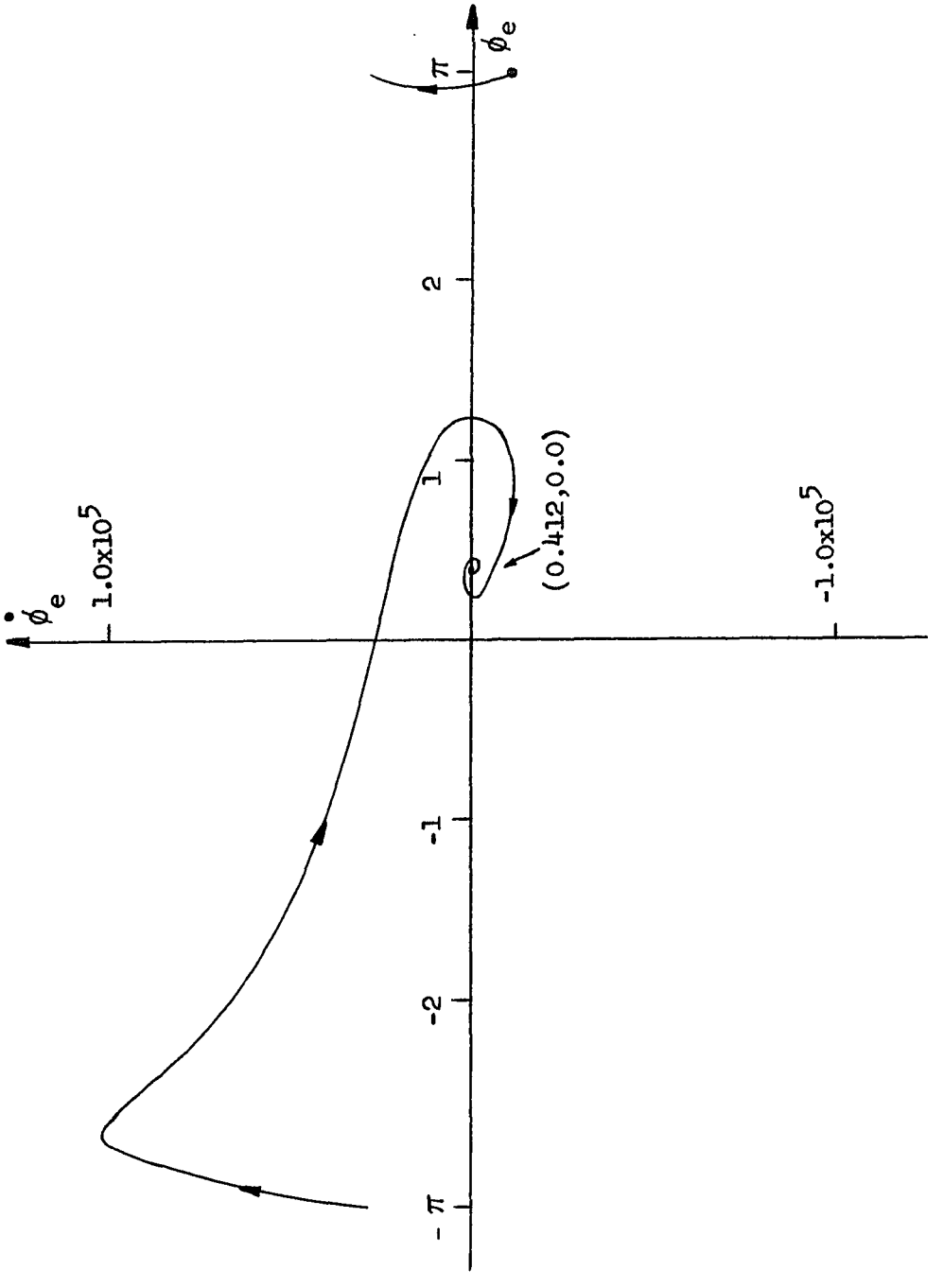

Fig. 5-32. Phase plane trajectory for $\Delta\omega_i/K = 0.4$, $\alpha = 0.9$, $\dot{\phi}_e(0) = -1.0\text{x}10^4$ and $\phi_e(0) = \pi$.

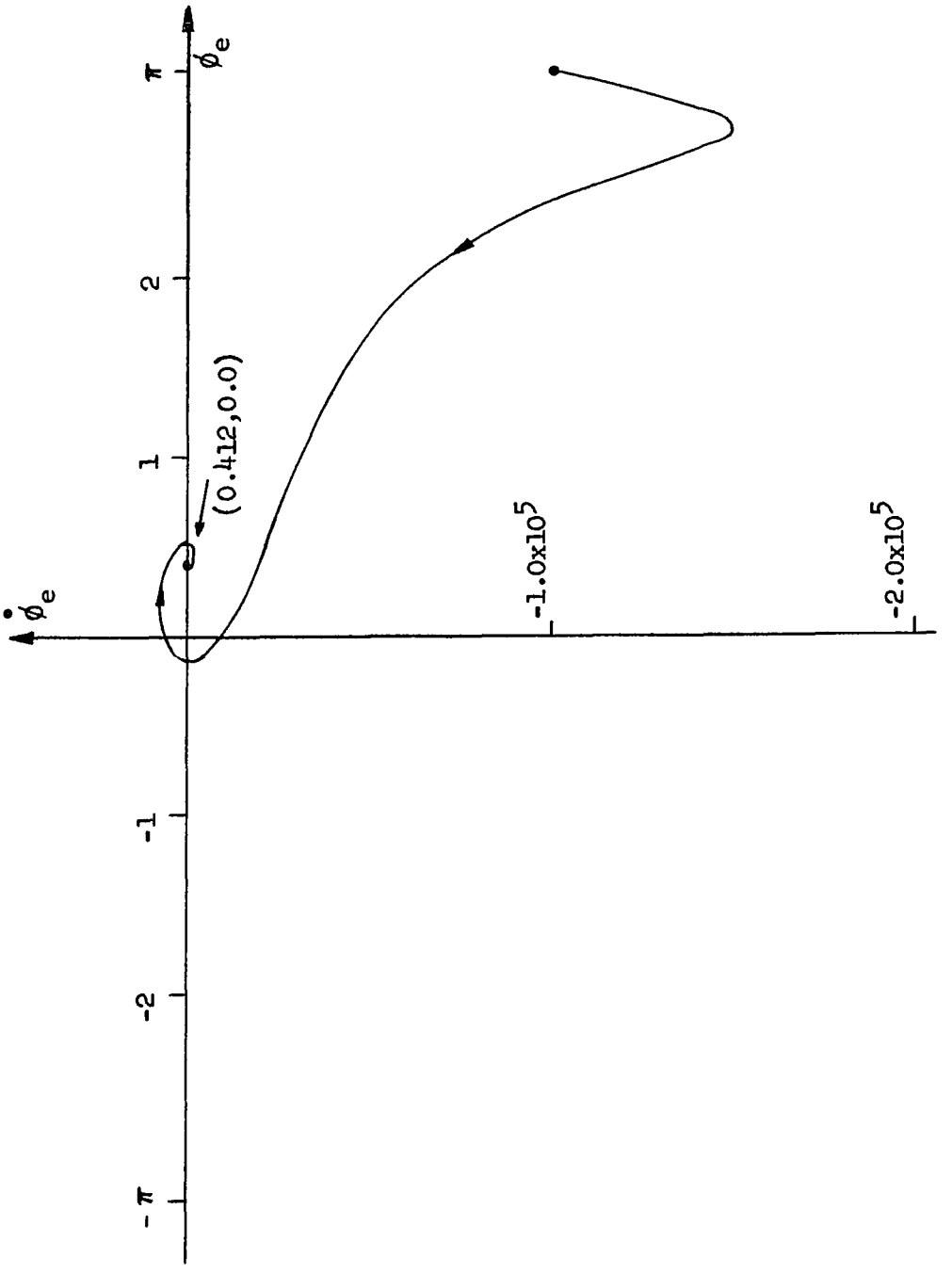

Fig. 5-33. Phase plane trajectory for $\Delta\omega_i/K = 0.4$, $\alpha = 0.9$, $\dot{\phi}_e(0) = -1.0x10^5$ and $\phi_e(0) = \pi$.

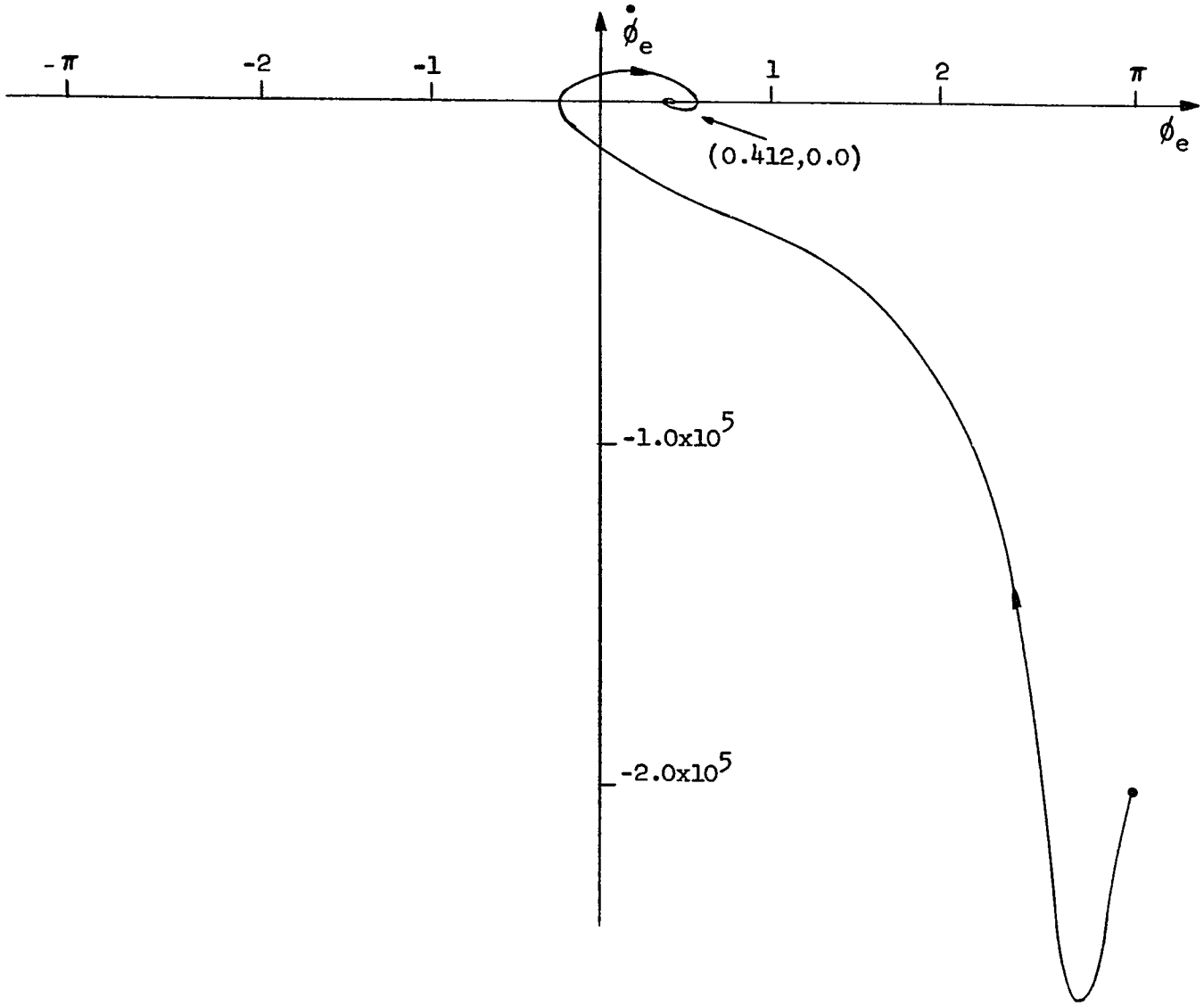

Fig. 5-34. Phase plane trajectory for $\Delta\omega_i/K = 0.4$, $\alpha = 0.9$, $\dot{\phi}_e(0) = -2.0\text{x}10^5$ and $\phi_e(0) = \pi$.

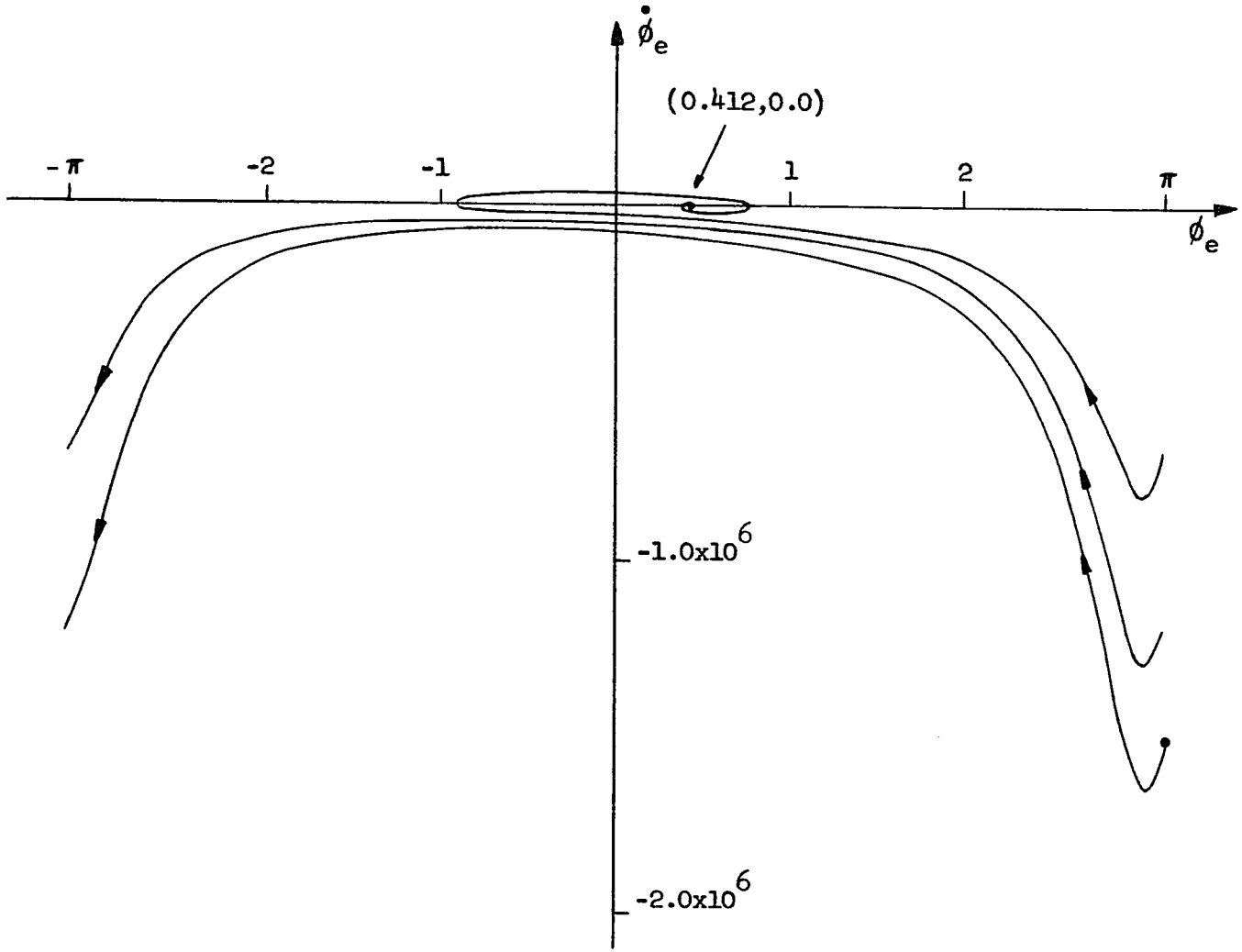

Fig. 5-35. Phase plane trajectory for $\Delta\omega_i/K = 0.4$, $\alpha = 0.9$, $\dot{\phi}_e(0) = -1.5\text{x}10^6$ and $\phi_e(0) = \pi$.

At this point it is of interest to reflect back to the discussion on isoclines in Sec. 5.3.3. The purpose of this is twofold. First, the isoclines serve as an added check on the computer generated trajectories. In addition, the isoclines give supplementary detail on the behavior of the trajectories. Figs. 5-8 through 5-10 show the m = o isoclines, i.e., the locus of points for which the trajectories in the phase plane have zero slope, for the preceding cases. From Eq. 5-12 it is noted that for $\alpha < 1$ the $m = \infty$ isoclines can only occur at y = o, i.e., along the x-axis. A check on the computer generated trajectories show them to indeed agree with the isocline predictions.

Consider next the effect of increasing the frequency offset $\Delta\omega_i$. Figs. 5-36 through 5-39 show pertinent trajectories for $\Delta\omega_i / K = 0.6$ and $\alpha = 0.1$. As $\Delta\omega_i$ is increased, the stable focus and and saddle point more closer to each other as dictated by Eq.5-22. This is shown in Fig. 5-36 along with the trajectory for a small initial negative frequency error. In this case the trajectory does not lock in but rather enters the upper half plane and skips cycles as it progresses towards the limit cycle at 2.6×10^5. Although this behavior is quite different from that observed in Fig. 5-25 for the same initial conditions, this same type of trajectory, occurs in the $\Delta\omega_i/K = 0.4$ case for very small negative initial frequency errors e.g., $\dot{\phi}_e(o) = -1.0 \times 10^3$ and $\phi_e(o) = \pi$.

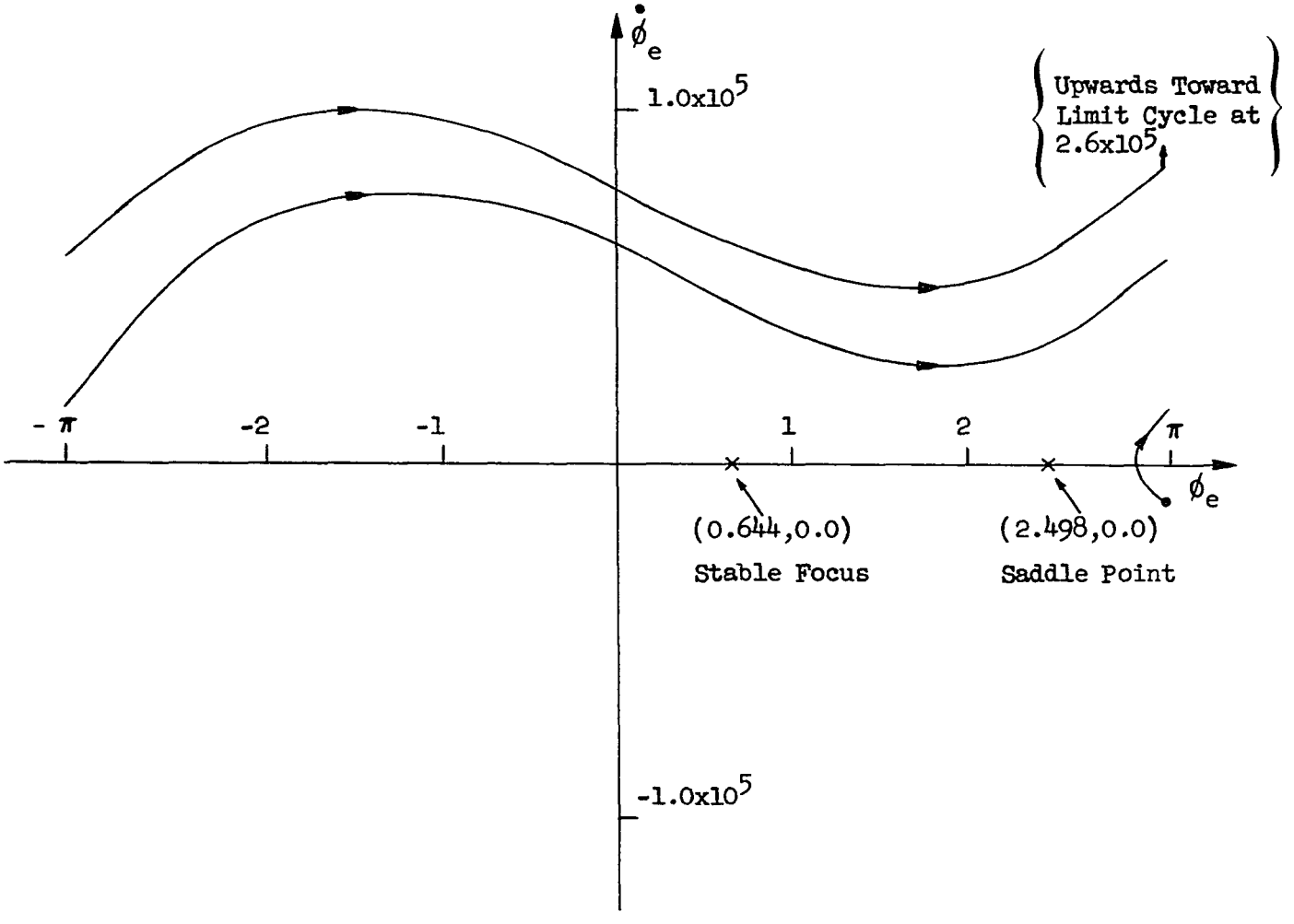

Fig. 5-36. Phase plane trajectory for $\Delta\omega_i/K = 0.6$, $\alpha = 0.1$, $\dot{\phi}_e(0) = -1.0\text{x}10^4$ and $\phi_e(0) = \pi$.

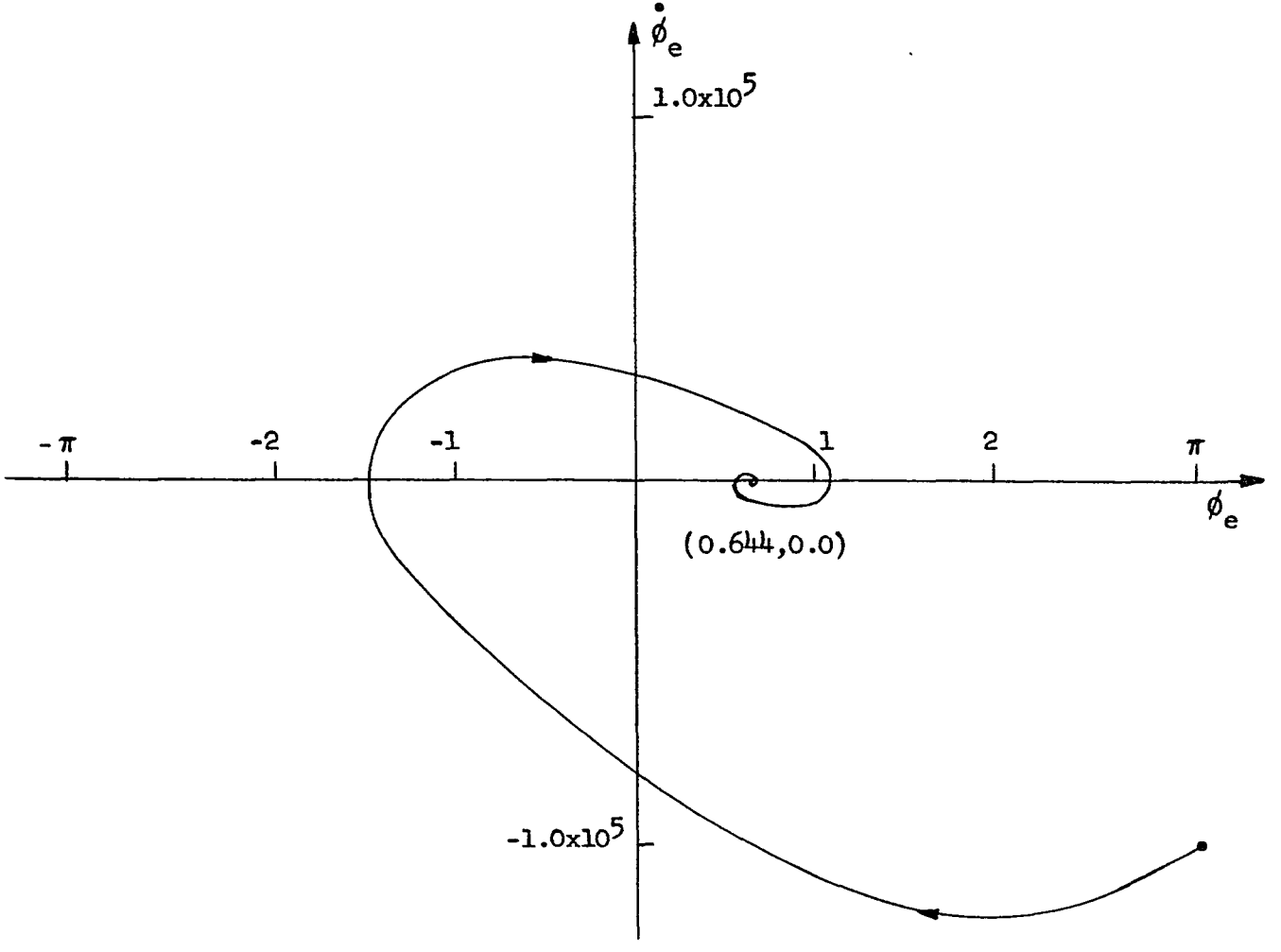

Fig. 5-37. Phase plane trajectory for $\Delta\omega_i/K = 0.6$, $\alpha = 0.1$, $\dot{\phi}_e(0) = -1.0\text{x}10^5$ and $\phi_e(0) = \pi$.

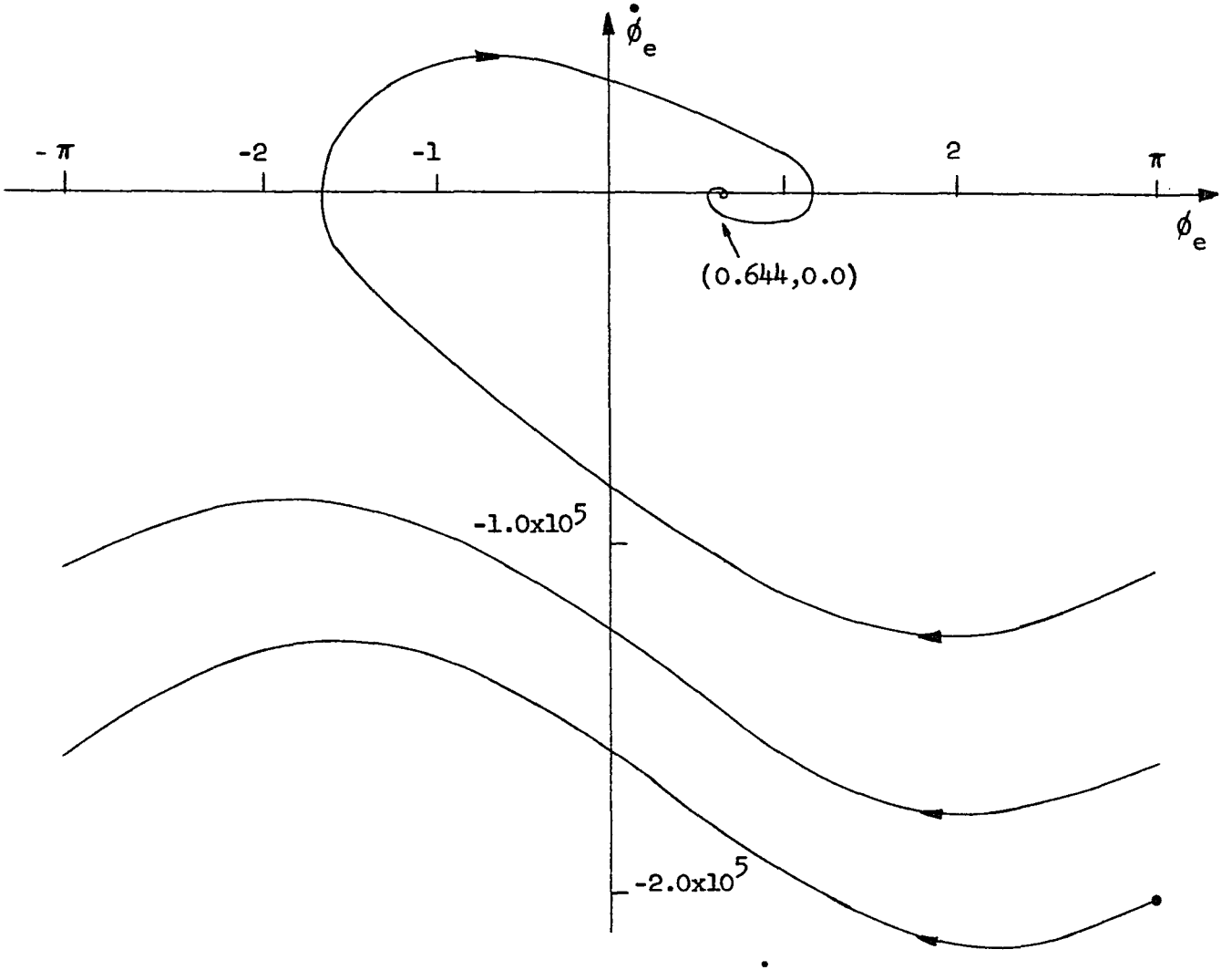

Fig. 5-38. Phase plane trajectory for $\Delta\omega_i/K = 0.6$, $\alpha = 0.1$, $\dot{\phi}_e(0) = -2.0x10^5$ and $\phi_e(0) = \pi$.

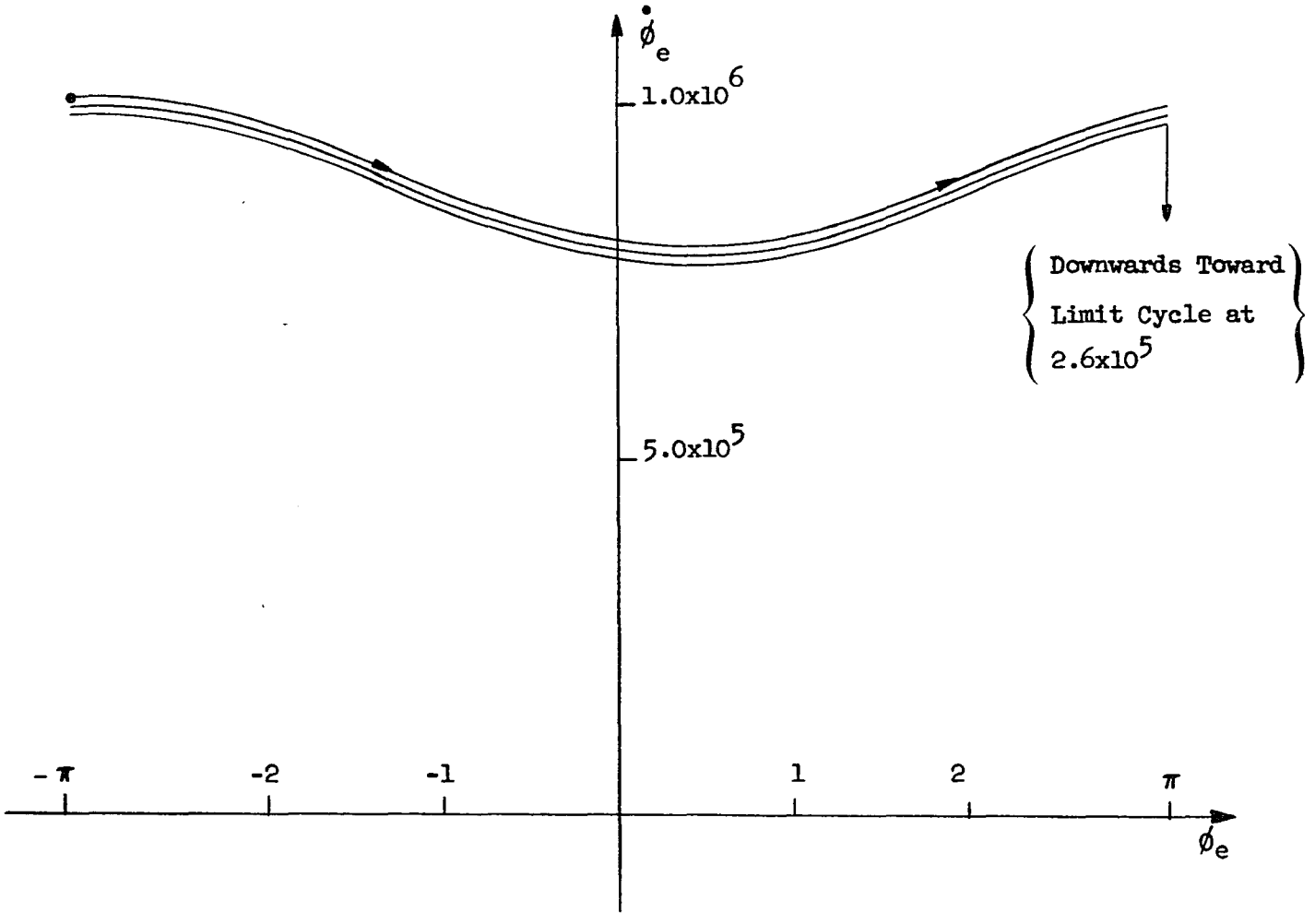

Fig. 5-39. Phase plane trajectory for $\Delta\omega_i/K = 0.6$, $\alpha = 0.1$, $\dot{\phi}_e(0) = 1.0x10^6$ and $\phi_e(0) = -\pi$.

Figs. 5-37 and 5-38 show the same general behavior as the $\Delta\omega_i/K = 0.4$ cases with the same initial conditions shown in Figs. 5-26 and 5-27, except that fewer cycles are skipped. Finally, Fig. 5-39 shows a downwards cycle slipping towards the limit cycle for a large positive initial frequency error.

Figs. 5-40 through 5-42 show pertinent trajectories for the $\Delta\omega_i/K = 0.6$ case with $\alpha = 0.5$ and 0.9. Again these results compared to their counterparts in the $\Delta\omega_i/K = 0.4$ case show similar types of trajectories but with fewer cycles slipped. Increasing $\Delta\omega_i$, then appears to have the effect of stretching the phase plane portrait in the vertical direction with the limit cycle occurring at a higher frequency error. This effect is also noted in the standard second-order PLL [Ref. 2, pp. 600-602].

The final case to be considered for values of α less than unity is $\Delta\omega_i/K = 0.9$. Recall that this value is approaching the limiting value of $\Delta\omega_i/K = 1.0$ beyond which the singularities on the x-axis vanish. Figs. 5-43 through 5-46 show pertinent trajectories for $\alpha = 0.1$. Fig 5-43, which shows the new position of the singularities, indicates that for a small negative frequency error the trajectory again enters the upper half plane and moves upwards towards the limit cycle at 4.13×10^5. This is the same type of behavior exhibited for the $\Delta\omega_i/K = 0.6$ case and as anticipated the position of the limit cycle again moves upward. As the initial

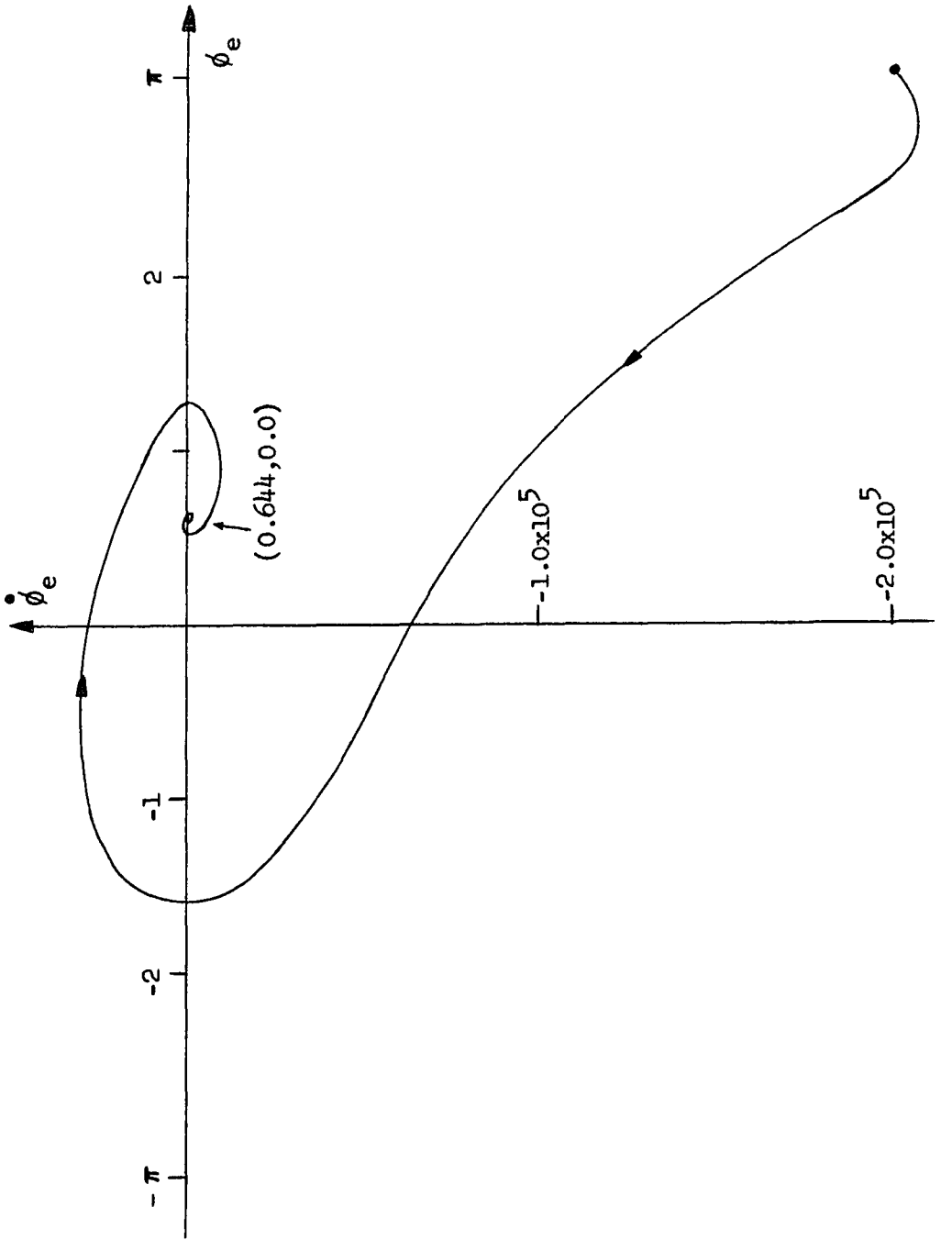

Fig. 5-40. Phase plane trajectory for $\Delta\omega_1/K = 0.6$, $\alpha = 0.5$, $\dot{\phi}_e(0) = -2.0\times10^5$ and $\phi_e(0) = \pi$.

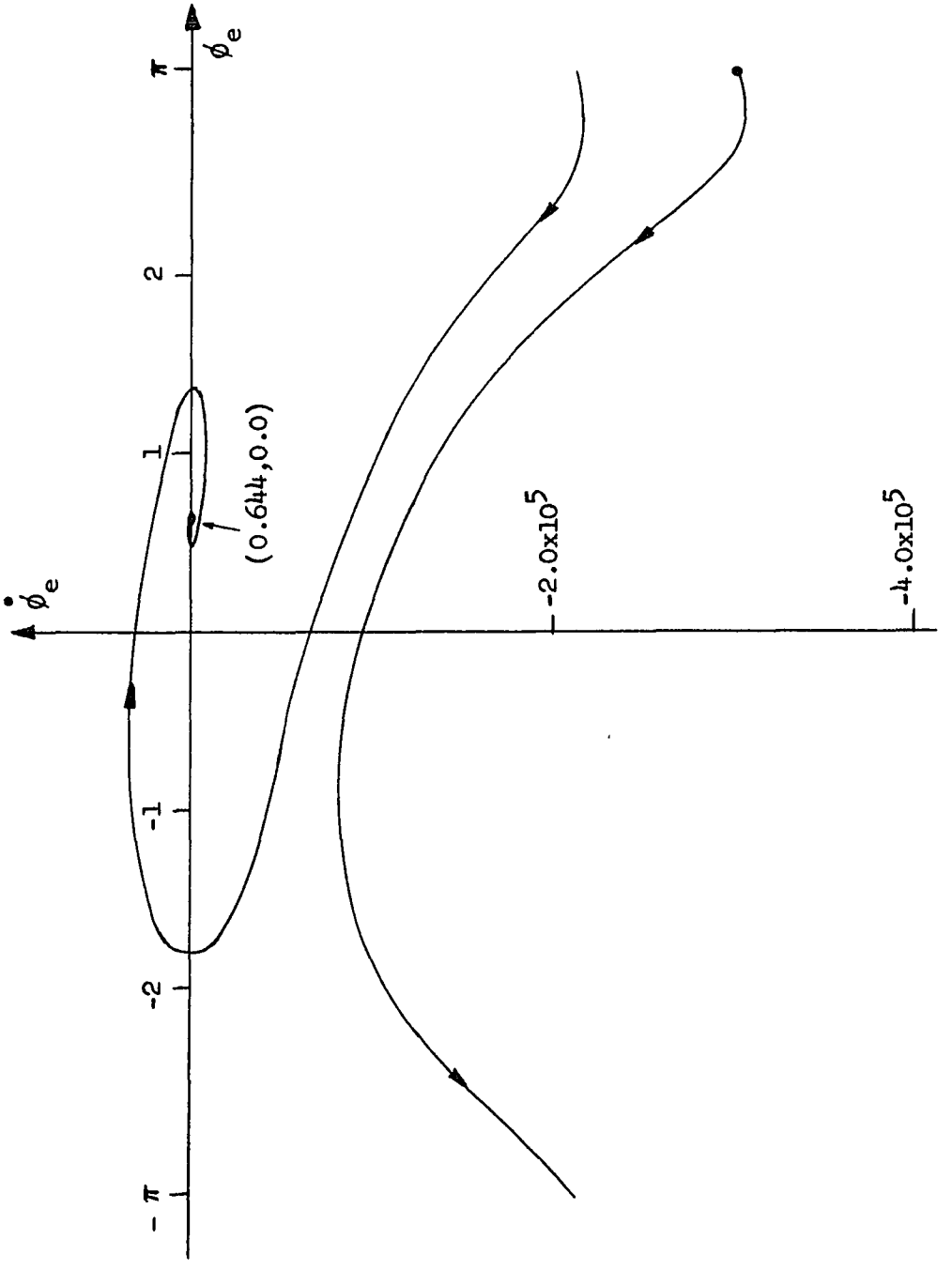

Fig. 5-41. Phase plane trajectory for $\Delta\omega_i/K = 0.6$, $\alpha = 0.5$, $\dot{\phi}_e(0) = -3.0\times10^5$ and $\phi_e(0) = \pi$.

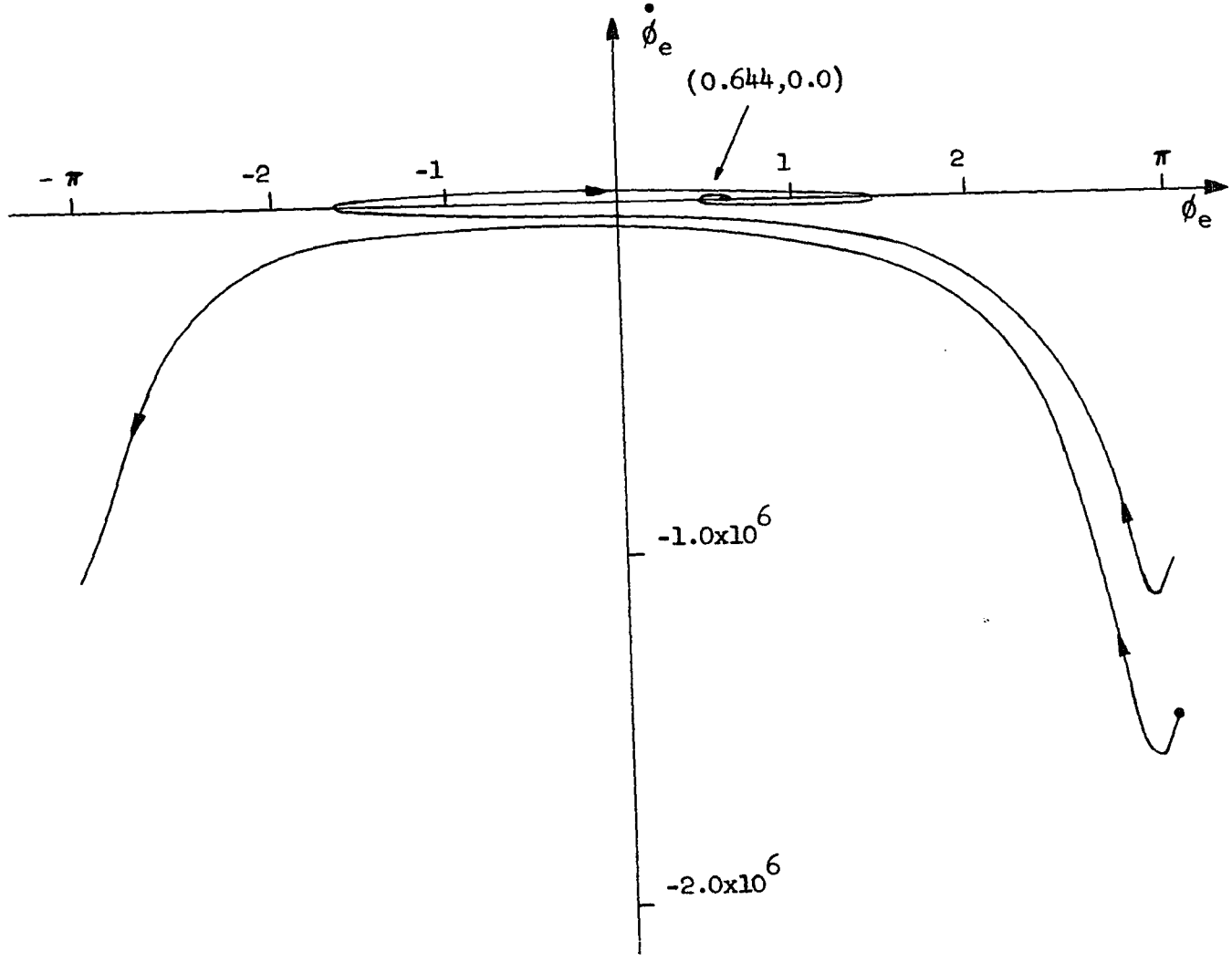

Fig. 5-42. Phase plane trajectory for $\Delta\omega_i/K = 0.6$, $\alpha = 0.9$, $\dot{\phi}_e(0) = -1.5\times10^6$ and $\phi_e(0) = \pi$.

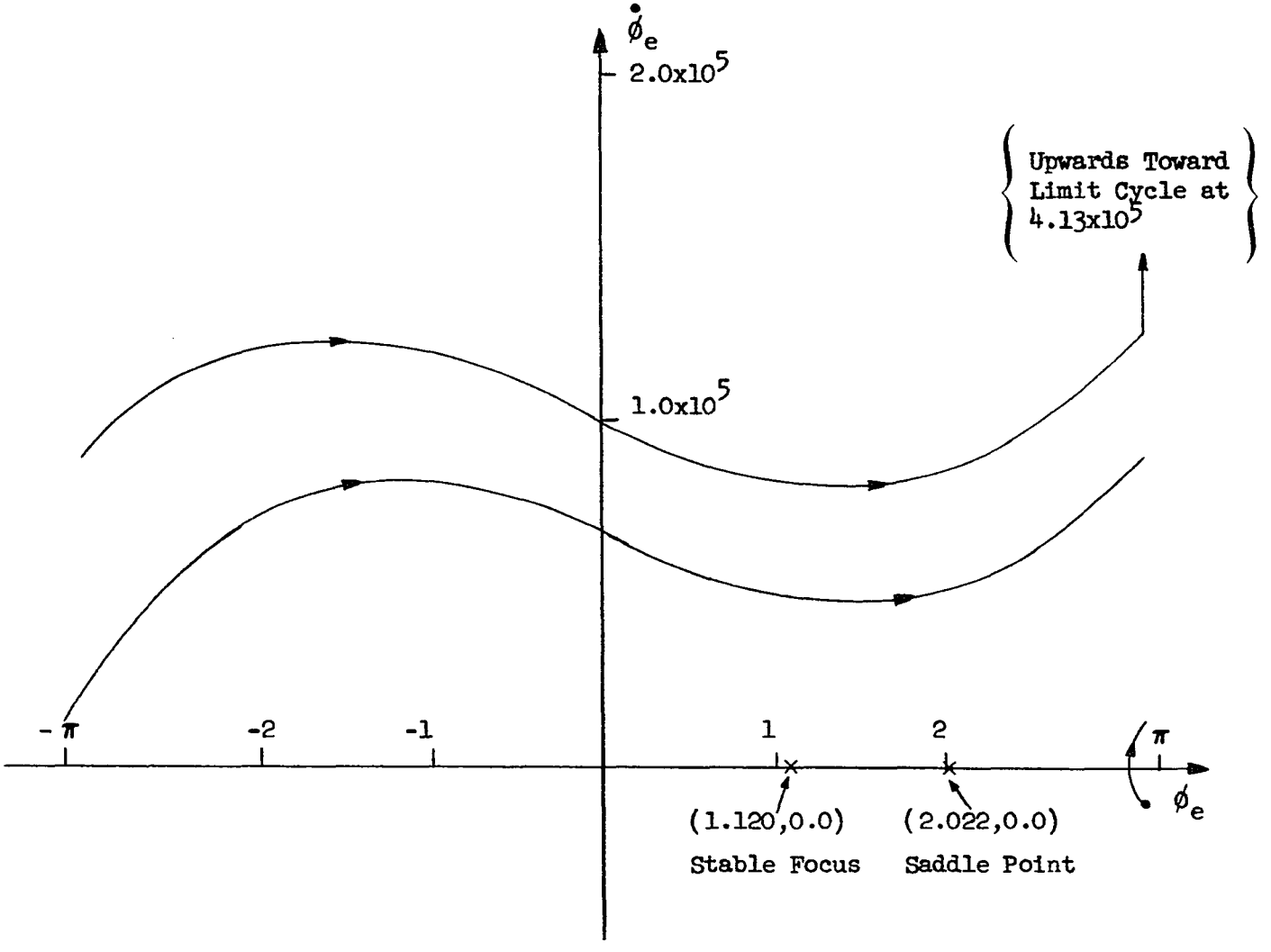

Fig. 5-43. Phase plane trajectory for $\Delta\omega_i/K = 0.9$, $\alpha = 0.1$, $\dot{\phi}_e(0) = -1.0x10^4$ and $\phi_e(0) = \pi$.

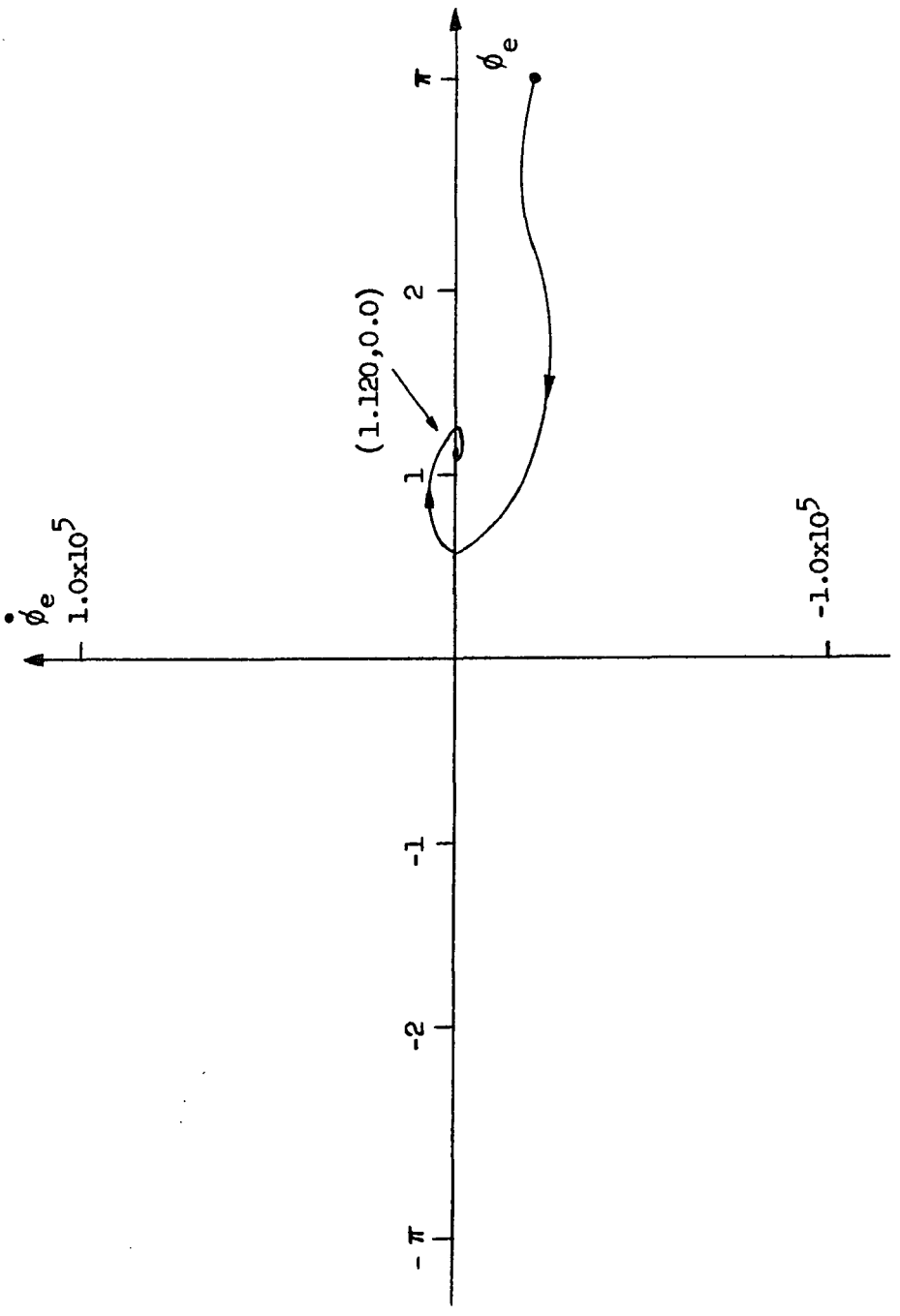

Fig. 5-44. Phase plane trajectory for $\Delta\omega_1/K = 0.9$, $\alpha = 0.1$, $\dot{\phi}_e(0) = -2.0\text{x}10^4$ and $\phi_e(0) = \pi$.

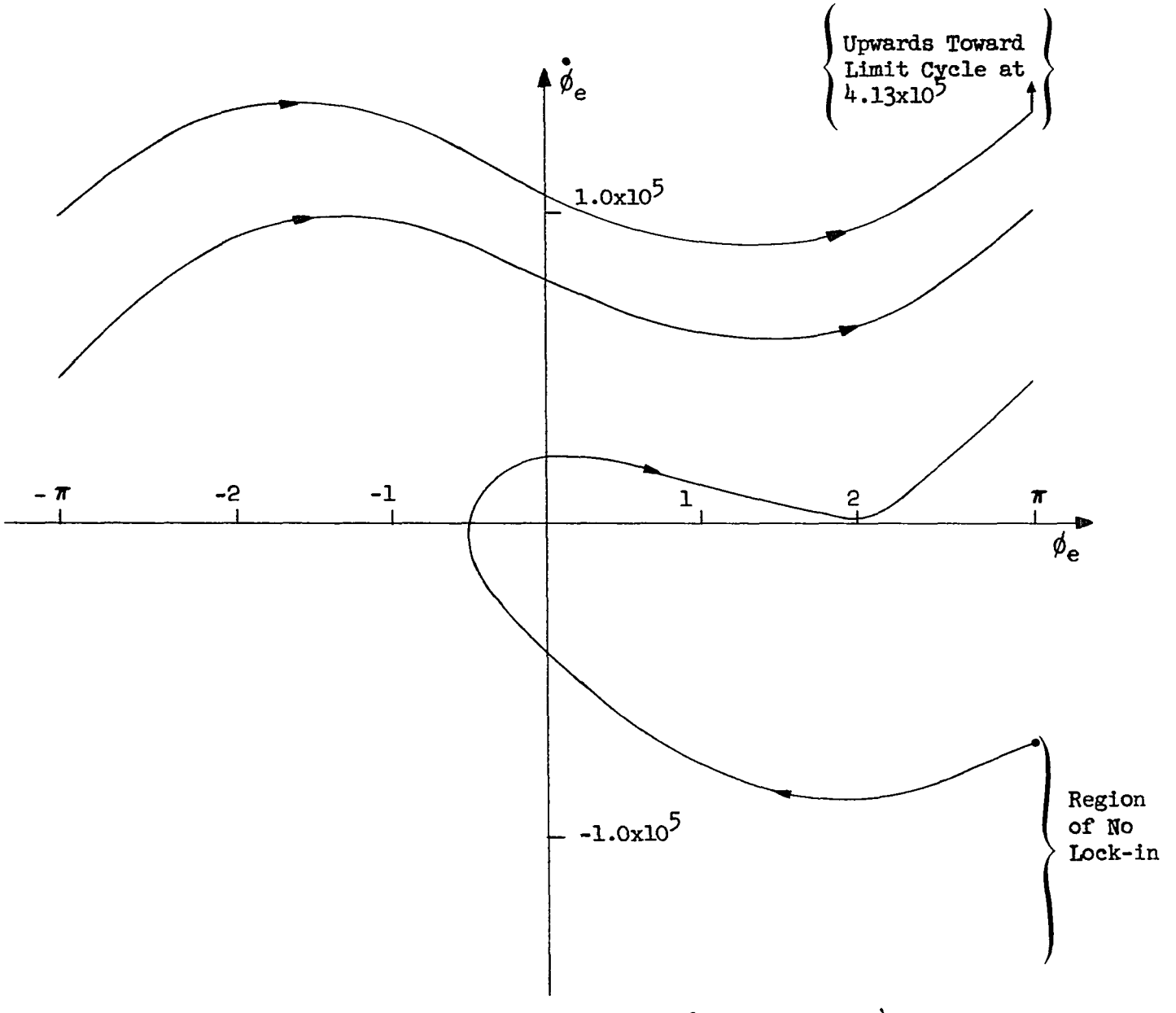

Fig. 5-45. Phase plane trajectory for $\Delta\omega_i/K = 0.9$, $\alpha = 0.1$, $\dot{\phi}_e(0) = -7.0\text{x}10^4$ and $\phi_e(0) = \pi$.

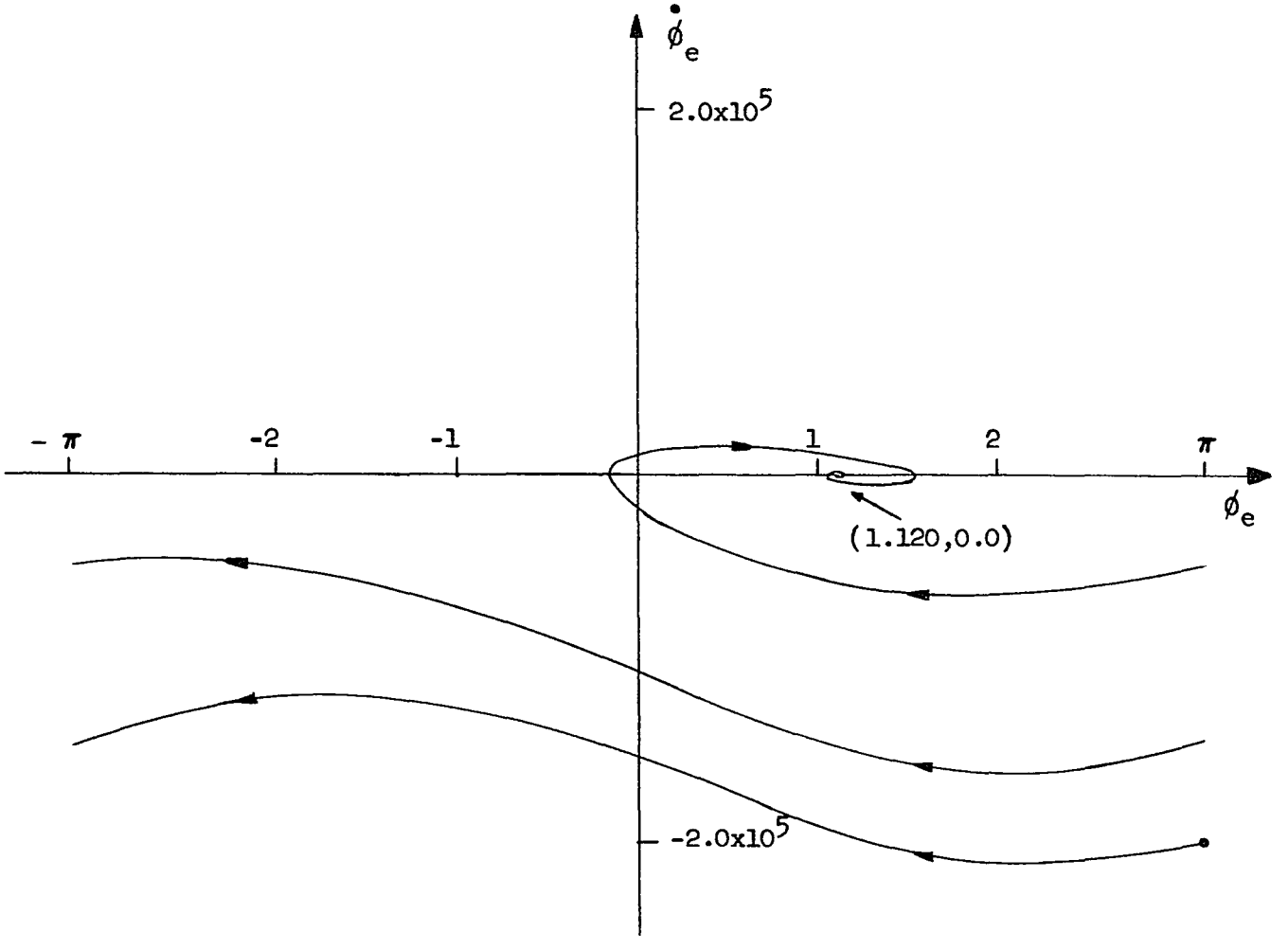

Fig. 5-46. Phase plane trajectory for $\Delta\omega_i/K = 0.9$, $\alpha = 0.1$, $\dot{\phi}_e(0) = -2.0\text{x}10^5$ and $\phi_e(0) = \pi$.

frequency error is made increasingly negative, the trajectories lock-in without skipping cycles as shown for example in Fig 5-44. At this point, an interesting phenomenon occurs. A slot is encountered for which the trajectories no longer lock-in but rather move into the upper half plane towards the limit cycle. An example of a trajectory in this region is shown in Fig. 5-45. After the no lock-in slot, a further negative decrease in the frequency error again results in trajectories which lock-in, however, they do so after skipping cycles. An example of such a trajectory is shown in Fig. 5-46. The effect of limiting the phase plane portrait to $-\pi < \phi_e \leq \pi$, then, causes alternating bands of lock-in and no lock-in trajectories. This same effect also occurs for smaller values of $\Delta\omega_i/K$, however, the band of no lock-in appears to widen substantially for values of $\Delta\omega_i/K$ approaching unity. This is in keeping with the observation discussed earlier that increasing $\Delta\omega_i/K$ towards unity tends to stretch the phase plane portrait in the vertical direction. For values of α greater than 0.1 and less than unity only partial data was obtained which indicate similar changes occur as was observed in the $\Delta\omega_i/K = 0.4$ and 0.6 cases. Fig. 5-47 shows an example for $\alpha = 0.5$ in which the increased peakedness of the trajectory is again apparent.

As discussed previously for $\alpha \geq 1$ additional singularities are introduced into the phase plane along the lines given by Eq. 5-23.

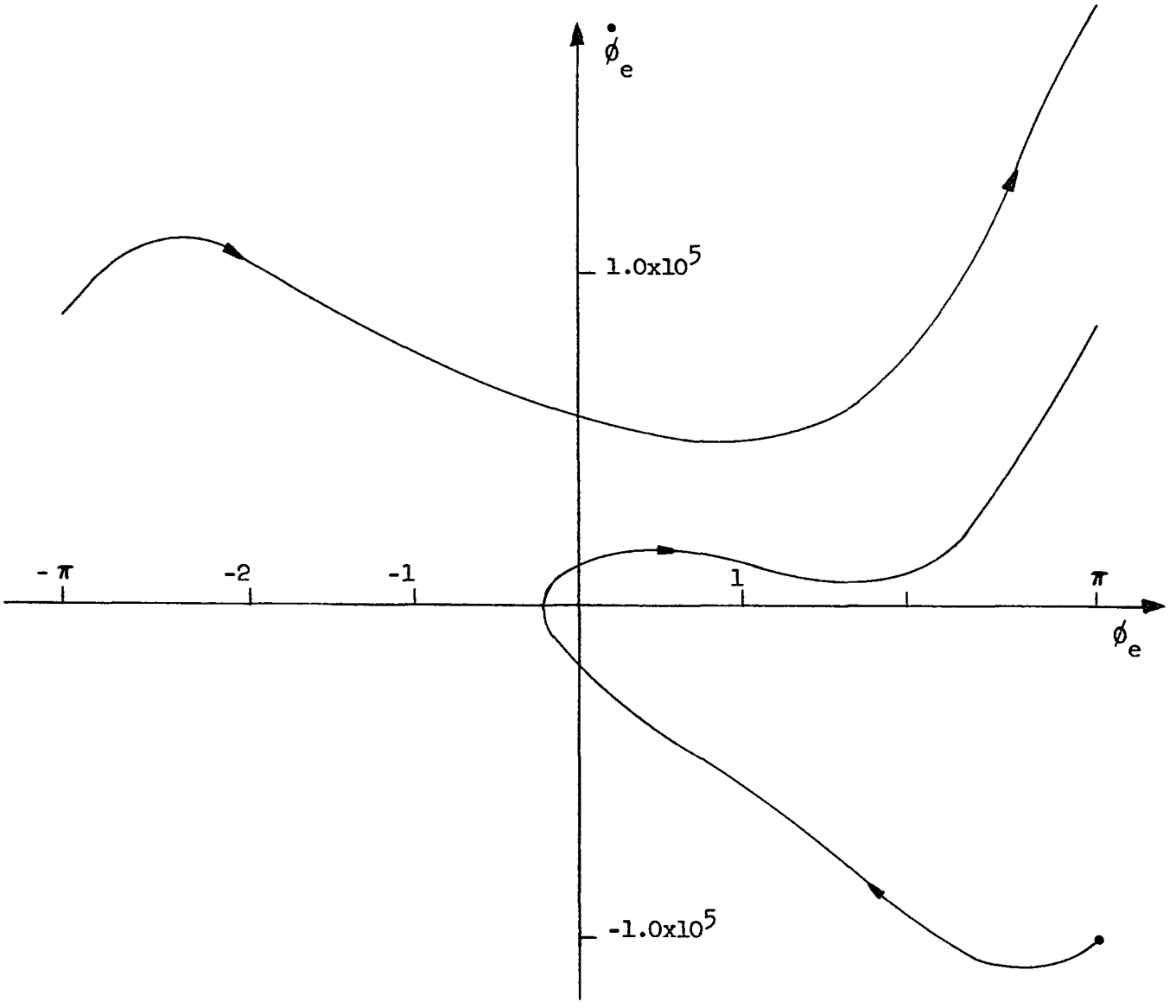

Fig. 5-47. Phase plane trajectory for $\Delta\omega_i/K = 0.9$, $\alpha = 0.5$, $\dot{\phi}_e(0) = -1.0 \times 10^5$ and $\phi_e(0) = \pi$.

The occurrence of these new singularities signals a dramatic change in the phase plane portrait as hinted by Figs. 5-4 through 5-6. From Eq. 5-12 it is noted that the lines along which the new singularities occur are also isoclines for m = ∞ i.e., the slope of the trajectories dy/dx along the lines

$$x = \cos^{-1}\left(-\frac{1}{\alpha}\right) \tag{5-23}$$

is infinite except at the singularities where it becomes indeterminate. Fig. 5-48 shows the phase plane portrait for $\Delta\omega_i/K = 0.4$, with $\alpha = 1.0$ and the remaining parameters being those of Acampora and Newton [Ref. 3]. There are two singularities along the x-axis; a stable focus at (0.412, 0.0) and a saddle point at (2.730, 0.0). In addition, there are saddle points at $(\pm\pi, -1.176 \times 10^4)$. From the figure it is noted that depending upon the initial conditions, some trajectories lock-in while others proceed towards an infinite frequency error in either the positive or negative direction. This brings out an obvious disparity with the physical system which has limits on the actual frequency error it can exhibit and is an area which deserves future investigation. For values of α greater than unity the positions of the added singularities change position according to Eq. 5-23, however the same basic types of trajectories just described occur.

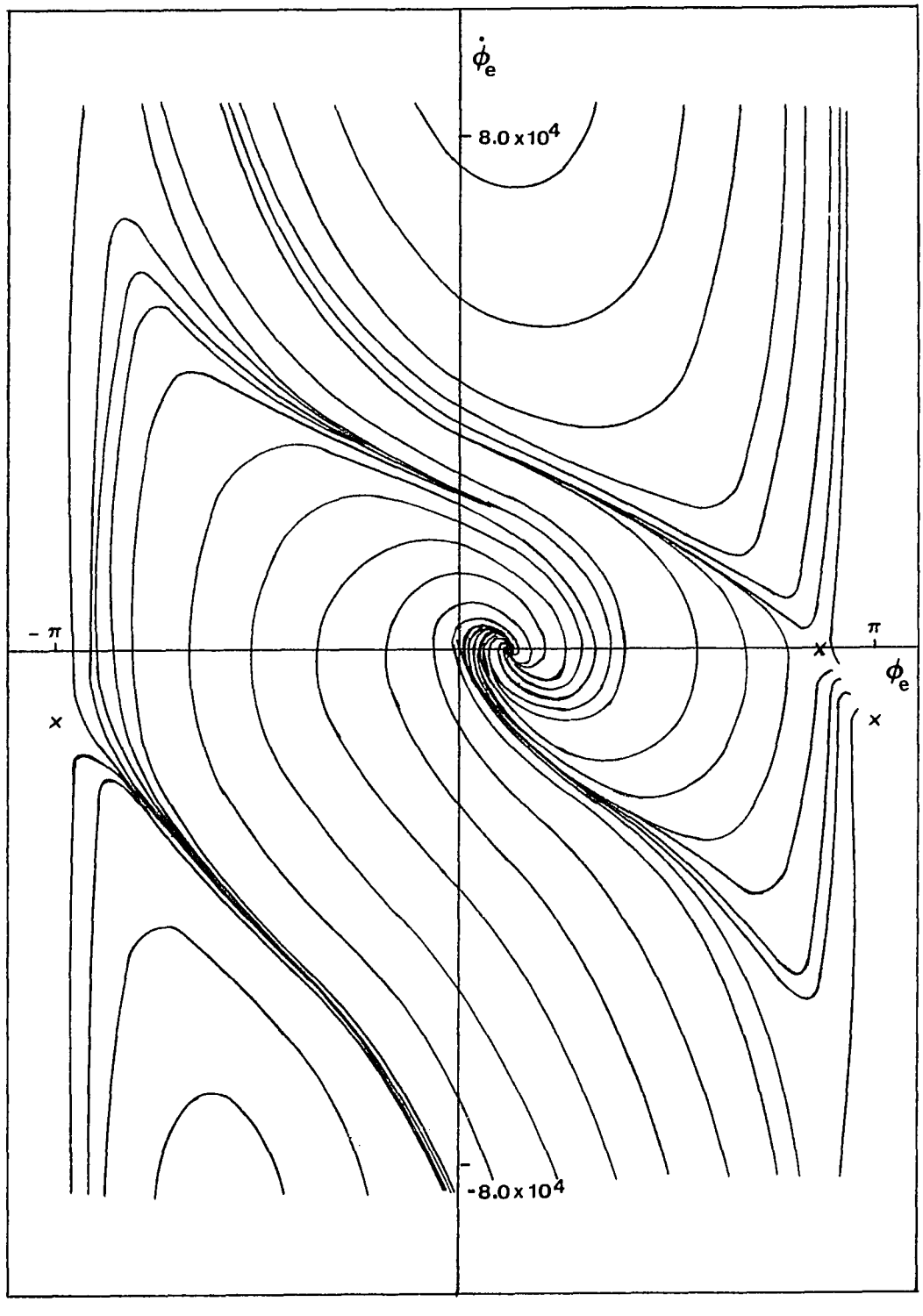

Fig. 5-48. Phase plane portrait for $\Delta\omega_i/K = 0.4$ and $\alpha = 1.0$.

In this chapter the basic acquisition and tracking behavior of the generalized second-order PLL has been developed. There are of course other facets of the non-linear behavior of the generalized second-order PLL which deserve investigation, e.g., the loop with linearly varying frequency input. This and other future investigative possibilities will be discussed in the next chapter.

References - Chapter 5

1. J. Klapper and J. Frankle, Phase-Locked and Frequency-Feedback Systems: Principles and Techniques, Academic Press, New York, 1972.

2. A. J. Viterbi, "Acquisition and Tracking Behavior of Phase-Locked Loops," Symposium on Active Networks and Feedback Systems, Polytechnic Institute of Brooklyn, April 1960.

3. A. Acampora and A. Newton, "Use of Phase Subtraction to Extend the Range of a Phase-Locked Demodulator, "RCA Review, Vol. 27, No. 3, pp. 577-599, December 1966.

4. R. Burington, Handbook of Mathematical Tables and Formulas, 4th Edition, McGraw-Hill Book Co., New York, 1965.

5. W. J. Cunningham, Introduction to Non-linear Analysis, McGraw-Hill Book Co., New York, 1958.

6. G. J. Thaler and M. P. Pastel, Analysis and Design of Non-linear Feedback Control Systems, McGraw-Hill Book Co., New York, 1962.

7. J. E. Gibson, Non-linear Automatic Control, McGraw-Hill Book Co., New York, 1963.

8. K. Ogata, Modern Control Engineering, Prentice-Hall Inc., Englewood Cliffs, New Jersey, 1970.

9. Y. H. Ku, Analysis and Control of Non-linear Systems, The Ronald Press, Co., New York, 1958.

10. R. C. Tausworthe, "Theory and Practical Design of Phase-Locked Receivers," Vol. 1, Technical Report No. 32-819, Jet Propulsion Laboratory, Pasadena, California, 1966.

CHAPTER VI

CONCLUSIONS

6.1 Conclusions

In this dissertation, a second-order PLL in which the loop filter contains complex zeros has been investigated. Prior designs used a filter containing a simple zero on the negative real axis. This "generalized" second-order PLL had been heretofore unexplored, although there was experimental evidence on a related loop (ERPLD) which suggested that considerable performance improvement was possible with this generality, in terms of threshold performance [Ref. 1, pp. 260-261 and Ref. 2]. The basic characteristics of the generalized second-order PLL including the open and closed-loop responses and the corresponding root locus were generated and compared against those of the conventional second-order PLL. As in the conventional second-order PLL case, the generalized second-order PLL was found to be unconditionally stable. The closed-loop response of the generalized second-order PLL indicates that the noise bandwidth of the device is theoretically infinite thus making the predetection filter critical to the performance of this PLL. Such is not the case in the conventional PLL.

A method was presented for achieving an optimum design for the generalized second-order PLL for a number of useful modulation types including a single-channel FM speech signal, FDM-FM and FDM-PM. This optimum design was in terms of threshold performance and requires a knowledge of "ν" the mean-square phase error at threshold for the device. Previous experimental and analytical evidence with conventional PLLs [Ref. 1, pp. 138-147, Ref. 3 and Ref. 4] has indicated a range of values of ν between 0.20 and 0.25. The optimum design was found to be relatively insensitive to a variation of ν over this range.

Using the Continuous System Modeling Program (CSMP), a non-linear model of the generalized second-order PLL was simulated for the test-tone modulation case both in the absence of noise and with the signal corrupted by bandpass Gaussian noise. In addition, preliminary results for the case of a single-channel FM voice signal were obtained and the methods for simulating the FDM-FM and FDM-PM cases were given. It was shown that by comparing the results obtained for the non-linear model against those predicted from the linear formulation, a measure of the mean-square phase error at threshold for the generalized second-order PLL is obtainable, and ranges between 0.25 and 0.30.

Additional insight into the operation of the generalized second-order PLL was obtained through investigation of its acquisition and tracking behavior. This was accomplished using phase plane techniques to study the non-linear differential equation which governs the loop operation. The results indicated that for $Kb/\beta < 1.0$ (see Sec. 5.2) the phase plane behavior of the generalized second-order PLL is similar to that of the conventional second-order PLL with differences in the trajectory shape and cycle slipping rates being noticed. However, for $Kb/\beta \geq 1.0$ the phase plane portrait is seen to change markedly with the introduction of additional singularities into the phase plane.

6.2 Suggestions for Future Work

The optimum design technique presented in Chapter 3 may have applications not only to the conventional and generalized second-order PLL but to higher order PLLs as well. Design and performance of PLLs of order greater than two are as yet largely unexplored [Ref. 1, p. 152] and the optimum design procedure presented in this dissertation holds the possibility of remedying this situation. It is also desirable to investigate an alternate optimization algorithm with the goal of decreasing the CPU time required to obtain the optimum loop parameters.

The computer simulation techniques and results of Chapter 4 should be an aid for more advanced work. It is desirable, for example, to perform the simulations for the FDM-FM and FDM-PM cases and obtain the corresponding data for the meansquare phase error at threshold. In addition, the possibility of refining the PSD models for the various modulation cases could be investigated in an effort to more closely simulate the actual physical situation thereby achieving more precise results. As discussed earlier, it is desirable to investigate PLLs of order greater than two. The computer simulation of such devices is an obvious and significant part of this investigation and should be explored.

It is also of interest to compare the acquisition times (see Sec. 5.3.5) of the conventional and generalized second-order PLL. This can be accomplished by again using the CSMP to obtain the corresponding time solutions of the differential equations governing the two PLLs.

The phase plane analysis of Chapter 5 yielded additional insight into the behavior of the generalized second-order PLL; however, it brought to light another question. For $K_b/\beta \geq 1.0$ the phase plane portrait shows an absence of cycle slipping and trajectories which theoretically move towards infinite frequency error (see Sec. 5.3.5). Exactly what significance these findings have in light of the performance and component limitations of the actual physical device remains yet to be answered.

References - Chapter 6

1. J. Klapper and J. Frankle, Phase - Locked and Frequency - Feedback Systems: Principles and Techniques, Academic Press, New York, 1972.

2. A. Acampora and A. Newton "Use of Phase Subtraction to Extend the Range of a Phase - Locked Demodulator, "RCA Review, vol. 27, No. 3, pp. 577-599, December 1966.

3. A. J. Viterbi, "Phase - Locked Loop Dynamics in the Presence of Noise by Fokker - Planck Techniques," Proc. IEEE, vol. 51, pp. 1737-1753, December 1963.

4. J. T. Frankle, "Threshold Performance of Analog FM Demodulators," RCA Review, vol. 27, No. 4, pp. 521-562, December 1966.

REFERENCES

1. A. Acampora and A. Newton, "Use of Phase Subtraction to Extend the Range of A Phase-Locked Demodulator," RCA Review, vol. 27, No. 3, pp. 577-599, December 1966.

2. G. S. Beveridge and R.S. Schechter, Optimization Theory and Practice, McGraw-Hill, New York, 1970.

3. R. Burington, Handbook of Mathematical Tables and Formulas, 4th Edition, McGraw-Hill Book Co., New York, 1965.

4. W. J. Cunningham, Introduction to Nonlinear Analysis, McGraw-Hill Book Co., New York, 1958.

5. R. L. Fox, Optimization Methods for Engineering Design, Addison-Wesley, Reading, MA, 1971.

6. J. Frankle, "Threshold Performance of Analog FM Demodulators," RCA Review 27, No. 4, pp. 521-562, 1966.

7. J. E. Gibson, Nonlinear Automatic Control, McGraw-Hill Book Co., New York, 1963.

8. E. Grabbe, S. Ramo and D. Wooldridge, Handbook of Automation, Computation and Control, vol. 2, John Wiley and Sons, New York, 1959.

9. E. A. Guillemin, Synthesis of Passive Networks, John Wiley and Sons, New York, 1957.

10. R. E. Heitzman, "A Study of the Threshold Power Requirements of FMFB Receivers," IRE Trans. SET-8, pp. 249-256, 1962.

11. IBM Application Program, System/360 Continuous System Modeling Program User's Manual, GH20-0367-4.

12. IBM Application Program, System/360 Continuous System Modeling Program Application Description, GH20-0240-3.

13. IBM Application Program, System/360 Continuous System Modeling Program System Manual, GY20-0111-0.

14. C. L. Johnson, Analog Computer Techniques, McGraw-Hill Book Co., New York, 1963.

15. S. Karni, Network Theory: Analysis and Synthesis, Allyn and Bacon Inc., Boston, MA, 1966.

16. J. Klapper, "Demodulator Threshold Performance and Error Rates in Angle-Modulated Digital Signals", RCA Review, vol. 27, No. 2, pp. 226-244, June 1966.

17. J. Klapper and J. Frankle, Phase-Locked and Frequency-Feedback Systems: Principles and Techniques, Academic Press, New York, 1972.

18. J. Klapper and G. M. Veiga, "Threshold Performance of a PLL with Phase Feedback," Proc. Allerton Conf. on Circuit and System Theory, Monticello, IL, October 1971.

19. R. Kochenburger, Computer Simulation of Dynamic Systems, Prentice Hall, Inc., Englewood Cliffs, NJ, 1972.

20. G. A. Korn, Random-Process Simulation and Measurements, McGraw-Hill Book Co., NY, 1966.

21. J. Kowalik and M. Osborne, Methods for Unconstrained Optimization Problems, Elseiver, NY, 1968.

22. Y. H. Ku, Analysis and Control of Nonlinear Systems, The Ronald Press Co., NY, 1958.

23. W. C. Lindsey, Synchronization Systems in Communication and Control, Prentice Hall, Inc., Englewood Cliffs, NJ, 1972.

24. D. D. McCracken, A Guide to FORTRAN IV Programming, John Wiley & Sons, NY, 1965.

25. M. MacLaren, M. Donald and G. Marsaglia, Uniform Random Number Generators, Journal of ACM, vol. 12, No. 1, pp. 83-89.

26. K. Ogata, Modern Control Engineering, Prentice-Hall, Inc., Englewood Cliffs, NJ, 1970.

27. P. F. Panter, Modulation, Noise, and Spectral Analysis, McGraw-Hill, NY, 1965.

28. M. J. Powell, "An Efficient Method for Finding the Minimum of a Function of Several Variables without Calculating Derivatives, Computer J, No. 7, p. 155, 1964.

29. L. M. Robinson, "Tanlock: A Phase Lock Loop of Extended Tracking Capability," Proc. Nat. Conf. Military Electron., Los Angeles, CA, pp. 396-421, February 1962.

30. S. M. Selby, editor, Standard Mathematical Tables, 17th Edition, The Chemical Rubber Co., Cleveland, Ohio, 1969.

31. R. C. Tausworthe, "Theory and Practical Design of Phase-Locked Receivers," vol. 1, Technical Report No. 32-819, Jet Propulsion Laboratory, Pasadena, CA, 1966.

32. G. J. Thaler and M. P. Pastel, Analysis and Design of Nonlinear Feedback Control Systems, McGraw-Hill Book Co., NY, 1962.

33. J. J. Uhran and J. C. Lindenlaub, "Effects of a Class of Phase Comparators on the Threshold and Lock Range of Phase Lock Loop Systems," Int. Conf. Commun. 3rd, Minneapolis, Minnesota, June 1967; "Experimental Results for Phase-Lock Loop Systems Having a Modified nth-order Tanlock Phase Detector," IEEE Trans., COMM-16, No. 6, pp. 787-795, 1968.

34. A. J. Viterbi, "Acquisition and Tracking Behavior of Phase-Locked Loops," Symposium on Active Networks and Feedback Systems, Polytechnic Institute of Brooklyn, April 1960.

35. A. J. Viterbi, "Phase-Locked Loop Dynamics in the Presence of Noise by Fokker-Planck Techniques," Proc. IEEE, vol. 51, pp. 1737-1753, December 1963.

36. A. Viterbi, Principles of Coherent Communication, McGraw-Hill Book Co., NY, 1966.

APPENDIX A

COMPUTER PROGRAMS USED TO EVALUATE MAGNITUDE AND PHASE RESPONSE OF THE ERPLD AND ROOT LOCUS OF THE GENERALIZED SECOND-ORDER PLL

```
      C  CLOSED LOOP MAGNITUDE RESPONSE OF ERPLD WITH VARYING ALPHA
1      10 READ(5,20) ALPHA
2      20 FORMAT (8F10.0)
3         A=2.94E4
4         B=1.88E3
5         XK=4.7E5
6         RFRQ=0.0
7         XNEWA=ALPHA/(XK*B)
8      30 XNEWB=1.0-(RFRQ**2)*XNEWA
9         XNEW1=XNEWB**2
10        XNEWC=1.0/A+ALPHA/XK
11        XNEWD=RFRQ*XNEWC
12        XNEW2=XNEWD**2
13        XNEWE=(1.0+ALPHA)/(XK*B)
14        XNEWF=1.0-(RFRQ**2)*XNEWE
15        XNEW3=XNEWF**2
16        XNEWG=1.0/A+(1.0+ALPHA)/XK
17        XNEWH=RFRQ*XNEWG
18        XNEW4=XNEWH**2
19        TRSQ=(XNEW1+XNEW2)/(XNEW3+XNEW4)
20        TRANS=SQRT(TRSQ)
21        TRANDB=10.0*ALOG10(TRANS)
22        FREQ=RFRQ/(2.0*3.1415927)
23        WRITE(6,40) TRANS , RFRQ , FREQ , ALPHA , TRANDB
24     40 FORMAT(1P5E16.6)
25        RFRQ-RFRQ+1000.0
26        IF(RFRQ.GT.3.0E5) GO TO 10
27        GO TO 30
28        STOP
29        END
```

```
C CLOSED LOOP PHASE RESPONSE OF ERPLD WITH VARYING ALPHA

 1        10  READ(5,20) ALPHA
 2        20  FORMAT(8F10.0)
 3            A=2.94E4
 4            B=1.88E3
 5            XK=4.7E5
 6            RFRQ=0.0
 7            XNEWA=ALPHA/(XK*B)
 8        30  XNEW1=1.0-(RFRQ**2)*XNEWA
 9            IF(ABS(XNEW1).LT.1.0E-30) GO TO 99
10            XNEWB=1.0/A+ALPHA/XK
11            XNEW2=RFRQ*XNEWB
12            XNEWR=XNEW2/XNEW1
13            IF(XNEW1.LT.0.0) GO TO 40
14            THETA1=ATAN(XNEWB)
15            GO TO 50
16        40  THETA1=ATAN(XNEWR)+3.1415927
17        50  XNEWC=(1.0+ALPHA)/(XK*B)
18            XNEW3=1.0-(RFRQ**2)*XNEWC
19            IF(ABS(XNEW3).LT.1.0E-30) GO TO 99
20            XNEWD=1.0/A+(1.0+ALPHA)/XK
21            XNEW4=RFRQ*XNEWD
22            XNEWS=XNEW4/XNEW3
23            IF(XNEW3.LT.0.0) GO TO 60
24            THETA2=ATAN(XNEWS)
25            GO TO 70
26        60  THETA2=ATAN(XNEWS)+3.1415927
27        70  THETA=THETA1-THETA2
28            THETAD=(180.0/3.1415927)*THETA
29            FREQ=RFRQ/(2.0*3.1415927)
30            WRITE(6,80) THETAD , RFRQ , FREQ , ALPHA , THETA
31        80  FORMAT(1P5E16.6)
32        99  RFRQ=RFRQ+1000.0
33            IF(RFRQ.GT.3.0E5) GO TO 10
34            GO TO 30
35            STOP
36            END
```

```
C GENERALIZED SECOND-ORDER PLL-ROOT LOCUS

      B=1.88E3
      BETA=8.836E8
      GAMMA=2.767E4
      XK=1.0E5
   10 XNEW1=1.0/XK+1.0/GAMMA
      XNEW2=1.0/(XK*B)+1.0/BETA
      RE1=(XNEW1/XNEW2)*(-0.5)
      XNEW3=XNEW1**2
      XNEW4=4.0*(XNEW2**2)
      XNEW5=XNEW3/XNEW4
      XNEW6=XNEW5-1.0/XNEW2
      IF(XNEW6.LT.0.0) GO TO 40
      RE2=SQRT(XNEW6)
      S1=RE1+RE2
      S2=RE1-RE2
      WRITE(6,20)
   20 FORMAT(1H , 16HREAL ROOT REGION)
      WRITE(6,30) S1,S2,XK
   30 FORMAT(1P3E16.6)
      GO TO 70
   40 XNEW7=ABS(XNEW6)
      XNEW8=SQRT(XNEW7)
      XIM1=XNEW8
      XIM2=XNEW8*(-1.0)
      WRITE(6,50)
   50 FORMAT(1H , 19HCOMPLEX ROOT REGION)
      WRITE(6,60) RE1,XIM1,XIM2,XK
   60 FORMAT(1P4E16.6)
   70 XK=XK+1.0E5
      IF(XK.GE.1.0E8) GO TO 80
      GO TO 10
   80 STOP
      END
```

APPENDIX B

DETAILED MATHEMATICS FOR CLOSED-FORM SOLUTION OF (CNRIF)TH FOR THE VOICE MODULATION CASE

In this Appendix, a detailed derivation of (CNRIF)TH in closed form for a single-channel FM speech signal is presented. Each of the four cases as given by Eqs. 3-28, 3-29, 3-37 and 3-46 is discussed. Beginning with Cases I and II, which may be combined for much of the derivation which follows, and realizing that the integrand in Eq. 3-24 is an improper polynomial function, a division is performed yielding

$$\int_0^{B_p/2} |H(j\omega)|^2 \, df \tag{B-1}$$

$$\frac{1}{2\pi} \int_0^{\pi B_p} \left[\frac{A}{C} - \frac{A}{C} \left(\frac{D\omega^2 + 1}{C\omega^4 + D\omega^2 + 1} \right) + \left(\frac{B\omega^2 + 1}{C\omega^4 + D\omega^2 + 1} \right) \right] d\omega$$

Consider first the third term in the integrand of Eq. B-1 and defining $X \equiv \omega$ for convenience yields

$$\frac{BX^2 + 1}{CX^4 + DX^2 + 1} = \frac{1}{C}\left[\frac{BX^2 + 1}{X^4 + \frac{D}{C}X^2 + \frac{1}{C}}\right] \tag{B-2}$$

The denominator of Eq. B-2 yields the roots

$$X^2 = -\frac{D}{2C} \pm \sqrt{\left(\frac{D}{2C}\right)^2 - \frac{1}{C}} \tag{B-3}$$

For Cases I and II, the roots of Eq. B-3 are seen to be complex and the following definition is made

$$X^4 + \frac{D}{C}X^2 + \frac{1}{C} \equiv (X^2 + G)(X^2 + G^*) \tag{B-4}$$

where

$$G = \frac{D}{2C} - j\sqrt{\frac{1}{C} - \left(\frac{D}{2C}\right)^2} \tag{B-5}$$

and G^* is the complex conjugate of G. Using the method of partial fraction expansion

$$\frac{BX^2+1}{(X^2+G)(X^2+G^*)} = \frac{MX+N}{X^2+G} + \frac{PX+Q}{X^2+G^*} \tag{B-6}$$

By using the conventional technique in Eq. B-6 of cross-multiplying and setting the coefficients of like powers of X equal to each other, the following set of conditions arises

$$\left.\begin{aligned} M+P &= 0 \\ N+Q &= B \\ MG^*+PG &= 0 \\ NG^*+QG &= 1 \end{aligned}\right\} \qquad \text{(B-7)}$$

The special case of $M = -P \neq 0$ implies that G must be purely real which reduces to Case IV, to be discussed subsequently. Excluding this case, it follows directly from the conditions of Eq. B-7 that

$$\left.\begin{aligned} M &= P = 0 \\ Q &= \frac{1 - BG^*}{G - G^*} \\ N &= \frac{1 - BG}{G^* - G} \end{aligned}\right\} \qquad \text{(B-8)}$$

Next, consider the roots of $X^2 + G$

$$X^2 = -G = \frac{-D}{2C} + j\sqrt{\frac{1}{C} - \left(\frac{D}{2C}\right)^2} \equiv R\angle\phi \qquad \text{(B-9)}$$

where

$$R = (1/C)^{1/2} \tag{B-10}$$

$$\phi = \tan^{-1}\left(\frac{\sqrt{\frac{1}{C} - \left(\frac{D}{2C}\right)^2}}{D/2C}\right) , \quad \text{for CASE I}$$

$$\phi = \tan^{-1}\left(\frac{\sqrt{\frac{1}{C} - \left(\frac{D}{2C}\right)^2}}{D/2C}\right) + \pi , \quad \text{for CASE II}$$

The expressions for ϕ for Cases I and II are arrived at using the following reasoning. For Case I, D is negative and the real part of the complex expression in Eq. B-9 is positive. The angle ϕ is then in the first quadrant and the expression for ϕ for Case I in Eq. B-10 holds. If, on the other hand, D is positive, ϕ falls in the second quadrant. But, since the arctangent function of a negative number gives the principle value, i.e., a value in the fourth quadrant, a factor of π must be added to achieve the correct angle.

The two roots of X^2+G are then

$$\left.\begin{aligned} X &= R^{1/2}\underline{/\phi/2} \quad \equiv -J \\ X &= R^{1/2}\underline{/\phi/2} + \pi \quad \equiv J \end{aligned}\right\} \tag{B-11}$$

where the relationship between ϕ and θ used in Chapter 3 is given by the more convenient definition for J

$$J = M \angle \theta \tag{3-33}$$

In a similar manner

$$X^2 = -G^* = \frac{-D}{2C} - j\sqrt{\frac{1}{C} - \left(\frac{D}{2C}\right)^2} = R \angle -\phi \tag{B-12}$$

These two roots are then

$$\left.\begin{aligned} X &= R^{1/2} \angle -\phi/2 \equiv -K \\ X &= R^{1/2} \angle -\phi/2 + \pi \equiv K \end{aligned}\right\} \tag{B-13}$$

From Eqs. B-11 and B-13, it is noted that

$$K = J^* \tag{B-14}$$

Again, using the method of partial fraction expansion

$$\left.\begin{aligned} \frac{N}{X^2+G} &= \frac{N}{(X+J)(X-J)} = \frac{N/2J}{X-J} - \frac{N/2J}{X+J} \\ \frac{Q}{X^2+G^*} &= \frac{Q}{(X+K)(X-K)} = \frac{Q/2K}{X-K} - \frac{Q/2K}{X+K} \end{aligned}\right\} \qquad \text{(B-15)}$$

Eq. B-6 may then be expressed as

$$\frac{BX^2+1}{(X^2+G)(X^2+G^*)} = \frac{N}{2J}\left(\frac{1}{X-J} - \frac{1}{X+J}\right) + \frac{Q}{2K}\left(\frac{1}{X-K} - \frac{1}{X+K}\right) \qquad \text{(B-16)}$$

Defining the complex variable Z as

$$Z = X + J$$

then

$$dZ = dX \qquad \text{(B-17)}$$

and

$$\int \frac{dX}{X+J} = \int \frac{dZ}{Z} = \ell n\, Z = \ell n\,(X+J)$$

Integrating both sides of Eq. B-16 yields

$$\int \frac{BX^2 + 1}{(X^2 + G)(X^2 + G^*)} dX = \tag{B-18}$$

$$\frac{N}{2J}\left[\ell n(X - J) - \ell n(X + J)\right] + \frac{Q}{2K}\left[\ell n(X - K) - \ell n(X + K)\right] =$$

$$\frac{N}{2J}\,\ell n\left(\frac{X - J}{X + J}\right) + \frac{Q}{2K}\,\ell n\left(\frac{X - K}{X + K}\right)$$

Utilizing Eqs. B-8 and B-14 in Eq. B-18, above, yields

(B-19)

$$\int \frac{BX^2 + 1}{(X^2 + G)(X^2 + G^*)} dX =$$

$$\frac{1 - BG}{2J(G^* - G)}\,\ell n\left(\frac{X - J}{X + J}\right) + \frac{1 - BG^*}{2J^*(G - G^*)}\,\ell n\left(\frac{X - J^*}{X + J^*}\right)$$

Recalling that G and J are complex constants, B is a real constant and X is a real variable, it is noted that the first term in Eq. B-19 is the complex conjugate of the second term, therefore

$$\int \frac{BX^2 + 1}{X^4 + \frac{DX^2}{C} + \frac{1}{C}}\, dX = \tag{B-20}$$

$$2\,\mathrm{Re}\left[\frac{1 - BG}{2J\,(G^* - G)} \cdot \ln\left(\frac{X - J}{X + J}\right)\right]$$

This result may be used to evaluate the entire integral in Eq. B-1, yielding

$$\int_0^{B_p/2} |H(j\omega)|^2\, df = \tag{B-21}$$

$$\frac{1}{2\pi}\left\{\frac{AX}{C} - \frac{A}{C^2}\,\mathrm{Re}\left[\frac{1 - DG}{J(G^* - G)} \ln\left(\frac{X - J}{X + J}\right)\right] + \frac{1}{C}\,\mathrm{Re}\left[\frac{1 - BG}{J(G^* - G)} \ln\left(\frac{X - J}{X + J}\right)\right]\right\}\Bigg|_0^{\pi B_p}$$

Following through the evaluation

(B-22)

$$\int_0^{Bp/2} |H(j\omega)|^2 \, df =$$

$$\frac{1}{2\pi}\left\{ \frac{\pi A B_p}{C} - \frac{A}{C^2} \mathrm{Re}\left[\frac{1-DG}{J(G^*-G)} \ln\left(\frac{\pi B_p - J}{\pi B_p + J} \right) \right] \right.$$

$$+ \frac{1}{C} \mathrm{Re}\left[\frac{1-BG}{J(G^*-G)} \ln\left(\frac{\pi B_p - J}{\pi B_p + J} \right) \right] + \frac{A}{C^2} \mathrm{Re}\left[\frac{1-DG}{J(G^*-G)} \ln(-1) \right]$$

$$\left. - \frac{1}{C} \mathrm{Re}\left[\frac{1-BG}{J(G^*-G)} \ln(-1) \right] \right\}$$

Combining terms in Eq. B-22 simplifies the expression to the form

(3-30)

$$\int_0^{B_p/2} |H(j\omega)|^2 \, df =$$

$$\frac{1}{2\pi C}\left\{ \pi A B_p + \mathrm{Re}\left[\frac{(1 - BG) - A/C(1 - DG)}{J(G^* - G)} \ln\left(\frac{J - \pi B_p}{J + \pi B_p}\right)\right]\right\}$$

where the parameters are defined by Eqs. 3-22, 3-32 and 3-33.

Next, the evaluation of $\overline{\phi_{es}^2(t)}$ in closed form is considered. From Eqs. 3-6, 3-11, 3-13 and 3-25, $\overline{\phi_{es}^2(t)}$ may be expressed as

(B-23)

$$\overline{\phi_{es}^2(t)} =$$

$$\frac{(2\pi)^2 f_a f_b (\Delta\omega_{rms})^2}{f_b - f_a} \int_{f_a}^{f_b} \frac{1}{\omega^4} \cdot \frac{A'\omega^4 + B'\omega^2}{C\omega^4 + D\omega^2 + 1} \, df =$$

$$\frac{\omega_a \omega_b (\Delta\omega_{rms})^2}{\omega_b - \omega_a} \int_{\omega_a}^{\omega_b} \frac{1}{\omega^4} \cdot \frac{A'\omega^4 + B'\omega^2}{C\omega^4 + D\omega^2 + 1} \, d\omega$$

where the coefficients of the integrand are defined in Eq. 3-22. Again, letting $X \equiv \omega$, the integrand in Eq. B-23 may be expressed as

(B-24)

$$\frac{1}{X^4} \cdot \frac{A'X^4 + B'X^2}{CX^4 + DX^2 + 1} =$$

$$\frac{A'}{CX^4 + DX^2 + 1} + \frac{B'}{X^2(CX^4 + DX^2 + 1)}$$

By making use of Eq. B-20 with B=0, the integral of the first term on the right side of Eq. B-24 can be immediately evaluated as

(B-25)

$$\frac{A'}{C}\int_{\omega_a}^{\omega_b}\frac{1}{\omega^4+\frac{D}{C}\omega^2+\frac{1}{C}}\,d\omega =$$

$$\frac{A'}{C}\,Re\left[\frac{1}{J\,(G^*-G)}\,\ell n\left(\frac{\omega-J}{\omega+J}\right)\right]\Bigg|_{\omega_a}^{\omega_b} =$$

$$\frac{A'}{C}\,Re\left[\frac{1}{J\,(G^*-G)}\,\ell n\left(\frac{\omega_b-J}{\omega_b+J}\cdot\frac{\omega_a+J}{\omega_a-J}\right)\right]$$

Next, consider the second term on the right side of Eq. B-24 which using B-4, can be expressed as

$$\frac{B'}{C}\left[\frac{1}{X^2\left(X^4+\frac{D}{C}X^2+\frac{1}{C}\right)}\right] = \frac{B'}{C}\left[\frac{1}{X^2(X^2+G)(X^2+G^*)}\right] \qquad \text{(B-26)}$$

Using the method of partial fraction expansion

$$\frac{1}{X^2(X^2+G)(X^2+G^*)} = \frac{MX+N}{X^2+G} + \frac{PX+Q}{X^2+G^*} + \frac{R}{X^2} + \frac{S}{X} \qquad \text{(B-27)}$$

By again using the conventional technique in Eq. B-27 of cross-multiplying and setting the coefficients of like powers of X equal to each other, the following set of conditions arises

$$\left.\begin{aligned} M+P+S &= 0 \\ N+Q+R &= 0 \\ MG^*+PG+SG+SG^* &= 0 \\ NG^*+QG+RG+RG^* &= 0 \\ SGG^* &= 0 \\ RGG^* &= 1 \end{aligned}\right\} \qquad \text{(B-28)}$$

From Eq. B-28, except for the trivial case of G=0, S must equal zero. In addition, once more, the special case of $M=-P \neq 0$ implies that G must be purely real which reduces to Case IV to be discussed subsequently. Excluding these special cases, it follows directly from the conditions of Eq. B-28 that

$$M = P = S = 0 \tag{B-29}$$

$$N = \frac{1}{G(G-G^*)}$$

$$Q = \frac{1}{G^*(G^*- G)}$$

$$R = \frac{1}{GG^*}$$

Combining the first two terms of Eq. B-27 yields

(B-30)

$$\frac{\dfrac{1}{G\,(\,G - G^*\,)}}{X^2 + G} + \frac{\dfrac{1}{G^*\,(\,G^* - G\,)}}{X^2 + G^*} =$$

$$\frac{-\left(\dfrac{1}{G\,G^*}\right)(\,X^2 + G + G^*\,)}{(\,X^2 + G\,)(\,X^2 + G^*\,)} =$$

$$\frac{-\left(\dfrac{G + G^*}{G\,G^*}\right)\left(\dfrac{X^2}{G + G^*} + 1\right)}{X^4 + \dfrac{D}{C}X + \dfrac{1}{C}}$$

Note that this result is consistent with partial fraction theory in that $G+G^*$ and GG^* are real numbers. The result of Eq. B-30 fits the form already evaluated in Eq. B-20. Performing the desired integration yields

(B-31)

$$-\left(\frac{G + G^*}{GG^*}\right)\int \frac{\frac{X^2}{G + G^*} + 1}{X^4 + \frac{D}{C}X^2 + \frac{1}{C}}\, dX =$$

$$\mathcal{R}e\left[\frac{1}{GJ\,(G - G^*)}\, \ell n\left(\frac{X - J}{X + J}\right)\right]$$

Next, considering the third and final term in Eq. B-27, yields

(B-32)

$$\frac{1}{GG^*}\int \frac{dX}{X^2} = \left(\frac{1}{GG^*}\right)\left(-\frac{1}{X}\right)$$

The entire expression in Eq. B-26 can now be integrated between the desired limits of ω_a to ω_b using the results of Eqs. B-31 and B-32. This proceeds as follows

(B-33)

$$\frac{B'}{C} \int_{\omega_a}^{\omega_b} \frac{1}{\omega^2 \left(\omega^4 + \frac{D}{C}\omega^2 + \frac{1}{C} \right)} \, d\omega =$$

$$\frac{B'}{C} \left\{ \mathrm{Re} \left[\frac{1}{GJ (G - G^*)} \ln \left(\frac{\omega - J}{\omega + J} \right) \right] - \left(\frac{1}{GG^*} \right) \left(\frac{1}{\omega} \right) \right\} \Bigg|_{\omega_a}^{\omega_b} =$$

$$\frac{B'}{C} \left\{ \mathrm{Re} \left[\frac{1}{GJ (G - G^*)} \ln \left(\frac{\omega_b - J}{\omega_b + J} \cdot \frac{\omega_a + J}{\omega_a - J} \right) \right] \right.$$

$$\left. + \frac{1}{GG^*} \left(\frac{1}{\omega_a} - \frac{1}{\omega_b} \right) \right\}$$

Finally, the results of Eqs. B-25 and B-33 may be combined along with Eq. B-23, yielding the desired expression

(3-31)

$$\overline{\phi_{es}^2(t)} =$$

$$\frac{\omega_a \omega_b (\Delta\omega_{rms})^2}{\omega_b - \omega_a} \left\{ \frac{1}{C} \mathcal{R}e \left[\frac{B' - A'G}{GJ(G - G^*)} \ln \left(\frac{\omega_b - J}{\omega_b - J} \cdot \right. \right. \right.$$

$$\left. \left. \left. \frac{\omega_a + J}{\omega_a + J} \right) \right] + \frac{B'}{CGG^*} \left(\frac{1}{\omega_a} - \frac{1}{\omega_b} \right) \right\}$$

Next, consider Case III defined by Eq. 3-37. Starting with Eq. B-2, it is seen that the roots of the denominator may be expressed as follows

$$X^4 + \frac{D}{C} X^2 + \frac{1}{C} = (X^2 + R_1^2)(X^2 + R_2^2) \qquad \text{(B-34)}$$

where R_1 and R_2 are both positve real constants defined by Eq. 3-43. Eq. B-2 may then be expressed as

(B-35)

$$\frac{B X^2 + 1}{C X^4 + D X^2 + 1} = \frac{1}{C}\left[\frac{B X^2 + 1}{(X^2 + R_1^2)(X^2 + R_2^2)}\right]$$

Using the method of partial fraction expansion

(B-36)

$$\frac{B X^2 + 1}{(X^2 + R_1^2)(X^2 + R_2^2)} = \frac{M X + N}{X^2 + R_1^2} + \frac{P X + Q}{X^2 + R_2^2}$$

Again, using the conventional technique of cross-multiplying and setting like powers of X equal to each other, the following set of conditions arises.

$$\left.\begin{aligned} M+P &= 0 \\ N+Q &= B \\ MR_2^2 + PR_1^2 &= 0 \\ NR_2^2 + QR_1^2 &= 1 \end{aligned}\right\} \qquad \text{(B-37)}$$

The special case of $M = -P \neq 0$ implies that $R_1^2 = R_2^2$ which again reduces to Case IV, to be discussed subsequently. Excluding this case, it follows directly from the conditions of Eq. B-37 that

$$\left.\begin{aligned} M &= P = 0 \\ Q &= \frac{1 - B R_2^2}{R_1^2 - R_2^2} \\ N &= \frac{1 - B R_1^2}{R_2^2 - R_1^2} \end{aligned}\right\} \qquad \text{(B-38)}$$

Carrying through the desired integration of Eq. B-35 yields

(B-39)

$$\frac{1}{C}\int \frac{BX^2 + 1}{(X^2 + R_1^2)(X^2 + R_2^2)}\, dX =$$

$$\frac{1}{C}\int \frac{\frac{1 - BR_1^2}{R_2^2 - R_1^2}}{X^2 + R_1^2}\, dX + \frac{1}{C}\int \frac{\frac{1 - BR_2^2}{R_1^2 - R_2^2}}{X^2 + R_2^2}\, dX =$$

$$\frac{1}{C}\left[\frac{1 - BR_1^2}{R_2^2 - R_1^2}\left(\frac{1}{R_1}\tan^{-1}\frac{X}{R_1}\right) + \frac{1 - BR_2^2}{R_1^2 - R_2^2}\left(\frac{1}{R_2}\tan^{-1}\frac{X}{R_2}\right)\right]$$

This result may be used to evaluate the entire integral in Eq. B-1 as follows

(B-40)

$$\int_0^{B_p/2} |H(j\omega)|^2 \, df =$$

$$\frac{1}{2\pi}\left\{\frac{AX}{C} - \frac{A}{C^2}\left[\frac{1-DR_1^2}{R_2^2-R_1^2}\left(\frac{1}{R_1}\tan^{-1}\frac{X}{R_1}\right)+\right.\right.$$

$$\left.\frac{1-DR_2^2}{R_1^2-R_2^2}\left(\frac{1}{R_2}\tan^{-1}\frac{X}{R_2}\right)\right] + \frac{1}{C}\left[\frac{1-BR_1^2}{R_2^2-R_1^2}\left(\frac{1}{R_1}\tan^{-1}\frac{X}{R_1}\right)\right.$$

$$\left.\left.\left.+\frac{1-BR_2^2}{R_1^2-R_2^2}\left(\frac{1}{R_2}\tan^{-1}\frac{X}{R_2}\right)\right]\right\}\right|_0^{\pi B_p}$$

and

(3-41)

$$\int_0^{B_p/2} |H(j\omega)|^2 \, df$$

$$\frac{1}{2\pi C}\left\{\left[\frac{1-BR_1^2}{R_2^2-R_1^2}\left(\frac{1}{R_1}\tan^{-1}\frac{\pi B_p}{R_1}\right)+\frac{1-BR_2^2}{R_1^2-R_2^2}\left(\frac{1}{R_2}\tan^{-1}\frac{\pi B_p}{R_2}\right)\right]\right.$$

$$-\frac{A}{C}\left[\frac{1-DR_1^2}{R_2^2-R_1^2}\left(\frac{1}{R_1}\tan^{-1}\frac{\pi B_p}{R_1}\right)+\frac{1-DR_2^2}{R_1^2-R_2^2}\left(\frac{1}{R_2}\tan^{-1}\frac{\pi B_p}{R_2}\right)\right]$$

$$\left.+A\pi B_p\right\}$$

Next, the evaluation of $\overline{\phi_{es}^2(t)}$ in closed form for Case III is considered. Starting with Eq. B-24, it is recognized that the first term on the right side of this equation can be evaluated immediately using the results of Eq. B-39 with B=0. Following this procedure yields

(B-41)

$$\frac{A'}{C}\int_a^b \frac{1}{\omega^4 + \frac{D}{C}\omega^2 + \frac{1}{C}}\, d\omega =$$

$$\frac{A'}{C}\left[\frac{1}{R_2^2 - R_1^2}\left(\frac{1}{R_1}\tan^{-1}\frac{\omega}{R_1}\right) + \frac{1}{R_1^2 - R_2^2}\left(\frac{1}{R_2}\tan^{-1}\frac{\omega}{R_2}\right)\right]\Bigg|_{\omega_a}^{\omega_b} =$$

$$\frac{A'}{C(R_1^2 - R_2^2)}\left[\frac{1}{R_2}\left(\tan^{-1}\frac{\omega_b}{R_2} - \tan^{-1}\frac{\omega_a}{R_2}\right) + \frac{1}{R_1}\left(\tan^{-1}\frac{\omega_a}{R_1} - \tan^{-1}\frac{\omega_b}{R_1}\right)\right]$$

Next, consider the second term on the right side of Eq. B-24, which may be expressed as

(B-42)

$$\frac{B'}{C}\left[\frac{1}{X^2\left(X^4 + \frac{D}{C}X^2 + \frac{1}{C}\right)}\right] = \frac{B'}{C}\left[\frac{1}{X^2(X^2 + R_1^2)(X^2 + R_2^2)}\right]$$

Using the method of partial fraction expansion

(B-43)

$$\frac{1}{X^2(X^2+R_1^2)(X^2+R_2^2)} = \frac{MX+N}{X^2+R_1^2} + \frac{PX+Q}{X^2+R_2^2} + \frac{R}{X^2} + \frac{S}{X}$$

Cross-multiplying and setting coefficients of like powers of X equal to each other yields

(B-44)

$$M+P+S = 0$$

$$N+Q+R = 0$$

$$MR_2^2 + PR_1^2 + SR_1^2 + SR_2^2 = 0$$

$$NR_2^2 + QR_1^2 + RR_1^2 + RR_2^2 = 0$$

$$S\,R_1^2\,R_2^2 = 0$$

$$R\,R_1^2\,R_2^2 = 1$$

Once more, the special case of S=0 and M= -P $\neq$ 0 reduces to Case IV to be discussed subsequently. Excluding this case, it follows directly from Eq. B-44 that

$$M = P = S = 0 \qquad \text{(B-45)}$$

$$N = \frac{1}{R_1^2 \left(R_1^2 - R_2^2\right)}$$

$$Q = \frac{1}{R_2^2 \left(R_2^2 - R_1^2\right)}$$

$$R = \frac{1}{R_1^2 R_2^2}$$

Then

$$\frac{B'}{C}\int_{\omega_a}^{\omega_b}\frac{1}{\omega^2\left(\omega^4+\frac{D}{C}\omega^2+\frac{1}{C}\right)}\,d\omega = \tag{B-46}$$

$$\frac{B'}{C}\left[\frac{1}{R_1^3\left(R_1^2-R_2^2\right)}\tan^{-1}\frac{\omega}{R_1}+\frac{1}{R_2^3\left(R_2^2-R_1^2\right)}\tan^{-1}\frac{\omega}{R_2}+\frac{1}{R_1^2R_2^2}\left(-\frac{1}{\omega}\right)\right]\Bigg|_{\omega_a}^{\omega_b}=$$

$$\frac{B'}{C(R_1^2-R_2^2)}\left[\frac{1}{R_1^3}\left(\tan^{-1}\frac{\omega_b}{R_1}-\tan^{-1}\frac{\omega_a}{R_1}\right)+\frac{1}{R_2^3}\left(\tan^{-1}\frac{\omega_a}{R_2}-\tan^{-1}\frac{\omega_b}{R_2}\right)\right]$$

$$+\frac{B'}{CR_1^2R_2^2}\left(\frac{1}{\omega_a}-\frac{1}{\omega_b}\right)$$

Combining the results of Eq. B-41 and B-46 along with Eq. B-23, yields the expression

(3-42)

$$\overline{\phi_{es}^2(t)} = \frac{\omega_a \omega_b (\Delta\omega_{rms})^2}{\omega_b - \omega_a} \cdot$$

$$\left\{ \frac{A'}{C(R_1^2 - R_2^2)} \left[\frac{1}{R_2} \left(\tan^{-1} \frac{\omega_b}{R_2} - \tan^{-1} \frac{\omega_a}{R_2} \right) + \frac{1}{R_1} \left(\tan^{-1} \frac{\omega_a}{R_1} - \tan^{-1} \frac{\omega_b}{R_1} \right) \right] \right.$$

$$+ \frac{B'}{C(R_1^2 - R_2^2)} \left[\frac{1}{R_1^3} \left(\tan^{-1} \frac{\omega_b}{R_1} - \tan^{-1} \frac{\omega_a}{R_1} \right) + \frac{1}{R_2^3} \left(\tan^{-1} \frac{\omega_a}{R_2} - \tan^{-1} \frac{\omega_b}{R_2} \right) \right]$$

$$\left. + \frac{B'}{C R_1^2 R_2^2} \left(\frac{1}{\omega_a} - \frac{1}{\omega_b} \right) \right\}$$

Finally, consider Case IV, defined by Eq. 3-46. Starting with Eq. B-2, it is seen that the roots of the denominator may be expressed as follows

$$X^4 + \frac{D}{C} X^2 + \frac{1}{C} = (X^2 + R_o^2)^2 \qquad \text{(B-47)}$$

where R_o is a positive real constant defined by Eq. 3-49. Eq. B-2 may then be expressed as

(B-48)

$$\frac{B X^2 + 1}{C X^4 + D X^2 + 1} = \frac{1}{C}\left[\frac{B X^2}{(X^2 + R_o^2)^2} + \frac{1}{(X^2 + R_o^2)^2}\right]$$

Eq. B-48 can be integrated directly using standard integral tables yielding the result

(B-49)

$$\frac{1}{C}\int_0^{\pi B_p} \frac{B\omega^2 + 1}{\omega^4 + \frac{D}{C}\omega^2 + \frac{1}{C}}\, d\omega =$$

$$\frac{1}{2C}\left[-\frac{B\omega}{\omega^2 + R_0^2} + \frac{B}{R_0}\tan^{-1}\frac{\omega}{R_0} + \frac{\omega}{R_0^2(\omega^2 + R_0^2)}\right.$$

$$\left. + \frac{1}{R_0^3}\tan^{-1}\frac{\omega}{R_0}\right]\Bigg|_0^{\pi B_p} =$$

$$\frac{1}{2C}\left[\left(\frac{\pi B_p}{\pi^2 B_p^2 + R_0^2}\right)\left(\frac{1}{R_0^2} - B\right) + \left(\frac{1}{R_0}\tan^{-1}\frac{\pi B_p}{R_0}\right)\left(\frac{1}{R_0^2} + B\right)\right]$$

This result may be used to evaluate the entire integral in Eq. B-1 yielding

(3-47)

$$\int_0^{B_p/2} |H(j\omega)|^2 \, df =$$

$$\frac{1}{4\pi C}\left\{\left[\left(\frac{\pi B_p}{\pi^2 B_p^2 + R_0^2}\right)\left(\frac{1}{R_0^2} - B\right) + \left(\frac{1}{R_0} \tan^{-1}\frac{\pi B_p}{R_0}\right)\left(\frac{1}{R_0^2} + B\right)\right]\right.$$

$$-\frac{A}{C}\left[\left(\frac{\pi B_p}{\pi^2 B_p^2 + R_0^2}\right)\left(\frac{1}{R_0^2} - D\right) + \left(\frac{1}{R_0} \tan^{-1}\frac{\pi B_p}{R_0}\right)\left(\frac{1}{R_0^2} + D\right)\right]$$

$$\left. + 2\pi A B_p\right\}$$

Next, the evaluation of $\overline{\phi_{es}^2(t)}$ in closed form for Case IV is considered. Starting with Eq. B-24, the first term on the right side can be evaluated immediately, using Eq. B-49 with B=0 and a change in limits on the integral. This yields

(B-50)

$$\frac{A'}{C}\int_{\omega_a}^{\omega_b} \frac{1}{(\omega^2 + R_o^2)^2}\, d\omega =$$

$$\frac{A'}{2R_o^2C}\left[\frac{\omega_b}{\omega_b^2 + R_o^2} - \frac{\omega_a}{\omega_a^2 + R_o^2}\right.$$

$$\left.\frac{1}{R_o}\left(\tan^{-1}\frac{\omega_b}{R_o} - \tan^{-1}\frac{\omega_a}{R_o}\right)\right]$$

The second term on the right side of Eq. B-24 may be expressed as

(B-51)

$$\frac{B'}{X^2\,(CX^4 + DX^2 + 1)} = \frac{B'}{C}\left[\frac{1}{X^2\,(X^2 + R_o^2)^2}\right]$$

This term may be integrated directly using standard integration tables yielding the following

(B-52)

$$\frac{B'}{C}\int_{\omega_a}^{\omega_b} \frac{1}{\omega^2(\omega^2+R_0^2)^2}\, d\omega =$$

$$-\frac{B'}{R_0^4 C}\left[\frac{1}{\omega} + \frac{3}{2}\left(\frac{1}{R_0}\tan^{-1}\frac{\omega}{R_0}\right) + \frac{\omega}{2(\omega^2+R_0^2)}\right]\Bigg|_{\omega_a}^{\omega_b}$$

$$-\frac{B'}{R_0^4 C}\left[\frac{\omega_b}{2(\omega_b^2+R_0^2)} - \frac{\omega_a}{2(\omega_a^2+R_0^2)}\right.$$

$$\left. + \frac{3}{2R_0}\left(\tan^{-1}\frac{\omega_b}{R_0} - \tan^{-1}\frac{\omega_a}{R_0}\right) + \frac{1}{\omega_b} - \frac{1}{\omega_a}\right]$$

Combining Eqs. B-51 and B-52 along with Eq. B-23, yields the desired expression

(3-48)

$$\overline{\phi_{es}^2(t)} = \frac{\omega_a \omega_b (\Delta\omega_{rms})^2}{\omega_b - \omega_a} \cdot$$

$$\left\{ \frac{A'}{2R_o^2 C} \left[\frac{\omega_b}{\omega_b^2 + R_o^2} - \frac{\omega_a}{\omega_a^2 + R_o^2} + \frac{1}{R_o} \left(\tan^{-1} \frac{\omega_b}{R_o} - \tan^{-1} \frac{\omega_a}{R_o} \right) \right] \right.$$

$$- \frac{B'}{2R_o^4 C} \left[\frac{\omega_b}{\omega_b^2 + R_o^2} - \frac{\omega_a}{\omega_a^2 + R_o^2} + \frac{3}{R_o} \left(\tan^{-1} \frac{\omega_b}{R_o} - \tan^{-1} \frac{\omega_a}{R_o} \right) \right]$$

$$\left. + \frac{B'}{R_o^4 C} \left(\frac{1}{\omega_a} - \frac{1}{\omega_b} \right) \right\}$$

APPENDIX C

COMPUTATION OF (CNRIF)TH FOR VOICE MODULATION CASE USING NUMERICAL INTEGRATION TECHNIQUES

In this Appendix, a computer program is presented which was used to evaluate (CNRIF)TH using the trapezoidal method for numerical integration. This was done for a set of parameters for each of the cases defined by Eqs. 3-28, 3-29, 3-37, and 3-46. The purpose of this procedure was to check the closed-form solutions previously derived. The sets of parameters used are given as follows

CASE I:

$$\left.\begin{aligned} \beta &= 8.836\times10^{8} \quad (\text{rad/sec})^2 \\ \gamma &= 2.767\times10^{4} \quad \text{rad/sec} \\ b &= 1.88\times10^{3} \quad \text{rad/sec} \\ K &= 4.7\times10^{5} \quad \text{sec}^{-1} \end{aligned}\right\} \qquad \text{(C-1)}$$

CASE II:

$$\left.\begin{aligned} \beta &= 8.836\times10^{8} \\ \gamma &= 1.5\times10^{4} \\ b &= 1.88\times10^{3} \\ K &= 4.7\times10^{5} \end{aligned}\right\} \qquad \text{(C-2)}$$

CASE III:

$$\left.\begin{aligned} \beta &= 8.836\times10^{8} \\ \gamma &= 1.0\times10^{4} \\ b &= 1.88\times10^{3} \\ K &= 4.7\times10^{5} \end{aligned}\right\} \qquad \text{(C-3)}$$

CASE IV:

$$\left.\begin{aligned} \beta &= 6.776\times10^{8} \\ \gamma &= 1.0\times10^{4} \\ b &= 1.88\times10^{3} \\ K &= 4.7\times10^{5} \end{aligned}\right\} \qquad \text{(C-4)}$$

The computer program used in this analysis is given by

```
 1 C COMPUTATION OF (CNRIF)TH FOR VOICE MODULATION CASE
 2 C
 3 C FIRST CALCULATE AREA UNDER CURVE OF CLOSED-LOOP TRANSFER
 4 C FUNCTION SQUARED VS FREQUENCY
 5 C
 6 C INSERT LOOP PARAMETERS
 7             BETA=8.836E8
 8             GAMMA=1.5E4
 9             B=1.88E3
10             XK=4.7E5
11 C COMBINE LOOP PARAMETERS INTO NEW CONSTANTS
12             XNEWA=1.0/(BETA**2)
13             XNEWB=1.0/(GAMMA**2)-2.0/BETA
14             XNEWC=(1.0/XK*B)+1.0/BETA)**2
15             XNEWD=1.0/XK+1.0/GAMMA)**2-2.0*(1.0/(XK*B)*1.0/BETA)
16 C EMPLOY TRAPEZOIDAL RULE FOR NUMERICAL INTEGRATION
17             SUM1=0.0
18             DO 200 I=1, 17501
19             J=I-1
20             FREQ1=J
21             RFRQ1=(2.0*3.1415927)*FREQ1
22 C EVALUATE FACTORS IN NUMERATOR AND DENOMINATOR OF MAGNITUDE
23 C OF CLOSED-LOOP TRANSFER FUNCTION SQUARED
24             XNEW1=XNEWA*RFRQ1**4+XNEWB*RFRQ1**2+1.0
25             XNEW2=XNEWC*RFRQ1**4+XNEWD*RFRQ1**2+1.0
26             TRSQ1=XNEW1/XNEW2
27             IF(I.EQ.1) GO TO 100
28             IF(I.EQ.17501) GO TO 100
29             GO TO 150
30             TRSQ1=TRSQ1/2.0
31  150        CONTINUE
32  200 SUM1=SUM1+TRSQ1
33             AREA1=SUM1
34             WRITE(6,300) AREA1
35  300 FORMAT(1P1E16.6)
36 C NEXT EVALUATE MEAN-SQUARE PHASE ERROR SIGNAL COMPONENT
37 C
38 C EVALUATE VOICE PSD MODULATION CONSTANT
39             FA=300.0
40             FB=3300.0
41             DELSQ=(2.0*3.1415927)**2*1.0E7
42             ETA=((2.0*3.145927)**2*FA*FB*DELSQ)/(FB-FA)
43 C COMBINE ADDITIONAL LOOP PARAMETERS INTO NEW CONSTANTS
44             XNEWE=1.0/(XK*B)**2
45             XNEWF=1.0/XK**2
```

```
C EMPLOY TRAPEZOIDAL RULE FOR NUMERICAL INTEGRATION
      SUM2=0.0
      DO 700 I=300,3300
      FREQ2=I
      RFRQ2=(2.0*3.1415927)*FREQ2
C EVALUATE FACTORS WITHIN INTEGRAND
      XNEW3=XNEWE*RFRQ2**4+XNEWF*RFRQ2**2
      XNEW4=XNEWC*RFRQ2**4+XNEWD*RFRQ2**2+1.0
      TRSQ2=(1.0/RFRQ2**4)*(XNEW3/XNEW4)*ETA
      IF(I.EQ.300) GO TO 500
      IF(I.EQ.3300) GO TO 500
      GO TO 600
 500  TRSQ2=TRSQ2/2.0
 600  CONTINUE
 700  SUM2=SUM2+TRSQ2
      AREA2=SUM2
      WRITE(6,800)AREA2
 800  FORMAT(1P1E16.6)
C INSERT REMAINING PARAMETERS TO DETERMINE CNR
      XNU=0.25
      BP=3.5E4
C DETERMINE CNR
      CNRTH=AREA1/(BP*XNU-AREA2))
       C CONVERT TO DB
      CNRTH=10.0*ALOG10(CNRTH)
      WRITE(6,900) CNRTH,CNRTHD
 900  FORMAT(1P2E16.6)
      STOP
      END
```

The results of the computer runs as shown in Table C-1 show the validity of the closed-form solutions. The small differences between the numerical integration results and that of the closed-form solutions are explained by the size of the integration intervals used in the former technique. Finer integration intervals will bring the two results into even closer agreement.

Table C-1. Comparison of $(CNR_{IF})_{TH}$ obtained by numerical integration methods and the closed-form solution.

Case	(CNRIF)TH in dB Numerical Integration Method	(CNRIF)TH in dB Closed-form Solution
I	5.614×10^{-1}	5.730×10^{-1}
II	8.612×10^{-1}	8.730×10^{-1}
III	1.314	1.324
IV	1.292	1.302

APPENDIX D

DETAILED MATHEMATICS FOR CLOSED FORM SOLUTION OF (CNRIF)TH FOR FDM-FM CASE

In this Appendix, a detailed derivation of (CNRIF)TH in closed form for the FDM-FM case is presented. Beginning with Eq.. 3-52, it is noted that the integral in the numerator has already been evaluated in closed form in Appendix B for all four cases. Next, consider the determination of $\overline{\phi_{es}^2(t)}$ in closed form. Cases I and II, defined by Eqs. 3-28 and 3-29, can, again, be combined for the basic derivation. Putting Eq. 3-53 into more convenient form yields

(D-1)

$$\overline{\phi_{es}^2(t)} = \frac{(\Delta\omega_{rms})^2}{\omega_b - \omega_a} \cdot \frac{B'}{C} \int_{\omega_a}^{\omega_b} \frac{\left(\frac{A'}{B'}\right)\omega^2 + 1}{\omega^4 + \frac{D}{C}\omega^2 + \frac{1}{C}} \, d\omega$$

But, the integral in Eq. D-1 is of the same form as that in Eq. B-20, permitting the following solution

(D-2)

$$\overline{\phi_{es}^2(t)} = \frac{(\Delta\omega_{rms})^2}{\omega_b - \omega_a} \cdot \left(\frac{B'}{C}\right) Re\left[\frac{1 - \left(\frac{A'}{B'}\right)G}{J(G^* - G)} ln\left(\frac{\omega - J}{\omega + J}\right)\right] \Bigg|_{\omega_a}^{\omega_b}$$

$$= \frac{(\Delta\omega_{rms})^2}{\omega_b - \omega_a} \cdot \frac{1}{C} \Bigg\{ Re\left[\frac{B' - A'G}{J(G^* - G)} ln\left(\frac{\omega_b - J}{\omega_b + J}\right)\right]$$

$$- Re\left[\frac{B' - A'G}{J(G^* - G)} ln\left(\frac{\omega_a - J}{\omega_a + J}\right)\right]\Bigg\}$$

Eq. D-2 simplifies directly to

(3-54)

$$\overline{\phi_{es}^2(t)} =$$

$$\frac{(\Delta\omega_{rms})^2}{\omega_b - \omega_a} \cdot \frac{1}{C} \mathcal{R}e \left[\frac{B' - A'G}{J(G^* - G)} \ln\left(\frac{\omega_b - J}{\omega_b + J} \cdot \frac{\omega_a + J}{\omega_a - J} \right) \right]$$

where G and J for Cases I and II are given by Eq. 3-32 through Eq. 3-36.

Next, consider Case III, defined by Eq. 3-37. For this case, Eq. D-1 reduces to

(D-3)

$$\overline{\phi_{es}^2(t)} =$$

$$\frac{(\Delta\omega_{rms})^2}{\omega_b - \omega_a} \cdot \left(\frac{B'}{C}\right) \int_{\omega_a}^{\omega_b} \frac{\left(\frac{A'}{B'}\right)\omega^2 + 1}{(\omega^2 + R_1^2)(\omega^2 + R_2^2)} \, d\omega$$

Using the results of Eq. B-39, this integral can be directly evaluated yielding the result

(D-4)

$$\overline{\phi_{es}^2(t)} = \frac{(\Delta\omega_{rms})^2}{\omega_b - \omega_a}\left(\frac{B'}{C}\right) \cdot$$

$$\left\{ \frac{1 - \left(\frac{A'}{B'}\right) R_1^2}{R_2^2 - R_1^2}\left(\frac{1}{R_1} \tan^{-1} \frac{\omega}{R_1}\right) + \frac{1 - \left(\frac{A'}{B'}\right) R_2^2}{R_1^2 - R_2^2}\left(\frac{1}{R_2} \tan^{-1} \frac{\omega}{R_2}\right) \right\} \Bigg|_{\omega_a}^{\omega_b}$$

Substitution of the limits in Eq. D-4 yields the desired result

(3-55)

$$\overline{\phi_{es}^2(t)} = \frac{(\Delta\omega_{rms})^2}{\omega_b - \omega_a} \cdot \frac{1}{C(R_1^2 - R_2^2)} \cdot$$

$$\left\{\left[\frac{B' - A'R_2^2}{R_2}\left(\tan^{-1}\frac{\omega_b}{R_2} - \tan^{-1}\frac{\omega_a}{R_2}\right)\right] + \left[\frac{B' - A'R_1^2}{R_1}\left(\tan^{-1}\frac{\omega_a}{R_1} - \tan^{-1}\frac{\omega_b}{R_1}\right)\right]\right\}$$

where R_1 and R_2 are defined by Eq. 3-43.

Finally, consider Case IV, defined by Eq. 3-46. For this case, Eq. D-1 reduces to

$$\overline{\phi_{es}^2(t)} = \frac{(\Delta\omega_{rms})^2}{\omega_b - \omega_a}\left(\frac{B'}{C}\right)\int_{\omega_a}^{\omega_b} \frac{\left(\frac{A'}{B'}\right)\omega^2 + 1}{(\omega^2 + R_o^2)^2}\, d\omega \tag{D-5}$$

Using the results of Eqs. B-48 and B-49, this integral may be evaluated as follows

$$\overline{\phi_{es}^2(t)} = \frac{(\Delta\omega_{rms})^2}{\omega_b - \omega_a}\left(\frac{B'}{2C}\right)\left[\frac{-\left(\frac{A'}{B'}\right)\omega}{\omega^2 + R_o^2} + \frac{\left(\frac{A'}{B'}\right)}{R_o}\tan^{-1}\frac{\omega}{R_o} + \frac{\omega}{R_o^2(\omega^2 + R_o^2)} + \frac{1}{R_o^3}\tan^{-1}\frac{\omega}{R_o}\right]\Bigg|_{\omega_a}^{\omega_b} \tag{D-6}$$

Substitution of the limits in Eq. D-6 yields

(D-7)

$$\overline{\phi_{es}^2(t)} = \frac{(\Delta\omega_{rms})^2}{\omega_b - \omega_a}\left(\frac{1}{2C}\right)\left[\frac{-A'\omega_b}{\omega_b^2 + R_o^2} + \frac{A'\omega_a}{\omega_a^2 + R_o^2}\right.$$

$$+ \frac{A'}{R_o}\tan^{-1}\frac{\omega_b}{R_o} - \frac{A'}{R_o}\tan^{-1}\frac{\omega_a}{R_o}$$

$$+ \frac{B'\omega_b}{R_o^2(\omega_b^2 + R_o^2)} - \frac{B'\omega_a}{R_o^2(\omega_a^2 + R_o^2)}$$

$$\left. + \frac{B'}{R_o^3}\tan^{-1}\frac{\omega_b}{R_o} - \frac{B'}{R_o^3}\tan^{-1}\frac{\omega_a}{R_o}\right]$$

Simplification of Eq. D-7 gives

(3-56)

$$\overline{\phi_{es}^2(t)} = \frac{(\Delta\omega_{rms})^2}{\omega_b - \omega_a}\left(\frac{1}{2C}\right)\cdot$$

$$\left[\left(\frac{B'}{R_o^2} - A'\right)\left(\frac{\omega_b}{\omega_b^2 + R_o^2} - \frac{\omega_a}{\omega_a^2 + R_o^2}\right)\right.$$

$$\left. + \left(\frac{B'}{R_o^2} + A'\right) \cdot \frac{1}{R_o}\left(\tan^{-1}\frac{\omega_b}{R_o} - \tan^{-1}\frac{\omega_a}{R_o}\right)\right]$$

APPENDIX E

DETAILED MATHEMATICS FOR CLOSED FORM SOLUTION OF (CNRIF)TH FOR FDM-PM CASE

In this Appendix, a detailed derivation of (CNRIF)TH in closed form for the FDM-PM case is presented. Beginning with Eq. 3-59, it is noted that the integral in the numerator has already been evaluated in closed form in Appendix B for all four cases. Next, consider the determination of $\overline{\phi_{es}^2(t)}$ in closed form. Cases I and II, defined by Eqs. 3-28 and 3-29, can again be combined for the basic derivation. Starting with the integrand in Eq. 3-60

(E-1)

$$\frac{A'\omega^4 + B'\omega^2}{C\omega^4 + D\omega^2 + 1} =$$

$$\frac{A'}{C} - \frac{A'}{C^2}\left[\frac{(D - B'C/A')\omega^2 + 1}{\omega^4 + \frac{D}{C}\omega^2 + \frac{1}{C}}\right]$$

The signal-induced mean-square phase error may then be expressed as

$$\overline{\phi_{es}^2(t)} = \frac{3(\Delta\omega_{rms})^2}{\omega_b^3 - \omega_a^3} \int_{\omega_a}^{\omega_b} \left\{ \frac{A'}{C} - \frac{A'}{C^2} \left[\frac{(D - B'C/A')\omega^2 + 1}{\omega^4 + \frac{D}{C}\omega^2 + \frac{1}{C}} \right] \right\} d\omega \qquad \text{(E-2)}$$

The first term within the integrand of Eq. E-2 can be integrated directly and the second term fits the form of Eq. B-20. Carrying through the integration then results in

(E-3)

$$\overline{\phi_{es}^2(t)} = \frac{3(\Delta\omega_{rms})^2}{\omega_b{}^3 - \omega_a{}^3}\left\{ \frac{A'}{C}(\omega_b - \omega_a) \right.$$

$$\left. - \frac{A'}{C^2}\,\mathrm{Re}\left[\frac{1-(D-B'C/A')G}{J(G^*-G)}\,\ln\left(\frac{\omega - J}{\omega + J}\right)\right]\Bigg|_{\omega_a}^{\omega_b} \right\} =$$

$$\frac{3(\Delta\omega_{rms})^2}{\omega_b{}^3 - \omega_a{}^3}\left\{ \frac{A'}{C}(\omega_b - \omega_a) - \frac{A'}{C^2}\,\mathrm{Re}\left[\frac{1-(D-B'C/A')G}{J(G^*-G)}\cdot \right.\right.$$

$$\left.\left. \ln\left(\frac{\omega_b - J}{\omega_b + J}\right)\right] + \frac{A'}{C^2}\,\mathrm{Re}\left[\frac{1-(D-B'C/A')}{J(G^*-G)}\,\ln\left(\frac{\omega_a - J}{\omega_a + J}\right)\right] \right\}$$

Eq. E-3 simplifies directly to

(3-61)

$$\overline{\phi_{es}^2(t)} =$$

$$\frac{3\,(\Delta\omega_{rms})^2}{\omega_b^3 - \omega_a^3}\left\{\frac{A'}{C}\,(\omega_b - \omega_a) - \frac{A'}{C^2}\,\mathrm{Re}\left[\frac{1 - (D - B'C/A')G}{J(G^* - G)}\,\ln\left(\frac{\omega_b - J}{\omega_b + J}\cdot\frac{\omega_a + J}{\omega_a - J}\right)\right]\right\}$$

where G and J for Cases I and II are given by Eqs. 3-32 through 3-36.

Next, consider Case III, defined by Eq. 3-37. For this case, Eq. E-21 reduces to

$$\overline{\phi_{es}^2(t)} = \frac{3\,(\Delta\omega_{rms})^2}{\omega_b^3 - \omega_a^3} \cdot \int_{\omega_a}^{\omega_b} \left\{ \frac{A'}{C} - \frac{A'}{C^2} \left[\frac{(D - B'C/A')\omega^2 + 1}{(\omega^2 + R_1^2)(\omega^2 + R_2^2)} \right] \right\} d\omega \tag{E-4}$$

The first term may be integrated directly. The second term may be integrated using the results of Eq. B-39. This procedure yields

(E-5)

$$\overline{\phi_{es}^2(t)} = \frac{3\,(\Delta\omega_{rms})^2}{\omega_b^3 - \omega_a^3} \left\{ \frac{A'}{C}\omega - \right.$$

$$\frac{A'}{C^2}\left[\frac{1 - (D - B'C/A')\,R_1^2}{R_2^2 - R_1^2} \left(\frac{1}{R_1} \tan^{-1} \frac{\omega}{R_1} \right) + \right.$$

$$\left. \left. \frac{1 - (D - B'C/A')\,R_2^2}{R_1^2 - R_2^2} \left(\frac{1}{R_2} \tan^{-1} \frac{\omega}{R_2} \right) \right] \right\} \Bigg|_{\omega_a}^{\omega_b}$$

Substitution of the limits into Eq. E-5 yields the desired result

(3-62)

$$\overline{\phi_{es}^2(t)} = \frac{3\,(\Delta\omega_{rms})^2}{\omega_b^3 - \omega_a^3}\left\{\frac{A'}{C}\,(\omega_b - \omega_a) - \right.$$

$$\frac{A'}{(R_1^2 - R_2^2)C^2}\left[\frac{1 - (D - B'C/A')\,R_2^2}{R_2}\left(\tan^{-1}\frac{\omega_b}{R_2} - \tan^{-1}\frac{\omega_a}{R_2}\right) + \right.$$

$$\left.\left.\frac{1 - (D - B'C/A')\,R_1^2}{R_1}\left(\tan^{-1}\frac{\omega_a}{R_1} - \tan^{-1}\frac{\omega_b}{R_1}\right)\right]\right\}$$

where R_1 and R_2 are defined by Eq. 3-43.

Finally, consider Case IV defined by Eq. 3-46. For this case, Eq. E-2 reduces to

$$\overline{\phi^2_{es}(t)} = \frac{3\,(\Delta\omega_{rms})^2}{\omega_b^3 - \omega_a^3} \cdot \tag{E-6}$$

$$\int_{\omega_a}^{\omega_b} \left\{ \frac{A'}{C} - \frac{A'}{C^2}\left[\frac{(D - B'C/A')\omega^2 + 1}{(\omega^2 + R_o^2)^2} \right] \right\} d\omega$$

Again, the first term within the integrand can be integrated directly and the second term may be integrated using the results of Eqs. B-48 and B-49, yielding

$$\overline{\phi^2_{es}(t)} = \frac{3\,(\Delta\omega_{rms})^2}{\omega_b^3 - \omega_a^3} \left\{ \frac{A'}{C}\omega - \right. \tag{E-7}$$

$$\frac{A'}{2C^2}\left[- \frac{(D - B'C/A')\omega}{\omega^2 + R_o^2} + \right.$$

$$\left. \left. \frac{(D - B'C/A')}{R_o} \tan^{-1}\frac{\omega}{R_o} + \frac{\omega}{R_o^2(\omega^2 + R_o^2)} + \frac{1}{R_o^3} \tan^{-1}\frac{\omega}{R_o} \right] \right\} \Bigg|_{\omega_a}^{\omega_b}$$

Substitution of the limits in Eq. E-7 results in

(E-8)

$$\overline{\phi_{es}^{2}(t)} = \frac{3(\Delta\omega_{rms})^2}{\omega_b^3 - \omega_a^3}\left\{\frac{A'}{C}(\omega_b - \omega_a) - \frac{A'}{2C^2}\left[-\frac{(D - B'C/A')\,\omega_b}{\omega_b^2 + R_0^2}\right.\right.$$

$$+\frac{(D - B'C/A')\,\omega_a}{\omega_a^2 + R_0^2} + \frac{(D - B'C/A')}{R_0}\left(\tan^{-1}\frac{\omega_b}{R_0} - \tan^{-1}\frac{\omega_a}{R_0}\right)$$

$$\left.\left.+\frac{\omega_b}{R_0^2(\omega_b^2 + R_0^2)} - \frac{\omega_a}{R_0^2(\omega_a^2 + R_0^2)} + \frac{1}{R_0^3}\left(\tan^{-1}\frac{\omega_b}{R_0} - \tan^{-1}\frac{\omega_a}{R_0}\right)\right]\right\}$$

Simplification of Eq. E-8 yields the desired result

(3-63)

$$\phi_{es}^2(t) = \frac{3(\Delta\omega rms)^2}{\omega_b^3 - \omega_a^3}\left\{\frac{A'}{C}(\omega_b - \omega_a)\right.$$

$$-\frac{A'}{2C^2}\left[\left(\frac{1}{R_o^2} - D + \frac{B'C}{A'}\right)\left(\frac{\omega_b}{\omega_b^2 + R_o^2} - \frac{\omega_a}{\omega_a^2 + R_o^2}\right)\right.$$

$$\left.\left.+\left(\tan^{-1}\frac{\omega_b}{R_o} - \tan^{-1}\frac{\omega_a}{R_o}\right)\left(\frac{1}{R_o^3} + \frac{D - B'C/A'}{R_o}\right)\right]\right\}$$

where R_o is defined by Eq. 3-49.

APPENDIX F

COMPUTER PROGRAM FOR EVALUATION OF (CNRIF)TH FOR THE TEST-TONE CASE

```
      COMPLEX G,J,CPXL1,CPLX2,CPLX3,CPLX4,CPLX5,CPLX6
      REAL K,MAGNT,INTVL,NU
      ALPHA=1.0
      K=4.7E5
      A=2.94E4
      B=1.88E3
      BPPRM=2.2E5
      BP=3.5E4
      NU=0.25
      DELOMG=2.0*3.1415927*1.0E4
      OMGTT=2.0*3.1415927*1.0E3
50    XNEWA=(ALPHA/(K*B))**2
      XNEWB=(1.0/A+ALPHA/K)**2-2.0*(ALPHA/(K*B))
      XNEWC=((1.0+ALPHA /(K*B))**2
      XNEWD=((1.0+ALPHA)/K+1.0/A)**2-2.0*((1.0+ALPHA)/K*B))
      XNEW1=XNEWD/(2.0*XNEWC)
      XNEW2=(-1.0)*SQRT(1.0/XNEWC-(XNEWD/(2.0*XNEWC))**2)
      G=CMPXL(XNEW1,XNEW2)
      IF(XNEWD.GE.0.0,GO TO 75
      XNEW3=ATAN(XNEW2/XNEW1)
      GO TO 80
      XNEW3=ATAN(XNEW2/XNEW1)+3.1415927
80    XNEW4=XNEW3/2.0
      THETA=XNEW4+3.1415927
      MAGNT=SQRT(SQRT(1.0/XNEWC))
      XNEW5=MAGNT*COS(THETA)
      XNEW6=MAGNT*SIN(THETA)
      J=CMPXL(XNEW5,XNEW6)
      CPLX1=1.0-XNEWB*G-(1.0-XNEWD*G)*(XNEWA/XNEWC)
      CPLX2=J*(CONJG(G)-G)
      CPLX3=CPLX1/CPLX2
      CPLX4=(J-BPPRM/2.0)/(J+BPPRM/2.0)
      CPLX5=CLOG(CPLX4)
      CPLX6=CPLX3*CPLX5
      XNEW7=REAL(CPLX6)
      XNEW8=XNEWA*(BPPRM/2.0)+XNEW7
      XNEW9=1.0/(2.0*3.1415927*XNEWC)
      INTVL=XNEW8*XNEW9
C EVALUATE MEAN SQUARE SIGNAL PHASE ERROR
      XNEW10=(OMGTT**4)/((K*B)**2)
      XNEW11=(OMGTT**2)/(K**2)
      XNEW12=XNEW10+XNEW11
      XNEW13=(1.0-(OMGTT**2)*((1.0+ALPHA)/(K*B)))**2
```

```
      XNEW14=(OMGTT*((1.0/A)+(1.0+ALPHA)/K))**2
      XNEW15=XNEW13+XNEW14
      XNEW16=XNEW12/XNEW15
      XNEW17=(DELOMG/OMGTT)**2
      XNEW18=XNEW17/2.0
      PHISQ=XNEW18*XNEW16
      CNRTH1=INTVL/(BP*(NU-PHISQ))
      CNRTH2=10.0*ALOG10(CNRTH1)
      WRITE(6,300)CNRTH1,CNRTH2
300   FORMAT(1P2E16.6)
      STOP
      END
```

APPENDIX G

COMPUTER PROGRAM USED TO IMPLEMENT POWELL'S METHOD AND RELATED SUBPROGRAMS

Basic Optimization Program

```
1       PROGRAM POWELL
2 C THIS ALGORITHM USES THE POWELL SEARCH TECHNIQUE IN CONJUGATE DIRECTIONS.
3       DIMENSION X(50,4),ESV(4,4),Y(50),B(5),XO(4),X1(4),XC(4),DL(4),O(4)
4       DIMENSION X3(4)
5       READ 5,N,KMAX,C,STEP,TCLX,FLN
6     5 FORMAT (2I3,2F5,1,2F7,4)
7       READ 10, (X(1,J),J = 1,N)
8    10 FORMAT (F10.1)
9       DO 11 IK=1,N
10      DO 11 JK=1,N
11   11 ESV(JK,IK)=0.0
12      DO 15 IK=1,N
13   15 ESV(IK,IK)=1.0
14      I=1
15   20 DELTM=0.0
16      MTEST=0
17      J=1
18      DO 22 IK=1,N
19   22 X3(IK)=X(1,IK)
20      Y(I)=FIT(X3)
21      B(J)=Y(I)
22      BJT=B(J)
23   25 DO 30 JK=1,N
24   30 XO(JK)-X(I,JK)
25 C  THE UNRESTRICTED SEARCH BEGINS.
26 C  IN THE RARE CASE WHERE TWO SUCCESSIVE FUNCT ARE EXACTLY EQUAL
27 C  SEARCH IS STOPPED AND THE PROGRAM TERMINATED.
28      KR=1
29   35 DO 100 K=1,KMAX
30   40 S=2.0**(K-1)*STEP
31      DO 50 IK=1,N
32   50 XO(IK)=XO(IK)+S*ESV(IK,J)
33      YT=FIT(XO)
34      IF(C*YT-C*BJT) 60,350,100
35   60 IF(K-1) 70,90,70
36   70 IF(KR=1) 73,73,110
37   73 DO 80 IK=1,N
38      X1(IK)=XO(IK)
39   80XO(IK)=XO(IK)-(S+((2.0**(K-2))*STEP))*ESV(IK,J)
40      GO TO 110
```

```
41     90    DO 95 IK=1,N
42     95    X1(IK)=XO(IK)
43           STEP=-STEP
44           KR=KR+1
45     100   BJT=YT
46           GO TO 340
47     110   R=3.0*((2.0**(K-2))*ABS(STEP))
48           NM=1.0-4.75*ALOG10(FLN/R)
49           DO 120 IK=1,N
50           DL(IK)=0.618*(X1(IK)-XO(IK))
51           XO(IK)=X1(IK)-DL(IK)
52     120   X1(IK)=X1(IK-0.618*DL(IK)
53           W=FIT(XO)
54           V=FIT(X1)
55           DO 180 KNM=1,NM
56           DO 130 IK=1,N
57     130   DL(IK)=0.618*DL(IK)
58           IF(ABS(W-V)-0.01*TOLX) 185,135,135
59     135   IF(C*W-C*V) 160,350,140
60     140   DO 150 IK=1,N
61           XC(IK)=X1(IK)
62           X1(IK)=XO(IK)
63     150   XO(IK)=XC(IK)-DL(IK)
64           V=W
65           W=FIT(XO)
66           GO TO 180
67     160   DO 170 IK=1,N
68           XC(IK)=XO(IK)
69           XO(IK)=XL(IK)
70     170   X1(IK)=XC(IK)+DL(IK)
71           W=V
72           V=FIT(X1)
73     180   CONTINUE
74     185   J=J+1
75           DO 190 IK=1,N
76     190   XO(IK)=0.5*(XO(IK)+X1(IK))
77 C     THE FOLLOWING STATEMENTS TO 280 DETERM THE NEW SEARCH DIRECT
78           B(J)=FIT(XO)
79           BJT=B(J)
80           DELT=ABS(B(J)-B(J-1))
81           IF(DELTM-DELT) 200,210,210
82     200   DELTM=DELT
83           MAX=J-1
84     210   KR=1
85           IF(J-N) 35,35,220
86     220   AMPU=0.000001
87           DO 230 IK=1,N
88           U(IK)=XO(IK)-X(I,IK)
89           AMPU=AMPU+U(IK)**2
90     230   X1(IK)=2.0*XO(IK)-X(I,IK)
```

```
91          DO 232 IK=1,N
92    232   U(IK)=U(IK)/SQRT(AMPU)
93          YT=FIT(X1)
94          IF(C*YT-C*B(1)) 290,290,240
95    240   A=(B(1)-2.0*B(N+1)+YT)*(B(1)-B(N+1)-DELTM)**2
96          BT=0.5*DELTM*(B(1)-YT)**2
97          IF(C*A-C*BT) 290,290,250
98    250   IF(MTEST-1) 260,20,20
99    260   N1=N-1
100         IF(MAX-N1) 265,265,275
101   265   DO 270 JK=MAX,N1
102         DO 270 IK=1,N
103   270   ESV(IK,JK)=ESV(IK,JK+1)
104   275   DO 280 IK=1,N
105   280   ESV(IK,N)=U(IK)
106         DELTM=0.0
107         J=N
108         MTEST=1
109         GO TO 35
110   290   DO 300 IK=1,N
111         IF(ABS(XO(IK)-X(I,IK))-TOLX) 300,310,310
112   300   CONTINUE
113         GO TO 330
114   310   I=I+1
115         DO 320 IK=1,N
116   320   X(I,IK)=XO(IK)
117         IF(I-40) 20,20,500
118   330   YOPT=FIT(XO)
119         PRINT 331
120   331   FORMAT ('OTHIS IS THE VALUE OF YOPT')
121         PRINT 332,YOPT
122   332   FORMAT (F22.6)
123         PRINT 333
124   333   FORMAT ('OTHESE ARE THE VALUES OF X(1),X(2)')
125         PRINT 334,(XO(IK),IK=1,N)
126   334   FORMAT (2F22.6)
127   500   PRINT 335
128   335   FORMAT ('OTHESE ARE THE BASE POINTS')
129         PRINT 336,((X(IJ,IK),IK=1,N),IK=1,I)
130   336   FORMAT (2F22.6)
131         PRINT 337
132   337   FORMAT ('OTHESE ARE THE FUNCTION VALUES AT THE BASE POINTS')
133         PRINT 338,(Y(IK),IK=1,I)
134   338   FORMAT (F22.6)
135         IF(I-40) 400,400,390
136   390   PRINT 395
137   395   FORMAT ('OTHE SOLUTION DID NOT CONVERGE')
138         GO TO 400
139   340   PRINT 345
140   345   FORMAT ('OTHERE IS NO MAX,MIN')
```

```
141          GO TO 400
142    350   PRINT 360
143    360   FORMAT ('OTWO FUNCTION VALUES ARE EQUAL')
144    400   CONTINUE
145          STOP
146          END
```

Subprogram for Generalized Second-Order PLL-Voice Modulation Case

```
 1          FUNCTION FIT(X3)
 2          DIMENSION X3(4)
 3          REAL K,MAGNT,INTVL,NU
 4          COMPLEX G,J,CPLX1,CPLX2,CPLX3,CPLX4,CPLX5,CPLX6,CPLX7,CPLX8
 5          COMPLEX CPLX9,CPLX10,CPLX11,CPLX12
 6          SBETA=X3(1)
 7          SGAMMA=X3(2)
 8          SB=X3(3)
 9          SK=X3(4)
10          BETA=SBETA*1.0E8
11          GAMMA=SGAMMA*1.0
12          B=SB*1.0E3
13          K=SK*1.0E5
14          BPPRM=2.2E5
15          BP=3.5E4
16          NU=0.25
17          OMEGA=1.88E3
18          OMEGB=2.07E4
19          DELSQ=4.0*(3.1415927**2)*1.0E7
20          APRIM=1.0/(K*B)**2
21          BPRIM=1.0/K**2
22          XNEWA=1.0/(BETA**2)
23          XNEWB=1.0/(GAMMA**2)-2.0/BETA
24          XNEWC=(1.0/(K*B)*1.0/BETA)**2
25          XNEWD=(1.0/K+1.0/GAMMA)**2-2.0*(1.0/(K*B)+1.0/BETA)
26          XNEW1=XNEWD/(2.0*XNEWC)
27          XNEWM=XNEW1**2
28          XNEWN=1.0/XNEWC
29          IF(XNEWM.GT.XNEWN.AND.XNEWD.GT.0.0) GO TO 150
31          XNEW2=(-1.0)*SQRT(1.0/XNEWC-(XNEWD/(2.0*XNEWC))**2)
32          G=CMPLX(XNEW1,XNEW2)
33          IF(XNEWD.GE.0,0)GO TO 75
34          XNEW3=ATAN(XNEW2/XNEW1)
35          WRITE(6,50)
36    50    FORMAT (1H  ,  13HCASE 1 REGION)
37          GO TO 80
38    75    XNEW3=ATAN(XNEW2/XNEW21)+3.14145927
39          WRITE(6,60)
40    60    FORMAT(1H  ,  13HCASE 2 REGION)
41    80    XNEW4=XNEW3/2.0
42          THETA=XNEW4+3.1415927
43          MAGNT=SQRT(SQRT(1.0/XNEWC))
44          XNEW5=MAGNT*COS(THETA)
45          XNEW6=MAGNT*SIN(THETA)
46          J=CMPLX(XNEW5,XNEW6)
47          CPLX1=1.0-XNEWB*G-(1.0-XNEWD*G)*(XNEWA/XNEWC)
48          CPLX2=J*(CONJG(G)-G)
49          CPLX3=CPLX1/CPLX2
50          CPLX4=(J-BPPRM/2.0)/(J*BPPRM/2.0)
```

```
      CPLX5=CLOG(CPLX4)
      CPLX6=CPLX3*CPLX5
      XNEW7=REAL(CPLX6)
      XNEW8=XNEWA*(BPPRM/2,0)+XNEW7
      XNEW9=1.0/(2.0*3.1415927*XNEWC)
      INTVL=XNEW8*XNEW9
      CPLX7=((OMEGB-J)/(OMEGB+J))*((OMEGA+J)/(OMEGA-J))
      CPLX8=CLOG(CPLX7)
      CPLX9=(BPRIM-APRIM*G)/(G*J*(G-CONJG(G)))
      CPLX10=CPLX8*CPLX9
      XNEW10=REAL(CPLX10)
      CPLX11=BPRIM/(XNEWC*G*CONJG(C))
      XNEW11=1.0/OMEGA-1.0/OMEGB
      CPLX12=XNEW11*CPLX11
      XNEW12=REAL(CPLX12)
      XNEW13=(1,0/XNEWC)*XNEW10+XNEW12
      XNEW14=(OMEGA*OMEGB*DELSQ)/(OMEGB-OMEGA)
      PHISQ=XNEW13*XNEW14
      GO TO 90
  150  CONTINUE
      WRITE(6,160)
  160  FORMAT(1H , 13HCASE 3 REGION)
      YNEW1=SQRT(XNEWM-XNEWN)
      RS1=XNEW1+YNEW1
      RS2=XNEW1-YNEW1
      R1=SQRT(RS1)
      R2=SQRT(RS2)
      YNEW2=(1.0/R1)*ATAN(3.1415927*BP/R1)
      YNEW3=(1.0/R2)*ATAN(3.1415927*BP/R2)
      YNEW4=(1.0-XNEWB*RS1)/(RS2-RS1)
      YNEW5=(1.0-XNEWB*RS2)/(RS1-RS2)
      SUBT1=YNEW4*YNEW2+YNEW5*YNEW3
      YNEW6=(1.0-XNEWD*RS1)/(RS2-RS1)
      YNEW7=(1.0-XNEWD*RS2)/(RS1-RS2)
      SUBT2=YNEW6*YNEW2+YNEW7*YNEW3
      SUBT3=XNEWA*3.1415927*BP
      SUBT4=SUBT1-(XNEWA/XNEWC)*SUBT2+SUBT3
      INTVL=SUBT4/(2.0*3.1415927*XNEWC)
      YNEW8=ATAN(OMEGA/R1)
      YNEW9=ATAN(OMEGA/R2)
      YNEW10=ATAN(OMEGB/R1)
      YNEW11=ATAN(OMEGB/R2)
      YNEW12=YNEW11-YNEW9
      YNEW13=YNEW8-YNEW10
      SUBT5=(1.0/R2)*YNEW12+(1.0/R1)*YNEW13
      YNEW14=-YNEW13
      YNEW15=-YNEW12
      SUBT6=(1.0/R1**3)*YNEW14+(1.0/R2**3)*YNEW15
      SUBT7=1.0/OMEGA-1.0/OMEGB
      YNEW16=APRIM/((XNEWC)*(RS1-RS2))
```

```
101         YNEW17=BPRIM/((XNEWC)*(RS1-RS2))
102         YNEW18=BPRIM/(XNEWC*RS1*RS2)
103         SUBT8=YNEW16*SUBT5+YNEW17*SUBT6+YNEW18*SUBT7
104         YNEW19=(OMEGA*OMEGB*DELSQ)/(OMEGB-OMEGA)
105         PHISQ=YNEW19*SUBT8
106      90 CNRTH-INTVL/(BP*(NU-PHISQ))
107         WRITE(6,100)CNRTH,BETA,GAMMA,B,K
108     100 FORMAT(1P5E16.6)
109         FIT=CNRTH
110         RETURN
111         END
```

Subprogram for Generalized Second-Order PLL - FDM-FM Case

```
      FUNCTION FIT(X3)
      DIMENSION X3(4)
      REAL K,MAGNT,INTVL,NU
      COMPLEX G,J,CPLX1,CPLX2,CPLX3,CPLX4,CPLX5,CPLX6,CPLX7,CPLX8
      COMPLEX CPLX9,CPLX10,CPLX11,CPLX12
       SBETA=X3(1)
      SGAMMA=X3(2)
      SB=X3(3)
      SK=X3(4)
      BETA=SBETA*1.0E15
      GAMMA=SGAMMA*1.0E7
      B=SB*1.0E5
      K=SK*1.0E9
      BPPRM=3.142E8
      BP=5.0E7
      NU=0.25
      OMEGA=3.770E5
      OMEGB=1.596E7
      DELSQ=1.990E15
      APRIM=1.0/(K*8)**2
      BPRIM=1.0/K**2
      XNEWA=1.0/(BETA**2)
      XNEWB=1.0/(GAMMA**2)-2.0/BETA
      XNEWC=(1.0/(K*B)=1.0/BETA)**2
      XNEWD=(1.0/K+1.0/GAMMA)**2-2.0*(1.0/(K*B)+1.0/BETA)
      XNEW1=XNEWD/(2.0*XNEWC)
      XNEWM=XNEW1**2
      XNEWN=1.0/XNEWC
      IF(XNEWM.GT.XNEWN.AND.XNEWD.GT.0.0) GO TO 150
      XNEW2=(-1.0)*SQRT(1.0/XNEWC-(XNEWD/(2.0*XNEWC))**2)
      G=CMPLX(XNEW1,XNEW2)
      IF(XNEWD.GE.0.0)GO TO 75
      XNEW3=ATAN(XNEW2/XNEW1)
      WRITE(6,50)
50    FORMAT(1H , 13HCASE 1 REGION)
      GO TO 80
75    XNEW3=ATAN(XNEW2/XNEW1)+3.1415927
      WRITE(6,60)
60    FORMAT(1H , 13HCASE 2 REGION)
80    XNEW4=XNEW3/2.0
      THETA=XNEW4+3.1415927
      MAGNT=SQRT(SQRT(1.0/XNEWC))
      XNEW5=MAGNT*COS(THETA)
       XNEW6=MAGNT*SIN(THETA)
      J=CMPLX(XNEW5,XNEW6)
      CPLX1=1.0-XNEWB*G-(1.0-XNEWD*G)*(XNEWA/XNEWC)
      CPLX2=J*(CONJG(G)-G)
```

```
48          CPLX3=CPLX1/CPLX2
49          CPLX4=(J-BPPRM/2.0)/(J+BPPRM/2.0)
50          CPLX5-CLOG(CPLX4)
51          CPLX6=CPLX3*CPLX5
52          XNEW7=REAL(CPLX6)
53          XNEW8=XNEWA*(BPPRM/2.0)+XNEW7
54          XNEW9=1.0/(2.0*3.1415927*XNEWC)
55          INTVL=XNEW8*XNEW9
56          CPLX7=((OMEGB-J)/(OMEGB+J))*((OMEGA+J)/(OMEGA-J))
57          CPLX8=CLOG(CPLX7)
58          CPLX9=(BPRIM-APRIM*G)/(J*(CONJG(G)-G))
59          CPLX10=CPLX8*CPLX9
60          XNEW10=REAL(CPLX10)
61          XNEW11=DELSQ/(OMEGB-OMEGA)
62          XNEW12=XNEW11/XNEWC
63          PHISQ=XNEW10*XNEW12
64          GO TO 90
65    150   CONTINUE
66          WRITE(6,160)
67    160   FORMAT(1H , 13HCASE 3 REGION)
68          YNEW1=SQRT(XNEWM-XNEWN)
69          RS1=XNEW1+YNEW1
70          RS2=XNEW1-YNEW1
71          R1=SQRT(RS1)
72          R2=SQRT(RS2)
73          YNEW2=(1.0/R1)*ATAN(3.1415927*BP/R1)
74          YNEW3=(1.0/R2)*ATAN(3.1415927*BP/R2)
75          YNEW4=(1.0-XNEWB*RS1)/(RS2-RS1)
76          YNEW5=(1.0-XNEWB*RS2)/(RS1-RS2)
77          SUBT1=YNEW4*YNEW2+YNEW5*YNEW3
78          YNEW6=(1.0-XNEWD*RS1)/(RS2-RS1)
79          YNEW7=(1.0-XNEWD*RS2)/(RS1-RS2)
80          SUBT2=YNEW6*YNEW2+YNEW7*YNEW3
81          SUBT3=XNEWA*3.1415927*BP
82          SUBT4=SUBT1-(XNEWA/XNEWC)*SUBT2+SUBT3
83          INTVL=SUBT4/(2.0*3.1415927*XNEWC)
84          YNEW8=ATAN(OMEGA/R1)
85          YNEW9=ATAN(OMEGA/R2)
86          YNEW10=ATAN(OMEGB/R1)
87          YNEW11=ATAN(OMEGB/R2)
88          YNEW12=YNEW11-YNEW9
89          YNEW13=YNEW8-YNEW10
90          YNEW14=(BPRIM-APRIM*RS2)/R2
91          YNEW15=(BPRIM-APRIM*RS1)/R1
92          SUBT5=YNEW14*YNEW12+YNEW15*YNEW13
93          YNEW16=1.0/(XNEWC*(RS1-RS2))
94          YNEW17=DELSQ/(OMEGB-OMEGA)
95          YNEW18=YNEW16*YNEW17
96          PHISQ=YNEW18*SUBT5
97    90    CNRTH=INTVL/(BP*(NU-PHISQ))
```

```
98          WRITE(6,100)CNRTH,BETA,GAMMA,B,K
99   100    FORMAT(1P5E16.6)
100         FIT=CNRTH
101         RETURN
102         END
```

APPENDIX H

SPECTRAL ANALYSIS OF A SAMPLED SINUSOIDAL WAVEFORM

In Section 4.2.3 of Chapter 4, it was indicated that initial attempts to simulate the equivalent filter ERPLD or the generalized second-order PLL for the sinusoidal test-tone case yielded erroneous results. For example, Fig. H-1 shows a segment of the phase error as a function of time for the equivalent filter ERPLD for a 1kHz test-tone in the absence of noise using the linear model. This model is the same as that shown in Fig. 4-4 with the sinusoidal function removed from the phase detector. Unlike the results predicted by linear circuit theory which would indicate that the phase error should be sinusoidal after the transient portion of the response, the results of Fig. H-1 are highly nonsinusoidal and show the influence of higher frequencies. As indicated in Section 4.2.3, the basic problem was pinpointed to the differentiator within the equivalent filter and the generalized second-order PLL filter. The differentiator by nature emphasizes higher frequencies. Unlike a true analog computer in which the simulated parameters are continuous, CSMP being a digital computer program must handle the parameters as discrete variables. It is of interest therefore, to determine the spectrum of these parameters. In particular, the spectrum of a sinusoid as handled by CSMP shall be investigated in order to gain additional insight into the problems encountered in the test-tone case. Consider the spectrum Fs $(j\omega)$ of a sampled waveform $f_s(t)$

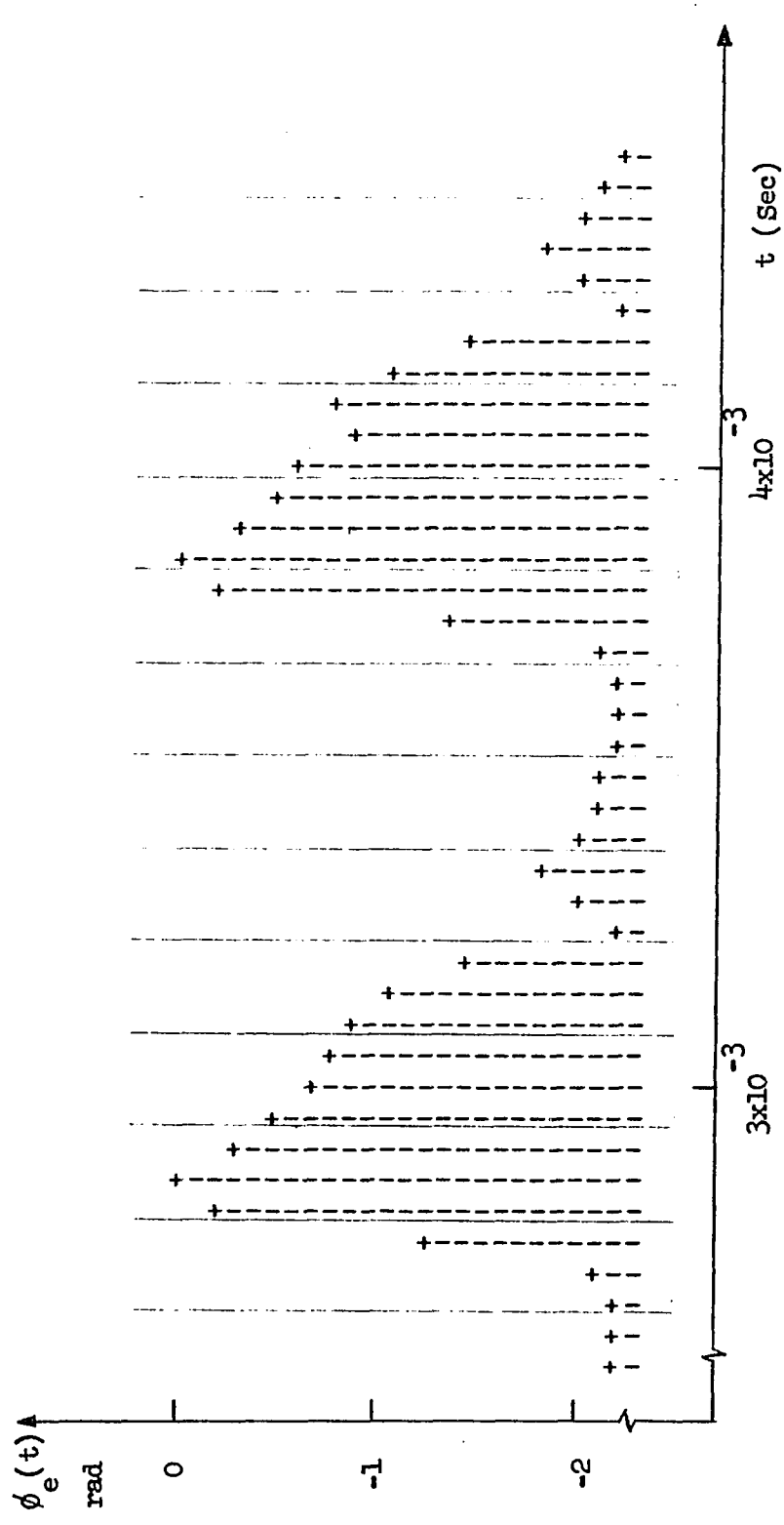

Fig. H-1. Segment of phase error response for equivalent filter ERPLD with perfect differentiator.

such as that encountered using CSMP. $f_s(t)$ may be expressed by

$$f_s(t) = f(t) \sum_{n=-\infty}^{\infty} \delta(t - n\Delta t) = \sum_{n=-\infty}^{\infty} f(n\Delta t) \delta(t - n\Delta t) \tag{H-1}$$

where f(t) is the continuous function being approximated by the digital computer and Δt is the integration interval. It can be readily shown [Ref. 1, p. 515] that Fs $(j\omega)$ is given by

$$F_s(j\omega) = \sum_{n=-\infty}^{\infty} \frac{1}{\Delta t} F \left[j(\omega - n\omega_s) \right] \tag{H-2}$$

where

$$\omega_s = \frac{2\pi}{\Delta t} \tag{H-3}$$

Consider the case

$$f(t) = A \cos \omega_{TT} t \tag{H-4}$$

Then

$$F(j\omega) = A\pi\delta(\omega - \omega_{TT}) + A\pi\delta(\omega + \omega_{TT}) \tag{H-5}$$

and

$$F_s(j\omega) = \sum_{n=-\infty}^{\infty} \frac{A\pi}{\Delta t}\left[\delta(\omega - n\omega_s - \omega_{TT}) + \delta(\omega - n\omega_s - \omega_{TT})\right] \tag{H-6}$$

Fs(jω) therefore consists of a spectral line at the test-tone frequency f_{TT} plus additional spectral component pairs centered about multiples of the sampling frequency $1/\Delta t$ and separated from this frequency by f_{TT} Hz.

Next, consider the case where the sinusoidal waveform is represented by a sample-and-hold approximation indicative of simple rectangular integration. It can readily be shown for this case that

$$F_s(j\omega) = \frac{\text{Sin}(\omega\Delta t/2)}{\omega\Delta t/2} \sum_{n=-\infty}^{\infty} F\left[j(\omega - n\omega_s)\right] \tag{H-7}$$

For the sinusoidal test-tone case of Eq. H-4, Fs (jω) may be expressed as follows

$$F_s(j\omega) = \frac{A\pi\,\text{Sin}(\omega\Delta t/2)}{\omega\Delta t/2} \tag{H-8}$$

$$\cdot \sum_{n=-\infty}^{\infty} \left[\delta(\omega - n\omega_s - \omega_{TT}) + \delta(\omega - n\omega_s - \omega_{TT})\right]$$

In this case, the same spectral lines occur as in the impulse sampling case; however, a Sinc weighting factor is introduced. The preceding analysis has shown that a sinusoid simulated by a discrete approximation contains additional spectral components due to the sampling. When a differentiator is required in a digital simulation, erroneous results can sometimes occur because of its property of emphasizing higher frequencies. As indicated in Chapter 4, by using an imperfect differentiator, this problem can be eliminated.

Reference

P. F. Panter, Modulation, Noise, and Spectral Analysis, McGraw-Hill, New York, 1965.

APPENDIX I

ANALYTICAL CHECK ON THE BASIC GENERALIZED SECOND-ORDER PLL MODEL

In Section 4.2.3, it was indicated that the substitution of an imperfect differentiator for the ideal device corrected the erroneous results originally observed in the equivalent filter ERPLD and the generalized second-order PLL. In this Appendix, as a check on the validity of the new model with the imperfect differentiator, an analysis was performed on the linear model of the generalized second-order PLL for the test-tone case in the absence of noise using Laplace Transform techniques.

The linear model of the generalized second-order PLL used in the analysis which follows is shown in Fig. I-1. Although, of course, any parameter within the model can be determined, the phase error is of prime interest and shall be determined. As shown in Chapter 1, the phase error may be expressed in terms of the closed-loop transfer function as follows

$$\Phi_e(s) = \Phi_i(s) \left[1 - H(s) \right] \qquad \text{(I-1)}$$

where

$$H(s) = \frac{K F(s)}{s + K F(s)} \qquad \text{(I-2)}$$

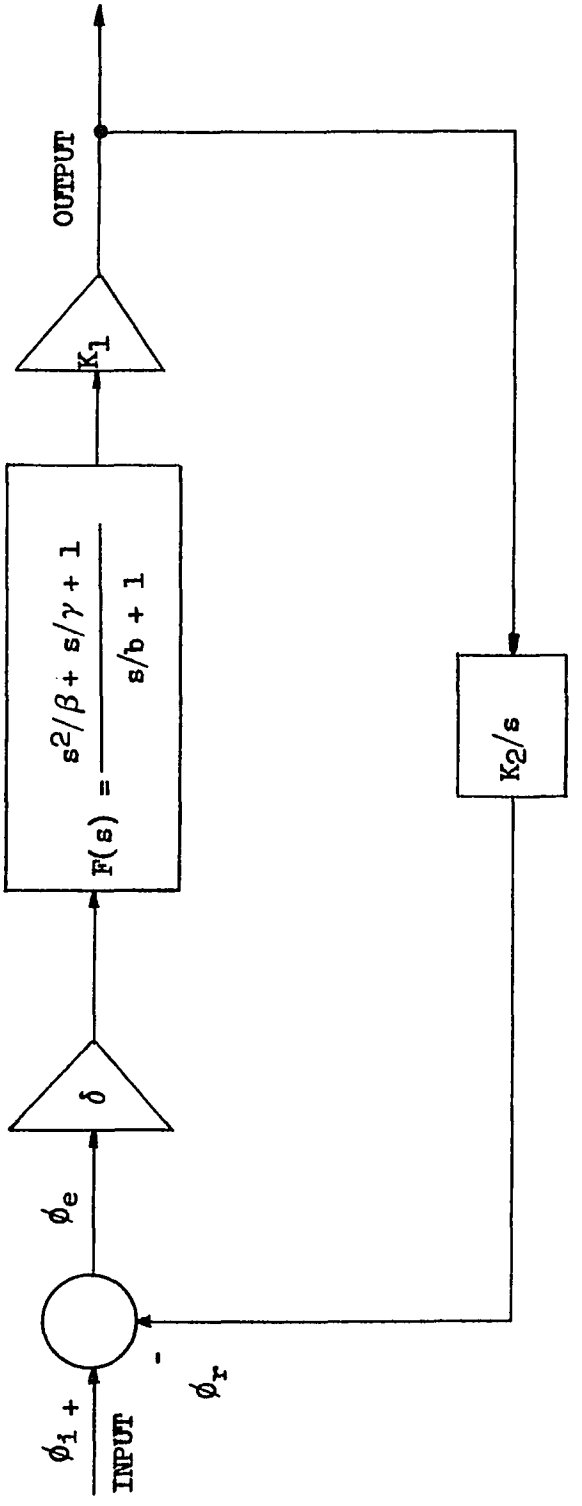

Fig. I-1. Linear model of the generalized second-order PLL in the absence of noise.

$$F(s) = \frac{s^2/\beta + s/\gamma + 1}{s/b + 1} \qquad \text{(I-3)}$$

and

$$K = K_1 K_2 \delta \qquad \text{(I-4)}$$

continuing the development

$$1-H(s) = \frac{s^2/Kb + s/K}{s^2\left[\frac{1}{Kb} + \frac{1}{\beta}\right] + s\left[\frac{1}{K} + \frac{1}{\gamma}\right] + 1} \qquad \text{(I-5)}$$

If the input is a sinusoidal test-tone expressed by

$$\phi_i(t) = A\sin\omega_o t \qquad \text{(I-6)}$$

then

$$\Phi_i(s) = \frac{A\omega_o}{s^2 + \omega_o^2} \qquad \text{(I-7)}$$

The parameters to be used are those of Acampora and Newton [Ref. 1] converted to generalized second-order PLL form which are given by

$$\left.\begin{array}{lll} \beta = 8.836 \times 10^{8} & (\text{rad/sec})^2 \\ \gamma = 2.767 \times 10^{4} & \text{rad/sec} \\ b = 1.88 \times 10^{3} & \text{rad/sec} \\ K = 4.7 \times 10^{5} & \text{sec}^{-1} \\ A = 10 & \text{rad} \\ \omega_o = 6.283 \times 10^{3} & \text{rad/sec} \end{array}\right\} \qquad \text{(I-8)}$$

The expression for the phase error in the Laplace Transform domain is then given by

$$\Phi_e(s) = \frac{6.283\times10^{4}}{s^2 + (6.283\times10^{3})^2} \cdot \frac{s^2 + 1.880\times10^{3}\,s}{2s^2 + 3.381\times10^{4}\,s + 8.836\times10^{8}} \qquad \text{(I-9)}$$

using the method of partial fraction expansion, Eq. I-9 may be expressed as follows

$$\frac{(3.142\times10^{4})(s^2 + 1.880\times10^{3}\,s)}{(s^2 + 3.948\times10^{7})(s^2 + 1.691\times10^{4}\,s + 4.418\times10^{8})} = \qquad \text{(I-10)}$$

$$\frac{C_1 s + C_2}{(s^2 + 3.948\times10^{7})} + \frac{C_3 s + C_4}{s^2 + 1.691\times10^{4} s + 4.418\times10^{8}}$$

The first term on the right side of Eq. I-10 represents the steady-state component, while the second term yields the transient response.

By cross-multiplying in Eq. I-10, and setting like powers of "s" equal to each other, the constants of the partial fraction expansion can be evaluated yielding

$$\left.\begin{aligned} C_1 &= 2.584\text{x}10^{-1} \\ C_2 &= -2.655\text{x}10^{3} \\ C_3 &= -2.584\text{x}10^{-1} \\ C_4 &= 2.970\text{x}10^{4} \end{aligned}\right\} \qquad \text{(I-11)}$$

The Laplace Transform expression of Eq. I-10 can then be inverted yielding the time domain expression

$$\phi_e(t) = 0.495 \cos\left(6.283\text{x}10^{3}\, t + 58.6^{\circ}\right) + 1.677\, e^{-8.455\text{x}10^{3}\, t} \sin\left(1.924\text{x}10^{4}\, t - 8.86^{\circ}\right) \qquad \text{(I-12)}$$

Fig. I-2 shows a plot of Eq. I-12 for the first millisecond. Fig. I-3 shows the CSMP solution for the generalized second-order PLL for the same loop parameters. The results are virtually identical, adding additional confidence to the model. The equivalent filter ERPLD and the original Acampora and Newton ERPLD were also simulated using the same basic set of parameters for the linear case. As anticipated, the results were again identical to a high degree of accuracy. Fig. I-4 shows the CSMP program used for the generalized second-order PLL, linear model,

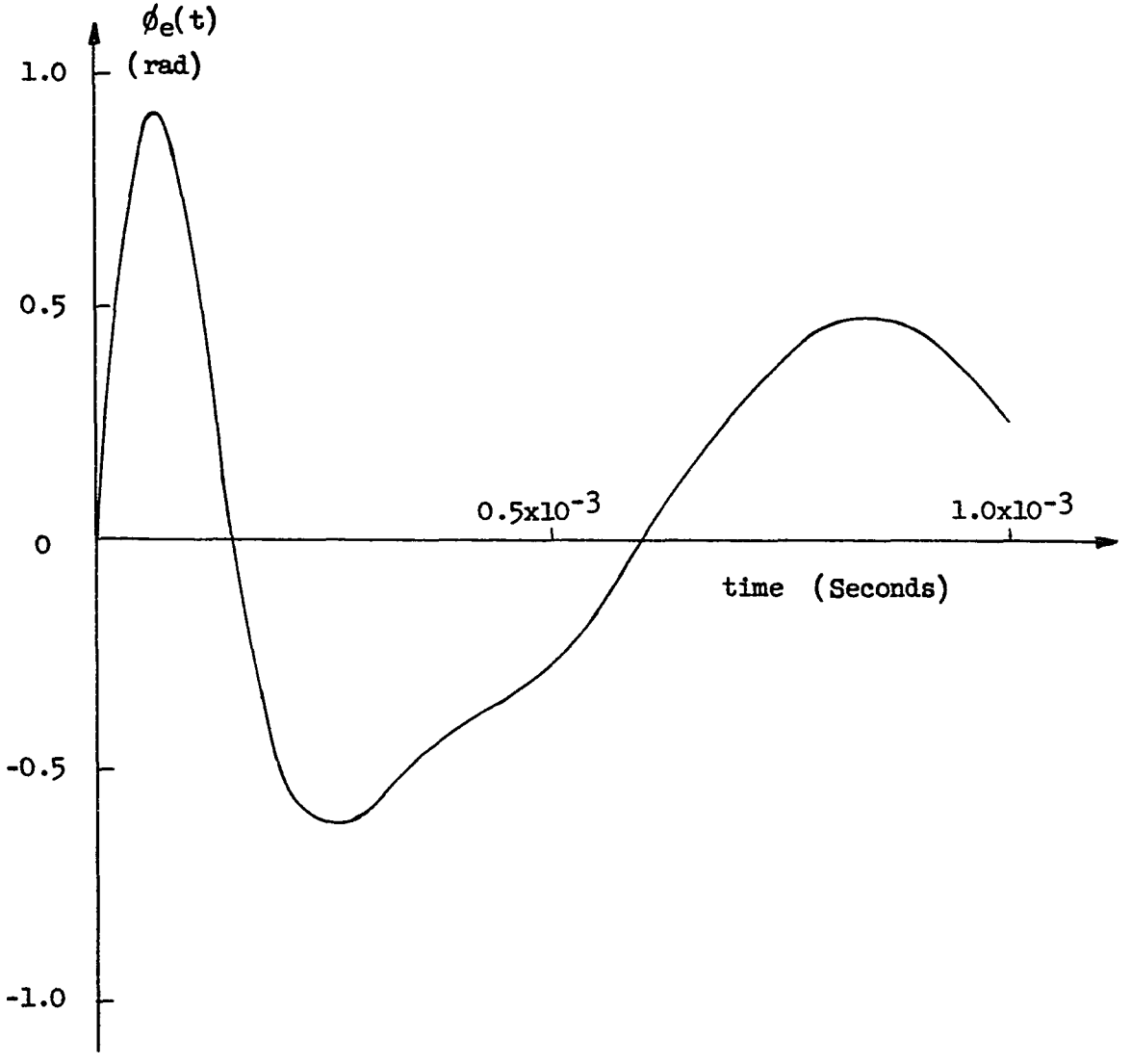

Fig. I-2. Phase error vs time for generalized second-order PLL from analytical solution.

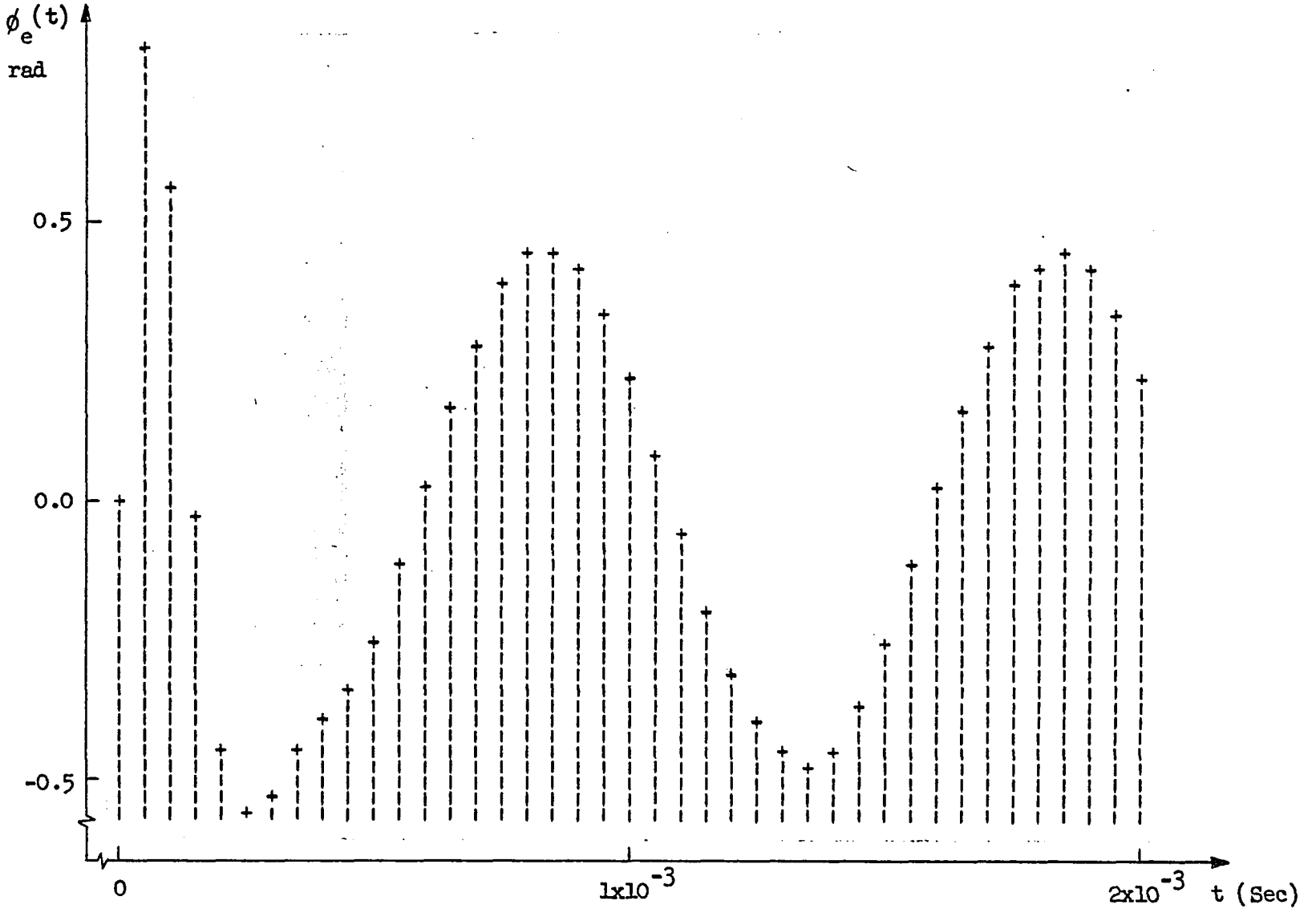

Fig. I-3. CSMP solution of phase error vs time for linear model of the generalized second-order PLL.

```
TITLE GENERALIZED SECOND-ORDER PLL, TEST-TONE CASE, LINEAR MODEL
INITIAL
CONSTANT XK=4.7E5
CONSTANT BETA=8.836E8,GAMMA=2.767E4,B=1.88E3
CONSTANT C1=3.1415E5
         C=1.0/C1
DYNAMIC
       ERROR=XINPUT-RETSIG
          EI=ERROR*XK
       XNEWA=(1.0/BETA)*EI
       XNEWB=INTGRL(0.0,EI)
       XNEWC=(1.0/GAMMA)*XNEWB
       XNEWD=INTGRL(0.0,XNEWB)
       XNEWE=XNEWA+XNEWC+XNEWD
       XNEWF=XNEWE-XNEWH
       XNEWG=B*XNEWF
       XNEWH=INTGRL(0.0,XNEWG)
          EO=DERIV(0.0,XNEWG)
         EOP=REALPL(0.0,C,EO)
      RETSIG=INTGRL(0.0,EOP)
       XNEW1=SINE(0.0,6.283E3,0.0)
      XINPUT=XNEW1*10.0
       XNEW2=ERROR**2
       XNEW3=INTGRL(0.0,XNEW2)
       XNEW4=RAMP(0.0)
      XMSQER=XNEW3/XNEW4
TIMER DELT=1.0E-6,OUTDEL=5.0E-5,FINTIM=1.0E-2
PRTPLOT ERROR
LABEL PHASE ERROR VS TIME
PRTPLOT XMSQER
LABEL MEAN-SQUARE PHASE ERROR
METHOD RECT
END
STOP
```

Fig. I-4. CSMP program for the generalized second-order PLL; test-tone, linear model.

test-tone case. Fig. I-5 shows the CSMP program used for the equivalent filter ERPLD, linear model, test-tone case. By re-inserting the sinusoidal function into the phase detector expression in Figs. I-4 and I-5, the non-linear CSMP programs used in Chapter 4 are obtained. Fig. I-6 shows the results obtained for the non-linear model of the generalized second-order PLL test-tone case in the absence of noise. Note that there are some differences between this figure and that of Fig. I-3 caused by the sinusoidal non-linearity.

Reference

A. Acampora and A. Newton, "Use of Phase Subtraction to Extend the Range of a Phase-Locked Demodulator," RCA Review, Vol 27, No. 3, pp. 577-599, December 1966.

```
TITLE ERPLD EQUIVALENT FILTER, LINEAR MODEL, NO NOISE
INITIAL
CONSTANT A=2.94E4,B=1.88E3
CONSTANT C=3.1415E5
          APRIM=1.0/A
          BPRIM=1.0/B
          CPRIM=1.0/C
CONSTANT DELK1=2.93E-1,XK2=1.6E6,XKD=2.13E-6
DYNAMIC
          ERROR=XINPUT=RETSIG
          XNEW1=ERROR*DELK1
          XNEW2=LEDLAG(APRIM,BPRIM,XNEW1)
          XNEW3=XNEW1*XKD
          XNEW4=DERIV(0.0,XNEW3)
         XNEW4A=REALPL(0.0,CPRIM,XNEW4)
         OUTPUT-XNEW2+XNEW4A
          XNEW5=OUTPUT*XK2
         RETSIG=INTGRL(0.0,XNEW5)
          XNEW6=SINE(0.0,6.283E3,0.0)
         XINPUT=XNEW6*10.0
          XNEW7=ERROR**2
          XNEW8=INTGRL(0.0,XNEW7)
          XNEW9-RAMP(0.0)
         XMSQER=XNEW8/XNEW9
TIMER DELT=1.0E-6,OUTDEL=5.0E-5,FINTIM=1.0E-2
PRTPLOT ERROR
LABEL PHASE ERROR VS TIME
PRTPLOT OUTPUT
LABEL OUTPUT VS TIME
PRTPLOT XNEW2
LABEL XNEW2
PRTPLOT XNEW4
LABEL XNEW4
PRTPLOT XMSQER
LABEL MEAN SQUARE PHASE ERROR
METHOD RECT
END
STOP
```

Fig. I-5. CSMP program for the equivalent filter ERPLD; test-tone, linear model.

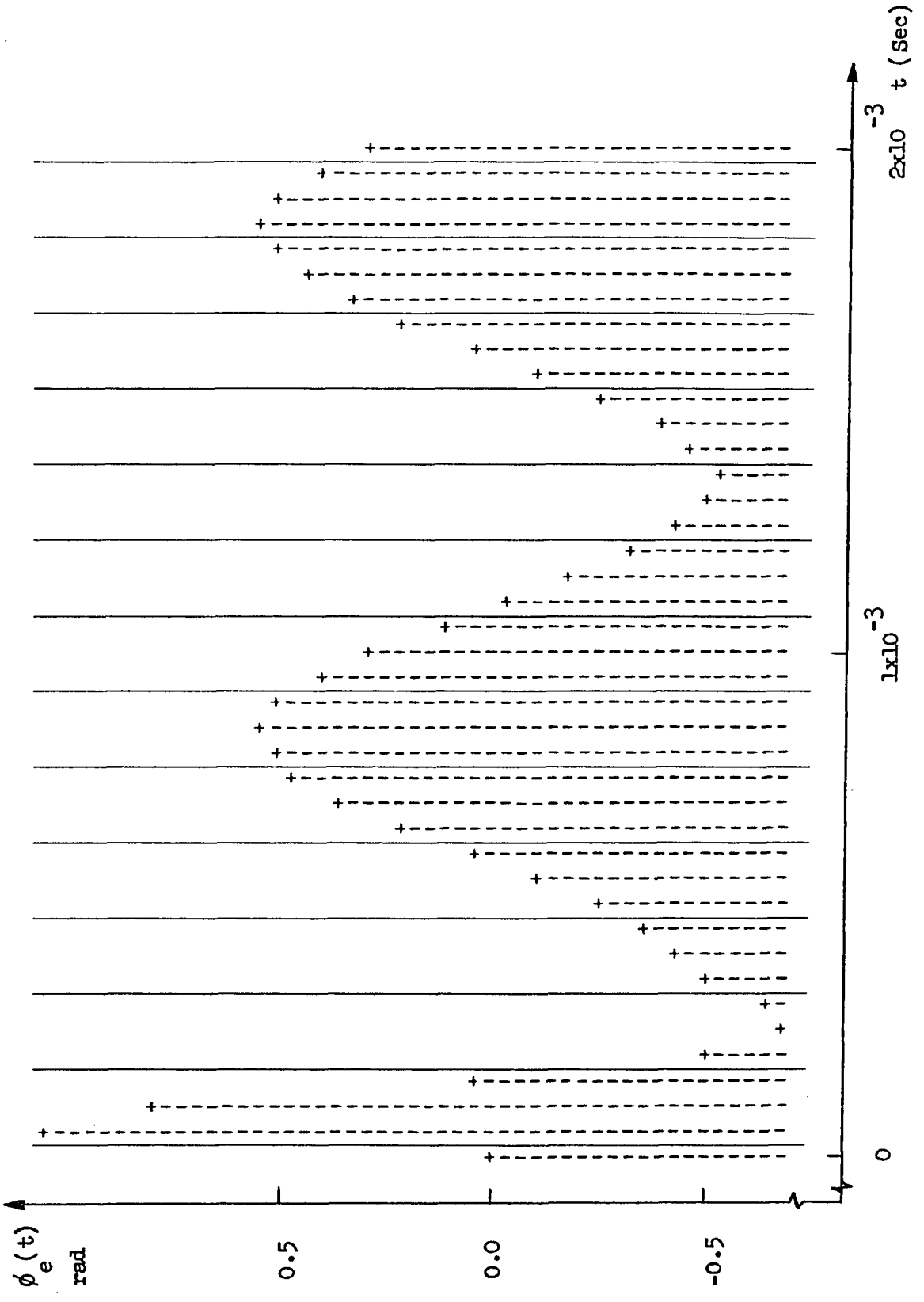

Fig. I-6. CSMP solution of phase error vs time for non-linear model of the generalized second-order PLL.

APPENDIX J

BUTTERWORTH FILTER IMPLEMENTATION USING THE CSMP

In this Appendix, a detailed discussion of Butterworth filter implementation using the CSMP will be given. Included will be the low-pass implementation used in the equivalent noise source and the high-pass implementation used in the voice modulation PSD simulation. The expression for the sixth-order normalized Butterworth low-pass filter transfer function is given by [Ref. 1, p. 347]

$$\frac{1}{(s^2+0.518s+1)(s^2+1.414s+1)(s^2+1.932s+1)} \qquad \text{(J-1)}$$

$H_B(s)$ can be reexpressed in terms of a generalized cutoff frequency ω_c by making the substitution

$$s = j\frac{\omega}{\omega_c} \qquad \text{(J-2)}$$

in Eq. J-1 yielding

$$H_B(s) = \frac{1}{\left[\left(j\frac{\omega}{\omega_c}\right)^2+0.518j\frac{\omega}{\omega_c}+1\right]\left[\left(j\frac{\omega}{\omega_c}\right)^2+1.414j\frac{\omega}{\omega_c}+1\right]\left[\left(j\frac{\omega}{\omega_c}\right)^2+1.932j\frac{\omega}{\omega_c}+1\right]} \qquad \text{(J-3)}$$

The low-pass Butterworth transfer function for a cutoff frequency of ω_c is then given by

$$H_B(s) = \frac{\omega_c^6}{(s^2+0.518\,\omega_c\,s+\omega_c^2)(s^2+1.414\,\omega_c s+\omega_c^2)(s^2+1.932\,\omega_c s+\omega_c^2)} \qquad \text{(J-4)}$$

substituting the desired cutoff frequency of 17.5kHz into Eq. J-4 yields

$$H_B(s) = \frac{1.772\times10^{30}}{(s^2+5.698\times10^4\,s+1.21\times10^{10})(s^2+1.555\times10^5 s+1.21\times10^{10})(s^2+2.125\times10^5\,s+1.21\times10^{10})} \qquad \text{(4-24)}$$

The CSMP CMPXPL function (see Eq. 4-27) can be used directly to realize each of the quadratic terms in the denominator of $H_B(s)$. The tenth-order Butterworth low-pass filter transfer function is determined in a similar manner. Starting with the normalized expression given by

$$H_B(s) = \frac{1}{(s^2+0.313s+1)(s^2+0.908s+1)(s^2+1.414s+1)(s^2+1.782s+1)(s^2+1.975s+1)} \qquad \text{(J-5)}$$

Transformation of Eq. J-5 to a cutoff frequency of 17.5 kHz yields

$$H_B(s) = \frac{2.594 \times 10^{50}}{(s^2+3.441\times10^4 s+1.21\times10^{10})(s^2+9.988\times10^4 s+1.21\times10^{10})(s^2+1.556\times10^5 s+1.21\times10^{10})} \cdot \frac{1}{(s^2+1.960\times10^5 s+1.21\times10^{10})(s^2+2.173\times10^5 s+1.21\times10^{10})} \qquad \text{(J-6)}$$

Again, the CSMP CMPXPL function can be used to realize each of the quadratic terms. Fig. J-1 shows the CSMP program for the approximate equivalent noise source using a tenth-order Butterworth low-pass filter.

Next, consider the high-pass Butterworth filter required for the voice modulation case. By substituting 1/s for s in Eq. J-1, a low-pass to high-pass transformation is achieved yielding

$$H_B(s) = \frac{s^6}{(s^2+0.518s+1)(s^2+1.414s+1)(s^2+1.932s+1)} \qquad \text{(J-7)}$$

```
TITLE APPROX. EQUIVALENT NOISE SOURCE TEST PROG.

DYNAMIC
       XNEW1=GAUSS (5,0.0,5.35)
       XNEW2=CMPXPL(0.0,0.0,1.564E-1,1.1E5,XNEW1)
       XNEW3=XNEW2*1.21E10
       XNEW4=CMPXPL(0.0,0.0,4.540E-1,1.1E5,XNEW3)
       XNEW5=XNEW4*1.21E10
       XNEW6=CMPXPL(0.0,0.0,7.071E-1,1.1E5,XNEW5)
       XNEW7=XNEW6*1.21E10
       XNEW8=CMPXPL(0.0,0.0,8.910E-1,1.1E5,XNEW7)
       XNEW9=XNEW8*1.21E10
       XNEW10=CMPXPL(0.0,0.0,9.877E-1,1.1E5,XNEW9)
       EQNOIN=XNEW10*1.21E10
       XNEW11=EQNOIN**2
       XNEW12=INTGRL(0.0,XNEW11)
       XNEW13=RAMP(0.0)
       XMSQ=XNEW12/XNEW13
TIMER DELT=2.5E-7,OUTDEL=1.0E-4,FINTIM=5.0E-2
PRTPLOT XMSQ
LABEL MEAN-SQUARE VALUE OF NOISE SOURCE
PRTPLOT EQNOIN
LABEL APPROXIMATE EQUIVALENT NOISE SOURCE
METHOD RECT
END
STOP
```

Fig. J-1. CSMP program for approximate noise source using tenth-order Butterworth filter.

Substituting Eq. J-2 into Eq. J-7 yields the Butterworth high-pass filter transfer function with a cutoff frequency ω_c given by

$$H_B(s) = \qquad \text{(J-8)}$$

$$\frac{s^6}{(s^2+0.518\omega_c s+\omega_c^2)(s^2+1.414\omega_c s+\omega_c^2)(s^2+1.932\omega_c s+\omega_c^2)}$$

Substituting the desired cutoff frequency of 1kHz into Eq. J-8 yields

$$H_B(s) = \qquad \text{(4-48)}$$

$$\frac{s^6}{(s^2+3.255\times10^3 s+3.948\times10^7)(s^2+8.884\times10^3 s+3.948\times10^7)(s^2+1.214\times10^4 s+3.948\times10^7)}$$

Once more the CSMP CMPXPL function can be used to realize the quadratic functions in the denominator of $H_B(s)$. The numerator can be realized using CSMP DERIV functions. The tenth-order Butterworth high-pass filter transfer function is determined in a similar manner. Starting with the normalized expression given by

$$H_B(s) = \qquad \text{(J-9)}$$

$$\frac{s^{10}}{(s^2+0.313s+1)(s^2+0.908s+1)(s^2+1.414s+1)(s^2+1.782s+1)(s^2+1.975s+1)}$$

Transformation of Eq. J-9 to a cutoff frequency of 1kHz yields

$$H_B(s) = \qquad \text{(J-10)}$$

$$\frac{s^{10}}{(s^2+1.965\times10^3 s+3.948\times10^7)(s^2+5.705\times10^3 s+3.948\times10^7)(s^2+8.885\times10^3 s+3.948\times10^7)}$$

$$\cdot \quad \frac{1}{(s^2+1.120\times10^4 s+3.948\times10^7)(s^2+1.241\times10^4 s+3.948\times10^7)}$$

Fig. J-2 shows the complete voice PSD simulator using a tenth-order high-pass Butterworth filter.

Reference

S. Karni, Network Theory: Analysis and Synthesis, Allyn and Bacon Inc., Boston, Massachusetts, 1966.

```
TITLE VOICE PSD SIMULATOR TEST PROGRAM
DYNAMIC
          XNEW1=GAUSS(1,0.0,6.447E9)
          XNEW2=CMPXPL(0.0,0.0,1.564E-1,6.283E3,XNEW1)
          XNEW3=DERIV(0.0,XNEW2)
          XNEW4=DERIV(0.0,XNEW3)
          XNEW5=CMPXPL(0.0,0.0,4.540E-1,6.283E3,XNEW4)
          XNEW6=DERIV(0.0,XNEW5)
          XNEW7=DERIV(0.0,XNEW6)
          XNEW8=CMPXPL(0.0,0.0,7.071E-1,6.283E3,XNEW7)
          XNEW9=DERIV(0.0,XNEW8)
         XNEW10=DERIV(0.0,XNEW9)
         XNEW11=CMPXPL(0.0,0.0,8.913E-1,6.28E3,XNEW10)
         XNEW12=DERIV(0.0,XNEW11)
         XNEW13=DERIV(0.0,XNEW12)
         XNEW14=CMPXPL(0.0,0.0,9.876E-1,6.283E3,XNEW13)
         VOIPSD=XNEW14
         XNEW15=VOIPSD**2
         XNEW16=INTGRL(0.0,XNEW15)
         XNEW17=RAMP(0.0)
         XMSQVL=XNEW16/XNEW17
TIMER DELT=2.5E-7,PRDEL=1.0E-4,OUTDEL=1.0E-4,FINTIM=2.5E-2
PRTPLOT XMSQVL
LABEL MEAN SQUARE VALUE OF VOICE SIGNAL
PRTPLOT VOIPSD
LABEL VOICE SIGNAL VS TIME
METHOD RECT
END
STOP
```

Fig. J-2. CSMP program for voice PSD simulator using tenth-order Butterworth filter.

APPENDIX K

CSMP PROGRAM FOR THE GENERALIZED SECOND-ORDER PLL IN THE PRESENCE OF NOISE, TEST-TONE CASE

```
TITLE GENERALIZED SECOND-ORDER PLL, TEST-TONE CASE
INITIAL
CONSTANT  XK=4.7E5
CONSTANT CPRIM=6.283E5
      C=1.0/CPRIM
CONSTANT BETA=8.836E8,GAMMA=2.767E4,B=88E3
DYNAMIC
      ERROR=XINPUT-RETSIG
     PHDEOT=SIN(ERROR)
      XNEWA=GAUSS(5,0.0,2.390)
      XNEWB=IMPULS(0.0,5.0E-7)
      XNEWC=XNEWA*XNEWB
      XNEWD=XNEWC**2
      EQNOA=ZHOLD(XNEWD,XNEWC)
      XNEWE=CMPXPL(0.0,0.0,2.590E-1,1.1E5,EQNOA)
      XNEWF=XNEWE*1.21E10
      XNEWG=CMPXPL(0.0,0.0,7.068E-1,1.1E5,XNEWF)
      XNEWH=XNEWG*1.21E10
      XNEWI=CMPXPL(0.0,0.0,9.659E-1,1.1E5,XNEWH)
      EQNO1=XNEWI*1.21E10
      XNEWJ=IMPULS(2.5E-7,5.0E-7)
      XNEWK=XNEWA*XNEWJ
      XNEWL=XNEWK**2
      EQNOB=ZHOLD(XNEWL,XNEWK)
      XNEWM=CMPXPL(0.0,0.0,2.590E-1,1.1E5,EQNOB)
      XNEWN=XNEWM*1.21E10
      XNEWO=CMPXPL(0.0,0.0,7.068E-1,1.1E5,XNEWN)
      XNEWP=XNEWO*1.21E10
      XNEWQ=CMPXPL(0.0,0.0,9.659E-1,1.1E5,XNEWP)
      EQNO2=XNEWQ*1.21E10
      YNEWA=SIN(RETSIG)
      YNEWB=COS(RETSIG)
      YNEWC=EQNO1*YNEWA
      YNEWD=EQNO2*YNEWB
     EQNOIN=YNEWD-YNEWC
         E1=PHDEOT+EQNOIN
         EI-XK*E1
      XNEW1=DERIV(0.0,EI)
      XNEW2=REALPL(0.0,C,XNEW1)
      XNEW3=(1.0/BETA)*XNEW2
      XNEW4=(1.0/GAMMA)*EI
      XNEW5=INTGRL(0.0,EI)
      XNEW6=XNEW3+XNEW4+XNEW5
```

```
      XNEW7=INTGRL(0.0,E0)
      XNEW8=(-1.0)*XNEW7
      XNEW9=XNEW8+XNEW6
         E0=B*XNEW9
      RETSIG=INTGRL(0.0,E0)
      XNEW10=SINE(0.0,6.283E3,0.0)
      XINPUT=XNEW10*10.0
       ZNEW1=ERROR**2
       ZNEW2=INTGRL(0.0,ZNEW1)
       ZNEW3=RAMP(0.0)
      XMSQER=ZNEW2/ZNEW3
        ZNEW4=EQNO1**2
        ZNEW5=INTGRL(0.0,ZNEW4)
        XMSQ1=ZNEW5/ZNEW3
        ZNEW6=EQNO2**2
        ZNEW7=INTGRL(0.0,ZNEW6)
        XMSQ2=ZNEW7/ZNEW3
TIMER DELT=2.5E-7,FINTIM=1.0E-2
PRTPLOT ERROR
LABEL PHASE ERROR VS TIME
PRTPLOT XMSQER
LABEL MEAN-SQUARE PHASE ERROR
PRTPLOT XMSQ1
LABEL MEAN-SQUARE OF NOISE COMPONENT 1
PRTPLOT XMSQ2
LABEL MEAN-SQUARE OF NOISE COMPONENT 2
METHOD RECT
END
STOP
```

APPENDIX L

DETAILED DERIVATION OF THE DIFFERENTIAL EQUATION FOR THE GENERALIZED SECOND-ORDER PHASE-LOCKED LOOP

In this Appendix, the detailed mathematics for deriving the differential equation for the generalized second-order PLL in standard form is given. Starting with Eq. 5-3

$$\dot{\phi}_e(t) = \dot{\phi}_i(t) - K\left[\frac{p^2/\beta + p/\gamma + 1}{p/b + 1}\right] \text{Sin } \phi_e(t) \tag{5-3}$$

Eliminating P/b + 1 from the denominator of the filter function and multiplying through by "b" results in

$$\left[p + b\right] \dot{\phi}_e(t) = \left[p + b\right] \dot{\phi}_i(t) - Kb\left[p^2/\beta + p/\gamma + 1\right] \text{Sin } \phi_e(t) \tag{L-1}$$

Carrying through the differential operator evaluations yields

$$p\ (\ \text{Sin } \phi_e\ ) = \dot{\phi}_e \text{ Cos } \phi_e \tag{L-2}$$

and

$$p^2\ (\ \text{Sin } \phi_e\ ) = -\dot{\phi}_e^2 \text{ Sin } \phi_e + \ddot{\phi}_e \text{ Cos } \phi_e \tag{L-3}$$

Substitution of Eqs. L-2 and L-3 into Eq. L-1 and carrying through the remaining differential operator evaluations yields the result

$$\ddot{\phi}_e + b\dot{\phi}_e = \tag{L-4}$$

$$\ddot{\phi}_i + b\dot{\phi}_i - (Kb/\beta)\left[- \dot{\phi}_e^2 \operatorname{Sin} \phi_e + \ddot{\phi}_e \operatorname{Cos} \phi_e \right]$$

$$- Kb/\gamma \, \dot{\phi}_e \operatorname{Cos} \phi_e - Kb \operatorname{Sin} \phi_e$$

Simplifying and collecting terms yields the desired result

$$\ddot{\phi}_e = \tag{5-4}$$

$$\frac{\ddot{\phi}_i + b\dot{\phi}_i - Kb \operatorname{Sin} \phi_e - \left[b + (Kb/\gamma) \operatorname{Cos} \phi_e \right] \dot{\phi}_e + (Kb/\beta) \dot{\phi}_e^2 \operatorname{Sin} \phi_e}{1 + (Kb/\beta) \operatorname{Cos} \phi_e}$$

VITA

William A. Novick was born in , on . He received a Bachelor of Science in Electrical Engineering and a Master of Science in Electrical Engineering in 1966 and 1969, respectively, from Newark College of Engineering, Newark, New Jersey. He has been working toward the Doctor of Engineering Science Degree in Electrical Engineering at New Jersey Institute of Technology, Newark, New Jersey, since September 1969. From September 1969 through June 1972, he held the position of Teaching Fellow at New Jersey Institute of Technology. The research upon which this dissertation is based was conducted at New Jersey Institute of Technology from October 1971 through December 1975.

Since 1972, he has been working at the US Army Electronics Command, Fort Monmouth, New Jersey, where he has been involved in the areas of Electromagnetic (EM) Vulnerability and Electronics Counter-Countermeasures (ECCM).